NASA/TM–2005-212827
AFDD/TR-05-003

UH-60A Airloads Catalog

William G. Bousman
Aeroflightdynamics Directorate (AMRDEC)
U.S. Army Research, Development, and Engineering Command
Ames Research Center, Moffett Field, California

Robert M. Kufeld
Ames Research Center
Aeromechanics Branch
Moffett Field, California

August 2005

The NASA STI Program Office . . . in Profile

Since its founding, NASA has been dedicated to the advancement of aeronautics and space science. The NASA Scientific and Technical Information (STI) Program Office plays a key part in helping NASA maintain this important role.

The NASA STI Program Office is operated by Langley Research Center, the Lead Center for NASA's scientific and technical information. The NASA STI Program Office provides access to the NASA STI Database, the largest collection of aeronautical and space science STI in the world. The Program Office is also NASA's institutional mechanism for disseminating the results of its research and development activities. These results are published by NASA in the NASA STI Report Series, which includes the following report types:

- TECHNICAL PUBLICATION. Reports of completed research or a major significant phase of research that present the results of NASA programs and include extensive data or theoretical analysis. Includes compilations of significant scientific and technical data and information deemed to be of continuing reference value. NASA's counterpart of peer-reviewed formal professional papers but has less stringent limitations on manuscript length and extent of graphic presentations.

- TECHNICAL MEMORANDUM. Scientific and technical findings that are preliminary or of specialized interest, e.g., quick release reports, working papers, and bibliographies that contain minimal annotation. Does not contain extensive analysis.

- CONTRACTOR REPORT. Scientific and technical findings by NASA-sponsored contractors and grantees.

- CONFERENCE PUBLICATION. Collected papers from scientific and technical conferences, symposia, seminars, or other meetings sponsored or cosponsored by NASA.

- SPECIAL PUBLICATION. Scientific, technical, or historical information from NASA programs, projects, and missions, often concerned with subjects having substantial public interest.

- TECHNICAL TRANSLATION. English-language translations of foreign scientific and technical material pertinent to NASA's mission.

Specialized services that complement the STI Program Office's diverse offerings include creating custom thesauri, building customized databases, organizing and publishing research results . . . even providing videos.

For more information about the NASA STI Program Office, see the following:

- Access the NASA STI Program Home Page at *http://www.sti.nasa.gov*

- E-mail your question via the Internet to help@sti.nasa.gov

- Fax your question to the NASA Access Help Desk at (301) 621-0134

- Telephone the NASA Access Help Desk at (301) 621-0390

- Write to:
  NASA Access Help Desk
  NASA Center for AeroSpace Information
  7121 Standard Drive
  Hanover, MD 21076-1320

NASA/TM–2005-212827
AFDD/TR 05-003

UH-60A Airloads Catalog

William G. Bousman
Aeroflightdynamics Directorate (AMRDEC)
U.S. Army Research, Development, and Engineering Command
Ames Research Center, Moffett Field, California

Robert M. Kufeld
Ames Research Center
Aeromechanics Branch
Moffett Field, California

National Aeronautics and
Space Administration

Ames Research Center
Moffett Field, California 94035-1000

August 2005

Available from:

NASA Center for AeroSpace Information
7121 Standard Drive
Hanover, MD 21076-1320
(301) 621-0390

National Technical Information Service
5285 Port Royal Road
Springfield, VA 22161
(703) 487-4650

TABLE OF CONTENTS

LIST OF FIGURES

LIST OF TABLES

NOMENCLATURE

A	disk area
B	blade root flap transducer rotation angle
c	blade chord
C	Celsius
c.g.	center of gravity
C_n	section normal force coefficient, $N \Big/ \frac{1}{2} \rho V^2 c$
C_P	power coefficient, $P \Big/ \rho A(\Omega R)^3$
C_{pcg}	power coefficient correction for different c.g.
C_{pD}	power coefficient correction for the effect of drag
$C_{p\beta}$	power coefficient correction due to sideslip
C_T	thrust coefficient, $T \Big/ \rho A(\Omega R)^2$
C_W	weight coefficient, $GW \Big/ \rho A(\Omega R)^2$
e	offset of focal point
F	Fahrenheit
F_c	centrifugal force at focal point of bearing
GW	gross weight
fwd	forward
HP	pressure altitude
$K_{i,\ i=1\ to\ 10}$	blade root motions calibration constants
M	Mach number
M_f	first harmonic hub moment
N	normal section force
N_R	rotor rotational speed, percent
N_r	rotor rotational speed, percent
n_z	aircraft load factor
P	total engine power
P_s	static pressure
mph	miles per hour
fpm	feet per minute
ft/min	feet per minute

psia	pounds per square inch, absolute
P_t	stagnation pressure
q	dynamic pressure
R	rotor radius
rwd	rearward
s	rotor solidity
T	thrust
T	blade root pitch transducer rotation angle
T_d	time duration
V	velocity
Vh	max aircraft horizontal velocity
Z	blade root lead-lag transducer rotation angle
4P	4 per rev component
α_s	shaft angle of attack
α_{TPP}	tip-path-plane angle
β	blade root flapping angle
β	sideslip angle
β	first harmonic of the flapping angle
β_{lc}	cosine flapping angle
γ	flightpath
ζ	blade root motion lead-lag angle
θ	blade root motion pitch angle
Θ	temperature ratio
μ	advance ratio
ρ	air density
σ	rotor solidity, $Nc/\pi R$
ψ	rotor azimuth
Ω	rotor rotation speed, rad/sec

TRENDS Wordscan Notation

AOB	angle of bank
ATM TURBULENCE	atmospheric turbulence conditions
CA	collision avoidance
CON.FIX	control fixed in one position
CCW	counter clockwise
CW	clockwise
CWS	weight coefficient over solidity
DEG	degree
DG	degree
D/S	degrees per second
G	aircraft load factor
HDG	compass heading
HEAT	aircraft heater turn on
KIAS	indicated airspeed, knots
KIASB	indicated airspeed, boom system, knots
KIASH	indicated airspeed
LEVEL FLT	level flight
RAD	flightpath turn radius
ROLL REV	roll reversal
STAB	stabilator position
S/S	sideslip
VNE	never exceed velocity
2311	control input

TRENDS Item Codes Descriptions

AF53.HN4	vertical acceleration of pilot's seat, 4^{th} harmonic
AH0Z.AVO	vertical acceleration of hub, average component
AH0Z.HN4	vertical acceleration of hub, 4^{th} harmonic
AMU	advance ratio
AZCG	aircraft vertical acceleration
AZIM	data item code rotor azimuth
BCART	ballast cart position
BH12	blade 1 pitch RVDT

BH22	blade 2 pitch RVDT
BH32	blade 3 pitch RVDT
BH42	blade 4 pitch RVDT
BH11	blade 1 flap RVDT
BH21	blade 2 flap RVDT
BH31	blade 3 flap RVDT
BH42	blade 4 flap RVDT
BH10	blade 1 lead-lag RVDT
BH20	blade 2 lead-lag RVDT
BH30	blade 3 lead-lag RVDT
BH40	blade 4 lead-lag RVDT
CP	power coefficient
FLP1	blade 1 corrected flap measurement
FLP2	blade 2 corrected flap measurement
FLP3	blade 3 corrected flap measurement
FLP4	blade 4 corrected flap measurement
HPB	pressure altitude, boom system
H001	static pressure
KIAS	indicated airspeed, knots
KIASB	indicated airspeed, boom system, knots
KIASH	indicated airspeed, HADS
LAG1	blade 1 corrected lead-lag measurement
LAG2	blade 2 corrected lead-lag measurement
LAG3	blade 3 corrected lead-lag measurement
LAG4	blade 4 corrected lead-lag measurement
LSSZ	HADS downwash velocity
LSSX	HADS forward velocity
LSSY	HADS sideways velocity
MRFLAP1	blade 1 corrected flap measurement
PITCHATT	aircraft pitch attitude
PTC1	blade 1 corrected pitch measurement
PTC2	blade 2 corrected pitch measurement
PTC3	blade 3 corrected pitch measurement
PTC4	blade 4 corrected pitch measurement

P701	blade pressure, 92%R, 1%c, top surface
RQ10	main rotor shaft torque
RQ12	main rotor shaft bending moment
SGMA	air density ratio
T100	outside air temperature
VR04	rotor speed
VR05	rotor speed
VTAS	true airspeed, boom system
VTRU	true velocity, combine HADS and boom system
V001	dynamic pressure
WINDSP	Crows Landing Airfield wind speed
WINDR	Crows Landing Airfield wind direction
XLASER	Crows Landing Airfield laser tracking X measurement
XLDOT	Crows Landing Airfield laser tracking velocity measurements
YLASER	Crows Landing Airfield laser tracking Y measurement
YLDOT	Crows Landing Airfield laser tracking velocity measurements
ZLDOT	Crows Landing Airfield laser tracking velocity measurements
ZRADAR	Crows Landing Airfield radar tracking Z measurements

Acronyms

AACT	Air-to-Air Combat Test
AGL	Above Ground Level
ADAS	Airframe Data Acquisition System
AEFA	U.S. Army Aviation Engineering Flight Activity
AFCS	Automatic Flight Control System
BMH	Blade Motion Hardware
DCS	Derived Counter Set
ESSS	Extended Stores Support System
FPS	Flight Path Stabilization
HADS	Helicopter Airspeed Data Sensor
HIRSS	Hover Infrared Suppression System
IGE	In-Ground Effect
ILS	Instrument Landing System
LaRC	Langley Research Center

LASSIE	Low Airspeed Sensing and Indicating Equipment
LVDT	Linear Variable Differential Transformers
MRP	Military Rated Power
OGE	Out-of-Ground Effect
PBA	Pitch Bias Actuator
PCM	Pulse Code Modulation
RDAS	Rotating Data Acquisition System
SAS	Stability Augmentation System
TRENDS	Tilt Rotor Engineering Database System
UTTAS	Utility Tactical Transport Aerial System
VFR	Visual Flight Rules
VRS	Vortex Ring State

TRENDS Commands

BHL
BH2
CALIBS
CVF
GATEWAY
HARMONIC
MINMAX
MULTIPLOT
NORMALIZE
OUTDATA
PLOT
PRINT
TIMEHIST
VIEW
WORDSCAN

SUMMARY

As a part of the NASA-Army UH–60A Airloads Program, instrumented rotor blades were designed and built for the UH–60A helicopter that included 241 pressure tranducers on one blade and a suite of strain gauges and accelerometers on a second blade. These blades were then installed on a UH–60A at NASA Ames Research Center and a special purpose data acquisition system was designed and built to acquire the rotating system measurements. The aircraft was also instrumented with conventional aircraft state measurements as well as a suite of fuselage accelerometers.

Test flights of the highly-instrumented UH–60A were flown from August 1993 to February 1994 and an extensive data base was acquired. A total of 31 research flights were made with the majority of the flights flown out of Moffett Field, California. The test data, in general, were acquired in isolated airspace over the San Joaquin Valley. An exception to this procedure is that nine flights were made in cooperation with NASA Langley Research Center, and for these tests the aircraft was flown out of the Modesto airport and the data were acquired at the Crows Landing Naval Auxiliary Air Field, also within the San Joaquin Valley.

Over 900 different test conditions, or counters, were recorded, processed, and stored in an electronic data base as a part of this test program. The electronic data base, currently at NASA Ames Research Center, includes approximately 30 GBytes of data obtained from the test program. This Technical Memorandum summarizes the kinds of data that are in the data base to assist interested users. Each set of test conditions is presented in a table which contains a unique identifying number that is termed the counter number, the written description of the counter that is within the database, and the duration of the counter in seconds. Within each table the counters are listed in chronological order, and in some cases counters may be included within two or more tables if they meet different criteria.

1. INTRODUCTION

The UH–60A Airloads Aircraft, flight tested from August 1993 to February 1994, is shown in flight over the Livermore Valley of California in figure 1. The testing has been summarized in reference 1 and results from these tests, to date, have been presented in references 2–15. A summary description of the 31 test flights is provided here as table 1. The airloads program test objectives were quite broad and included not only classical flight test conditions as might be encountered in an aircraft development program, but also flight tests in conjunction with a ground-acoustic array where flightpath control, aircraft tracking, and data sychronization issues were important as well as formation flight with a YO–3A aircraft for airborne acoustic measurements. The differing requirements of the program's test objectives have affected the data reduction procedures and the structure of the data base. There is a need for a comprehensive description of all the data that were acquired in this test program as well as explanatory material as to how the data were acquired, reduced, and stored in the data base. The purpose of the present Technical Memorandum is to provide this comprehensive description of the data that were acquired as well as to provide the reader with information on data acquistion and reduction issues.

This Technical Memorandum is designed to list all of the flight counters (as well as some pseudo-counters) in tables. Counters have been selected and assigned to tables using a variety of criteria. For instance, there are tables that include hover conditions, level flight conditions, climbs, descents, turns, and so forth. In some cases counters may be listed in more than one table. In providing tables of the flight counters an effort has also been made to show examples of test data, and in this way to provide a qualitative appreciation of the data that have been acquired. However, these examples are quite limited and cannot be considered comprehensive.

The initial section of this report provides a general summary of the test procedures, data acquisition, data reduction, and data base storage. Following the summary, section 3 discusses the calibration of the instrumentation, the use of housekeeping points to track data integrity, and the procedures for airspeed calibrations. The remaining sections of the report discuss the specific kinds of data that were obtained. Section 4 summarizes the data that were obtained in steady flight, and this includes forward flight sweeps, hover conditions, and a number of miscellaneous cases. Section 5 describes the portion of the test where data were obtained in conjunction with acoustic measurements. This section includes both tests with a ground-acoustic array and inflight airborne acoustic measurements. Section 6 describes climb and descent data and these include steady climbs and descents, vertical climbs, high-speed dives, and autorotational descents. Section 7 covers cases where the aircraft was in a steady turn, a diving turn, or a maneuver associated with a steady turn. Section 8 treats maneuvering flight including pull-ups, pushovers, rolling pullouts, and roll reversals. Section 9 finishes the recitation of data with flight dynamic data that includes 3-2-1-1 flight dynamic maneuvers and frequency sweeps. Finally, section 10 provides some concluding remarks.

Figure 1.– UH–60A Airloads Aircraft over the Livermore Valley.

Table 1.– Summary of UH–60A Airloads Program flights.

FLT	FLIGHT OBJECTIVE	DATA ACQUIRED
82	Low Airspeed Calibration	Ground paced, 30 mph rwd to 70 mph fwd; Nr sweep on ground
83	High Airspeed Calibration	Air-paced level flight, 80–160 kts; Nr sweep, 1 in. stick inputs on ground
84	Steady & Maneuvering Airloads[a]	Level flight, 20 kts to Vh (127 kts) at C_W/s=0.09; accel./decel., hover to 50 kts
85	Steady & Maneuvering Airloads[a]	Level flight, 20 kts to Vh (138 kts), steady turns at C_W/s=0.08; roll reversals
88	Steady & Maneuvering Airloads[a]	Level flight, 15 kts to Vh (122 kts), steady turns at C_W/s=0.10; heading changes; decel.
89	Steady & Maneuvering Airloads[a]	Level flight, 20 kts to Vh (109 kts), turns at C_W/s=0.11; roll rev; pull-ups; pushovers
90	Steady & Maneuvering Airloads[a]	Level flight, 20 kts to Vh (90 kts), turns at C_W/s=0.12 and 0.13; climbs
91	Ground Measured Acoustics	Level flight, 60–143 kts; ascents, descents, 6°–12° glide slope
92	Ground Measured Acoustics	Turns, 60 and 80 kts; heading changes, 15°–90°; ascents, descents, 6–12°
93	Ground Measured Acoustics	Level flight, 60–143 kts; ascents, descents, 6°–12°
94	Ground Measured Acoustics	Hover pedal turns, 250 ft AGL; ascents, descents, 3°–12°; climbs
95	Ground Measured Acoustics	Ascents and descents, 3°–12°; level flight, 100 kts
96	Ground Measured Acoustics	Constant radius turns, 60 kts, 1000, 1400, 1800 ft radii; low airspeed calibration
97	Ground Measured Acoustics	Terminal area traffic turns, 30°–90° heading changes, 60 kts
98	Ground Measured Acoustics	Constant radius turns, 60 kts, 1000, 1400, 1800 ft radii; low airspeed calibration
99	Ground Measured Acoustics	Terminal area traffic turns, 30°–90° heading changes, 60 kts
100	Airborne Measured Acoustics	Formation flight with YO-3A data acquisition aircraft, descents, 300–600 fpm
101	Airborne Measured Acoustics	Formation flight with YO-3A data acquisition aircraft, descents, 400–900 fpm
102	Airborne Measured Acoustics	Formation flight with YO-3A data acquisition aircraft, descents, 400–900 fpm
103	Airborne Measured Acoustics	Formation flight with YO-3 data acquisition aircraft, descents, 300–400 fpm
105	Flight Dynamics[a]	Frequency sweep control inputs (long., lat., col., ped.), 70 kts
106	Flight Dynamics[a]	Turbulent air gust response, 80 and 120 kts
107	Flight Dynamics[a]	Frequency sweeps control inputs (long., lat., col., ped.), 35 kts
108	Flight Dynamics[a]	Frequency sweep (lat.) and 2-3-1-1 control inputs (long., lat., col., ped.), 35 & 70 kts
110	Maneuvers[a]	Level flight, hover to 139 kts at C_W/s=0.08; dives; turns; roll rev. pull-ups; pushovers
111	Flight Dynamics[a]	Frequency sweeps control inputs (long., lat., col., ped.), hover
112	Flight Dynamics[a]	Frequency sweep and 2-3-1-1 control inputs (long., lat., col., ped.), hover
113	Airborne Measured Acoustics	YO-3A data acquisition aircraft, descents, 200–900 fpm; collective sweep on ground
114	Airborne Measured Acoustics	YO-3A data acquisition aircraft, descents, 200–1000 fpm; collective sweep on ground
115	Maneuvers[a]	Autorotations; climbs; turns; Nr sweeps, hover, 80, 120 kts
116	Maneuvers[a]	Wind-up turns; dives; Nr sweeps, 30 kts; accel., hover to 50 kts

[a]Aircraft longitudinal c.g. held constant by using movable ballast cart to offset fuel used.

2. FLIGHT TEST PROGRAM PROCEDURES

Test Procedures

Flight Card– Test planning for each flight began with the preparation of the flight card that listed the required test points to be covered during the upcoming flight. The card was developed by the Test Director and was reviewed with the Project Pilot and then the project team. Under normal circumstances the test flight was briefed on the afternoon prior to the flight. All flights were made under VFR conditions and in the absence of precipitation.

Flight Test Operation– On the day of a scheduled flight the aircraft was powered up in the hanger using a standard hydraulic mule. The rotor azimuth was set with Blade 1 over the nose of the aircraft, and the pilot controls were set to a neutral position that was used for all flights. Instrumentation power was turned on and tapes were loaded into the two tape drives. Preflight static cal records were taken after the instrumentation power had been on for at least half an hour to allow stabilization of the electronics. For performance flights the aircraft was weighed prior to leaving the hanger and fuel density measurements were obtained. The static pressure at the aircraft was measured with an independent instrument and this value was used to calibrate the ship and test boom static pressure sensors. The flight engineer used the weight and balance data to determine the c.g. position on the aircraft and to establish position requirements for the ballast cart that was used to control aircraft c.g. in flight.

Prior to a flight, the crew chief prepared the aircraft within the hanger, following a normal pre-flight checklist. The aircraft was then towed from the hanger to the ramp and the electrical systems were powered from an auxiliary power cart. The onboard instrumentation was turned on and a half-hour period was used to allow instrument system temperatures to stabilize. Once stabilized, the pre-flight static calibrations were recorded by the flight engineer. The pilots would then do their standard pre-flight checks for the aircraft. If control system calibrations were required, the aircraft hydraulic systems were powered by auxiliary cart. The pilots would then perform the required control system motions which were recorded. Following all checks and calibrations, the engines were started and the rotor brought up to operational speed.

The aircraft was then taxied onto the runway and lifted off to a hover at approximately 70 feet and an out-of-ground effect housekeeping point was taken. All instrumentation that could be examined on telemetry was then checked, and if the systems were working satisfactorily the aircraft departed for the flight test airspace in the San Joaquin Valley (about 20 minutes flying time from Ames Research Center). On the departure from Ames, a second housekeeping point was taken as the aircraft reached 1000-foot pressure altitude and an airspeed of 80 knots.

Once in approved airspace the test pilots would follow the test card for the flight. For performance and inflight acoustic tests it was necessary to select a flight altitude as specified by the value of the weight coefficient, C_W, on the test card. The aircraft telemetry signal included the outside air temperature, pressure, rotor speed, airspeed, and fuel burned, and the Test Director's workstation in the telemetry room was programmed to calculate the advance ratio, blade tip Mach number, and the C_W for the aircraft. The pilots were then instructed to increase or decrease altitude

or airspeed as appropriate to meet the assigned test condition. During a constant C_W flight it was necessary for the aircraft to increase its altitude with each test point to compensate for fuel burn-off. The flight engineer also monitored fuel burn-off and computed new settings for the ballast cart to maintain a constant c.g. position for the aircraft.

The UH–60A automatic flight control system (AFCS) has five major subsystems: (1) a limited authority stability augmentation system (SAS), (2) a trim system, (3) a flightpath stabilization system (FPS), (4) a pitch bias actuator (PBA), and (5) the stabilator control system (ref. 16). The SAS actuators are in series with the flight controls and have ±10% authority. The SAS was designed to provide the aircraft with three-axis rate damping and was left operational for all test flying, and the SAS actuator positions were measured as part of the basic instrumentation system installed on the aircraft. The trim system provided appropriate force-feel characteristics for normal operation of the vehicle and was turned off for performance counters but was left on for other flights cases. The FPS works through the trim system to provide attitude hold and turn coordination and it was turned off for all test flights. Similarly, the PBA, which was designed to provide longitudinal static and dynamic stability, was also turned off during test flights. The stabilator control system was operational for testing with the stabilator setting dependent upon airspeed and pitch attitude as determined by the AFCS computer. However, for one airspeed case during performance testing, the stabilator incidence was varied from +5 to –5 deg to examine the effects of variable stabilator incidence on loads and performance.

The length of the recorded data stream on the primary and back-up tape systems varied depending on the type of test condition. For steady flight conditions, a twenty-second record was normally obtained. Upon stabilizing at the desired flight condition, the pilot would notify the flight engineer who would turn on the flight tape recorders. The tape recorders were configured to automatically turn off after recording 20 seconds of data but could be manually shutdown at the flight engineer's discretion. The inflight acoustic test points (section 5) required 30 seconds of data instead of 20 seconds, while the length of the ground acoustic flyovers and maneuver data records were variable and the tape recorder was manually controlled for each test condition. Control frequency sweep records (section 9) generally required at least 90 seconds to complete and were also manually controlled by the flight test engineer.

During the flight, two data streams were telemetered to the ground for monitoring. One stream was obtained from the Airframe Data Acquisition System (ADAS) and one from the Rotating Data Acquisition System (RDAS). The ADAS data stream included typical aircraft state measurements, while the RDAS data stream included a limited number of blade pressures, strain-gauge outputs, and accelerometer measurements. These parameters were monitored to check signal quality, to determine if test card target values were achieved (in maneuvers, as an example), and to insure loads did not exceed aircraft limits.

Following completion of the flight test card or, as sometimes happened, the aircraft became low on fuel or there was insufficient data recording tape left, the aircraft was directed back to Ames. If sufficient recording tape remained, an inbound 80-knot housekeeping point was taken at 1000-foot pressure altitude while approaching Ames. Then, again, if there was sufficient tape, a final OGE hover housekeeping point was taken just off the taxiway. The aircraft then landed on the apron at the

hanger. Final static cal records were taken at this point and the aircraft was moved into the hanger and, for performance flights, was weighed once again.

Early Problem with Rotor Speed Measurements– The test aircraft had two measurements of rotor speed (item codes VR04 and VR05). Both measurements were based on a pulse train from the generator that provides the rotor speed signal for the ship's instrumentation and, in this sense, they were not redundant measurements. The VR04 measurement used a frequency-to-voltage converter to generate an analog signal of the rotor speed. The analog signal was then sampled by the ADAS and recorded with the aircraft state data. The VR05 measurement used the same pulse train as VR04, but the signal was never converted to an analog signal and was read directly as a digital signal on the ADAS. It was determined that the VR04 measurement was normally one or two rpm low, while the VR05 measurement was accurate. However, during early testing for weight coefficients of 0.08 and 0.09 (flights 84 and 85), VR04 was used in the real-time calculation of the weight coefficients. This resulted in slightly lower values of weight coefficients than were targeted; the values being lower by the square of the VR04 error. The values of the weight coefficients obtained and stored within the data base for these two flights, therefore, are 0.0791 and 0.0891 respectively. Once this error had been detected, VR05 was used for the real-time calculation of weight coefficients on all subsequent flights.

Post-Flight Data Processing– Post-flight data processing consisted of two basic steps. The first step added calibration files to the data records and aligned the data with proper time tags. This first step was performed in the ground station computers and resulted in a set of digital tapes based on the PCM tapes recorded in flight. The second step recomposed the data into time histories for each sensor that were properly tagged with the parameters names, and then calculated statistics and appropriate derived parameters. The data were then formatted and stored in the TRENDS data base (ref. 17). This second step was done using a VAX computer.

In general, the amount of data that was stored in the data base was reduced from the quantity recorded on the flight tapes through a process called “time slicing.” The concept behind time slicing was to select the best five seconds of data out of a 20-second record and store only these data in the data base. In this way the quantity of flight data was reduced by a factor of four. The appropriate time slice was determined by a subjective examination of a number of aircraft state parameters. The preferred means of making the examination was with the Test Director’s workstation in the telemetry room. As the flight data were being recorded, parameters on the telemetry stream were plotted in a “normalized” fashion where the mean value was removed and the data were normalized by the standard deviation. Depending upon the parameter being examined, this provided the Test Director information as to the best five seconds for data reduction. An example of normalized data plotted from the Test Director’s workstation is shown in figure 2.

Following the flight, the Test Director provided the ground station personnel with a table of start and stop times based on his assessment of the quality of the data, and these data were appropriately sliced in the first data reduction step.

An alternative and more time consuming approach to time slicing was to go through the two data-processing steps and then time slice afterwards using the NORMALIZE utility in TRENDS. A new set of start and stop times would then be provided to the TRENDS data base manager and the

second data reduction step would be repeated to save only the selected time slice. An example of data plotted from the NORMALIZE utility is shown in figure 3.

The first step in the data processing, performed at the ground station, would also vary if there were any failures in the primary flight data tape. The primary tape system recorded 10 streams of RDAS data merged as a single stream on one tape, while the secondary or backup system recorded each of the 10 RDAS streams as separate channels on the backup tape. In those cases where the primary system failed it was necessary to process the backup flight data tape at the ground station using a different data reduction program. However, the product of this first step was the same regardless of which flight tape was processed.

Data Base– As mentioned above, the data stored within the data base was only a subset of the data recorded. For a steady flight condition where 20 seconds of flight data were recorded, five seconds were saved in the data base. For longer records, as obtained in the ground-acoustic tests, inflight-acoustic tests, maneuvers, or flight dynamics tests, more than five seconds of data were generally archived in the data base. In addition, the use of the time-slicing technique provided flexibility in post-flight data processing so that multiple slices could be extracted from one counter and saved in the data base. In these cases, the flight tape was processed twice, once for each time slice. Normally, the first time slice was stored using the true flight counter number while the second time slice was saved with an artificial counter number or pseudo-counter number. The pseudo-counter numbers are identified in WORDSCAN in TRENDS by an "*" at the end of the test point description and can also be recognized by the absolute start time associated with the pseudo-counter. In the tables in this Technical Memorandum, pseudo-counters are also identified by an "*" at the end of the description line.

A special case of multiple time slices is related to the flights flown with respect to the ground-acoustic array (see section 7). For these counters, two sets of time slices were established, the first set by Ames investigators and the second by Langley personnel. The time-slicing criteria used at Ames for the ground-acoustic tests were the same as for all other flight conditions. The resulting data were stored in the same data base as the other flight data. The time-slicing criteria used by Langley engineers made use not only of aircraft state measurements but also of ground-acoustic measurements. In particular, for the Langley-selected data it was necessary to insure that the time slice was taken when the aircraft was near the acoustic array and there was good signal-to-noise in the acoustic measurements. A separate data base, therefore, was created for the Langley time slices. Users of TRENDS can access flight data in either the normal data base, labeled "BH2," or the Langley data base, labeled "BHL." Note, however, that there are no acoustic data in either of these data bases.

In addition to the second data base that was created to include the Langley time slices, a special partition of the BH2 data base was also made to store intermediate results from the ground-acoustic tests. This section consists of the counters from the nine ground acoustic flights (91 to 99) that were processed without the blade pressure transducer data. Unlike normal records, however, these counters cover the entire time that the tape recorder was on, that is, there was no time slicing. These full-record counters were obtained to provide a data base for the subsequent time slicing by the Ames and Langley organizations. Pressure data were not included to keep the size of this data base

tractable. Counter numbers for this special partition are created by using a prefix-4 with the original counter number. Thus, the full-record counter number equivalent to counter 9121 is 49121.

Ground-Acoustic Test Procedures

Test procedures during the ground-acoustic tests were similar to those described for the other tests. A total of nine flights were made over a 10-day period to accomplish these tests. The aircraft and the maintenance crew were stationed at the Modesto Airport during this portion of the program to allow for more efficient use of time for aircraft and instrumentation maintenance. The Langley acoustic crew was stationed at Crows Landing and they monitored the flights from acoustic vans adjacent to the Crows Landing laser tracking ground station. The flight crew and the Airloads test team were stationed at Ames. The flight crew was ferried back and forth to Modesto each morning for testing while the flight was monitored from the ground station at Ames which was done for other flights. Full radio and telemetry communication with both the Crows Landing's ground station and the aircraft was maintained during this testing.

The airfield at Crows Landing was selected because of the low level of flight activity in the region, the low background noise signature, the availability of the facilities including runways and fuel, a ground station equipped with radios, telemetry and a data acquisition system, a laser tracker, a redundant radar tracker, and a crash rescue crew for emergencies. The layout of the Crows Landing airfield is shown in figure 4. The figure has been digitized from a plot plan of the airfield used at Ames Research Center. The airfield has two runways (35 and 30), and Runway 35, with a nominal orientation of 355 deg magnetic, is oriented vertically in the figure. Based on the Crows Landing 7.5-minute topographic sheet dated 1980, the runway orientation is 11.1 deg east of true north and 6.5 deg west of magnetic north (353.5 deg magnetic).

The acoustic setup for these tests has been described in detail in reference 3, however, a brief overview is also provided here. The basic 18-microphone array was setup in a "T" shape with the center or reference microphone placed at the intersection of runways 35 and 30 as shown in figure 4. The aircraft flew a ground track perpendicular to Runway 35 from the west to the east as indicated in the figure. The airspeed, descent and ascent angles were varied to obtain a complete mapping of the acoustic signature of the UH–60A in a wide variety of low altitude takeoff and landing conditions. A major element in the successful testing of the UH–60A for ground acoustics was the accurate measurements of the aircraft position as it flew over the microphone array. These measurements were obtained with a laser tracker that was installed at the Crows Landing Airfield and its location is indicated in figure 4.

Flightpath guidance was supplied to the UH–60A pilots with a real-time position feedback system developed and operated at Crows. This was done by comparing the measured flight track as determined by the laser tracker with a prescribed flightpath. The calculated error was then transmitted to the aircraft using the Instrumented Landing System (ILS) frequencies and standard ILS instrumentation in the cockpit. The pilot would monitor the ILS and make altitude and azimuthal correction as he approached the microphone array. This system allowed the Airloads project team to complete the acoustic test matrix with a low number of repeat runs caused by out-of-tolerance flightpath errors.

During the ground-acoustic testing, wind velocities were measured with three different systems: (1) the normal ground system used at Crows Landing Airfield, (2) a 10-meter tower that was installed and operated by Langley Research Center, and (3) a tethered balloon, also installed and operated by Langley. The location of each of these systems is indicated in figure 4. The standard Crows wind measurements were recorded during the tests and are stored in the TRENDS data base as WINDSP and WINDR. The WINDR is specified within the Runway 35 axis system as shown in figure 4. Thus a 5-knot wind at 0 deg blows from north to south along the centerline of Runway 35, while a 5-knot wind at 90 deg blows from east to west across the runway. The data recorded by LaRC were not stored within this data base. A detailed analysis of all the Crows Landing hover and low speed flight data using the wind aloft data recorded by Langley has been completed and is discussed below in section 4.1.

The Langley Research Center anemometer tower or profiler measures wind speeds at five heights above the ground: 0.70 m, 2.62 m, 5.12 m, 7.00 m, and 10.00 m. The wind directions are measured at 0.70 m, 5.12 m, and 10.00 m. These data were acquired to support the ground-acoustic measurements and are not included in the TRENDS data base.

Langley also uses a tethered balloon to measure atmospheric properties at heights greater than the profiler. Under normal circumstances the balloon is raised and lowered between ground level and 500 ft, the wind speed, wind direction, turbulence level, temperature, and humidity are determined. As with the profiler data, these measurements are not included in the TRENDS data base.

Ground-acoustic data were collected for level flight, descents, and climbs as the UH–60A flew along the flight track indicated in figure 4. In addition, hover data were collected as the aircraft maintained a steady hover over the reference microphone at 250-ft elevation. The effects of turning flight were also evaluated by having the aircraft make left and right turns of 30, 45, 60, and 90 deg as it passed over the reference microphone. A second approach to the measurement of acoustics in turning flight used a different microphone layout (see section 10) and the aircraft flew a continuous circular flightpath centered about the reference microphone for one complete revolution. The airspeed was kept constant at 60 knots Indicated Airspeed (IAS) and three different radii were flown.

Air-to-Air Acoustic Test Procedures

Air-to-air or inflight acoustic measurements were made with the UH–60A in formation flight with a YO–3A aircraft that was used as a flying microphone platform. The two aircraft are shown in formation flight in figure 5. These measurements were made as a part of the NASA Ames Inflight Rotor Acoustic Program (IRAP)[18].

For these tests a matrix of airspeed and weight coefficients were selected that matched wind tunnel data taken with a model-scale UH–60A rotor (ref. 19). The airspeeds, weight coefficients, and rates of descent are shown in table 2. At each test point the flight elevation was set so that the desired weight coefficient would be obtained during the data record. The YO–3A established the

proper airspeed and descent rate for the test condition and the UH–60A would follow above and behind the YO–3A. The distance between the UH–60A and the YO–3A was measured with a hand-held laser tracking device and, based on these measurements, the UH–60A pilot was directed to move his aircraft either closer to or further from the YO–3A so as to obtain a separation distance of 1.5 rotor radii. As the target altitude was approached, synchronized data were recorded on both aircraft for 30 seconds. Each test condition was repeated several times to ensure that at least one counter would provide a suitable steady measurement. The time slices saved to the data base were determined after the flight following a review of both the UH–60A and YO–3A data. Typically, 14 seconds of data from the UH–60A were loaded in the BH2 data base.

Flight Dynamics Testing Procedures

Two approaches were used to obtain flight dynamic data during the UH–60A Airloads Program. First, a specified 2-3-1-1 input was used for each control to provide a fairly broadband excitation to the aircraft and, second, a frequency sweep method was used to allow identification of the aircraft characteristics (ref. 20). Both approaches were used at three airspeeds: hover, 35 KIASB, and 70 KIASB. The hover testing (Flight 111 and 112) were done at the Crows Landing Airfield in order to use the laser tracker at that facility and was performed out of ground effect. For these tests the SAS and FPS systems were disabled and the stabilator was fixed at the appropriate position for the selected flight speed. The position data from these tests is integrated into the data base, just as it was for the ground acoustic test data. The airloads measurements were considered of secondary importance for these flights, but it is believed that the airload information collected during this testing is of unique value and may well provide useful data for future research.

2-3-1-1 Control Input Testing– The 2-3-1-1 control input is a series of four step inputs made sequentially in alternate directions. The duration of each step is defined by the numeric value given in its name. Specifically, the numbers define a unit length of time that a control input is held. For example, if the unit of time is one second, then 3 represents an input that is held for 3 seconds, and the total maneuver input sequence would last 7 seconds. Alternatively, if the unit of time was 2 seconds, the 3 would stand for 6 seconds, and the total maneuver input sequence would last 14 seconds. The unit of time is selected based on the predicted frequencies of the various flight modes. For the UH–60A Airloads test this base unit of time was 0.5 seconds and this results in a total length for the control input sequence of 3.5 seconds. During the control inputs the pilot attempted to avoid control motions in other control axes to isolate the input to the control axis of interest. The average length of records for these tests was 20 seconds which included a steady flight portion prior to the input and a period of time for recovery following the input. The length of these records allowed them to be handled with the same procedures used for typical flight cases.

Frequency Sweep Inputs– Frequency sweep control inputs were used to provide data that could be analyzed in the frequency domain to identify aircraft flight dynamic modes. The pilot started the frequency sweep from a steady flight condition with a sine wave input to a single control with a frequency of about 0.1 Hertz. The pilot shortened the period of each successive oscillation in a smooth fashion until a cutoff frequency was reached. This cutoff frequency in most cases was a consequence of pilot limitations, but in some cases the frequency sweep was terminated because of excessive aircraft structural response. In general, the highest frequency achieved was of the order of

5 or 6 Hz and the entire record would take about one minute to complete. Particularly at the lower frequencies there was a tendency for the aircraft to depart from a trimmed flight condition, and it was necessary for the pilot to maintain trim simultaneously with the swept frequency input. This piloting task was made more difficult by the need to avoid any inputs in the other control axes.

The long length of the frequency sweep counters required adjustments in the normal data recording and processing steps. During the test point the flight test engineer incremented the flight counter roughly every 20 seconds. Then, during ground processing, each of these counters was treated as an independent segment of the test point. Within the data base these segments are identified as “SEG 1,” “SEG 2,” and so forth. In processing the segments, approximately a tenth of a second of overlap was included in the data base. To analyse these data records using the frequency domain methods[20], it is necessary to concatenate the individual counters outside of the TRENDS data base.

Table 2.– Test matrix for IRAP flights.

AIRSPEED, KIASB	C_W/σ	RATES OF DESCENT, FT/MIN
65	0.070	0–900
65	0.086	200–900
68	0.070	200–1000
75	0.070	0–900
95	0.070	300–400

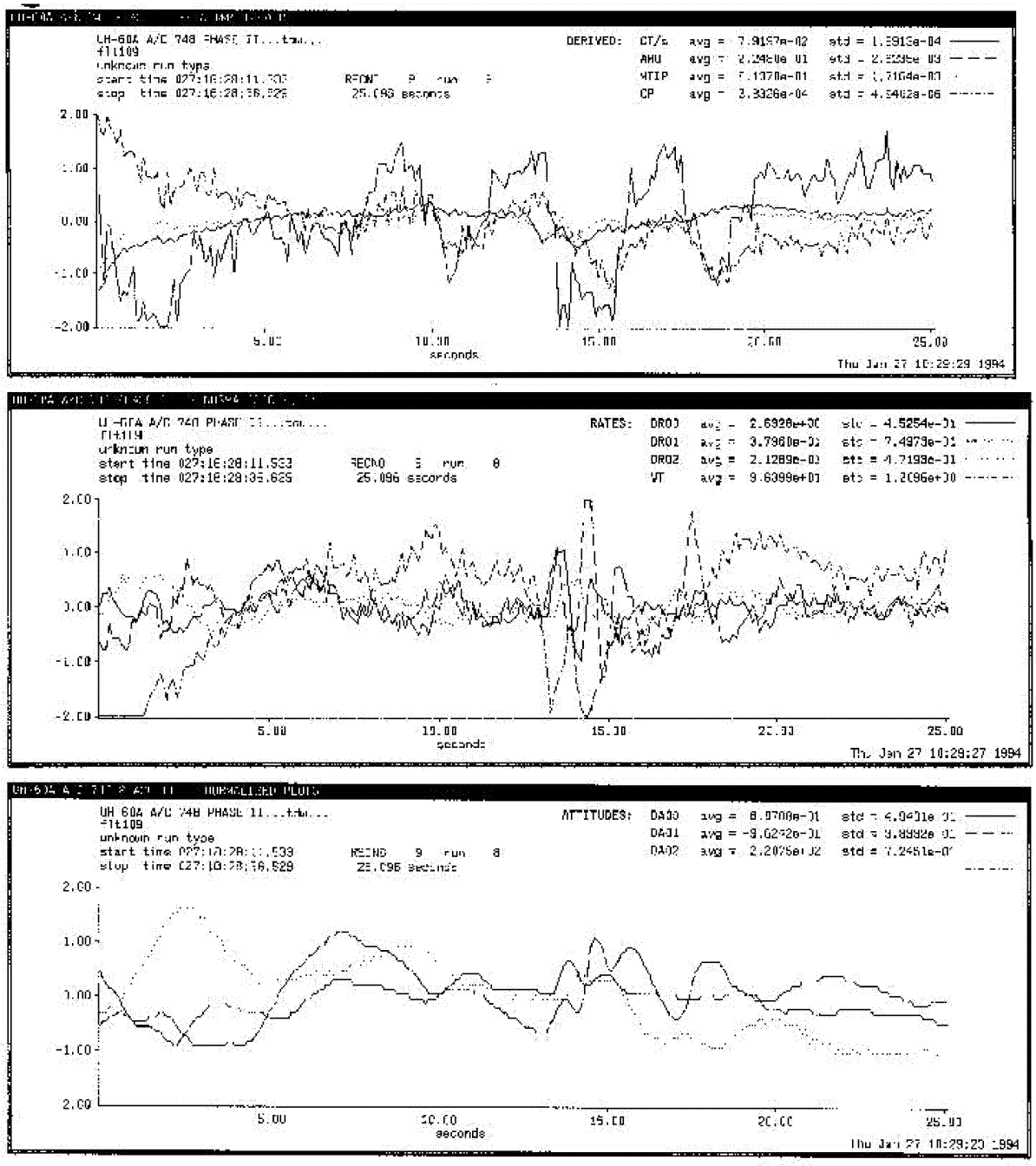

Figure 2.– Sample normalized plots from the Test Director's workstation, obtained during flight (flt 109 counter 9).

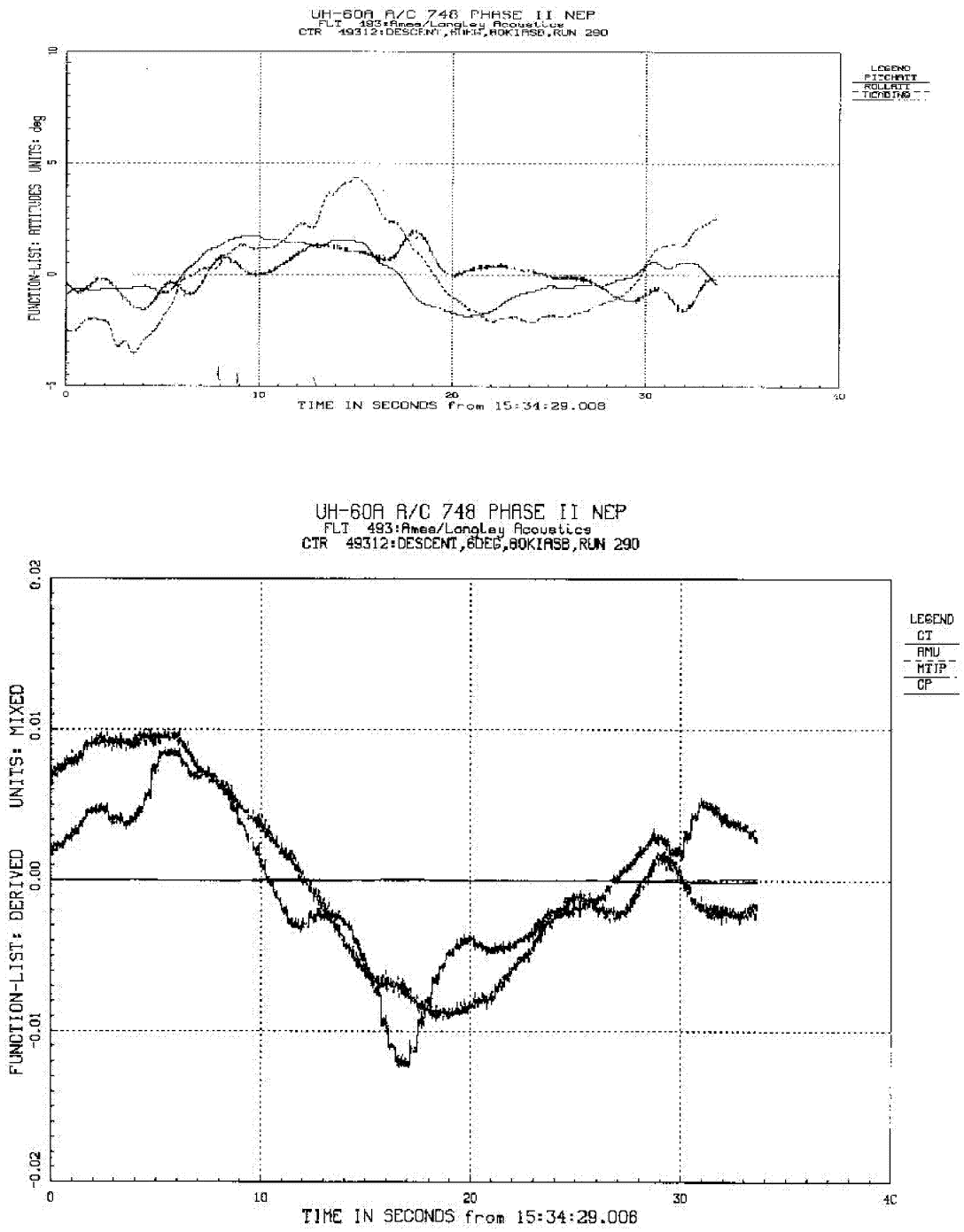

Figure 3.– Sample plots from NORMALIZE utility in TRENDS, obtained after initial ground-station processing to determine post-flight time slices (flt 94 counter 12).

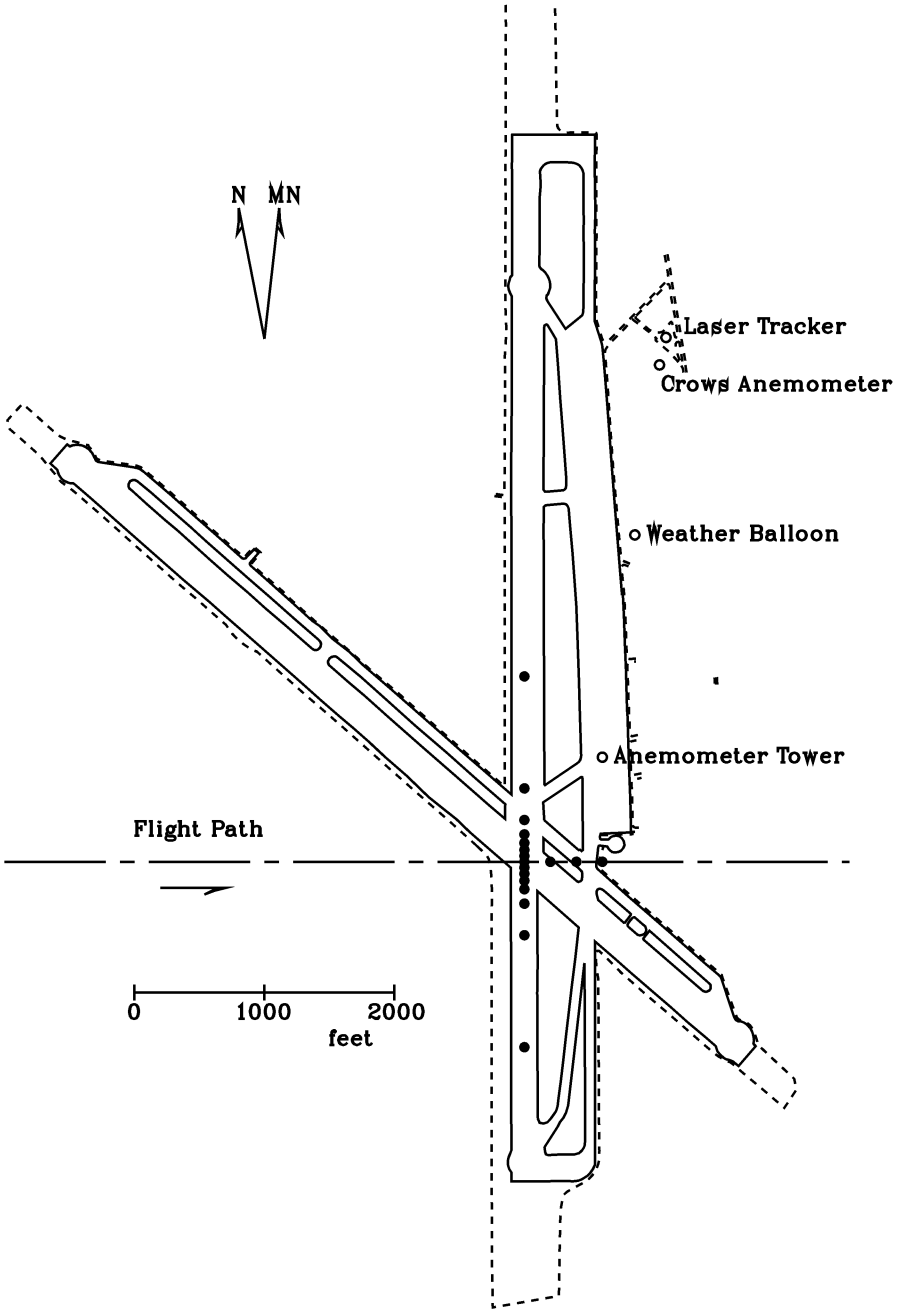

Figure 4.– Overview of Crows Landing Airfield as set up for ground-acoustic tests.

Figure 5.– UH–60A airloads aircraft in formation flight with YO–3A.

3. CALIBRATIONS

Two types of calibrations were used for instrumentation for the Airloads Project: linear and nonlinear. The vast majority of sensor calibrations used the classical approach where the measurement in engineering units is related to the measurement in PCM counts as:

$$P = mx + b \tag{1}$$

where P is the measured value in engineering units, m is the calibration slope, x is the measurement in counts, and b is the bias or offset. Nonlinear calibrations of the form

$$P = a_0 + a_1 + a_2 x^2 \tag{2}$$

where the a_i are the coefficients of a second-order polynomial, were used for the flight control displacements. Nonlinear calibrations were also used for airspeed and the blade root angles determined from the blade motion hardware (BMH).

Linear Calibrations

Each pressure transducer was calibrated in the laboratory prior to installation in the pressure blade to determine its response to pressure and temperature. These laboratory calibrations covered a range from 2 to 20 psia in pressure and 40 to 140 deg F in temperature. Frequency response tests were also performed on these transducers using an acoustic microphone so as to measure the frequency response within the range of the instrumentation filters. The pressure transducers were also calibrated as installed in the blade during the flight test program using a sealed bag that surrounded the blade. The bag was evacuated, to reduce pressure, but was not pressurized above atmospheric pressure. Hence, these bag cals ranged from 8 to about 15 psia. The temperature for the calibration was not controlled. The bag cals were performed irregularly during the flight program. The calibration slopes determined from each bag cal were used in the data reduction programs until replaced by the next bag cal.

Strain gauges on the strain-gauge blade were calibrated in the laboratory with the blade locked in a fixture. The blade was aligned so that the clevis was at zero deg pitch angle, which resulted in nonzero inclination of the principal axes at the outboard radial stations. The largest inclination was +8.6 deg at 0.20R. The flap and chord bending moments calibration slopes were not corrected for these inclinations.

The shaft bending and shaft torque strain gauges were calibrated by Sikorsky Aircraft using their standard calibration fixture.

Calibration slopes for those accelerometers that could be easily removed from the blades, hub, or fuselage were determined by turnover cals. However, there was no access to a number of accelerometers within the blade and these calibrations were obtained from blade turnover cals performed when the blade was in the laboratory.

The calibration slopes of various other parameters such as the actuator motions determined by Linear Variable Differential Transformers (LVDTs), string pots, tail rotor torque, tail rotor pitch, and so on were obtained in laboratory calibrations.

The offset, b, in Eq. (1) was obtained from pre- and post-flight static cals. Pre-flight static cals were obtained in the hanger prior to the flight, while post-flight static cals were normally obtained on the runway apron following the flight. In both cases, Blade 1 was positioned directly over the nose of the aircraft. The static cal counters used for the flight test program are identified in table 3.

In general, the static cals were used to determine the bias term based in Eq. (1)

$$b = P(0) - \frac{1}{2} m(x_1 - x_2) \tag{3}$$

where x_1 is the counts obtained from the pre-flight static cal, x_2 is the counts from the post-flight static cal, and $P(0)$ is an established offset value. For some sensors, $P(0)$ is simply zero. In many cases, however, $P(0)$ was assigned a known value at the time of the static cal. For example, the aircraft outside air temperature (OAT) measurement was set to values measured at the aircraft before and after the flight. Figure 6 shows the pre- and post-flight OATs that were obtained over the course of the flight program. This figure was made in TRENDS by first creating a Derived Counter Set (DCS) of all pre- and post-flight static cals. Then the temperatures (T100) were plotted as a function of the counter number using the MINMAX menu in TRENDS. The initial flights were from July (Flight 81) to September (Flight 90) and the ground OATs were close to 20 deg C during that period. The ground acoustic flights (Flights 91-99) were flown in November and a characteristic pattern is seen as a consequence of flying two flights a day. The pre-flight temperature is below 9 deg C for the pre-flight cal of the first flight, but it is generally over 20 deg C for the post-flight cal after the second flight. Flights 100 to 116 were flown in January and February and the colder temperatures for the static cals are evident.

For the strain gauges on the rotor blades, $P(0)$ was determined based on blade mass properties (refs. 21 and 22). The $P(0)$ values for the bending and torsion moments are given in table 4. The calculated static flap and chord bending moments at each station are caused by the mass of the blade outboard of the station. These moments are quite large at the most inboard stations. Static chord bending moment occurs because of the inclination of the blade's principal axes at each station. The torsion moment is caused by slight torsional mass offsets that occur along the blade and these corrections are quite small.

The $P(0)$ bias used for vertically-mounted accelerometers was 1.0.

Equation (3) was modified for the offset calculation for the blade pressure transducers in that only the pre-flight static cal was used to determine b. $P(0)$ in this case is the atmospheric pressure measured at the aircraft at the time of the pre-flight cal. Figure 7 shows the pressure recorded for the static cals for P701, the transducer at $0.92R$ and $0.01c$. These pressure measurements were calculated and plotted in TRENDS in the same manner as the outside air temperature discussed above. As expected these measurements tend to group around the nominal sea level pressure, 14.7 psia.

The calibration coefficients and offset values for all flights are stored in the TRENDS data base and can be accessed through the TRENDS menu item CALIBS.

Nonlinear Calibrations

Flight Controls– The cockpit control positions and flight control positions were calibrated by fitting a second order polynomial to data obtained over the entire motion range, and these calibrations were used for data reduction. The zero and first-order terms are contained in the CALIBS files in the TRENDS data base, but the second-order terms are not accessible. Periodically during the program these calibrations were checked, particularly for bias, and corrections were made.

Airspeed Calibrations– The Airloads aircraft used three airspeed systems during the test program. Two of the airspeed systems were pitot-static systems. One pitot-static system was installed on an instrumentation boom while the second was the ship's system. A low-speed measuring system, called HADS, for Helicopter Airspeed Data Sensor, was generally used below 20 knots. The boom and low-speed measuring systems were calibrated as part of the test program.

The two pitot-static systems measured the static pressure, P_s, and the dynamic pressure, q. These are related by

$$q = P_t - P_s \tag{4}$$

where P_t is the total or stagnation pressure. Errors can occur in either total pressure or static pressure because of the effects of the vehicle on the air stream and, at low speeds, by rotor downwash. These errors are influenced by changes in vehicle angle of attack or sideslip, whether caused by climb, descent, center of gravity location, or control inputs. For the calibration of the boom system it was assumed that an error occurred only in the measurement of the static pressure. This error, referred to as the position error, was calculated based on the indicated and calibrated airspeeds. The indicated airspeed was obtained from the compressible, isentropic Bernoulli's equation. The calibrated airspeed was obtained by fitting airspeed calibration data obtained on Flights 82 and 83.

Calibration data for Flight 82 were obtained using a ground pace vehicle. Paired north and south runs were used to correct for winds. Data were obtained from hover to 70 miles per hour in 5 mph increments. The counters for these low airspeed tests are shown in table 5. The pace car speed, item code VPAC, is stored in the TRENDS data base. Only data above about 30 or 40 knots were used

for calibration of the pressure measurements. The remaining data were used for calibration of the low-speed system as is discussed below.

Calibration data for Flight 83 were obtained by paced flying with a special purpose T–34 aircraft. At the time of the airspeed calibration the T–34 was based at the U.S. Army Aviation Engineering Flight Activity at Edward Air Force Base, and it flew to Moffett Field for the airspeed calibration. The counters for these airspeed calibration tests are shown in table 6. The aircraft was equipped with two independent airspeed systems. The calibration of the T–34 airspeed systems depends upon periodic flights with a trailing bomb. The trailing bomb, in turn, has been calibrated in the NASA Ames 7- by 10-Foot Wind Tunnel. On this flight, the UH–60A was flown from 80 knots indicated airspeed up to 160 knots in 10 knot increments and was paced at each flight speed by the T–34. For speeds above 135 knots the UH–60A was required to dive to obtain sufficient airspeed. However, above 160 knots the T–34 could not match both the airspeed and the dive angle of the UH–60A and this provided the upper limit for the airspeed calibration.

Using the indicated airspeed computed from the pitot-static system and the calibrated airspeed based on a fit of the data from Flights 82 and 83, a position error was determined for the boom system. This position error was then used to correct the static pressure (H001) and the dynamic pressure (V001). The true airspeed was then determined as a function of the corrected dynamic pressure, the static pressure, and the density.

For the ship’s system, a previous derivation of calibrated airspeed was used to compute the position error and the ship’s system true airspeed was then computed in the same manner as the boom system.

At low airspeed the boom and ship’s system become inaccurate because the pressure differential between total and static pressure becomes small and other effects, such as the rotor downwash, become more important. The HADS system does not rely on differential pressure for the determination of velocity. Instead, the HADS system places a total pressure probe within the rotor downwash that is mounted so it can act as a weather vane. As the aircraft moves forward, backward, or sideways the weather vane system measures the change of the downwash angle of the rotor induced flow. The measured downwash angles and total pressure are then related to the vehicle's velocity through calibration. The HADS supplied three separate measurements to the data base, downwash velocity (LSSZ), forward velocity (LSSX), and sideways velocity (LSSY).

Two approaches were used for calibration of the HADS system. In the first approach, on Flight 82, the aircraft was flown along the runway and ground speed was determined with a pace vehicle. The counters for this flight are in table 5. Repeat north and south runs were averaged to correct for wind effects. This calibration was largely in ground effect, although the rotor height above the ground varied with airspeed. The second calibration method, on Flights 96 and 98, was used during the ground-acoustic portion of the test program and is discussed in section 5. The counters for the second calibration are listed in table 7. Data were obtained from about –10 knots to +40 knots in 5 knot increments at a test altitude of 250 feet. The three components of measured velocity from the HADS system, LSSX, LSSY, and LSSZ, and the three components of velocity measured by the laser tracker, XLDOT, YLDOT, and ZLDOT, are stored in the TRENDS data base. A tethered weather balloon provided by Langley Research Center was used for estimates of wind speed and

direction at the test altitude, and these wind estimates were used to correct the inertial measurements to provide the true airspeed of the aircraft. The corrected inertial measurements for the calibration cases are shown in table 8 as three components of advance ratio. A second-order polynomial was used to relate the LSSX velocities to the corrected inertial measurements.

The data obtained during the second calibration are considered to be more accurate and have been used for the HADS calibration in the TRENDS data base. The calibrated LSSX values for the HADS system are compared with the corrected inertial velocities in figure 8. The LSSX values have been extracted from TRENDS using VIEW, while the corrected values are from table 8. Generally good agreement is observed between about zero airspeed and 20 knots which is the range used for the calibration. Above 30 knots the HADS system reads 5–10 knots low and is not trustworthy.

Figure 9 compares the HADS airspeed data (LSSX) and the calibrated airspeed (VTRU) obtained with the pace car calibration on Flight 82. The HADS airspeed data, the calibrated airspeed data, and the pace car speed have been extracted from TRENDS using VIEW and averaged for the appropriate north-south pairs of paced flight. The HADS data are nonlinear and are not suitable for calibration. Using the corrected velocities, based on the second calibration, the airspeed values are mostly correct, but show local nonlinearities. It is speculated that the presence of a ground vortex in the airspeed range from 10 to 25 knots is responsible for this behavior.

The high-speed and low-speed calibrations are combined in the parameter VTRU. Below 20 knots, VTRU is equivalent to the calibrated LSSX airspeed from the HADS system and above 20 knots is equivalent to the VTAS airspeed that is based on the boom system. Figure 10 shows an example of the overlap between the airspeed measurements for the airspeed sweep obtained on Flight 85. Below 20 knots the VTRU and LSSX are identical, while the boom speed shows erroneous results. Above 20 knots, VTRU and the boom speed, VTAS, exactly match while the HADS airspeed is in error.

Blade Root Angle Calibrations– The root motions of the UH–60A rotor blades were measured with a linkage mounted between the hub and the blade root and included three rotating hinges that used Rotary Variable Differential Transformers (RVDTs) to measure hinge rotation. This linkage was referred to as the Blade Motion Hardware (BMH) and is illustrated in figure 11 for one blade.

The blade root motions are related to the hinge point rotations as measured by the RVDTs by three nonlinear, kinematic equations. The equations for the blade root pitch angle, θ, the blade root flapping angle, β, and the blade root lead-lag angle, ζ, are:

$$\theta = (k_5 T^2 + k_6 T)\left(\frac{1 - k_7 \tan B}{\sqrt{\cos B}}\right) + k_{10}\left[Z - \frac{k_8 T}{(1+\sin B)^{k_9}}\right] \tag{5}$$

$$\beta = k_1 B^2 + k_2 B + k_3 + k_4\left(\frac{1-\cos T}{1+\sin B}\right) \tag{6}$$

$$\zeta = Z - \frac{k_8 T}{(1+\sin B)^{k_9}} \tag{7}$$

where T, B, and Z are the pitch, flap, and lead-lag RVDT rotation angles and k_1 through k_{10} are calibration constants. These equations are originally from reference 23, although some minor sign errors have been corrected. Although not apparent from these equations, the nonlinearities and coupling are fairly weak for the pitch and flap angles and it is possible to approximate these motions with a linear calibration. The lead-lag motion, however, is strongly coupled and depends upon all three of the RVDT measurements.

The ten BMH calibration constants for each blade were obtained by setting the blade to specific pitch, flap, and lead-lag angles and recording the RVDT outputs. A calibration angle matrix was established that covered the full range of angular deflections and also had sufficient points to properly identify the coupling terms in the equations. These calibrations required somewhat more than a day for each blade and were performed only once, at the start of the test program. Unlike conventional measurements where zero shifts are measured for each run, no equivalent procedure exists for the BMH measurements and there was a degradation in measurement accuracy over the course of the test program because of zero shifts in the RVDT measurements.

Both the uncalibrated RVDT voltages and the converted blade root motions are stored in the TRENDS data base. Table 9 lists the item codes for these parameters.

Table 3.– Static cals.

FLIGHT	COUNTER	DESCRIPTION	DURATION
FLT 82	CTR 8202	PREFLIGHT STATIC CAL	5.00 Seconds
FLT 82	CTR 8264	POSTFLIGHT STATIC CAL	4.99 Seconds
FLT 83	CTR 8303	PREFLIGHT STATIC CAL	5.00 Seconds
FLT 83	CTR 8341	POSTFLIGHT STATIC CAL	4.99 Seconds
FLT 84	CTR 8405	PREFLIGHT STATIC CAL	5.00 Seconds
FLT 84	CTR 8435	POSTFLIGHT STATIC CAL	4.99 Seconds
FLT 85	CTR 8503	PREFLIGHT STATIC CAL	5.00 Seconds
FLT 85	CTR 8540	POSTFLIGHT STATIC CAL	4.99 Seconds
FLT 88	CTR 8802	PREFLIGHT STATIC CAL	5.00 Seconds
FLT 88	CTR 8838	POSTFLIGHT STATIC CAL	4.99 Seconds
FLT 89	CTR 8902	PREFLIGHT STATIC CAL	5.99 Seconds
FLT 89	CTR 8935	POSTFLIGHT STATIC CAL	5.37 Seconds
FLT 90	CTR 9002	PREFLIGHT STATIC CAL	5.00 Seconds
FLT 90	CTR 9034	POSTFLIGHT STATIC CAL	4.99 Seconds
FLT 91	CTR 9102	PREFLIGHT STATIC CAL	6.00 Seconds
FLT 91	CTR 9126	POSTFLIGHT STATIC CAL	5.40 Seconds
FLT 92	CTR 9202	PREFLIGHT STATIC CAL	5.91 Seconds
FLT 92	CTR 9224	POSTFLIGHT STATIC CAL	5.99 Seconds
FLT 93	CTR 9302	PREFLIGHT STATIC CAL	5.00 Seconds
FLT 93	CTR 9329	POSTFLIGHT STATIC CAL	1.81 Seconds
FLT 94	CTR 9402	PREFLIGHT STATIC CAL	5.00 Seconds
FLT 94	CTR 9430	POSTFLIGHT STATIC CAL	4.99 Seconds
FLT 95	CTR 9502	PREFLIGHT STATIC CAL	5.00 Seconds
FLT 95	CTR 9531	POSTFLIGHT STATIC CAL	4.99 Seconds
FLT 96	CTR 9602	PREFLIGHT STATIC CAL	2.00 Seconds
FLT 96	CTR 9646	POSTFLIGHT STATIC CAL	1.99 Seconds
FLT 97	CTR 9702	PREFLIGHT STATIC CAL	5.00 Seconds
FLT 97	CTR 9731	POSTFLIGHT STATIC CAL	1.99 Seconds
FLT 98	CTR 9802	PREFLIGHT STATIC CAL	5.00 Seconds
FLT 98	CTR 9844	POSTFLIGHT STATIC CAL	5.00 Seconds
FLT 99	CTR 9902	PREFLIGHT STATIC CAL	4.78 Seconds
FLT 99	CTR 9929	POSTFLIGHT STATIC CAL	1.99 Seconds
FLT 100	CTR 10002	PREFLIGHT STATIC CAL	3.00 Seconds
FLT 100	CTR 10017	POSTFLIGHT STATIC CAL	2.00 Seconds
FLT 101	CTR 10103	PREFLIGHT STATIC CAL	2.00 Seconds
FLT 101	CTR 10119	POSTFLIGHT STATIC CAL	1.99 Seconds
FLT 102	CTR 10202	PREFLIGHT STATIC CAL	2.00 Seconds
FLT 102	CTR 10223	POSTFLIGHT STATIC CAL	2.00 Seconds
FLT 103	CTR 10302	PREFLIGHT STATIC CAL	2.00 Seconds
FLT 103	CTR 10314	POSTFLIGHT STATIC CAL	1.99 Seconds
FLT 105	CTR 10502	PREFLIGHT STATIC CAL	5.99 Seconds
FLT 106	CTR 10602	PREFLIGHT STATIC CAL	2.00 Seconds
FLT 106	CTR 10611	POSTFLIGHT STATIC CAL	1.99 Seconds

Table 3.– Concluded.

FLIGHT	COUNTER	DESCRIPTION	DURATION
FLT 107	CTR 10704	PREFLIGHT STATIC CAL	1.99 Seconds
FLT 107	CTR 10739	POSTFLIGHT STATIC CAL	1.99 Seconds
FLT 108	CTR 10803	PREFLIGHT STATIC CAL	2.00 Seconds
FLT 108	CTR 10840	POSTFLIGHT STATIC CAL	1.99 Seconds
FLT 110	CTR 11002	PREFLIGHT STATIC CAL	1.20 Seconds
FLT 110	CTR 11035	POSTLFIGHT STATIC CAL	1.99 Seconds
FLT 111	CTR 11102	PREFLIGHT STATIC CAL	2.00 Seconds
FLT 111	CTR 11144	POSTFLIGHT STATIC CAL	1.99 Seconds
FLT 112	CTR 11246	POSTFLIGHT STATIC CAL	1.99 Seconds
FLT 113	CTR 11302	PREFLIGHT STATIC CAL	2.00 Seconds
FLT 113	CTR 11332	POSTFLIGHT STATIC CAL	2.00 Seconds
FLT 114	CTR 11402	PREFLIGHT STATIC CAL	2.00 Seconds
FLT 114	CTR 11427	POSTFLIGHT STATIC CAL	1.99 Seconds
FLT 115	CTR 11502	PREFLIGHT STATIC CAL	2.00 Seconds
FLT 115	CTR 11545	POSTFLIGHT STATIC CAL	1.99 Seconds
FLT 116	CTR 11647	PREFLIGHT STATIC CAL	2.00 Seconds
FLT 116	CTR 11690	POSTFLIGHT STATIC CAL	2.00 Seconds

Table 4.– Strain-gauge blade static offsets used for pre- and post-flight static calibration offset.

r/R	FLAP BENDING MOMENT, IN-LB	CHORD BENDING MOMENT, IN-LB	TORSION MOMENT, IN-LB
0.113	–27422	3000	—
0.200	–22056	3534	—
0.300	–17048	2264	53
0.400	–12715	1323	—
0.500	–9008	674	22
0.600	–5792	265	—
0.700	–2826	61	–1
0.800	–1298	22	—
0.900	–203	—	18

Table 5.– Low-airspeed calibration data obtained on Flight 82 using a ground pace vehicle.

FLIGHT	COUNTER	DESCRIPTION	DURATION
FLT 82	CTR 8213	HOVER IGE, NR=100%, NORTH	4.99 Seconds
FLT 82	CTR 8214	FWD FLT, 5 MPH, NORTH	4.99 Seconds
FLT 82	CTR 8215	FWD FLT, 10 MPH, NORTH	4.99 Seconds
FLT 82	CTR 8216	FWD FLT, 15 MPH, NORTH	4.99 Seconds
FLT 82	CTR 8217	HOVER IGE, NR=100%, SOUTH	3.97 Seconds
FLT 82	CTR 8218	FWD FLT, 5 MPH, SOUTH	4.99 Seconds
FLT 82	CTR 8219	FWD FLT, 10 MPH, SOUTH	4.99 Seconds
FLT 82	CTR 8220	FWD FLT, 15 MPH, SOUTH	4.99 Seconds
FLT 82	CTR 8221	RT SIDE FLT, 5 MPH, NORTH	4.99 Seconds
FLT 82	CTR 8222	RT SIDE FLT, 10 MPH, NORTH	4.99 Seconds
FLT 82	CTR 8223	RT SIDE FLT, 15 MPH, NORTH	4.99 Seconds
FLT 82	CTR 8224	RT SIDE FLT, 5 MPH, SOUTH	4.99 Seconds
FLT 82	CTR 8225	RT SIDE FLT, 10 MPH, SOUTH	4.99 Seconds
FLT 82	CTR 8226	RT SIDE FLT, 15 MPH, SOUTH	4.99 Seconds
FLT 82	CTR 8227	LT SIDE FLT, 5 MPH, NORTH	4.99 Seconds
FLT 82	CTR 8228	LT SIDE FLT, 10 MPH, NORTH	4.99 Seconds
FLT 82	CTR 8229	LT SIDE FLT, 15 MPH, NORTH	4.99 Seconds
FLT 82	CTR 8230	LT SIDE FLT, 5 MPH, SOUTH	4.99 Seconds
FLT 82	CTR 8231	LT SIDE FLT, 10 MPH, SOUTH	4.99 Seconds
FLT 82	CTR 8232	LT SIDE FLT, 15 MPH, SOUTH	4.99 Seconds
FLT 82	CTR 8233	REAR FLT, 5 MPH, NORTH	4.99 Seconds
FLT 82	CTR 8234	REAR FLT, 10 MPH, NORTH	4.99 Seconds
FLT 82	CTR 8235	REAR FLT, 15 MPH, NORTH	4.99 Seconds
FLT 82	CTR 8236	REAR FLT, 5 MPH, SOUTH	4.99 Seconds
FLT 82	CTR 8237	REAR FLT, 10 MPH, SOUTH	4.99 Seconds
FLT 82	CTR 8238	REAR FLT, 15 MPH, SOUTH	4.99 Seconds
FLT 82	CTR 8239	FWD FLT, 20 MPH, NORTH	4.99 Seconds
FLT 82	CTR 8240	FWD FLT, 25 MPH, NORTH	4.99 Seconds
FLT 82	CTR 8241	FWD FLT, 20 MPH, SOUTH	4.99 Seconds
FLT 82	CTR 8242	FWD FLT, 25 MPH, SOUTH	4.99 Seconds
FLT 82	CTR 8243	FWD FLT, 30 MPH, NORTH	4.99 Seconds
FLT 82	CTR 8244	FWD FLT, 35 MPH, NORTH	4.99 Seconds
FLT 82	CTR 8245	FWD FLT, 30 MPH, SOUTH	4.99 Seconds
FLT 82	CTR 8246	FWD FLT, 35 MPH, SOUTH	2.99 Seconds
FLT 82	CTR 8247	FWD FLT, 40 MPH, NORTH	3.99 Seconds
FLT 82	CTR 8248	FWD FLT, 40 MPH, SOUTH	4.99 Seconds
FLT 82	CTR 8249	FWD FLT, 45 MPH, NORTH	4.99 Seconds
FLT 82	CTR 8250	FWD FLT, 45 MPH, SOUTH	4.99 Seconds
FLT 82	CTR 8251	FWD FLT, 50 MPH, NORTH	4.99 Seconds
FLT 82	CTR 8252	FWD FLT, 50 MPH, SOUTH	4.99 Seconds
FLT 82	CTR 8253	FWD FLT, 55 MPH, NORTH	4.52 Seconds
FLT 82	CTR 8254	FWD FLT, 55 MPH, SOUTH	4.99 Seconds
FLT 82	CTR 8255	FWD FLT, 60 MPH, NORTH	4.99 Seconds

Table 5.– Concluded.

FLIGHT	COUNTER	DESCRIPTION	DURATION
FLT 82	CTR 8256	FWD FLT, 60 MPH, SOUTH	4.99 Seconds
FLT 82	CTR 8257	FWD FLT, 65 MPH, NORTH	4.99 Seconds
FLT 82	CTR 8258	FWD FLT, 65 MPH, SOUTH	4.99 Seconds
FLT 82	CTR 8259	FWD FLT, 70 MPH, NORTH	4.99 Seconds
FLT 82	CTR 8260	FWD FLT, 70 MPH, SOUTH	4.99 Seconds
FLT 82	CTR 8261	HOVER IGE, NR=100%, NORTH	4.99 Seconds
FLT 82	CTR 8262	HOVER IGE, NR=100%, SOUTH	4.99 Seconds

Table 6.– Airspeed calibration data obtained on Flight 83 using a T–34 aircraft.

FLIGHT	COUNTER	DESCRIPTION	DURATION
FLT 83	CTR 8319	LEVEL FLT, 80 KIASB, 4000'HP	4.99 Seconds
FLT 83	CTR 8321	LEVEL FLT, 90 KIASB, 4000'HP	4.99 Seconds
FLT 83	CTR 8322	LEVEL FLT, 100 KIASB, 4000'HP	5.00 Seconds
FLT 83	CTR 8323	LEVEL FLT, 110 KIASB, 4000'HP	4.99 Seconds
FLT 83	CTR 8326	LEVEL FLT, 120 KIASB, 5000'HP	4.99 Seconds
FLT 83	CTR 8327	LEVEL FLT, 130 KIASB, 5000'HP	4.99 Seconds
FLT 83	CTR 8328	LEVEL FLT, VH(136KIB), 5000'HP	4.99 Seconds
FLT 83	CTR 8329	DESCENT, 150 KIASB, 5000'HP	4.99 Seconds
FLT 83	CTR 8330	DESCENT, 160 KIASB, 5000'HP	4.99 Seconds
FLT 83	CTR 8331	LEVEL FLT, 133 KIASB, 5000'HP	4.99 Seconds
FLT 83	CTR 8332	LEVEL FLT, 125 KIASB, 5000'HP	4.99 Seconds
FLT 83	CTR 8333	LEVEL FLT, 115 KIASB, 5000'HP	4.99 Seconds
FLT 83	CTR 8334	LEVEL FLT, 105 KIASB, 5000'HP	4.99 Seconds
FLT 83	CTR 8336	LEVEL FLT, 95 KIASB, 5000'HP	4.99 Seconds
FLT 83	CTR 8337	LEVEL FLT, 85 KIASB, 5000'HP	4.99 Seconds

Table 7.– Low-airspeed calibration using laser tracker.

FLIGHT	COUNTER	DESCRIPTION	DURATION
FLT 96	CTR 9605	LOW AIRSPEED CAL, HOVER	4.99 Seconds
FLT 96	CTR 9606	LOW AIRSPEED CAL, 5 KIASH	4.99 Seconds
FLT 96	CTR 9607	LOW AIRSPEED CAL, 10 KIASH	4.99 Seconds
FLT 96	CTR 9608	LOW AIRSPEED CAL, 15 KIASH	4.99 Seconds
FLT 96	CTR 9609	LOW AIRSPEED CAL, 21 KIASH	4.99 Seconds
FLT 96	CTR 9610	LOW AIRSPEED CAL, 26 KIASH	4.99 Seconds
FLT 96	CTR 9611	LOW AIRSPEED CAL, MARGINAL	4.99 Seconds
FLT 96	CTR 9612	LOW AIRSPEED CAL, 30 KIASH	4.99 Seconds
FLT 96	CTR 9613	LOW AIRSPEED CAL, 35 KIASH	4.99 Seconds
FLT 96	CTR 9614	LOW AIRSPEED CAL, 42 KIASH	4.99 Seconds
FLT 98	CTR 9805	FWD AIRSPEED CAL, 10 KIASH	4.99 Seconds
FLT 98	CTR 9806	FWD AIRSPEED CAL, 8 KIASH	4.99 Seconds
FLT 98	CTR 9807	FWD AIRSPEED CAL, 1 KIASH	4.03 Seconds
FLT 98	CTR 9808	AFT AIRSPEED CAL, 5 KIASH	4.99 Seconds
FLT 98	CTR 9809	AFT AIRSPEED CAL, 10 KIASH	4.99 Seconds

Table 8.– Corrected inertial measurements for low-airspeed calibration.

COUNTER	DESCRIPTION	μ_x	μ_y	μ_z
CTR 9605	LOW AIRSPEED CAL, HOVER	0.001	0.000	0.002
CTR 9606	LOW AIRSPEED CAL, 5 KIASH	0.016	0.003	0.006
CTR 9607	LOW AIRSPEED CAL, 10 KIASH	0.027	–0.004	0.000
CTR 9608	LOW AIRSPEED CAL, 15 KIASH	0.040	0.005	0.004
CTR 9609	LOW AIRSPEED CAL, 21 KIASH	0.050	–0.001	0.002
CTR 9610	LOW AIRSPEED CAL, 26 KIASH	0.077	–0.001	–0.001
CTR 9611	LOW AIRSPEED CAL, MARGINAL	0.091	–0.006	–0.002
CTR 9612	LOW AIRSPEED CAL, 30 KIASH	0.087	–0.008	–0.002
CTR 9613	LOW AIRSPEED CAL, 35 KIASH	0.101	0.001	0.003
CTR 9614	LOW AIRSPEED CAL, 42 KIASH	0.118	0.001	–0.005
CTR 9805	FWD AIRSPEED CAL, 10 KIASH	0.020	0.008	–0.002
CTR 9806	FWD AIRSPEED CAL, 8 KIASH	0.016	0.010	–0.002
CTR 9807	FWD AIRSPEED CAL, 1 KIASH	0.001	0.010	0.002
CTR 9808	AFT AIRSPEED CAL, 5 KIASH	–0.010	0.015	–0.001
CTR 9809	AFT AIRSPEED CAL, 10 KIASH	–0.027	0.015	–0.002

Table 9.– BMH and RVDT item codes.

BLADE	PITCH		FLAP		LEAD-LAG	
	RVDT	BMH	RVDT	BMH	RVDT	BMH
1	BH12	PTC1	BH11	FLP1	BH10	LAG1
2	BH22	PTC2	BH21	FLP2	BH20	LAG2
3	BH32	PTC3	BH31	FLP3	BH30	LAG3
4	BH42	PTC4	BH41	FLP4	BH40	LAG4

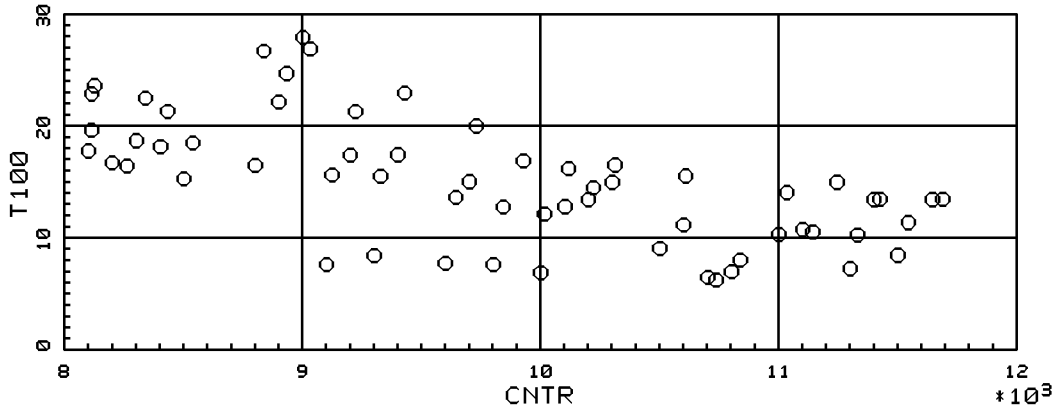

Figure 6.– OAT, deg C, for pre- and post-flight static cals (T100 is OAT mnemonic).

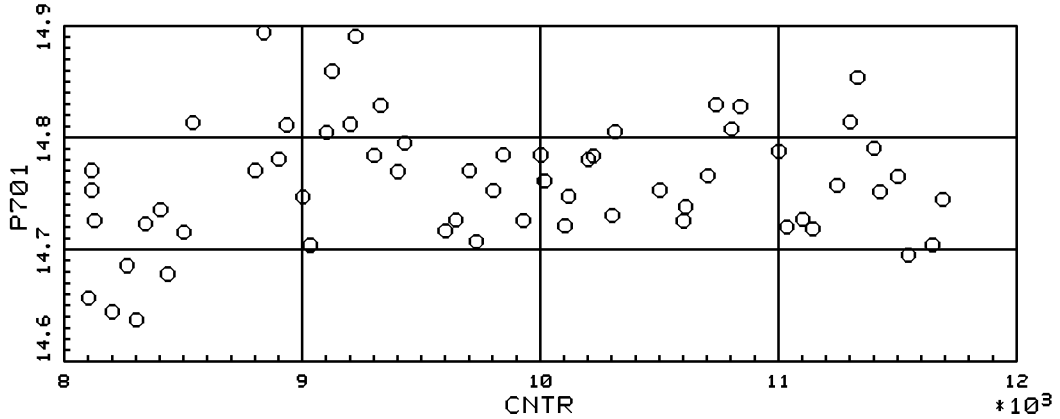

Figure 7.– Static pressure offset for pressure transducer P701 for pre- and post-flight static cals.

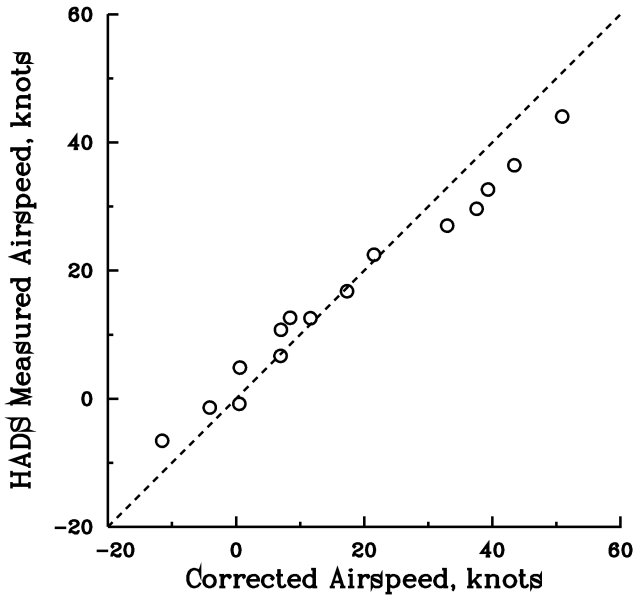

Figure 8.– Comparison of HADS x-velocity with corrected inertial velocity from second HADS calibration.

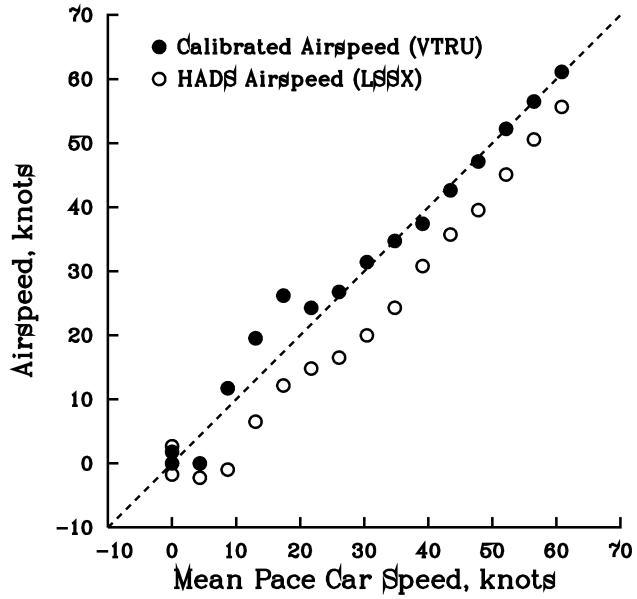

Figure 9.– Comparison of calibrated airspeed (VTRU) and HADS x-velocity (LSSX) during pace car speed sweep.

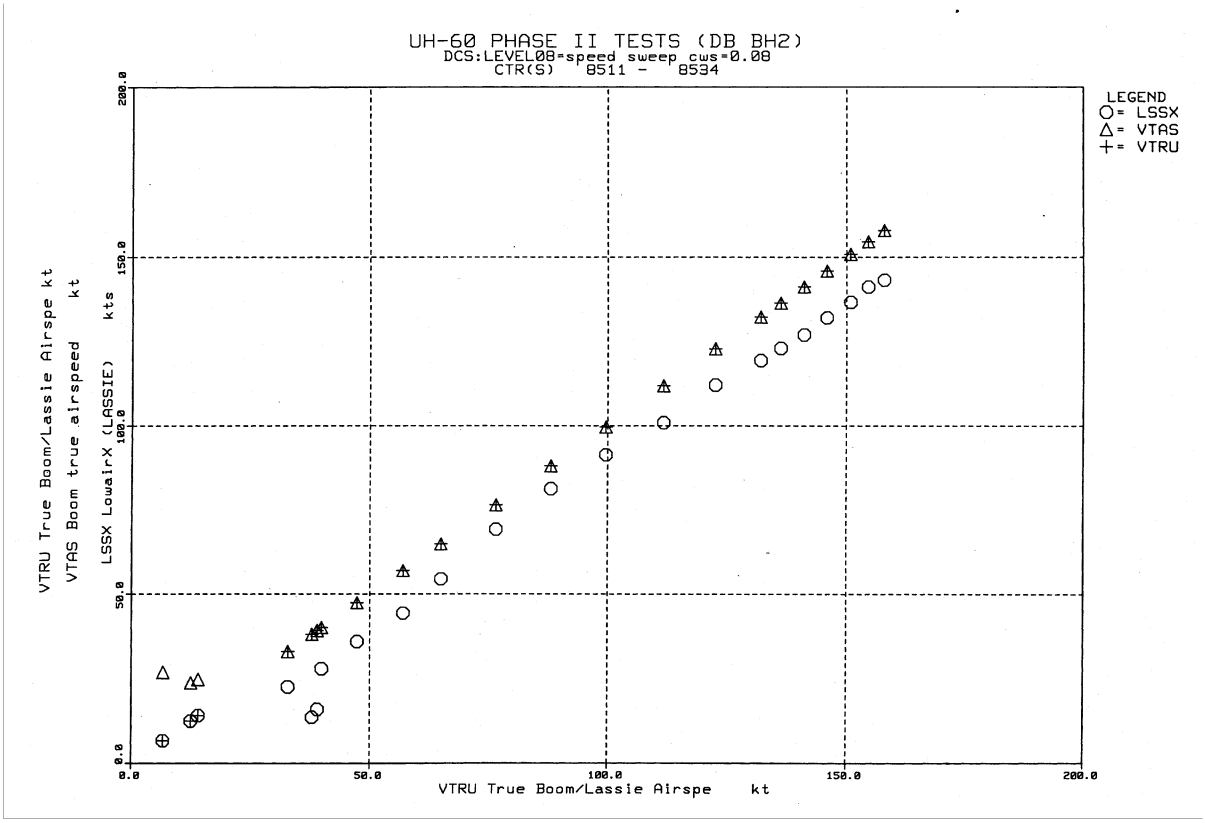

Figure 10.– Comparison of airspeed measurements for Flight 85.

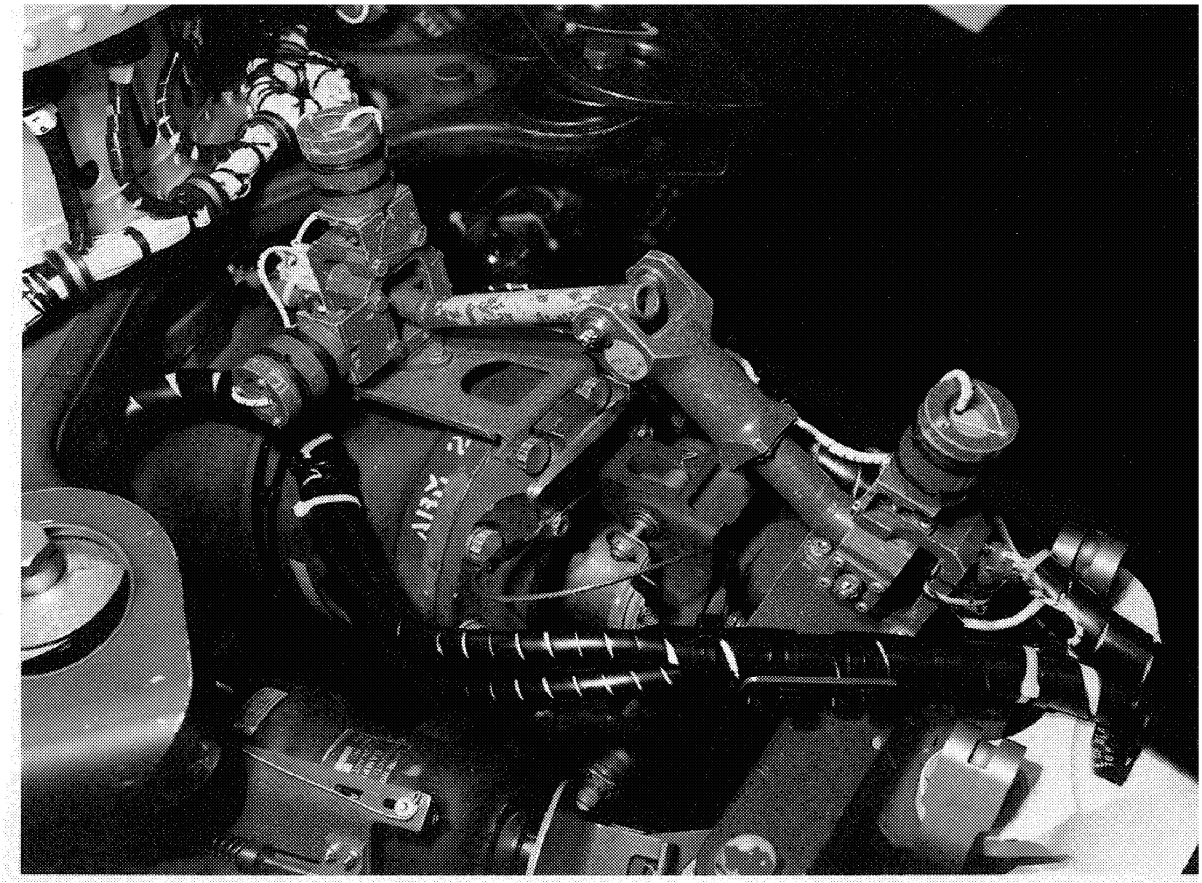

Figure 11.– Blade Motion Hardware (BMH) installation.

4. REFERENCE AND CHECKOUT CONDITIONS

Housekeeping Points

For most flights, two reference or housekeeping counters were obtained at the start of the flight and, if there was sufficient recording tape, at the end of the flight. The first of these housekeeping points was an out-of-ground effect hover that was obtained adjacent to the taxiway at Moffett Field immediately after liftoff. The rotor height for this initial point was approximately 80 feet. Following the OGE hover housekeeping point, the aircraft accelerated to forward flight and the second housekeeping point was obtained at 80 knots indicated airspeed (KIAS) once the aircraft reached 1000 feet pressure altitude. Returning housekeeping points were scheduled for most test flights but were often skipped because of a shortage of tape for the flight recorders. Although the housekeeping points were repeated for the same airspeeds and pressure altitudes for each flight, there was no attempt to control for aircraft weight or outside air temperature.

The hover housekeeping points for the program are listed in table 10. No hover housekeeping points were obtained during the ground acoustic tests when the aircraft was stationed in Modesto, California. Table 11 lists the 80-knot housekeeping counters.

Figure 12 shows the variation in C_P and C_W for the OGE hover housekeeping points from table 10. A range of weight coefficients is observed in this figure, in part because different portions of the flight program required different gross weights, but also because about a third of the flights included a returning housekeeping point where the aircraft was approximately 2,000 pounds lighter because of fuel burn-off. For comparison, curve fits to the test data obtained by the U.S. Army Aviation Engineering Flight Activity (AEFA) at Edwards on the First- through 12th-Year production aircraft (refs. 24–28) are also shown in this figure. The points were obtained for tethered hover conditions and include substantially higher weight coefficients than were flown in the Airloads Program. For both test programs the power was determined from measurements of the engine output shaft torque.

The test points from references 24–28 were obtained in winds of less than three knots to assure reliable performance data and the data repeatability is quite good. The OGE hover housekeeping points for the Airloads Program were recorded regardless of wind condition, as the purpose of these test points was to obtain reference data to cover the test program span and not to obtain performance data. It seems likely that some of the scatter in the Airloads data are a consequence of winds.

An Extended Stores Support System (ESSS) was added on the Sixth-Year production aircraft and the fairings for this system increase the power required in hover (ref. 26). Except for the original contract guarantee tests (ref. 24), the AEFA fits of the OGE hover data separate into two categories, that is, aircraft configurations with or without the ESSS fairings. The Airloads aircraft included the ESSS fairings and the hover data show general agreement with AEFA test results for aircraft with the ESSS fairings installed. The one set of tests that is anomalous, however, is the set obtained from the original contract guarantee tests (ref. 24). These data were obtained on a First-Year production aircraft without ESSS fairings, yet the data match the Sixth- and 12th-Year aircraft performance

rather than the First-Year performance data obtained from references 25 and 26. The reasons for this are unclear, although it is noted that the contract guarantee tests for OGE hover were performed with a highly-instrumented inlet cowling that did not fit the test aircraft adequately and left gaps between the cowling and the fuselage (ref. 24).

The purpose of the OGE hover housekeeping points was to assist in the detection of inoperative or inaccurate transducers by comparing recorded signals from one flight to another. However, this approach was ineffective as the blade pressures show large flight-to-flight variation for these OGE hover housekeeping points. As an example, figure 13 shows the upper surface pressure at 0.049c and 0.92R for all of the hover housekeeping points. Each azimuthal trace on this plot represents one housekeeping point. The data for these hover points show substantial variation from flight to flight and this is largely a result of small changes in wind velocity for these test conditions and the consequent effect on tip vortex loading of the blades. Thus, the hover housekeeping points have limited value for the detection of problems with the blade pressure transducers.

The 80-knot housekeeping points that were recorded on both the outboard and inboard legs of the test flights are considerably more useful for the qualitative assessment of the pressure transducers. Figure 14 compares all of the 80-knot housekeeping points for the same pressure transducer shown in figure 13. Although there is some variation from flight to flight, on a qualitative basis these data are quite repeatable and, therefore, these data are valuable for detecting problems with the pressure measurements.

On-ground Rotor Speed Variation

A limited number of ground test points were obtained to examine the effects of rotor speed variation on blade modal frequencies and these test points are listed in table 12. From an experimental point of view it would be have been desirable to have obtained on-ground test points over a range of rotors speeds. However, the engine controls do not allow stopping at rotor speeds between the flight idle condition at 60% N_R, and the nominal operating range from 96% to 104% N_R. Therefore, constant rotor test points were obtained only for 60%, 96%, and 104% N_R. In addition, transient records were made for two accelerations from flight idle to 100% N_R and a deceleration from 100% N_R to flight idle.

On-ground Rotor Moments

A series of test points were obtained on the ground with zero thrust on the rotor where the pilot was asked to make pure 1-inch stick inputs in each of four directions. The purpose of the test points was to make a number of instrumentation checks for a relatively straightforward, non-flight condition. These data can be used to assess that phase relations between the rotating system and the fixed system, to compare shaft bending with rotor blade motions, as well as other checks. The counters for these conditions are shown in table 13.

The first harmonic of the rotor hub moment in the rotating system, when resolved into the fixed system, provides the steady value of the aircraft pitch and roll moments. The rotating-system hub

moment may be approximated using either the blade flapping measurements or the main rotor shaft bending moment. The flapping measurements are essentially in the plane of the rotor disk, while the shaft bending moment is measured approximately 10 inches below the hub or disk center. The on-ground moment test points in table 12, therefore, are useful, first, in comparing the rotating- and fixed-system moments and, second, in comparing the two independent estimates of hub moment.

Before examining the rotating- and fixed-system hub moments, it is important to understand the hub reference systems used with the UH–60A data. Figure 15 provides a layout of the UH–60A hub as seen from above. The Hub Reference system is the datum used by Sikorsky Aircraft for the layout drawings of the hub and is also the reference system used in some of the comprehensive analysis models (refs. 29 and 30). The focal points of the elastomeric bearings on the UH–60A rotor are offset from the Hub Reference as shown in the figure. This torque offset is such that if the rotor were spun up in a vacuum the blades would line up with a reference about 7 deg forward of the Hub Reference. Hovering in air, the effect of the aerodynamic drag is such that the blades lag back about 7 deg so that they are roughly in line with the hub reference system.

The phase reference for the rotating data stored in TRENDS was determined by leveling the aircraft and orienting blade 1 towards the tail of the aircraft. A small theodolite was installed on the top of the RDAS “bucket” so that it was located exactly on the hub center. Two target points were established on blade 1, one inboard and one outboard. Both target points were aligned with the blade’s quarter chord location. Using the theodolite, the target points on blade 1 were aligned with each other and the formation light at the top of the vertical stabilizer. The reading of the azimuth encoder was recorded and used as an offset correction in the TRENDS data reduction. The alignment of blade 1, as described here, is exactly equivalent to a reference system that passes through the elastomeric bearing focal points and, hence, is defined as the TRENDS reference.

The first harmonic of the rotating-system hub moment is estimated using the flap angle measurements from the Blade Motion Hardware and a calculated value for the blade centrifugal force at the focal point.

$$M_f = 2F_c\, e \sin\beta \tag{1}$$

where M_f is the first harmonic hub moment, F_c is the centrifugal force at the focal point of the bearing, e is the offset of the focal point, and β is the first harmonic of the flap angle. The centrifugal force was calculated using CAMRAD/JA (ref. 29) and is 70,756 lbs. The hinge offset, as shown in figure 15, is 14.99 in.

The rotating-system hub moment is also estimated from the shaft bending moment (RQ12) assuming that the hub shears can be neglected for first harmonic motions. The longitudinal and lateral stick displacements and the resulting hub moments for the table 12 counters are shown in figure 16. With the stick centered there is a steady moment on the main rotor shaft as indicated by the center point. The remaining four counters show the 1 inch displacements in each axis. It is noted that the cyclic stick displacements are not as the pilot would see them from his seat. A forward motion of the cyclic stick (Counter 8312) causes a negative pitch moment, while an aft motion (Counter 8313) causes a positive pitch moment.

The pilot attempted to put in pure longitudinal and lateral inputs for the on-ground test points in figure 16. While the lateral displacements show no associated longitudinal displacements, there is a slight lateral displacement associated with the longitudinal stick inputs. The resulting aircraft moments are not purely in pitch and roll for the longitudinal and lateral displacements. In both cases there is a clockwise phase shift between eight and nine degrees.

All four of the flap angle measurements were functioning on Flight 83, and figure 16 shows that there is generally good agreement between the hub moment determined from the flap angles and from shaft bending. For these tests the difference ranges from –3.0% to +5.3%, while the rms error for all blades is 3.2%. For on-ground conditions, then, it appears that the influence of first harmonic hub shears can be ignored.

Ballast Cart Full Displacement Test

A ballast cart was installed in the Airloads Program UH–60A to control the c.g. location during the test program. As each test flight progressed, the Flight Test Engineer would record the fuel burnoff and adjust the ballast cart location accordingly. However, the available range of ballast cart displacement provided an opportunity to measure the aircraft response to an applied pitch moment in hover. Test counters were obtained on Flight 115 in an out-of-ground effect hover for three positions of the ballast cart as shown in table 14. Although these data were obtained sequentially, the slow travel rate of the ballast cart required about 12 minutes between test points. During these 12 minutes, the aircraft landed while waiting for the ballast cart to reach its next position.

The cyclic stick longitudinal and lateral displacements and the aircraft moments for the ballast cart full displacement test are shown in figure 17 in the same manner as was done for the on-ground moment tests, see figure 16. However, only one flap angle measurement was operational for Flight 115. Although the displacement of the ballast cart applies a pure pitch moment to the aircraft, the measured hub moment shows a small roll moment as well. For these tests there was a clockwise phase shift of about 18 deg and the cause of this shift is unknown. As during the on-ground moment tests, good agreement is observed between the steady hub moment from shaft bending and the one working flap angle measurement. The difference in this case is 3.6%.

Ground-Contact Collective Sweep

A series of test points were obtained for the aircraft on the ground where the collective pitch was varied from near a flat pitch condition (5% UP) to where the aircraft became light on its wheels (40% UP). The objective of the tests was to keep the cyclic stick and pedals centered as the collective was changed in 5% increments. A full range of collective sweep data was obtained on Flight 113, but it was determined that there was too much longitudinal stick and pedal displacements for the 30%, 35%, and 40% collective cases. Hence, these three cases were repeated on Flight 114. These counters are shown in table 15.

Table 10.– OGE hover housekeeping points.

FLIGHT	COUNTER	DESCRIPTION	DURATION
FLT 83	CTR 8316	HOVER OGE, 70 FT, 100% NR	4.99 Seconds
FLT 83	CTR 8340	HOVER OGE, 70 FT, 100% NR	4.99 Seconds
FLT 84	CTR 8434	HOVER OGE, 70 FT, 100% NR	4.99 Seconds
FLT 85	CTR 8509	HOVER OGE, 70 FT, 100% NR	4.99 Seconds
FLT 88	CTR 8804	HOVER OGE, 70 FT, 100% NR	3.42 Seconds
FLT 88	CTR 8837	HOVER OGE, 70 FT, 100% NR	4.25 Seconds
FLT 89	CTR 8904	HOVER OGE, 70 FT, 100% NR	5.99 Seconds
FLT 89	CTR 8934	HOVER OGE, 70 FT, 100% NR	4.36 Seconds
FLT 90	CTR 9004	HOVER OGE, 70 FT, 100% NR	4.99 Seconds
FLT 100	CTR 10004	HOVER OGE, 70 FT, 100% NR	4.99 Seconds
FLT 100	CTR 10016	HOVER OGE, 70 FT, 100% NR	4.99 Seconds
FLT 101	CTR 10118	HOVER OGE, 70 FT, 100% NR	4.99 Seconds
FLT 102	CTR 10204	HOVER OGE, 70 FT, 100% NR	4.99 Seconds
FLT 102	CTR 10221	HOVER OGE, 70 FT, 100% NR	4.99 Seconds
FLT 103	CTR 10313	HOVER OGE, 70 FT, 100% NR	4.99 Seconds
FLT 105	CTR 10504	HOVER OGE, 70 FT, 100% NR	5.51 Seconds
FLT 106	CTR 10610	HOVER OGE, 70',WIND:140@12KTS	4.99 Seconds
FLT 107	CTR 10705	HOVER OGE, 70 FT, 100% NR	4.99 Seconds
FLT 108	CTR 10805	HOVER OGE, 70 FT, 100% NR	4.99 Seconds
FLT 108	CTR 10839	HOVER OGE, 70 FT, 100% NR	4.99 Seconds
FLT 110	CTR 11004	HOVER OGE, 70 FT, 100% NR	4.99 Seconds
FLT 110	CTR 11034	HOVER OGE, 70 FT, 100% NR	4.99 Seconds
FLT 111	CTR 11104	HOVER OGE, 70 FT, 100% NR	4.99 Seconds
FLT 113	CTR 11304	HOVER OGE, 70 FT, 100% NR	4.99 Seconds
FLT 114	CTR 11407	HOVER OGE, 70 FT, 100% NR	4.99 Seconds
FLT 114	CTR 11426	HOVER OGE, 70 FT, 100% NR	4.99 Seconds
FLT 115	CTR 11505	HOVER OGE, 70 FT, 100% NR	4.99 Seconds
FLT 116	CTR 11649	HOVER OGE, 70 FT, 100% NR	4.99 Seconds
FLT 116	CTR 11689	HOVER OGE, 70 FT, 100% NR	4.99 Seconds

Table 11.– 80-knot forward flight housekeeping points.

FLIGHT	COUNTER	DESCRIPTION	DURATION
FLT 83	CTR 8317	HOUSEKEEPING POINT, 80 KIASB	4.99 Seconds
FLT 83	CTR 8339	HOUSEKEEPING POINT, 80 KIASB	4.99 Seconds
FLT 84	CTR 8412	HOUSEKEEPING POINT, 80 KIASB	4.99 Seconds
FLT 84	CTR 8433	HOUSEKEEPING POINT, 80 KIASB	4.99 Seconds
FLT 85	CTR 8510	HOUSEKEEPING POINT, 80 KIASB	4.99 Seconds
FLT 88	CTR 8805	HOUSEKEEPING POINT, 80 KIASB	4.99 Seconds
FLT 88	CTR 8828	HOUSEKEEPING POINT, 80 KIASB	4.99 Seconds
FLT 89	CTR 8905	HOUSEKEEPING POINT, 78 KIASB	5.99 Seconds
FLT 89	CTR 8933	HOUSEKEEPING POINT, 80 KIASB	10.99 Seconds
FLT 90	CTR 9005	HOUSEKEEPING POINT, 80 KIASB	4.99 Seconds
FLT 94	CTR 9420	HOUSEKEEPING POINT, 80 KIASB	4.99 Seconds
FLT 95	CTR 9504	HOUSEKEEPING POINT, 80 KIASB	5.00 Seconds
FLT 96	CTR 9604	HOUSEKEEPING POINT, 80 KIASB	4.99 Seconds
FLT 97	CTR 9704	HOUSEKEEPING POINT, 80 KIASB	4.99 Seconds
FLT 98	CTR 9804	HOUSEKEEPING POINT, 80 KIASB	4.99 Seconds
FLT 100	CTR 10005	HOUSEKEEPING POINT, 80 KIASB	4.86 Seconds
FLT 101	CTR 10105	HOUSEKEEPING POINT, 80 KIASB	4.99 Seconds
FLT 102	CTR 10205	HOUSEKEEPING POINT, 80 KIASB	4.99 Seconds
FLT 103	CTR 10304	HOUSEKEEPING POINT, 80 KIASB	4.99 Seconds
FLT 103	CTR 10312	HOUSEKEEPING POINT, 80 KIASB	4.99 Seconds
FLT 105	CTR 10505	HOUSEKEEPING POINT, 80 KIASB	5.99 Seconds
FLT 106	CTR 10604	HOUSEKEEPING POINT, 80 KIASB	4.99 Seconds
FLT 107	CTR 10706	HOUSEKEEPING POINT, 80 KIASB	4.99 Seconds
FLT 108	CTR 10806	HOUSEKEEPING POINT, 80 KIASB	5.00 Seconds
FLT 110	CTR 11005	HOUSEKEEPING POINT, 80 KIASB	4.99 Seconds
FLT 110	CTR 11033	HOUSEKEEPING POINT, 80 KIASB	4.99 Seconds
FLT 111	CTR 11105	HOUSEKEEPING POINT, 80 KIASB	4.99 Seconds
FLT 112	CTR 11242	HOUSEKEEPING POINT, 80 KIASB	4.99 Seconds
FLT 113	CTR 11305	HOUSEKEEPING POINT, 80 KIASB	4.99 Seconds
FLT 114	CTR 11408	HOUSEKEEPING POINT, 80 KIASB	4.99 Seconds
FLT 115	CTR 11511	HOUSEKEEPING POINT, 80 KIASB	5.00 Seconds
FLT 116	CTR 11651	HOUSEKEEPING POINT, 80 KIASB	4.99 Seconds
FLT 116	CTR 11687	HOUSEKEEPING POINT, 80 KIASB	4.99 Seconds

Table 12.– On-ground rotor speed variation.

FLIGHT	COUNTER	DESCRIPTION	DURATION
FLT 82	CTR 8209	LOW PITCH, GROUND IDLE, NR=60%	4.99 Seconds
FLT 82	CTR 8210	ROTOR ACCEL: NR=60% TO 100%	45.00 Seconds
FLT 82	CTR 8211	LOW PITCH, ON GROUND, NR=96%	4.41 Seconds
FLT 82	CTR 8212	LOW PITCH, ON GROUND, NR=104%	4.77 Seconds
FLT 82	CTR 8263	ROTOR DECEL: NR=100% TO %	24.00 Seconds
FLT 83	CTR 8310	ROTOR ACCEL: NR=60% TO 100%	51.00 Seconds

Table 13.– On-ground hub moment checks.

FLIGHT	COUNTER	DESCRIPTION	DURATION
FLT 83	CTR 8311	GROUND RUN, FLAT PITCH, 100%NR	4.99 Seconds
FLT 83	CTR 8312	GROUND RUN, 1"FWD STK, 100%NR	4.99 Seconds
FLT 83	CTR 8313	GROUND RUN, 1"AFT STK, 100%NR	4.99 Seconds
FLT 83	CTR 8314	GROUND RUN, 1"RT STK, 100%NR	4.99 Seconds
FLT 83	CTR 8315	GROUND RUN, 1"LT STK, 100%NR	4.99 Seconds

Table 14.– Ballast cart full displacement test.

FLIGHT	COUNTER	DESCRIPTION	DURATION
FLT 112	CTR 11243	HOVER, 70 FT, BCART FULL AFT	4.99 Seconds
FLT 112	CTR 11244	HOVER, 70 FT, BCART MID	4.99 Seconds
FLT 112	CTR 11245	HOVER, 70 FT, BCART FULL FWD	4.99 Seconds

Table 15.– Ground-contact collective sweep.

FLIGHT	COUNTER	DESCRIPTION	DURATION
FLT 113	CTR 11323	ON GROUND, 40% COLL, 100% NR	5.99 Seconds
FLT 113	CTR 11324	ON GROUND, 35% COLL, 100% NR	4.99 Seconds
FLT 113	CTR 11325	ON GROUND, 30% COLL, 100% NR	4.99 Seconds
FLT 113	CTR 11327	ON GROUND, 25% COLL, 100% NR	4.99 Seconds
FLT 113	CTR 11328	ON GROUND, 20% COLL, 100% NR	4.99 Seconds
FLT 113	CTR 11329	ON GROUND, 15% COLL, 100% NR	4.99 Seconds
FLT 113	CTR 11330	ON GROUND, 10% COLL, 100% NR	4.99 Seconds
FLT 113	CTR 11331	ON GROUND, 5% COLL, 100% NR	4.99 Seconds
FLT 114	CTR 11404	ON GROUND, 30% COLL, 100% NR	4.99 Seconds
FLT 114	CTR 11405	ON GROUND, 35% COLL, 100% NR	4.99 Seconds
FLT 114	CTR 11406	ON GROUND, 40% COLL, 100% NR	4.99 Seconds

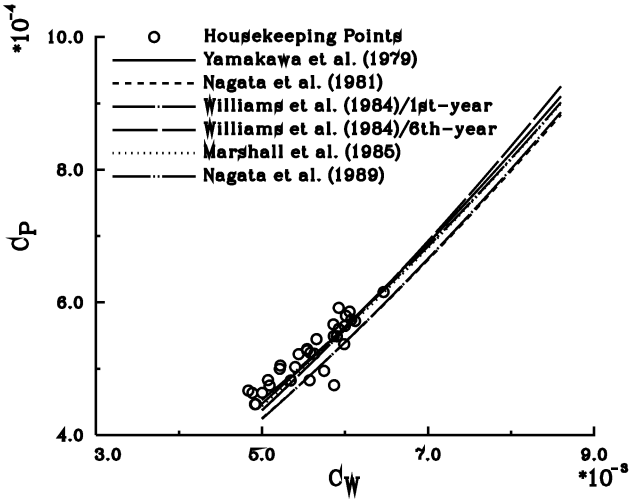

Figure 12.– OGE hover housekeeping points compared to USAAEFA hover performance data.

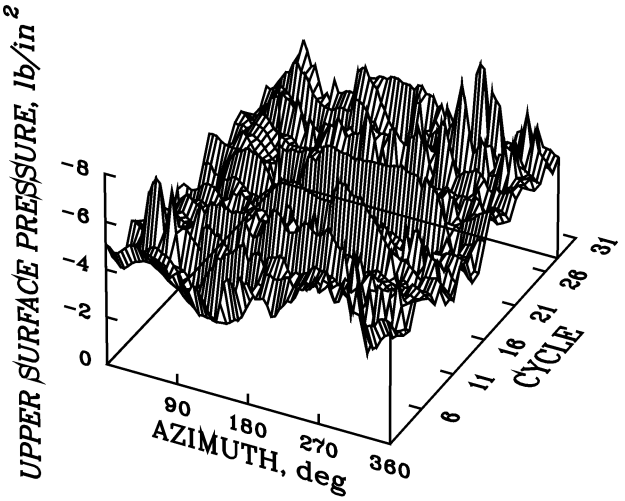

Figure 13.– Leading edge pressure variation for OGE hover housekeeping points; x/c = 0.049, r/R = 0.92.

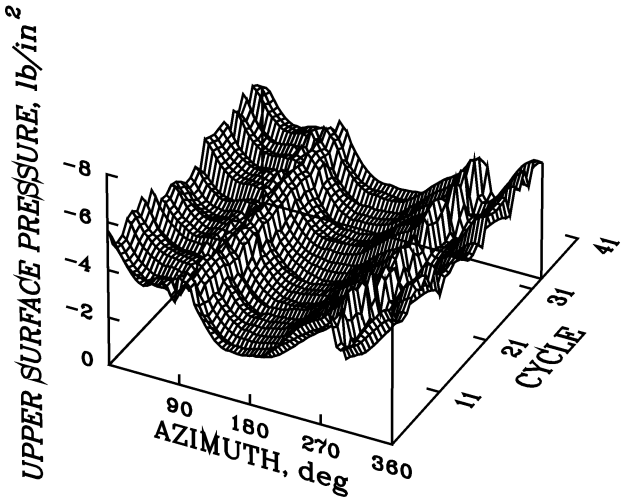

Figure 14.– Leading edge pressure variation for 80-knot housekeeping points; x/c = 0.049, r/R = 0.92.

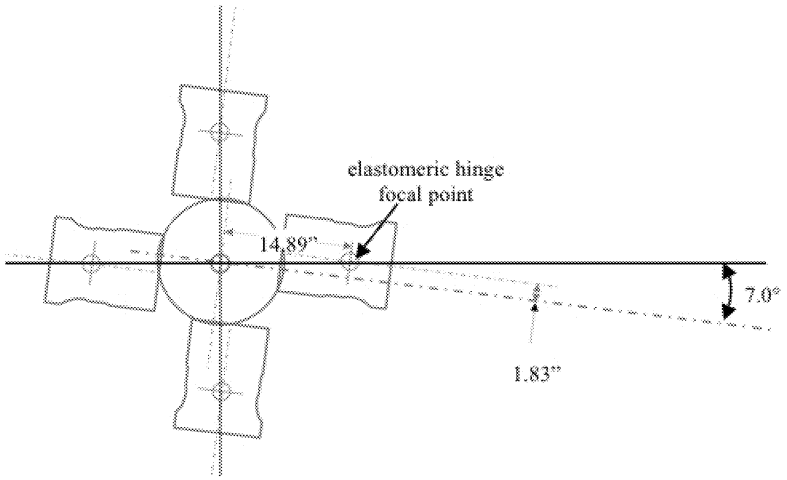

Figure 15.– Schematic of the UH–60A hub layout illustrating the two reference systems.

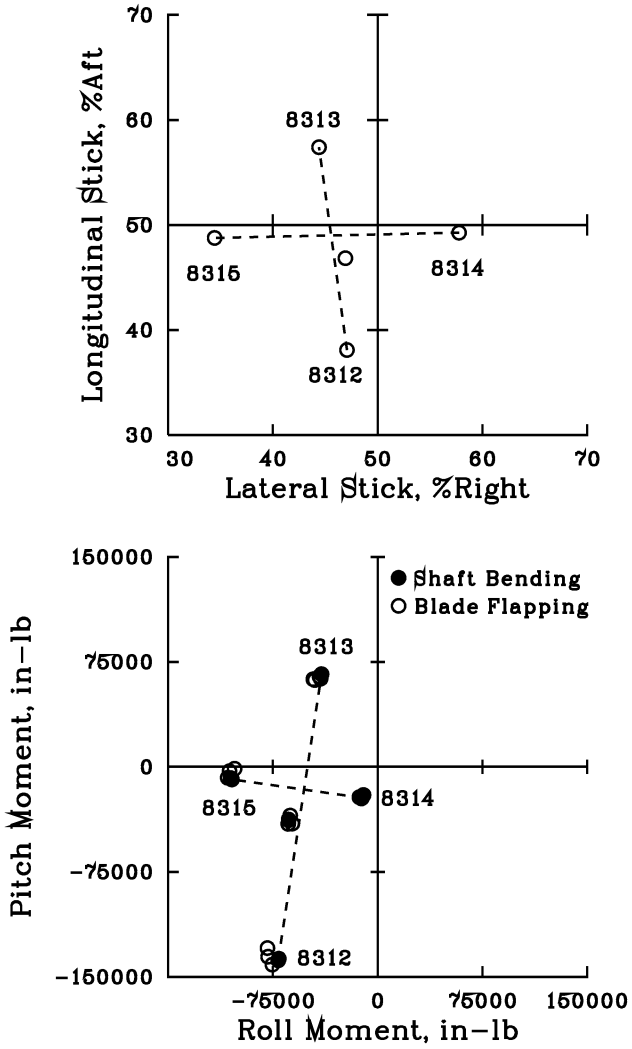

Figure 16.– Longitudinal and lateral stick displacements and aircraft moments during on-ground moment tests; Flight 83.

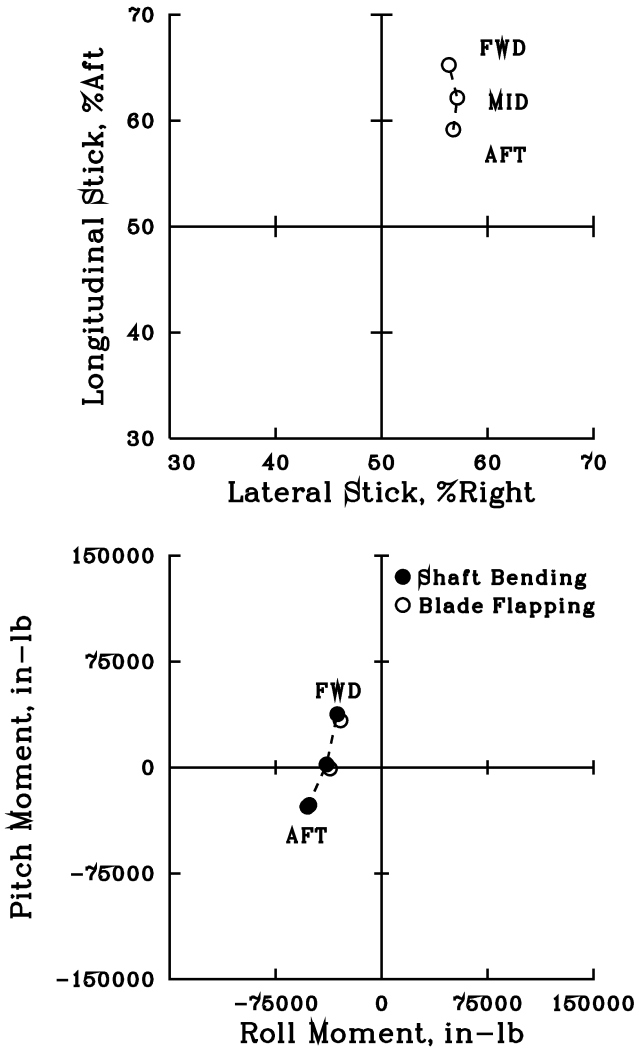

Figure 17.– Longitudinal and lateral stick displacements and aircraft moments during ballast cart full displacement test; Flight 115.

5. HOVER

Out-of-Ground-Effect Hover Data

Hover data were obtained during the Airloads Program in conjunction with other test objectives and are, in this sense, limited. Out-of-ground effect hover data were obtained during seven different types of tests: 1) housekeeping points, 2) a counter obtained during the low-airspeed calibration, 3) end points obtained as a part of forward flight airspeed sweeps, 4) counters obtained during ground-acoustic testing, 5) stabilized hover data prior to 2-3-1-1 inputs in flight dynamics tests, 6) stabilized hover data prior to frequency sweep measurements, and 7) counters obtained during rotor speed sweep testing. These seven sets of hover data are compared with hover performance data previously acquired by the U.S. Army Aviation Test Activity (AEFA), Edwards AFB, in figure 18. The AEFA data were acquired on a sixth-year production aircraft (ref. 27) and a twelfth-year production aircraft (ref. 28). The test aircraft used during the Airloads Program is a sixth-year aircraft and is therefore directly comparable to the reference 27 data. A number of configuration changes were made for the twelfth-year aircraft, but these changes are not believed to affect the hover data. For both the Airloads Program data and the AEFA data the power coefficient, C_P, is based on the measured engine output power that is equivalent to the sum of the main rotor power, the tail rotor power, accessory power, and gearbox losses. The weight coefficient, C_W, is based on aircraft weight, accounting for fuel burn-off and, for tethered flights, the force on the hook. The rotor thrust coefficient, which was not measured, will differ from the weight coefficient by the effects of download on the fuselage.

The OGE hover housekeeping counters were previously discussed in section 4 and the C_W/σ and C_P/σ data were compared to the AEFA data in figure 12. That comparison is repeated here as figure 18(a). The housekeeping counters were previously shown in table 10 and these are repeated in table 16, along with values of C_W/σ and C_P/σ from the TRENDS data base. The coefficients are average values obtained over the full duration of the record indicated in table 16.

Low-airspeed calibration data were obtained during the ground-acoustic testing portion of the program, as has been discussed in section 3. One point from this calibration series, Counter 9605, represents a hover condition and it is shown in figure 18(b) and listed in table 17. Combined with the calibration counter in figure 18(b) are two hover points that were obtained as end points for level flight airspeed sweeps, as will be discussed in section 6. The two level flight hover points are listed in table 18.

OGE hover data were also obtained during the ground-acoustic testing at Crows Landing. The data reduction procedures for the ground-acoustic testing differed from the other parts of the test program. Initially, rather than reducing a specific time slice of the flight record, the entire record was reduced and combined with tracking information from the laser and radar trackers. However, to keep the file size manageable, only the aircraft data were reduced and the rotor measurements were excluded. These initial records were placed in the Ames BH2 data base, but a prefix-4 was placed before the counter number. Subsequently, the prefix-4 data were used by Ames personnel to determine appropriate time slices for the BH2 data base and by Langley personnel to determine the time slices for the BHL data base. The hover cases in the prefix-4 data base are listed in table 19. The

time slices selected for the BH2 data base are listed in table 20. The hover cases in the BH2 data base are listed in table 21 and include C_W/σ and C_P/σ values. Figure 18c compares these ground-acoustic C_W/σ and C_P/σ data with the AEFA measurements.

Additional OGE hover data were obtained during the flight dynamics testing. Approximately the first five seconds of records for 2-3-1-1 input tests were obtained in a stabilized hover. The C_W/σ and C_P/σ data for the initial stabilized hover points are compared with the AEFA data in figure 18(d). The counters for these hover points are listed in table 22. Similarly, the first segment of each record obtained during frequency sweep tests also includes a steady hover point. The C_W/σ and C_P/σ data for the initial segment of the frequency sweep hover points are compared with the AEFA performance measurements in figure 18(e). The associated counters are shown in table 23.

Hover data were also obtained for five counters where the rotor speed was varied from 96% to 104% N_R. These data are compared with the AEFA curves in figure 18(f). The counters are listed in table 24.

The comparison of the Airloads Program OGE hover counters with the AEFA data illustrate two deficiencies in the Airloads hover data. First, the data were obtained over a reduced C_W/σ range compared to the AEFA data set and, second, the Airloads data show more variability in the power measurements. The increased range in C_W/σ for the AEFA tests was obtained by acquiring performance data in a tethered hover as well as testing at higher altitudes. For tether testing a tether cable connected the aircraft's cargo hook to an eyebolt set in concrete and the tether force was measured with a load cell. The tether force was added to the vehicle weight to compute the weight coefficient. This technique allowed the pilot to vary the collective pitch from a low-thrust condition, with barely any force on the tether, to a maximum power, high-thrust condition. An added benefit of this test approach was that the aircraft was fixed in inertial space and, if the winds were low, true hover data were obtained. High altitude testing was accomplished at Bishop (4120 feet) and Coyote Flats (9980 feet). Data in the Airloads Program were all obtained in untethered flight near sea level and the weight coefficient range is less than that obtained by AEFA.

The AEFA hover performance data are not shown in figure 18, rather the data are represented by a best fit of the original data (refs. 27, 28). As a consequence there is no indication of the variance observed for these data sets. An estimate of the standard deviation in C_P/σ obtained in earlier hover performance measurements on the UH–60A (ref. 25) is $\sigma \approx \pm 0.00010$. The housekeeping points show roughly three times this scatter with $\sigma = \pm 0.00027$. The other data sets show slightly less variance, with the ground-acoustics, 2-3-1-1 flight dynamics, and frequency sweep data showing respectively ±0.00019, ±0.00021, and ±0.00014. The low-airspeed calibration point in figure 18(b) shows excellent agreement with the AEFA data, but the two level flight sweep points are both offset from the AEFA data. Counter 8524 is about 0.00037 high and Counter 11008 is 0.00046 low. Curiously, the N_r sweep data appear to show less scatter than the other data sets, but the data are offset about +0.00032 from the AEFA performance curves.

The variability in the hover performance data for the Airloads Program is a result of winds, aircraft motion, or other unquantified factors. Generally, hover points were flown regardless of ground wind conditions and, in most cases, neither wind velocity nor inertial velocity were measured. For the ground-acoustics data in figure 18(c), however, both wind and inertial velocities

were obtained and their effects are discussed below. Some of the largest deviations from the AEFA performance curves in figure 18 are for the two level flight airspeed sweep end points. The flight altitude for Counter 8524 was 2564 feet while the altitude for Counter 11008 was 4056 feet. In neither case were there visual cues that the pilots could use to maintain hover. Instead the pilots used the HADS system, previously described in section 3, to achieve a relative wind as close to zero airspeed as possible. The HADS instrumentation was connected to a cockpit indicator and stabilized hover was obtained by zeroing the x- and y-velocities based on the cockpit indicator (there was no indication of z-velocity). Subsequent to the Airloads Program the HADS measurements had been calibrated for x-velocity (see section 3), but not for the y- or z-velocities. The x-velocities for counters 8524 and 11008 are less than three knots, but the y-velocity is unknown. An estimate of the z-velocity is obtained by looking at the rate of climb or descent based on the boom static pressure rate of change. For Counter 8524, the rate of climb is about 36 ft/min, which is close to a true hover. For Counter 11008, the rate of climb is about 600 ft/min, which is a significant departure from a hover condition. The differences between the two counters in rate of climb, however, does not explain the deviation from the AEFA data that is observed in figure 18(b) and these differences remain unexplained.

The accurate measurement of hover data on a flight vehicle depends upon a number of factors. The power required by the rotor depends upon the relative motion of the flight vehicle to the air mass and changes in power will differ depending upon whether the helicopter is climbing, descending, or moving in a horizontal plane. Even if the vehicle is perfectly still in an inertial frame, if there is motion of the air mass, similar changes will occur in power. For most of the hover data obtained during the Airloads Program there were no measurements of either inertial velocity or air mass velocity. However, for the ground-acoustic testing performed at Crows Landing, precise measurements were available for the motion of the aircraft in an inertial frame, using either a laser or radar tracker. In addition the motion of the air mass was measured over a range of heights. By analyzing these data it is possible to determine the relative motion between the aircraft and the air mass for all of the data acquired at Crows Landing.

Measurements of the UH–60A's vertical and horizontal position, for the ground-acoustic counters tabulated in table 21, are shown in figure 19. For these tests, the aircraft hovered over the center of the acoustic array at approximately 250 feet. To assist the pilot in accurately maintaining his position, two observers were located about 250 feet from the center of the acoustic array, one along the array's x-axis and the other along the y-axis. These observers used theodolites to locate the aircraft's position relative to the true center and communicated needed changes to the pilot by radio. Figure 19 shows the center point of the aircraft as measured with the radar tracker. As shown in this figure, during the five-second duration of a typical counter, there was limited aircraft motion. However, between test points, as the pilots changed heading, there were substantial shifts in the aircraft center point. The shifts in the center points in the x- and y-directions were as large as 50 feet and in the z-direction by up to 35 feet. The statistics for all of the center points are shown in table 25. The mean center point error varied from five feet for the x-axis to 14 feet for the z-axis, and the standard deviations ranged from 13 feet for the z-axis to 24 feet for the y-axis. However, during the period of data acquisition for each counter, the aircraft was essentially stationary. The standard deviation computed over the duration of the record ranged from about half a foot to a maximum of about five feet, depending upon the axis. The median value of the standard deviation for all of the counters varied between one to three feet as shown in table 26.

Wind velocities were measured at different elevations above the ground for these same tests. Measurements included the ground anemometer that is permanently installed at Crows Landing, an anemometer tower, and a tethered weather balloon. The anemometer tower and the weather balloon were installed by NASA Langley Research Center and are a normal part of their acoustic measurement suite. The location of the three wind velocity measurements is shown in figure 4.

The ground anemometer data were sampled at 100 Hz for the duration of the counter and the wind speed (WINDSP) and direction (WINDDR) are included in the TRENDS data base. The wind speed is measured in knots and the direction is measured with respect to the Crows Landing north-south runway as shown in figure 4. As discussed in section 2, this runway is 11.1 deg east of true north. The direction sense for WINDDR is clockwise, thus a northeast wind is at 45 deg, a south wind is at 180 deg, and so forth. For the ground-acoustic hover counters the wind speed varied from 1.7 to 6.3 knots. The variance, as measured by either the standard deviation or the range, was roughly proportional to the mean speed. For the standard deviation this variation was about 6% of the mean and for the range, about 12%.

The Langley Research Center anemometer tower (referred to as the profiler) measured wind speeds at five elevations from ground level to 10 meters, and direction at three of these elevations. Only the data obtained at the 10-m elevation are used here. These data were sampled once every 20 seconds (0.05 Hz) and, therefore, samples were not generally obtained at the time of the counter. The measurements shown below were taken from the sample that was nearest in time to the counter.

The weather balloon used by Langley Research Center was attached to a tether that allowed the balloon to be positioned anywhere from ground level to 500 feet. For the ground acoustic hover conditions, table 21, the balloon was fixed at 250 feet. The wind speed and direction were sampled every 10 sec (0.1 Hz). The five samples nearest the flight counter were used to estimate wind speed and direction. For the low-airspeed calibration conditions that include the table 18 hover case, the balloon elevation was continuously varied from the ground to 500 feet in a sawtooth pattern. For these cases, the sample point nearest in elevation and time was used to estimate the air mass velocity.

The measured wind speeds for the ground acoustic tests on Flights 93 and 94, and the low airspeed calibrations on Flights 96 and 98, are shown in figure 20. Normally, hover data are obtained only for wind speeds less than 3 knots at the ground. This criteria was met for Flight 93 and 96, but not for the other two flights. In particular, Flight 94 had ground winds from 2 to 6 knots and the winds at the 250 ft hover point were 6 to 11 knots. Therefore, it is expected that these hover points will be contaminated to some degree by these winds. However, the low airspeed calibration hover point, Counter 9605, was obtained for very low airspeed conditions. In reviewing figure 20 it is interesting to note that when ground winds exceeded 3 knots, the normal test criteria for acquiring steady data, the winds at 250 feet were always higher. However, for ground winds below 3 knots, the converse does not hold true. On both Flights 93 and 98, ground winds were less than 3 knots, but the winds aloft were 6 to 8 knots. This indicates that ground wind criteria may not be adequate to define conditions for acquiring steady OGE hover data.

The measured inertial velocities and measured wind speeds at the aircraft's test altitude were combined to provide the true advance ratios for the ground acoustic hover points, as shown in table 27, and the hover point obtained in the low-airspeed calibration, as shown in table 28. The influence of the air mass motion for the ground acoustic hover points is clearly seen in table 27. Depending upon the heading, non-zero advance ratios as high as 0.023 are observed. However, the low-airspeed calibration hover point is within 0.002 of a true zero advance ratio. (The true advance ratios for the remainder of the low-airspeed calibration points were previously shown in section 2, table 8.)

The variation of true advance ratio for the ground-acoustic hover counters and the low-airspeed calibration counter is examined in figure 21 by plotting the x- and y-components of the advance ratio. Figure 21(a) shows the ground-acoustic hover points and these are seen to trace out a rough semi-circle. The purpose of this series of test points was to obtain acoustic data as the aircraft's heading was varied in 15-deg increments around a half circle. As the prevailing winds were relatively constant during this test series, the relative wind varied in azimuth with the aircraft's heading. Thus the radius of the semi-circle represents the contaminating winds at 250 feet elevation.

The low-airspeed calibration points in figure 21(b) are in two groups: Flight 96 and Flight 98. The winds at 250 feet were less than 2 knots for Flight 96 (see fig. 20), and therefore the lateral advance ratios were generally less than 0.01, and this is particularly so for the three low-speed points in figure 21(b). However, on Flight 98, the winds at 250 feet were about 8 knots and the effects of the lateral component of these winds is apparent in figure 21(b).

Based on the examination of inertial and air mass velocities, Counter 9605 represents the steadiest hover case obtained in the Airloads Program. The airloads for this counter are shown in figure 22, where the normal force, M^2C_N, is shown at nine radial stations on the blade for one revolution. The two outboard stations show the greatest force and there is a clear reduction in this force from about 315 to 15 deg azimuth. This reduction occurs over the rear of the aircraft and is likely an effect of the tail boom or the tail rotor wake. Some unsteadiness in the lift is observed near the nose of the aircraft, from 0.775R out to 0.990R and this is particularly pronounced at 0.920R. The fluctuations in lift in figure 22 are likely caused by rapid changes in the blade angle of attack. The angle of attack related to these fluctuations can be approximated

$$\Delta\alpha \approx \frac{1}{2\pi\beta}\Delta C_N \tag{1}$$

where $\beta = \sqrt{1 - M^2}$. The peak-to-peak, angle-of-attack change associated with the lift fluctuations at 0.920R are approximately 2.7 deg. It is likely that this variation is a consequence of a blade-vortex interaction of some sort, although the source of the vortex, that is, whether the main rotor or tail rotor, is uncertain.

The variation of normal force is examined for three of the ground-acoustic hover points in figure 23. These counters: 9406, 9410, and 9416, were selected to provide different relative wind conditions (see fig. 21(a)). An outline of the UH–60A is placed above each figure to indicate the direction of the relative wind. For this aircraft, the tail rotor is located on the right side of the tail and its wake moves to the left. Figure 23(a) shows the normal force for Counter 9406, where the relative

wind is from the right aft quadrant. A great deal more unsteadiness is observed for this flight condition than was seen in figure 22. Apparent vortex interactions are seen from 0.865*R* to 0.990*R*, starting at an azimuth of about 240 deg and extending over 120 deg. Lesser unsteadiness is seen inboard at 0.775*R* and further inboard there are no significant fluctuations in the lift. The variation in angle of attack at the four outboard stations ranges from approximately 2.8 to 3.1 deg.

Figure 23(b) shows the lift fluctuations for Counter 9410, where the relative wind is from the right forward quadrant. Lift fluctuations are now seen primarily outboard and occur only in the fourth quadrant. Compared to figure 23(a), the angle of attack variation is reduced to about 2.6 deg. The third test point, Counter 9416, is shown in figure 23(c). In this case the relative wind is from the front left quadrant. Almost no lift fluctuations are observed in this case except at 0.920*R*, where an angle of attack excursion at 330 deg is about 2.9 deg in size.

Although not shown here, the correspondence in the load fluctuations at individual blade stations that is seen in figure 23, is repeated for subsequent cycles (revolutions) during the 19 or 20 cycles of the counter. However, these events move in azimuth over time as well as change in size and form. It seems likely that these blade vortex interactions are intimately tied into the rotor wakes, but the general structure of these interactions is not clear.

The two hover points obtained as a portion of an airspeed sweep, Counters 8524 and 11008, are shown in figures 24 and 25 respectively. Both hover points show lift fluctuations similar to what were seen for the ground-acoustic hover conditions in figure 23. The lift fluctuations for Counter 8524 extend over most of the retreating side of the blade and appear to extend over a greater area of the rotor disk than was observed for Counter 9406 in figure 23(a), which had the greatest extent of unsteady lift of the three ground-acoustic hover counters. Counter 11008 shows considerably less unsteadiness, at least at higher frequencies, although there is some low-frequency unsteadiness, particularly inboard on the rotor.

In-Ground-Effect Hover Data

During the low-airspeed system calibration on Flight 82, four test counters were obtained in an IGE hover, as listed in table 29. Based on the radar altimeter, the wheel height for these cases ranged from 8.4 to 9.6 feet. No measurements of the relative wind were obtained for these IGE hover conditions, however, the heading was reversed by 180 deg between test points.

Table 16.– OGE Hover housekeeping points.

FLIGHT	COUNTER	DESCRIPTION	DURATION	C_W/σ	C_P/σ
83	8316	HOVER OGE, 70 FT, 100% NR	4.99 Seconds	0.0676	0.00634
83	8340	HOVER OGE, 70 FT, 100% NR	4.99 Seconds	0.0594	0.00511
84	8411	HOVER OGE, 70 FT, 100% NR	4.99 Seconds	0.0741	0.00692
84	8434	HOVER OGE, 70 FT, 100% NR	4.99 Seconds	0.0674	0.00585
85	8509	HOVER OGE, 70 FT, 100% NR	4.99 Seconds	0.0734	0.00709
88	8804	HOVER OGE, 70 FT, 100% NR	3.42 Seconds	—	—
88	8837	HOVER OGE, 70 FT, 100% NR	4.25 Seconds	0.0725	0.00650
89	8904	HOVER OGE, 70 FT, 100% NR	5.99 Seconds	0.0782	0.00746
89	8934	HOVER OGE, 70 FT, 100% NR	4.36 Seconds	0.0709	0.00686
90	9004	HOVER OGE, 70 FT, 100% NR	4.99 Seconds	—	—
100	10004	HOVER OGE, 70 FT, 100% NR	4.99 Seconds	0.0631	0.00605
100	10016	HOVER OGE, 70 FT, 100% NR	4.99 Seconds	0.0591	0.00561
101	10118	HOVER OGE, 70 FT, 100% NR	4.99 Seconds	0.0585	0.00565
102	10204	HOVER OGE, 70 FT, 100% NR	4.99 Seconds	0.0648	0.00584
102	10221	HOVER OGE, 70 FT, 100% NR	4.99 Seconds	0.0605	0.00562
103	10313	HOVER OGE, 70 FT, 100% NR	4.99 Seconds	0.0616	0.00575
105	10504	HOVER OGE, 70 FT, 100% NR	5.51 Seconds	0.0696	0.00602
106	10610	HOVER OGE, 70', WIND:140@12KTS	4.99 Seconds	0.0711	0.00575
107	10705	HOVER OGE, 70 FT, 100% NR	4.99 Seconds	0.0709	0.00665
108	10805	HOVER OGE, 70 FT, 100% NR	4.99 Seconds	0.0714	0.00665
108	10839	HOVER OGE, 70 FT, 100% NR	4.99 Seconds	0.0671	0.00642
110	11004	HOVER OGE, 70 FT, 100% NR	4.99 Seconds	0.0726	0.00683
110	11034	HOVER OGE, 70 FT, 100% NR	4.99 Seconds	0.0654	0.00609
111	11104	HOVER OGE, 70 FT, 100% NR	4.99 Seconds	0.0728	0.00702
113	11304	HOVER OGE, 70 FT, 100% NR	4.99 Seconds	0.0717	0.00678
114	11407	HOVER OGE, 70 FT, 100% NR	4.99 Seconds	0.0671	0.00639
114	11426	HOVER OGE, 70 FT, 100% NR	4.99 Seconds	0.0597	0.00541
115	11505	HOVER OGE, 70 FT, 100% NR	4.99 Seconds	0.0705	0.00676
116	11649	HOVER OGE, 70 FT, 100% NR	4.99 Seconds	0.0735	0.00695
116	11689	HOVER OGE, 70 FT, 100% NR	4.99 Seconds	0.0682	0.00633

Table 17.– Low-airspeed calibration hover counter.

FLIGHT	COUNTER	DESCRIPTION	DURATION	C_W/σ	C_P/σ
96	9605	LOW AIRSPEED CAL, HOVER	4.99 Seconds	0.0668	0.00610

Table 18.– Airspeed sweep hover points.

FLIGHT	COUNTER	DESCRIPTION	DURATION	C_W/σ	C_P/σ
85	8524	HOVER, 0 KIASH, CWS=.08	4.995 Seconds	0.0792	0.00792
110	11008	HOVER, CWS=.08	4.995 Seconds	0.0804	0.00724

Table 19.– Hover cases from ground-acoustic testing; prefix-4 data base.

FLIGHT	COUNTER	DESCRIPTION	DURATION
493	49306	HOVER, HDG=173, RUN 600	24.17 Seconds
493	49307	HOVER, HDG=173, RUN 601	24.28 Seconds
493	49308	HOVER, HDG=188, RUN 605	42.88 Seconds
494	49404	HOVER, HDG=173, RUN 602	25.02 Seconds
494	49405	HOVER, HDG=188, RUN 607	24.71 Seconds
494	49406	HOVER, HDG=203, RUN 610	24.95 Seconds
494	49407	HOVER, HDG=218, RUN 615	24.59 Seconds
494	49408	HOVER, HDG=233, RUN 620	25.34 Seconds
494	49409	HOVER, HDG=248, RUN 625	14.99 Seconds
494	49410	HOVER, HDG=263, RUN 630	24.50 Seconds
494	49411	HOVER, HDG=278, RUN 635	24.88 Seconds
494	49412	HOVER, HDG=293, RUN 640	25.13 Seconds
494	49413	HOVER, HDG=308, RUN 645	24.67 Seconds
494	49414	HOVER, HDG=323, RUN 650	24.67 Seconds
494	49415	HOVER, HDG=338, RUN 655	24.47 Seconds
494	49416	HOVER, HDG=353, RUN 660	24.39 Seconds

Table 20.– Time slices for hover cases in prefix-4 and BH2 data bases.

PREFIX-4 DATA BASE			BH2 DATA BASE		
COUNTER	START TIME SEC	END TIME SEC	COUNTER	START TIME SEC	END TIME SEC
49306	0.00	24.17	9306	0.00	5.00
49307	0.00	24.28	9307	0.00	4.99
49308	0.00	42.89	9308	0.00	4.99
49404	0.00	25.02	9404	10.01	15.00
49405	0.00	24.71	9405	11.01	16.00
49406	0.00	24.94	9406	0.00	5.00
49407	0.00	24.59	9407	9.01	14.00
49408	0.00	25.34	9408	5.01	9.99
49409	0.00	14.99	9409	5.01	10.00
49410	0.00	24.50	9410	8.00	12.99
49411	0.00	24.87	9411	0.01	5.00
49412	0.00	25.13	9412	5.01	10.00
49413	0.00	24.66	9413	0.00	4.95
49414	0.00	24.67	9414	5.01	10.00
49415	0.00	24.47	9415	0.01	5.00
49416	0.00	24.38	9416	5.01	10.00

Table 21.– Ground-acoustic testing hover points.

FLIGHT	COUNTER	DESCRIPTION	DURATION	C_W/σ	C_P/σ
93	9306	HOVER, HDG=173, RUN 600	5.00 Seconds	0.0671	0.00622
93	9307	HOVER, HDG=173, RUN 601	4.99 Seconds	0.0668	0.00620
93	9308	HOVER, HDG=188, RUN 605	4.99 Seconds	0.0663	0.00609
94	9404	HOVER, HDG=173, RUN 602	5.00 Seconds	0.0684	0.00661
94	9405	HOVER, HDG=188, RUN 607	4.99 Seconds	0.0684	0.00623
94	9406	HOVER, HDG=203, RUN 610	4.99 Seconds	0.0684	0.00628
94	9407	HOVER, HDG=218, RUN 615	4.99 Seconds	0.0679	0.00636
94	9408	HOVER, HDG=233, RUN 620	4.99 Seconds	0.0678	0.00590
94	9409	HOVER, HDG=248, RUN 625	4.99 Seconds	0.0677	0.00582
94	9410	HOVER, HDG=263, RUN 630	4.99 Seconds	0.0664	0.00603
94	9411	HOVER, HDG=278, RUN 635	4.99 Seconds	0.0672	0.00626
94	9412	HOVER, HDG=293, RUN 640	4.99 Seconds	0.0671	0.00626
94	9413	HOVER, HDG=308, RUN 645	4.95 Seconds	0.0668	0.00631
94	9414	HOVER, HDG=323, RUN 650	4.99 Seconds	0.0663	0.00588
94	9415	HOVER, HDG=338, RUN 655	4.99 Seconds	0.0661	0.00581
94	9416	HOVER, HDG=353, RUN 660	4.99 Seconds	0.0663	0.00598

Table 22.– Stabilized hover points at beginning of 2-3-1-1 flight dynamic inputs.

FLIGHT	COUNTER	DESCRIPTION	DURATION	C_W/σ	C_P/σ
112	11206	PEDAL 2311, LEFT, HOVER	19.00 Seconds	0.0730	0.00654
112	11207	PEDAL 2311, RIGHT, HOVER	15.99 Seconds	0.0728	0.00676
112	11208	COLL 2311, UP, HOVER	18.00 Seconds	0.0728	0.00657
112	11209	COLL 2311, UP, HOVER	18.00 Seconds	0.0726	0.00653
112	11210	COLL 2311, DOWN, HOVER	19.00 Seconds	0.0724	0.00665
112	11211	LAT 2311, RIGHT, HOVER	18.00 Seconds	0.0725	0.00696
112	11212	LAT 2311, LEFT, HOVER	17.00 Seconds	0.0723	0.00676
112	11213	LONG 2311, AFT, HOVER	16.99 Seconds	0.0724	0.00683
112	11214	LONG 2311, FORWARD, HOVER	20.00 Seconds	0.0720	0.00663
112	11215	LONG 2311, FORWARD, HOVER	19.00 Seconds	0.0720	0.00690
112	11216	COLL 2311, DOWN, HOVER	19.00 Seconds	0.0719	0.00706

Table 23.– Stabilized hover points at beginning of multi-segmented, flight dynamic frequency sweeps. Stabilized hover point observed only during Segment 1.

FLIGHT	COUNTER	DESCRIPTION	DURATION	C_W/σ	C_P/σ
111	11106	PEDAL SWEEP A, SEG 1, HOVER	25.58 Seconds	0.0714	0.00669
111	11109	PEDAL SWEEP B, SEG 1, HOVER	27.28 Seconds	0.0712	0.00657
111	11112	PEDAL SWEEP C, SEG 1, HOVER	30.29 Seconds	0.0712	0.00660
111	11115	COLL SWEEP A, SEG 1, HOVER	25.29 Seconds	0.0708	0.00671
111	11118	COLL SWEEP B, SEG 1, HOVER	24.39 Seconds	0.0707	0.00675
111	11121	COLL SWEEP C, SEG 1, HOVER	26.06 Seconds	0.0705	0.00655
111	11124	LAT SWEEP A, SEG 1, HOVER	25.70 Seconds	0.0703	0.00665
111	11128	LAT SWEEP B, SEG 1, HOVER	26.25 Seconds	0.0699	0.00640
111	11131	LAT SWEEP C, SEG 1, HOVER	26.40 Seconds	0.0697	0.00655
111	11134	LONG SWEEP A, SEG 1, HOVER	25.70 Seconds	0.0696	0.00655
111	11137	LONG SWEEP B, SEG 1, HOVER	24.10 Seconds	0.0692	0.00659
111	11140	LONG SWEEP C, SEG 1, HOVER	26.66 Seconds	0.0690	0.00626
112	11217	PEDAL SWEEP A, SEG 1, HOVER	25.00 Seconds	0.0718	0.00660
112	11220	COLL SWEEP A, SEG 1, HOVER	24.30 Seconds	0.0717	0.00662
112	11223	LAT SWEEP A, SEG 1, HOVER	26.36 Seconds	0.0715	0.00671
112	11226	LAT SWEEP B, SEG 1, HOVER	27.06 Seconds	0.0714	0.00646
112	11230	LONG SWEEP A, SEG 1, HOVER	24.70 Seconds	0.0713	0.00642
112	11233	PEDAL SWEEP B, SEG 1, HOVER	25.00 Seconds	0.0712	0.00640
112	11236	COLL SWEEP B, SEG 1, HOVER	26.95 Seconds	0.0711	0.00637
112	11239	LONG SWEEP B, SEG 1, HOVER	25.80 Seconds	0.0709	0.00645

Table 24.– Rotor speed sweep in OGE hover.

FLIGHT	COUNTER	DESCRIPTION	DURATION	C_W/σ	C_P/σ
115	11505	HOVER OGE, 70 FT, 100% NR	4.99 Seconds	0.0705	0.00676
115	11506	HOVER OGE, 70 FT, 98% NR	4.99 Seconds	0.0732	0.00705
115	11507	HOVER OGE, 70 FT, 96% NR	4.99 Seconds	0.0766	0.00766
115	11508	HOVER OGE, 70 FT, 102% NR	4.99 Seconds	0.0676	0.00654
115	11509	HOVER OGE, 70 FT, 104% NR	4.99 Seconds	0.0656	0.00625

Table 25.– Center point variation between counters for ground-acoustic hover conditions; all table 21 counters.

DIRECTION	MEAN, FT	STANDARD DEVIATION, FT
X	5.1	22.9
Y	12.4	24.3
Z	236.2	13.1

Table 26.– Distribution of standard deviation measurements for each counter for ground-acoustic hover conditions; all table 21 counters.

DIRECTION	MEDIAN OF VARIATION, FT	RANGE OF VARIATION, FT
X	1.8	0.5 to 4.6
Y	3.1	0.7 to 4.4
Z	1.0	0.4 to 2.1

Table 27.– True advance ratios for ground-acoustic testing hover counters.

COUNTER	DESCRIPTION	μ_x	μ_y	μ_z
9306	HOVER, HDG=173, RUN 600	–0.010	0.015	0.000
9307	HOVER, HDG=173, RUN 601	–0.006	0.016	0.000
9308	HOVER, HDG=188, RUN 605	–0.008	0.014	–0.001
9404	HOVER, HDG=173, RUN 602	–0.016	0.012	0.000
9405	HOVER, HDG=188, RUN 607	–0.016	0.012	0.001
9406	HOVER, HDG=203, RUN 610	–0.018	0.015	–0.001
9407	HOVER, HDG=218, RUN 615	–0.003	0.017	0.000
9408	HOVER, HDG=233, RUN 620	–0.005	0.016	0.000
9409	HOVER, HDG=248, RUN 625	0.006	0.018	0.001
9410	HOVER, HDG=263, RUN 630	0.007	0.017	0.000
9411	HOVER, HDG=278, RUN 635	0.004	0.018	0.000
9412	HOVER, HDG=293, RUN 640	0.010	0.006	0.000
9413	HOVER, HDG=308, RUN 645	0.017	0.005	0.000
9414	HOVER, HDG=323, RUN 650	0.020	0.005	0.002
9415	HOVER, HDG=338, RUN 655	0.015	–0.007	0.000
9416	HOVER, HDG=353, RUN 660	0.018	–0.012	–0.001

Table 28.– True advance ratios for hover point flown during low-airspeed calibration.

COUNTER	DESCRIPTION	μ_x	μ_y	μ_z
9605	LOW AIRSPEED CAL, HOVER	0.001	0.000	0.002

Table 29.– In-Ground-Effect hover points.

FLIGHT	COUNTER	DESCRIPTION	DURATION	C_W/σ	C_P/σ
82	8213	HOVER IGE, NR=100%, NORTH	4.99 Seconds	0.0865	0.00554
82	8217	HOVER IGE, NR=100%, SOUTH	4.99 Seconds	0.0864	0.00550
82	8261	HOVER IGE, NR=100%, NORTH	4.99 Seconds	0.0646	0.00505
82	8262	HOVER IGE, NR=100%, SOUTH	4.99 Seconds	0.0644	0.00524

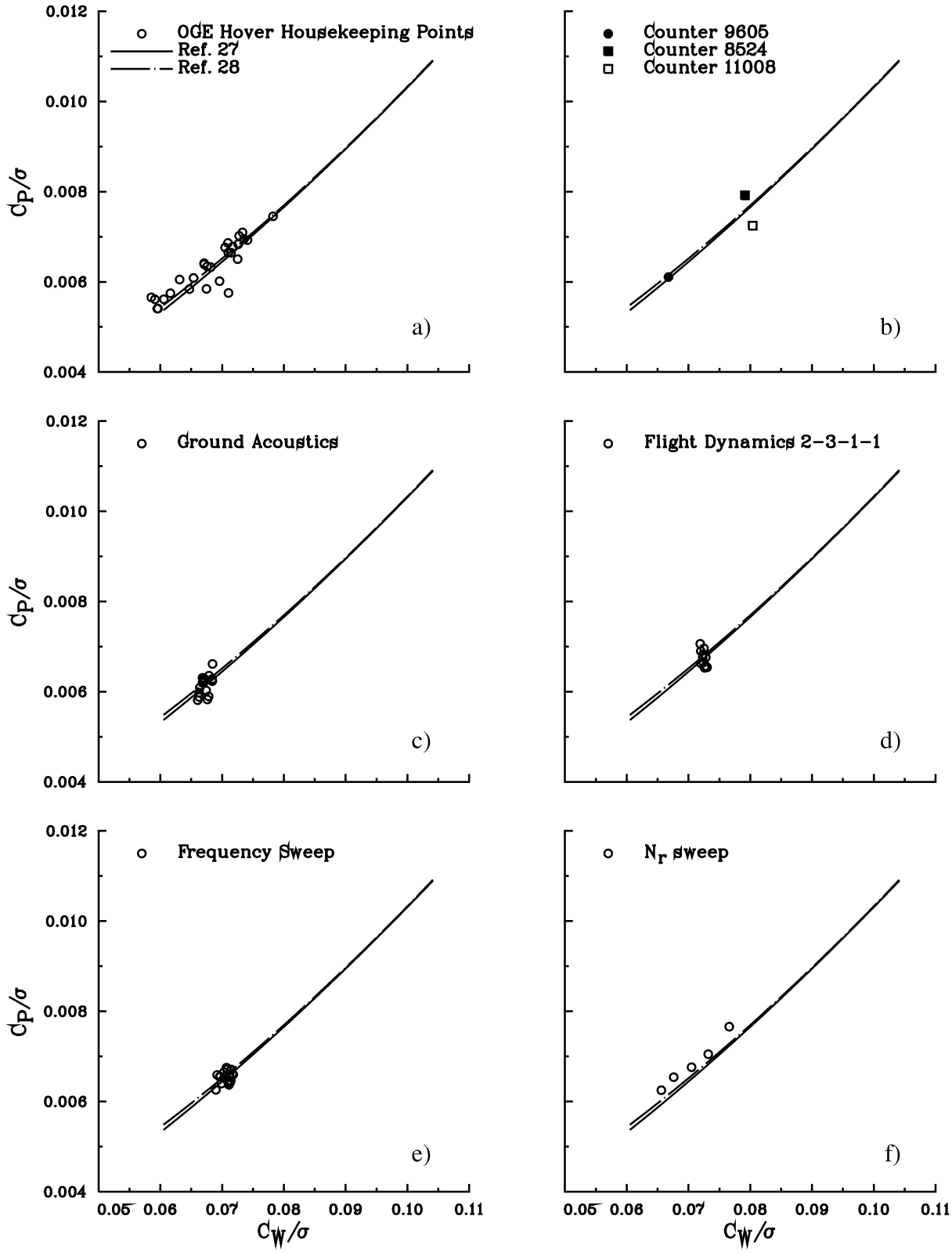

Figure 18.– Hover cases compared to previous performance measurements.

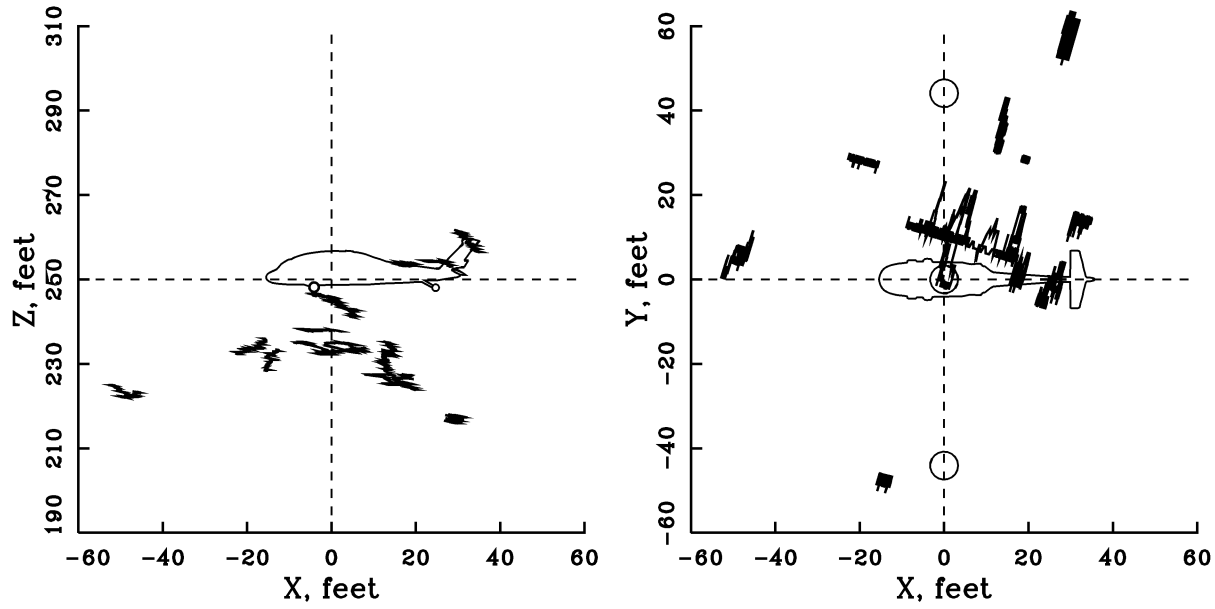

Figure 19.– Tracking data for ground-acoustic hover points. Outline of UH–60A is shown only for scale; the heading was changed between each test point.

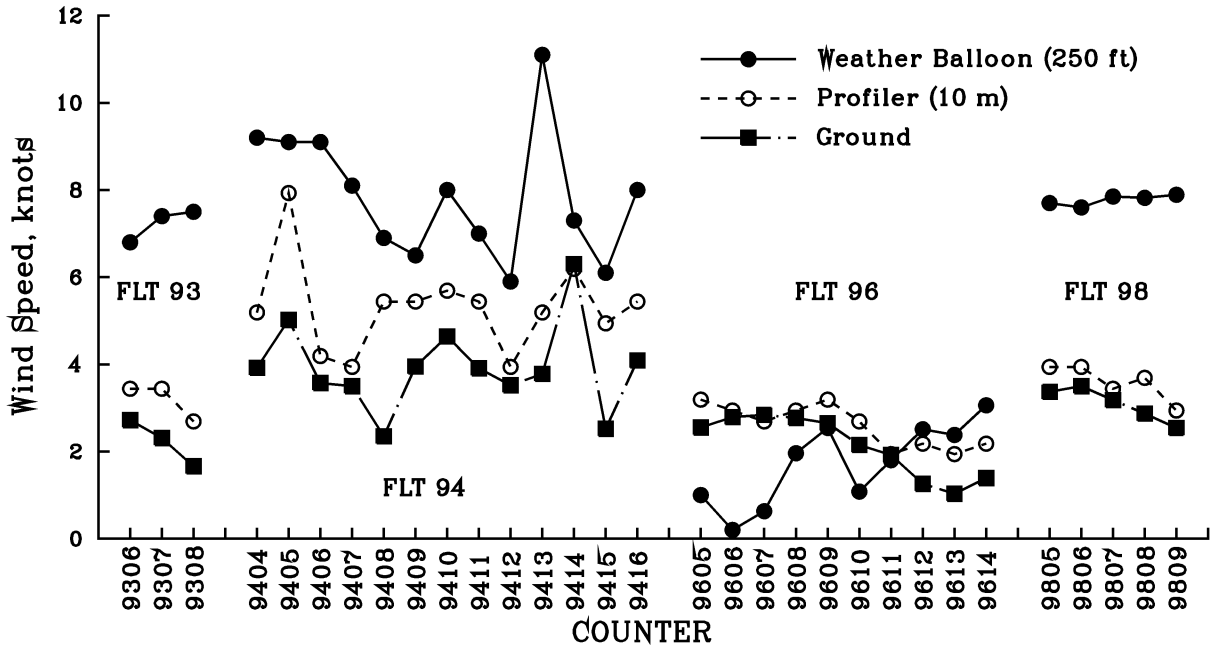

Figure 20.– Wind speeds associated with ground-acoustic and low-airspeed calibration counters.

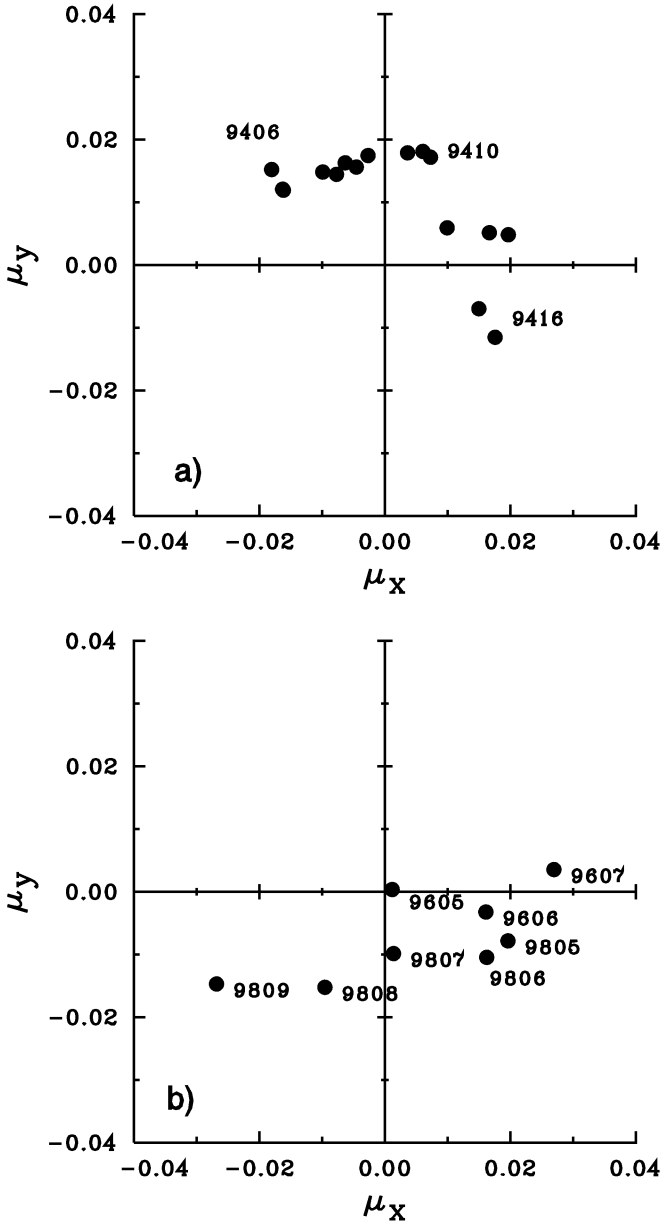

Figure 21.– True advance ratios for low-speed flight conditions: a) ground-acoustic hover counters; b) low-airspeed calibration counters.

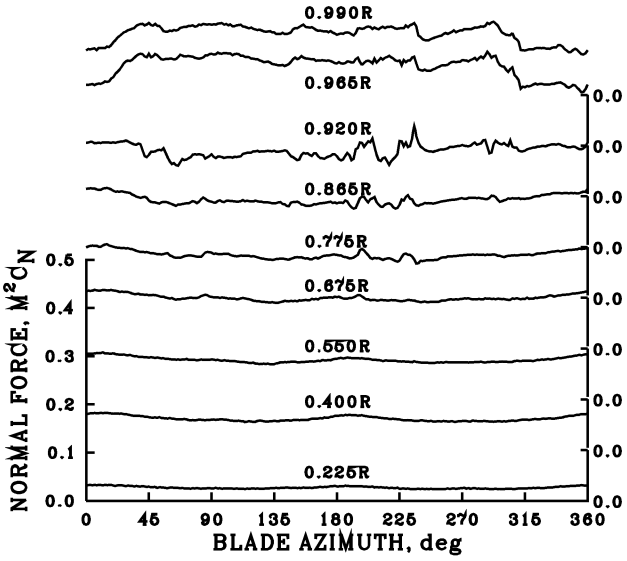

Figure 22.– Measured normal force for low-airspeed calibration hover point; counter 9605.

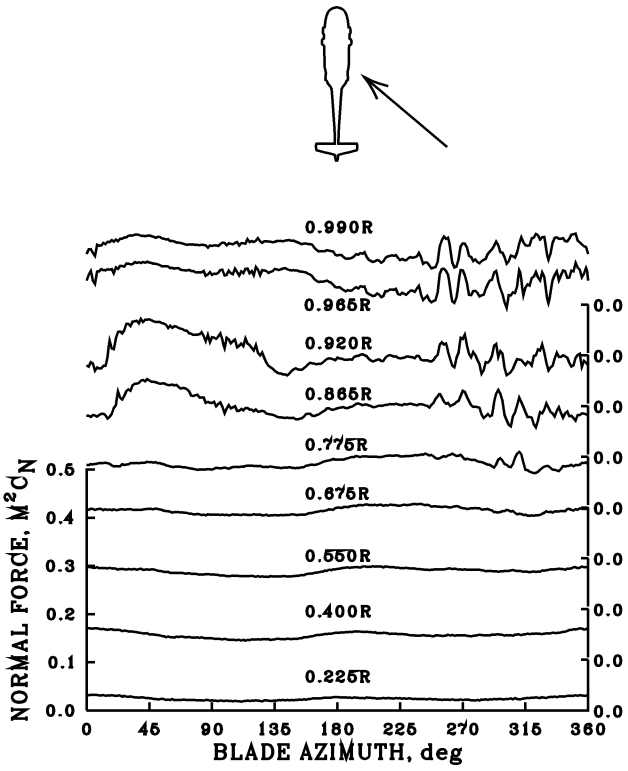

a) Counter 9406.

Figure 23.– Measured normal force for three ground-acoustic hover points with differing relative wind.

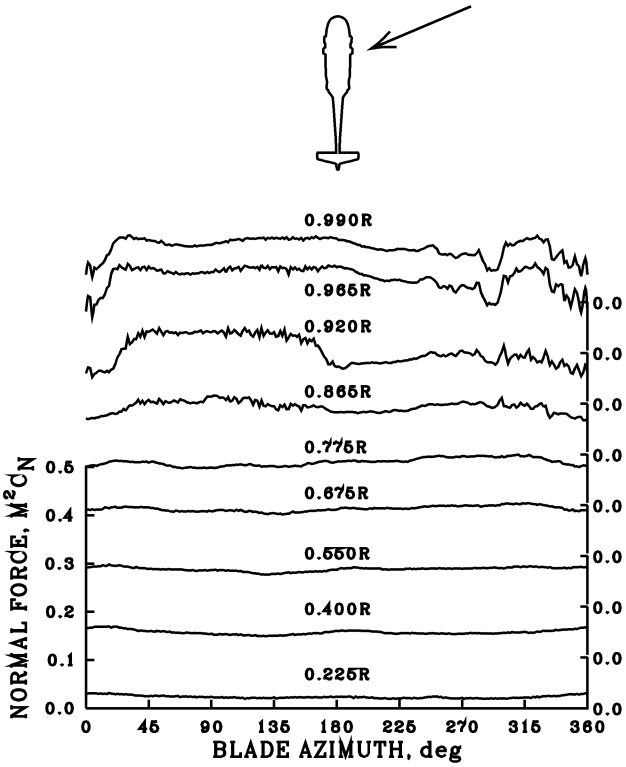

b) Counter 9410.

Figure 23.– Continued.

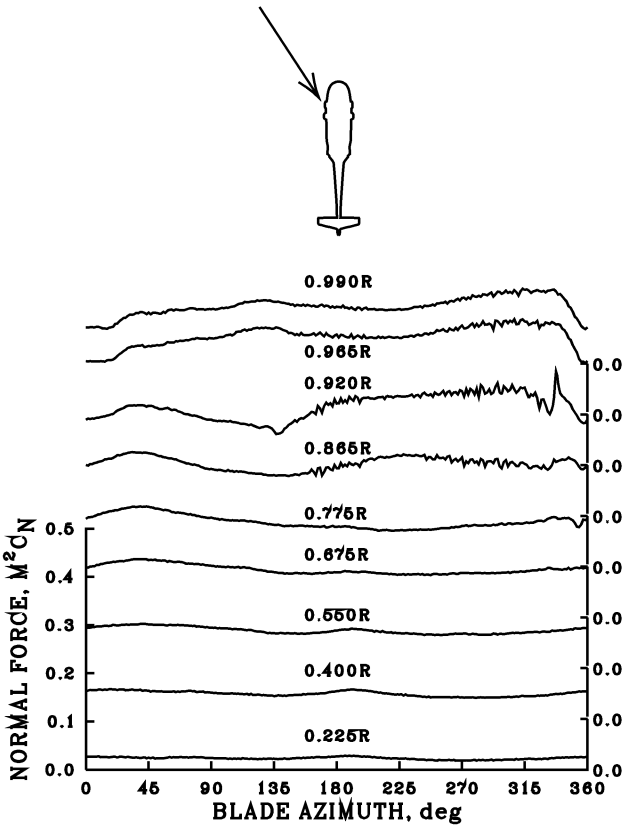

c) Counter 9416.

Figure 23.– Concluded.

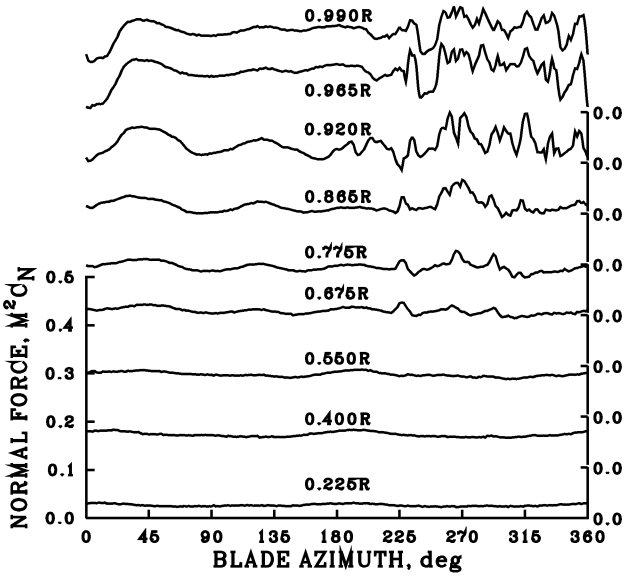

Figure 24.– Measured normal force for hover at altitude; counter 8524.

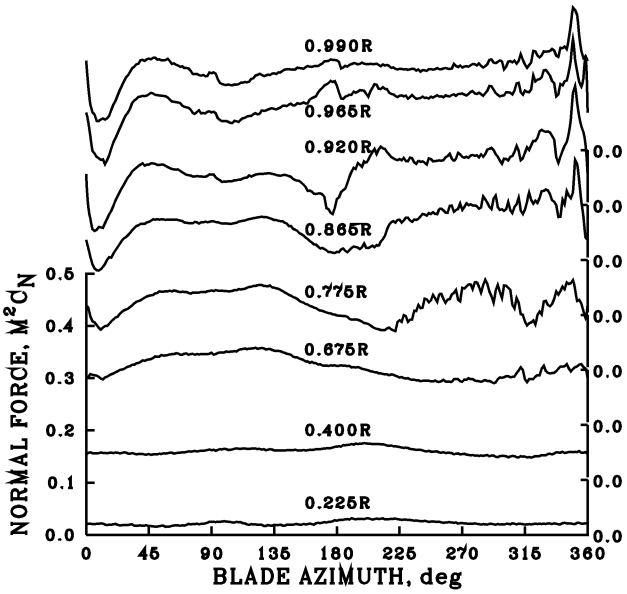

Figure 25.– Measured normal force for hover at altitude; counter 11008.

6. LEVEL FLIGHT

Level flight data were obtained for a number of different flight conditions including: 1) airspeed sweeps at six weight coefficients, 2) ground-acoustic and inflight-acoustic testing, 3) airspeed calibrations, 4) housekeeping points, 5) rotor speed changes, 6) a stabilator sweep, 7) roll angle/sideslip comparisons, and 8) in atmospheric turbulence. These various test data are shown in figure 26 where the test data C_W/σ values are plotted as a function of the advance ratio. The stall boundary measured by McHugh (ref. 31) is also shown in this figure. The weight coefficient and advance ratio data are average values obtained over the duration of the counter using VIEW in TRENDS.

The majority of the level flight data were obtained during a series of airspeed sweeps, with values of C_W/σ from 0.08 to 0.13 (see fig. 26(a)). The airspeeds for these data ranged from hover to the maximum speed of the aircraft, and are discussed below in the section on "Airspeed Sweeps." Level flight data were also obtained during acoustic testing, both for the ground-acoustic tests at Crows Landing, and for inflight-acoustic testing using the YO–3A (see fig. 26(b)). Aspects of these data are discussed below under "Acoustic Data." Figure 26(c) shows the airspeed calibration data and these are briefly discussed below in "Airspeed Calibration." The test procedures used to acquire the airspeed calibration data have been previously covered in section 3. The use of housekeeping points has been discussed before in section 4, and some limited additional discussion is also given here in "Housekeeping Points." The housekeeping data points are shown in figure 26(d).

The rotor speed was varied from 96 to 104% N_R at a number of different airspeeds and these data are shown in figure 26(e). These level flight data are discussed below in the section "Rotor Speed Sweeps." The aircraft stabilator angle was varied at one airspeed, as indicated in figure 26(f), and these data are covered in the section "Stabilator Angle Sweep." Pilots generally fly a helicopter in ball-centered flight, which provides a zero roll angle but allows residual sideslip. This flight approach is compared with flying at a zero sideslip angle in the "Roll Angle/Sideslip Comparison" section below, and these cases are shown in figure 26(g). The flight card on Flight 106 was terminated because the turbulence levels were considered to be too high, but limited data were obtained for these conditions and are discussed in the section "Turbulence Cases" below. The turbulence level flight cases are illustrated in figure 26(h).

Airspeed Sweeps

Level flight airspeed sweeps were flown at six non-dimensional thrust values from C_W/σ = 0.08 to 0.13. The weight of the aircraft was continuously computed by measuring the fuel used during the flight and this value was subtracted from the initial aircraft weight. The test altitude was then selected to provide the target value of C_W/σ. During an airspeed sweep a constant value of C_W/σ was maintained by increasing the flight altitude. The smallest practical adjustment in altitude that could be made by the pilots during these tests was about 50 feet. The pressure altitudes flown for the six airspeed sweeps are shown in figure 27. This figure was made in TRENDS by creating a Derived Counter Set using WORDSCAN, based on all counters that include "LEVEL FLT" in their description. The plot was then made in MINMAX with the pressure altitude shown as a function of counter number for Flights 84-90.

The counters for the six airspeed sweeps are tabulated in tables 30 through 35. Table 30 also includes additional flight counters that were obtained later in the test program at this same weight coefficient. Table 36 shows the same level flight counters from Flights 84 to 90, but orders them by weight coefficient and advance ratio.

The flight altitudes selected for the $C_W/\sigma = 0.08$ and 0.09 airspeed sweeps (tables 30 and 31) were computed using the VR04 rotor speed measurement. However, subsequent to these test flights, it was determined that this measurement had a –1% bias error and, therefore, the weight coefficients for these flights are slightly beneath the target values. The weight coefficients were computed using the VR05 rotor speed measurement for all subsequent flights and more accurate weight coefficients were achieved.

Table 30 also includes repeat level flight data obtained later in the program on Flights 110 and 115. In addition, counters are included that are reference conditions for tests to determine the effects of changes in the stabilator incidence and the effects of sideslip on trim (see below). The asterisk following the description for Counter 11040 indicates that this is a pseudo-counter obtained from a different time slice of a normal counter (in this case, Counter 11010). The word “HEAT” in the Counter 11512 description indicates that the aircraft’s heater was inadvertently turned on for this test point. The lowest speed point for this airspeed sweep, Counter 8524, was a hover condition. As there are no suitable ground references at the flight altitude it was necessary for the pilot to fly this hover point using the HADS low airspeed system. The maximum speed obtained for this weight coefficient, Counter 8534, was an advance ratio of 0.368. The maximum speed in this case was determined by the 30-minute power limit of the aircraft engines (Military Rated Power or MRP).

Flight conditions for $C_W/\sigma = 0.09$, table 31, were obtained in the same manner as for the lower weight coefficient, except in this case (and at all higher weight coefficients) it was not possible to obtain a hover point. The minimum advance ratio for which steady conditions were achieved was about 0.088. Attempts to fly at lower speeds resulted in a loss of vertical control, a situation referred to as “settling with power.” Records of two of the settling with power points were obtained and are discussed in section 8. The maximum speed point for this weight coefficient (Counter 8428) was an advance ratio of 0.368.

Prior to Flight 88 and the level airspeed sweep at $C_W/\sigma = 0.10$, table 32, the inboard end of the 100-pin connector used for pressure transducer wiring, was re-wired to correct a recurring problem of instrumentation shorts. Also, an “engine wash” was performed to remove dirt and other contaminants from the compressor blades. The wash is accomplished by spraying a cleaning solution into the engine inlet during a ground run. An additional 450 lbs of ballast was added to the aircraft, bringing the takeoff weight to 17,850 lbs. The minimum advance ratio for this sweep was 0.062 and the maximum was 0.355.

The airspeed sweep at $C_W/\sigma = 0.11$, table 33, required flight at 12,000 feet and it was therefore necessary to install an oxygen system in the aircraft for the use of the pilots and test engineer. The oxygen system added 85 lbs to the aircraft weight and was strapped down to the aircraft floor adjacent to the flight test engineer’s station. The minimum advance ratio for this flight was 0.076 and the maximum was 0.337.

The two highest weight coefficient airspeed sweeps, $C_W/\sigma = 0.12$ and 0.13 (tables 34 and 35), were both obtained on Flight 90. Again, as with Flight 89, supplementary oxygen was used by the crew. The $C_W/\sigma = 0.13$ airspeed sweep was flown first, requiring a flight altitude of 17,100 feet. The minimum advance ratio for this sweep was 0.066 and the maximum was 0.236. For $C_W/\sigma = 0.12$ the minimum advance ratio was 0.080 and the maximum was 0.296.

Power coefficient data for the UH–60A were calculated based on the measurement of the engine output shaft torque from both engines, rather than the main rotor torque. Therefore, this coefficient includes main rotor power, tail rotor power, aircraft system power, and all losses. The power coefficient data obtained during the six airspeed sweeps are shown in figure 28. These data are average values calculated in VIEW in TRENDS. For comparison, power coefficients calculated from data obtained in tests of the first-year production aircraft (ref. 24), the sixth-year production aircraft (refs. 16 and 27), and the 12th-year production aircraft (ref. 28) by the U.S. Army Aviation Engineering Flight Activity (AEFA) are also shown. The power coefficient data from these earlier tests have been corrected so that the data are comparable to the Airloads Program baseline, as discussed below. The power coefficient data in these reports are provided graphically and two different approaches have been used in the development of these data. In the first approach (refs. 25 and 27), the power coefficient is defined as

$$C_P = C_{P_1}(C_T, \mu, N_r/\sqrt{\theta}) + C_{P_\beta} + C_{P_{cg}} + C_{P_D} \tag{1}$$

where C_{P_1} is the power coefficient determined from graphs in these reports and is a function of the thrust coefficient C_T, the advance ratio μ, and rotor speed divided by the square root of the temperature ratio θ. The power coefficient C_{P_1}, in these references, is provided for an aircraft flying at zero sideslip. Corrections are then added to Eq. (1) for the effects of flying at non-zero sideslip C_{P_β}, for flight at a c.g. other than the one tested, $C_{P_{cg}}$, and for the effects of drag changes to the aircraft C_{P_D}. The second approach (refs. 16 and 28) defines the power coefficient as

$$C_P = C_{P_2}(C_T, \mu) + C_{P_{cg}} + C_{P_D} \tag{2}$$

In this approach C_{P_2} is the power coefficient obtained at a single rotor speed and in ball-centered flight. As the test data are obtained in ball-centered flight, there is no sideslip correction. The correction terms for c.g. changes and drag configuration are the same as in the first approach.

The first approach used by AEFA, where the power coefficient's dependency on rotor speed is included, allows direct comparison with flight test measurements over a wide range of rotor speeds. Thus, the power coefficient data of references 25 and 27 are suitable for comparison with the Airloads Program data. However, the power coefficient data from the second approach used by AEFA are for a single rotor speed and, hence, there is no correction for rotor speed variation. In the Airloads Program, the referred rotor speed varied from 254.1 rpm to 267.0 rpm, as shown in table 37. The average rotor speed at the three lower weight coefficients was within one and a half

percent of the nominal rotor speed of 258 rpm. As the rotor speed corrections are fairly small, it is assumed that the data sets of references 16 and 28 can be used to compare with the Airloads data at the three lower weight coefficients. However, at the higher weight coefficients, these data sets have not been used.

The power coefficients for the first approach, Eq. (1), are computed for the aircraft at zero sideslip. A correction term, C_{P_β}, is then used to account for ball-centered flight (non-zero sideslip). The correction term is based on an "inherent sideslip angle" which is a function of airspeed (ref. 27) or airspeed and thrust (ref. 29). A change in flat-plate drag is determined as a function of the inherent sideslip angle and is the basis for the correction. The inherent sideslip angles from references 27 and 29 for the Airloads Program conditions are shown in figure 29. For comparison, the measured sideslip angles for the six airspeed sweeps are also shown. These sideslip angles are average values computed in VIEW in TRENDS. For C_W/σ above 0.09, the inherent sideslip angle for the first-year aircraft is more negative than for the sixth-year aircraft. The latter angles show generally good agreement with the Airloads Program data, particularly for $\mu \geq 0.2$.

The power coefficient correction, $C_{P_{cg}}$, accounts for the effect of aircraft pitch attitude, as affected by aircraft c.g., on the configuration drag. The data reported in references 25, 27, and 28 was obtained at a forward c.g. (Sta. 347). However, the reference 16 tests and the Airloads Program were both flown with an aft c.g. (Sta. 361). At higher speeds the more nose-up attitude that occurs with an aft c.g. causes a reduction in negative angle of attack for the fuselage and therefore reduced drag. The reduction in drag for these conditions is equivalent to –2.0 ft^2 (ref. 16), and this value was used for the power coefficient correction for the coefficient data obtained with a forward c.g.

The aircraft drag configuration for each of the AEFA data sets is different, as is the drag configuration of the Airloads Program vehicle. For the power comparison shown in figure 28, flat plate drag corrections, C_{P_D}, have been added to each of the AEFA data sets to match the Airloads aircraft. Table 38 lists the flat plate area corrections that were used for each of these data sets. The Extended Stores Support System (ESSS) was added to the UH–60A between the first- and sixth-year production aircraft. The attachment points for the ESSS extend outside of the original aircraft contour, and fairings have been added that increase the aircraft drag. An estimate of 2.5 ft^2 was established by the testing reported in reference 26. The sixth-year production aircraft was tested with mounting brackets for the AN/ALQ-144(V) infrared countermeasures set and the M-130 chaff/flare dispenser installed. However, these brackets were not installed for the first-year and 12th-year tests, and were removed from the sixth-year aircraft prior to its transfer to NASA Ames Research Center. The drag of these components was estimated in reference 27. A number of external modifications were made between the first- and sixth-year production aircraft (ref. 27) including streamlining of the bifilar weights, the addition of an ice detector probe on the righthand nacelle, and the installation of an OAT sensor on the middle front window. Although drag comparisons between the first- and sixth-year aircraft were not entirely consistent, a drag increment of about 1.0 ft^2 was established by reference 27 to account for these miscellaneous changes.

A wire strike protection system was added to the UH–60A on the 12th-year production aircraft and its effect on drag was estimated to be 1.0 ft^2 (ref. 28). This system has been subsequently retrofitted to the UH–60A fleet and the retrofit was made to the Airloads Program ship prior to the

testing reported here. A number of other changes occurred between the sixth- and 12th-year aircraft and these include the Hover Infrared Suppression System (HIRSS), an extended sponson, and a number of miscellaneous changes (ref. 28). Based on the testing reported in reference 28, the drag increment for the HIRSS is considered to be 2.0 ft^2 while miscellaneous changes are accommodated with an additional 0.5 ft^2. With the 12th-year aircraft, the vibration absorber in the upper rear of the cabin was removed and two roll vibration absorbers were installed in the sponsons on either side of the aircraft. To accommodate the new absorbers the sponsons were extended about 4.75 in. on each side. This increased the aircraft's projected area by about 0.76 ft^2. The Airloads Program aircraft did not have an HIRSS installed nor had the sponsons been modified. In addition, it is assumed that the miscellaneous drag increments of reference 28 do not apply to the aircraft as tested.

The present aircraft, S/N 82-23748, was also tested at AEFA during an initial phase of the Airloads Project (ref. 16). For those tests, two sets of Blade Motion Hardware (BMH) were installed on the aircraft to measure the blade root angle motions, and a Low Airspeed Sensing and Indicating Equipment (LASSIE), made by Elliot, was placed on the right side of the aircraft in place of an FM antenna. The drag increment caused by this special purpose instrumentation was estimated to be 2.0 ft^2 (ref. 16). The standard test boom and other instrumentation used in all of the AEFA tests are considered to cause a drag increment of 0.833 ft^2.

The power supplies, amplifiers, and signal conditioners for the rotor measurements made during the Airloads Program were installed in a cylindrical structure referred to as the Rotating Data Acquisition System (RDAS). The RDAS, as installed on the Airloads Program UH–60A, is shown in figure 30. The projected area of the RDAS structure is 2.81 ft^2 and this drag increment has been added to all of the AEFA test data.

Figure 28 shows that as the weight coefficient increases there is a general trend toward increased scatter in the Airloads data, as well as between the various AEFA data sets. For $C_W/\sigma = 0.08$ to 0.10, little scatter is seen in the data, and the power coefficients calculated from the AEFA data sets show very good agreement with each other but are offset from the Airloads data. The Airloads power coefficients are about 0.0003 higher than the AEFA data and this appears to be consistent over the full advance ratio range. The independence of this offset with advance ratio suggests that it is caused by an increase in profile power. Although aircraft instrumentation near the blade root spoils the aerodynamic contour, it seems unlikely that this would cause such a large change in the profile power.

Increased scatter is seen in the data at the higher weight coefficients, and only two of the AEFA data sets have been used because of the rotor speed deviation from the AEFA data sets. The Airloads Program data generally show good agreement with the AEFA power coefficients at $C_W/\sigma = 0.11$ and 0.12, at least within the uncertainty of the AEFA data. At $C_W/\sigma = 0.13$, however, an advance ratio offset is seen between the Airloads Program coefficients and those calculated from the reference 25 data.

Blade pressure measurements have been extracted from TRENDS using the OUTDATA utility, and the measurements have been converted from the time base in TRENDS to an azimuth base using azimuth encoder values in AZIM. The pressures in this derived data base have been integrated to provide normal force and pitching moment. The normal force and moment are shown in figures 31

and 32 at the maximum airspeed for each of the airspeed sweeps. These values are only shown for the six outboard stations. At high speed, the normal force becomes negative for blade azimuths around 135 deg. With an increase in rotor thrust, the extent of this negative loading region is reduced. At $C_W/\sigma = 0.13$, the pitching moment data show two negative moment spikes in the fourth quadrant that are caused by shedding of leading edge vortices on the outer portion of the blade, that is, dynamic stall (ref. 12). The extent of the dynamic stall is reduced at $C_W/\sigma = 0.12$ and, at $C_W/\sigma = 0.11$, there is only a slight indication of stall at 0.865R.

A number of repeat level flight performance points were obtained towards the end of the flight test program on Flights 110 and 115 (see fig. 28(a) and table 30). To install the pressure transducers near the leading edge, it was necessary to etch oval cutouts in the titanium leading edge sheath at the transducer locations. Later, these areas were filled with potting compound. Over the course of the flight program, erosion was observed near the leading edge, as shown in figure 33. The pipette of the most forward transducer, at 0.010c, protruded from the blade material by about 0.020 inches, indicating the loss of at least this much material at this location. Substantially less erosion was observed at 0.030c and 0.049c. Figure 34 compares the repeat points from Flights 110 and 115 with the baseline data obtained on Flight 85. As discussed previously, the average C_W/σ for Flight 85 was about 1% low because of the bias error in the VR04 rotor speed measurement. A curve has been faired through the Flight 85 data, and this faired curve has been adjusted to represent a $C_W/\sigma = 0.080$ value to provide a reference for the Flight 110 and 115 data. The repeat data obtained on Flight 110 show differences in power ranging from –3.6% to +3.5%. The root-mean-square error for the six repeat points is 2.4%. The boom static pressure measurement failed on Flight 115, and the aircraft static pressure has been used to reduce the flight data. The Flight 115 repeat data show less satisfactory agreement with the baseline data than observed for Flight 110. It may be that the reduced accuracy of the aircraft static pressure measurement is the primary cause of the larger differences.

Acoustic Data

The procedures used in ground-acoustic and inflight-acoustic tests have been previously discussed in section 2. The primary objective of the ground-acoustic testing was to obtain steady flight over a microphone array laid out on the Crows Landing runway (see fig. 4). Flight conditions included climbs, descents, and level flight with the aircraft passing 250 feet above the center point of the array.

A two-step data reduction process was used for the ground-acoustic data. In the first step, the aircraft data from the full flight record were reduced and placed in the BH2 data base with a prefix-4 added to the counter number. Tracking data from laser and radar trackers were then combined with the prefix-4 counters. In the second step, time slices were selected from the prefix-4 data and the data were reduced a second time to include the rotor data. In this second step, Ames personnel generally selected a steady, five-second time slice, using the same criteria as for other flight cases. These slices were installed in the BH2 data base. Langley personnel selected time slices using different criteria to be correlated with their acoustic data base. These slices were also reduced a second time and were placed in the BHL data base as discussed in section 9. The level flight prefix-

4 counters are listed in table 39. The time slices used for counters for the BH2 data base are shown in table 40 and a list of the BH2 data base counters is given in table 41.

For level flight, repeat conditions were obtained as indicated in figure 26(b). The tracking data are shown in figure 35, which shows the vertical and lateral track as a function of the horizontal track. These data have been extracted from TRENDS using the OUTDATA utility and have been post-processed to provide x-, y-, and z-position on a per rev basis. The vertical and lateral track have a 20X exaggeration in the figure. Vertical flightpath reference angles (γ) and lateral flightpath reference angles (ψ) are shown on the figure. It is apparent that some of the ground-acoustic level flight conditions have small flightpath errors relative to level, straight-ahead flight. Some of these counters show climb or descent angles of two or three degrees and do not represent a true level flight condition. The lateral flightpath errors in the Ames data base, however, are considered unimportant.

The vertical flightpath angles and their variance are quantified in table 42 which shows the flightpath angle based on the laser tracking data and the standard error of estimate of the regression fit. The small errors in this case show that the flight data are steady although in some cases there is a slight climb or descent angle. Also in this table are the tip-path-plane angles and an estimate of variance based on the standard deviation of the tip-path-plane calculated on a per/rev basis over the length of the flight record. The variance in tip-path-plane angle is generally less than a degree for these level flight cases.

Inflight acoustic data were obtained for a limited airspeed range as compared to the ground-acoustic tests. This restricted airspeed range was governed primarily by flight envelope limitations of the YO–3A, which was used as an airborne microphone platform. Most of the inflight acoustic data were obtained in descending flight, but four points were for level flight conditions, as indicated in figure 28(b) and listed in table 43.

Airspeed Calibration

Airspeed calibration data were obtained in level flight except for the highest speed points. As discussed previously in section 3, three different types of airspeed calibrations were performed: (1) a high-speed calibration using a specially calibrated T–34 airplane; (2) a low-speed calibration using a pace car; and (3) a low-speed calibration using the laser tracking instrumentation at the Crows Landing airfield. Figure 28c shows the range of weight coefficients and advance ratio used for these calibrations. The relevant counters for these calibrations are shown in tables 5–7.

Housekeeping Points

Housekeeping points were obtained on most flights for nominal OGE hover conditions and at 80 knots. Figure 26(d) shows the two groups of housekeeping points in terms of weight coefficient and advance ratio. The use of these housekeeping points has been previously discussed in section 4. Considerable scatter is observed in the housekeeping points and this is expected. As discussed in section 4, there was variation in aircraft weight, particularly between housekeeping points at the

beginning and the end of a flight. In addition, points were obtained at a constant altitude regardless of temperature, which resulted in variations caused by density differences. The housekeeping point counters are shown in tables 10 and 11.

Rotor Speed Sweeps

Level flight data were obtained for rotor speed variations at four flight speeds including hover. The normal rotor speed operating range for the UH–60A is from 95 to 101% nominal speed. The rotor speed controller was adjusted for these tests to allow data to be obtained from 96 to 104% in 2% increments. The data were acquired at constant altitude and, therefore, the weight coefficient and advance ratio vary as rotor speed is changed, as shown in figure 28(e). The variable rotor speed flight counters are tabulated in table 44.

The primary effect of rotor speed variation is to change the rotor blade excitation frequency relative to the blade and fixed system natural frequencies. Although this ±4% frequency variation is relatively small, it does have a measurable effect on aircraft vibration. Figure 36 shows the rotor hub vertical vibration as a function of the rotor speed for the four airspeeds that were tested. The hub accelerometer is in the rotating system and is mounted within the RDAS container or "bucket." The vibration shown in figure 36 is the oscillatory or half peak-to-peak vibration and includes all harmonics. In general, the vibration gets worse for rotor speeds above 100%, and lessens at the lower rotor speeds. These oscillatory data were extracted from TRENDS using MINMAX by specifying AH0Z.AVO as the dependent parameter. A Derived Counter Set (DCS) was created by searching WORDSCAN for "NR" in the counter descriptions, and this DCS was used to define the output counters.

Stabilator Angle Sweep

The incidence of the stabilator on the UH–60A is varied to enhance the aircraft's handling qualities and to reduce changes in pitch attitude at various airspeeds. The incidence range of the stabilator is –10 to +40 deg. The stabilator incidence is controlled automatically depending upon airspeed, collective stick position, pitch rate, and lateral acceleration. The greatest effect on stabilator incidence is the airspeed, with the stabilator set at 30 to 38 deg in hover and at low speed to avoid pitch-up effects from the rotor downwash on the stabilator. The stabilator incidence is reduced to approximately zero deg from $\mu = 0.1$ to 0.2. The pilot can override the scheduled stabilator incidence and manually position the stabilator. The stabilator angle measured during the six level flight airspeed sweeps discussed previously is shown in figure 37. The average angles shown in the figure were extracted from TRENDS using VIEW.

The effect of stabilator angle variation was investigated at an advance ratio of 0.27. The pilot varied the angle from about –5 to +5 deg. A number of aircraft measurements are shown as a function of the stabilator angle in figure 38. The associated counters are listed in table 45. The flapping angle in figure 38(d) was obtained from TRENDS using HARMONIC. The oscillatory flap bending moment and the 4/rev cockpit vibration were obtained using MINMAX after defining a

Derived Counter Set using WORDSCAN. The remainder of the values were calculated in VIEW. For the nominal condition, with the stabilator incidence near zero degrees, there are about three degrees of blade flapping. Most of the flapping is positive cosine flapping, so the blade is flapping up at the rear of the aircraft and down at the nose, causing a nose-down pitching moment on the aircraft. The oscillatory shaft bending moment for this condition is largely 1/rev and also shows a nose-down pitching moment. An increase in the stabilator angle of attack increases the stabilator lift, which in turn causes a negative pitching moment on the aircraft. To balance the aircraft pitching moment, the pilot pulls back on the longitudinal stick which reduces the blade cosine flapping as well as the main rotor shaft bending moment. The effect of the moment shift between the stabilator and the main rotor causes the aircraft's pitch attitude to become more nose down. The relationships shown in figure 38(b) between stabilator incidence, rotor hub moment, longitudinal control position, and pitch attitude are approximately linear. The rotor oscillatory flap bending moment measured at 0.50*R* in figure 38(e) also appears to depend on the stabilator angle, although the dependency is slightly nonlinear. However, the pilot and co-pilot vertical vibration show little influence of the stabilator incidence.

Roll Angle/Sideslip Comparison

At low speed there is no direct control for the helicopter roll attitude. Thus, on lift off to hover, the trim roll attitude will depend upon the roll moment of the rotor, the lateral c.g., and tail rotor thrust. The combination of these roll moments may result in a non-zero roll attitude, which will be felt by the pilot as a slight lateral acceleration. As the aircraft is accelerated to normal flight speeds it is possible to reduce the roll angle to near zero by allowing a small amount of sideslip to induce a correcting roll moment through the aircraft's static dihedral. Flight with a zero roll attitude results in zero lateral acceleration on the pilot, and as the ball in the turn coordinator is centered, this is referred to as ball-centered flight. Generally a pilot will fly ball-centered as it is more comfortable. If the sideslip angle is more than a degree or two, however, it can create an increase in aircraft drag. This effect was investigated for the Airloads Program by flying a number of repeat points, first in ball-centered flight, and then with zero sideslip. This was feasible with the Airloads aircraft as there was a readout in the cockpit of the sideslip angle measured by the yaw vane on the test boom. The three pairs of roll angle/sideslip conditions are shown in table 46. The measured roll and sideslip angles are listed in table 47.

For the airspeed pair obtained at 35 knots, the measured roll angle is 1.2 to 1.3 deg. With the application of the pedals, the pilot was able to reduce the sideslip from 5.9 to 0.0 deg. However, at this low speed the aircraft static dihedral is ineffective and the roll angle was not reduced. At 85 knots, the residual roll angle was 0.7 deg in ball-centered flight and the sideslip angle was –4.0 deg. The pilot reduced this sideslip to –0.6 deg and this increased the roll angle to 2.0 deg. At the highest speed cases at 109 knots, the residual roll angle in ball-centered flight was only –0.6 deg with a sideslip angle of –4.6 deg. The pilot reduced the sideslip to –0.6 deg which increased the roll angle, slightly, to 1.0 deg. The power coefficients for these three cases are compared with a baseline faired curve in figure 39. Although slight changes in power were measured as the sideslip angle was reduced, these changes are not consistent. At 85 knots the power decreased 2.1% at zero sideslip, while at 109 knots it increased by 3.0%.

Turbulence Cases

Normally, test data were obtained during the Airloads Program for still air conditions. When turbulence was encountered, generally later in the day, the testing was terminated and the aircraft returned to Moffett Field. This situation occurred on Flight 106 and the decision was made to acquire limited turbulence data on the return flight to Moffett Field. The effect of turbulence was accentuated by flying at lower elevations over the Diablo Range. Five data records were obtained, including one of 20 sec. These counters are listed in table 48.

The 4/rev vertical acceleration, as measured on the rotating hub and at the pilot's seat, is shown in figure 40 as a function of advance ratio. Accelerometer data obtained on Flight 85 is shown for airspeeds from near hover to the maximum level flight speed, and these data represent an aircraft baseline. The acceleration increases rapidly from hover to a first peak at about $\mu = 0.09$ or 0.10 and then moderates until it starts to increase once again at high speed. The first peak in acceleration is caused by rotor wake effects in low-speed flight, while the vibration at high speed is caused by the large velocity variation as the blade travels around the rotor disk. The data for the Flight 106 turbulence cases are included in this figure and show about a 50% increase in aircraft vibration. The data shown in figure 40 were plotted in TRENDS using the MULTIPLOT utility. The level flight data from Flight 85 and the turbulence data from Flight 106 were treated as separate Derived Counters Sets.

Table 30.– Level flight airspeed sweep; $C_W/\sigma = 0.08$.

FLIGHT	COUNTER	DESCRIPTION	DURATION
85	8511	LEVEL FLT, 75 KIASB, CWS=.08	4.99 Seconds
85	8512	LEVEL FLT, 65 KIASB, CWS=.08	4.99 Seconds
85	8513	LEVEL FLT, 55 KIASB, CWS=.08	4.99 Seconds
85	8514	LEVEL FLT, 45 KIASB, CWS=.08	4.99 Seconds
85	8515	LEVEL FLT, 35 KIASB, CWS=.08	4.99 Seconds
85	8516	LEVEL FLT, 30 KIASB, CWS=.08	4.99 Seconds
85	8517	LEVEL FLT, 25 KIASB, CWS=.08	4.99 Seconds
85	8518	LEVEL FLT, 24 KIASB, CWS=.08	4.99 Seconds
85	8519	LEVEL FLT, 21 KIASB, CWS=.08	4.99 Seconds
85	8520	LEVEL FLT, 15 KIASH, CWS=.08	4.99 Seconds
85	8521	LEVEL FLT, 10 KIASH, CWS=.08	4.99 Seconds
85	8522	LEVEL FLT, 5 KIASH, CWS=.08	4.99 Seconds
85	8524	HOVER, 0 KIASH, CWS=.08	4.99 Seconds
85	8525	LEVEL FLT, 85 KIASB, CWS=.08	4.99 Seconds
85	8526	LEVEL FLT, 95 KIASB, CWS=.08	4.99 Seconds
85	8527	LEVEL FLT, 106 KIASB, CWS=.08	4.99 Seconds
85	8528	LEVEL FLT, 115 KIASB, CWS=.08	4.99 Seconds
85	8529	LEVEL FLT, 119 KIASB, CWS=.08	4.99 Seconds
85	8530	LEVEL FLT, 123 KIASB, CWS=.08	4.99 Seconds
85	8531	LEVEL FLT, 127 KIASB, CWS=.08	4.99 Seconds
85	8532	LEVEL FLT, 131 KIASB, CWS=.08	4.99 Seconds
85	8533	LEVEL FLT, 135 KIASB, CWS=.08	4.98 Seconds
85	8534	LEVEL FLT, 138 KIASB, CWS=.08	4.99 Seconds
110	11006	LEVEL FLT, 75 KIASB, CWS=.08	4.99 Seconds
110	11007	LEVEL FLT, 25 KIASB, CWS=.08	4.99 Seconds
110	11008	HOVER, CWS=.08	4.99 Seconds
110	11009	LEVEL FLT, 85 KIASB, CWS=.08	4.99 Seconds
110	11010	LEVEL FLT, 109 KIASB, CWS=.08	4.99 Seconds
110	11012	LEVEL FLT, 135 KIASB, CWS=.08	4.99 Seconds
110	11013	LEVEL FLT, 138 KIASB, CWS=.08	9.99 Seconds
110	11040	LEVEL FLT, 109 KIASB, CWS=.08*	2.59 Seconds
115	11512	LEVEL, 75 KIASB, CWS=.08, (HEAT)	4.99 Seconds
115	11513	LEVEL, 75 KIASB, CWS=.08	4.99 Seconds
115	11514	LEVEL, 35 KIASB, CWS=.08	4.99 Seconds
115	11516	LEVEL, 85 KIASB, CWS=.08	4.99 Seconds
115	11518	LEV, 100 KIASB, CWS=.08, STAB 0.0	4.99 Seconds

Table 31.– Level flight airspeed sweep; $C_W/\sigma = 0.09$.

FLIGHT	COUNTER	DESCRIPTION	DURATION
84	8413	LEVEL FLT, 75 KIASB, CWS=.09	4.99 Seconds
84	8414	LEVEL FLT, 65 KIASB, CWS=.09	9.99 Seconds
84	8415	LEVEL FLT, 55 KIASB, CWS=.09	4.99 Seconds
84	8416	LEVEL FLT, 45 KIASB, CWS=.09	4.99 Seconds
84	8417	LEVEL FLT, 35 KIASB, CWS=.09	4.99 Seconds
84	8418	LEVEL FLT, 26 KIASH, CWS=.09	4.99 Seconds
84	8419	LEVEL FLT, 30 KIASH, CWS=.09	4.99 Seconds
84	8420	LEVEL FLT, 20 KIASH, CWS=.09	4.99 Seconds
84	8422	LEVEL FLT, 83 KIASB, CWS=.09	4.99 Seconds
84	8423	LEVEL FLT, 96 KIASB, CWS=.09	9.99 Seconds
84	8424	LEVEL FLT, 107 KIASB, CWS=.09	4.99 Seconds
84	8425	LEVEL FLT, 115 KIASB, CWS=.09	4.99 Seconds
84	8426	LEVEL FLT, 120 KIASB, CWS=.09	14.99 Seconds
84	8427	LEVEL FLT, 123 KIASB, CWS=.09	4.99 Seconds
84	8428	LEVEL FLT, 127 KIASB, CWS=.09	4.99 Seconds
84	8429	LEVEL FLT, 127 KIASB, CWS=.09	9.99 Seconds
84	8430	LEVEL FLT, 77 KIASB, CWS=.09	4.99 Seconds

Table 32.– Level flight airspeed sweep; $C_W/\sigma = 0.10$.

FLIGHT	COUNTER	DESCRIPTION	DURATION
88	8806	LEVEL FLT, 70 KIASB, CWS=.10	4.99 Seconds
88	8807	LEVEL FLT, 63 KIASB, CWS=.10	4.99 Seconds
88	8808	LEVEL FLT, 54 KIASB, CWS=.10	4.99 Seconds
88	8809	LEVEL FLT, 44 KIASB, CWS=.10	4.99 Seconds
88	8810	LEVEL FLT, 35 KIASB, CWS=.10	4.99 Seconds
88	8812	LEVEL FLT, 30 KIASB, CWS=.10	4.99 Seconds
88	8813	LEVEL FLT, 25 KIASB, CWS=.10	5.19 Seconds
88	8814	LEVEL FLT, 20 KIASB, CWS=.10	4.99 Seconds
88	8815	LEVEL FLT, 15 KIASB, CWS=.10	4.99 Seconds
88	8817	LEVEL FLT, 74 KIASB, CWS=.10	5.00 Seconds
88	8818	LEVEL FLT, 84 KIASB, CWS=.10	4.99 Seconds
88	8819	LEVEL FLT, 97 KIASB, CWS=.10	9.99 Seconds
88	8820	LEVEL FLT, 105 KIASB, CWS=.10	4.99 Seconds
88	8821	LEVEL FLT, 114 KIASB, CWS=.10	4.99 Seconds
88	8822	LEVEL FLT, 119 KIASB, CWS=.10	9.99 Seconds
88	8823	LEVEL FLT, 123 KIASB, CWS=.10	4.99 Seconds

Table 33.– Level flight airspeed sweep; $C_W/\sigma = 0.11$.

FLIGHT	COUNTER	DESCRIPTION	DURATION
88	8827	LEVEL FLT, 75 KIASB, CWS=.11	3.82 Seconds
89	8906	LEVEL FLT, 75 KIASB, CWS=.11	5.99 Seconds
89	8907	LEVEL FLT, 65 KIASB, CWS=.11	5.99 Seconds
89	8908	LEVEL FLT, 55 KIASB, CWS=.11	5.99 Seconds
89	8909	LEVEL FLT, 46 KIASB, CWS=.11	10.99 Seconds
89	8910	LEVEL FLT, 35 KIASB, CWS=.11	10.99 Seconds
89	8911	LEVEL FLT, 31 KIASB, CWS=.11	5.99 Seconds
89	8912	LEVEL FLT, 24 KIASB, CWS=.11	10.9 Seconds
89	8913	LEVEL FLT, 20 KIASB, CWS=.11	20.99 Seconds
89	8914	LEVEL FLT, 75 KIASB, CWS=.11	5.99 Seconds
89	8915	LEVEL FLT, 85 KIASB, CWS=.11	5.99 Seconds
89	8916	LEVEL FLT, 96 KIASB, CWS=.11	4.51 Seconds
89	8917	LEVEL FLT, 105 KIASB, CWS=.11	5.99 Seconds
89	8918	LEVEL FLT, 109 KIASB, CWS=.11	5.99 Seconds
89	8919	LEVEL FLT, 101 KIASB, CWS=.11	5.99 Seconds

Table 34.– Level flight airspeed sweep; $C_W/\sigma = 0.12$.

FLIGHT	COUNTER	DESCRIPTION	DURATION
90	9020	LEVEL FLT, 75 KIASB, CWS=.12	4.99 Seconds
90	9021	LEVEL FLT, 64 KIASB, CWS=.12	4.99 Seconds
90	9022	LEVEL FLT, 54 KIASB, CWS=.12	4.99 Seconds
90	9023	LEVEL FLT, 45 KIASB, CWS=.12	5.00 Seconds
90	9024	LEVEL FLT, 36 KIASB, CWS=.12	4.99 Seconds
90	9025	LEVEL FLT, 31 KIASB, CWS=.12	4.99 Seconds
90	9026	LEVEL FLT, 24 KIASB, CWS=.12	4.99 Seconds
90	9027	LEVEL FLT, 20 KIASB, CWS=.12	4.99 Seconds
90	9028	LEVEL FLT, 77 KIASB, CWS=.12	4.99 Seconds
90	9029	LEVEL FLT, 87 KIASB, CWS=.12	4.99 Seconds
90	9030	LEVEL FLT, 90 KIASB, CWS=.12	11.01 Seconds

Table 35.– Level flight airspeed sweep; $C_W/\sigma = 0.13$.

FLIGHT	COUNTER	DESCRIPTION	DURATION
90	9011	LEVEL FLT, 68 KIASB, CWS=.13	4.99 Seconds
90	9012	LEVEL FLT, 64 KIASB, CWS=.13	4.99 Seconds
90	9013	LEVEL FLT, 52 KIASB, CWS=.13	4.99 Seconds
90	9014	LEVEL FLT, 45 KIASB, CWS=.13	4.99 Seconds
90	9015	LEVEL FLT, 33 KIASB, CWS=.13	4.99 Seconds
90	9016	LEVEL FLT, 28 KIASB, CWS=.13	4.99 Seconds
90	9017	LEVEL FLT, 69 KIASB, CWS=.13	4.99 Seconds

Table 36.– Level flight counters sorted by weight coefficient and advance ratio (continued).

COUNTER	DESCRIPTION	C_W/σ	μ
8524	HOVER, 0 KIASH, CWS=.08	0.0792	0.000
8521	LEVEL FLT, 10 KIASH, CWS=.08	0.0792	0.055
8520	LEVEL FLT, 15 KIASH, CWS=.08	0.0791	0.057
8522	LEVEL FLT, 5 KIASH, CWS=.08	0.0791	0.062
8519	LEVEL FLT, 21 KIASB, CWS=.08	0.0789	0.076
8518	LEVEL FLT, 24 KIASB, CWS=.08	0.0791	0.088
8517	LEVEL FLT, 25 KIASB, CWS=.08	0.0789	0.091
8516	LEVEL FLT, 30 KIASB, CWS=.08	0.0791	0.093
8515	LEVEL FLT, 35 KIASB, CWS=.08	0.0789	0.110
8514	LEVEL FLT, 45 KIASB, CWS=.08	0.0789	0.129
8513	LEVEL FLT, 55 KIASB, CWS=.08	0.0792	0.149
8512	LEVEL FLT, 65 KIASB, CWS=.08	0.0797	0.178
8511	LEVEL FLT, 75 KIASB, CWS=.08	0.0794	0.205
8525	LEVEL FLT, 85 KIASB, CWS=.08	0.0789	0.232
8526	LEVEL FLT, 95 KIASB, CWS=.08	0.0789	0.260
8527	LEVEL FLT, 106 KIASB, CWS=.08	0.0788	0.286
8528	LEVEL FLT, 115 KIASB, CWS=.08	0.0791	0.308
8529	LEVEL FLT, 119 KIASB, CWS=.08	0.0789	0.317
8530	LEVEL FLT, 123 KIASB, CWS=.08	0.0792	0.329
8531	LEVEL FLT, 127 KIASB, CWS=.08	0.0792	0.340
8532	LEVEL FLT, 131 KIASB, CWS=.08	0.0792	0.351
8533	LEVEL FLT, 135 KIASB, CWS=.08	0.0787	0.360
8534	LEVEL FLT, 138 KIASB, CWS=.08	0.0788	0.368
8420	LEVEL FLT, 20 KIASH, CWS=.09	0.0892	0.088
8418	LEVEL FLT, 26 KIASH, CWS=.09	0.0893	0.091
8419	LEVEL FLT, 30 KIASH, CWS=.09	0.0890	0.106
8417	LEVEL FLT, 35 KIASB, CWS=.09	0.0890	0.113
8416	LEVEL FLT, 45 KIASB, CWS=.09	0.0892	0.137
8415	LEVEL FLT, 55 KIASB, CWS=.09	0.0896	0.162
8414	LEVEL FLT, 65 KIASB, CWS=.09	0.0895	0.192
8413	LEVEL FLT, 75 KIASB, CWS=.09	0.0892	0.217
8430	LEVEL FLT, 77 KIASB, CWS=.09	0.0891	0.227
8422	LEVEL FLT, 83 KIASB, CWS=.09	0.0892	0.242
8423	LEVEL FLT, 96 KIASB, CWS=.09	0.0890	0.276
8424	LEVEL FLT, 107 KIASB, CWS=.09	0.0889	0.304
8425	LEVEL FLT, 115 KIASB, CWS=.09	0.0889	0.327
8426	LEVEL FLT, 120 KIASB, CWS=.09	0.0889	0.341
8427	LEVEL FLT, 123 KIASB, CWS=.09	0.0890	0.350
8429	LEVEL FLT, 127 KIASB, CWS=.09	0.0890	0.361
8428	LEVEL FLT, 127 KIASB, CWS=.09	0.0887	0.362
8815	LEVEL FLT, 15 KIASB, CWS=.10	0.1014	0.062
8814	LEVEL FLT, 20 KIASB, CWS=.10	0.1008	0.075
8813	LEVEL FLT, 25 KIASB, CWS=.10	0.1012	0.088
8812	LEVEL FLT, 30 KIASB, CWS=.10	0.1016	0.102
8810	LEVEL FLT, 35 KIASB, CWS=.10	0.1004	0.112

Table 36.– Level flight counters sorted by weight coefficient and advance ratio (concluded).

COUNTER	DESCRIPTION	C_W/σ	μ
8809	LEVEL FLT, 44 KIASB, CWS=.10	0.1002	0.130
8808	LEVEL FLT, 54 KIASB, CWS=.10	0.1003	0.164
8807	LEVEL FLT, 63 KIASB, CWS=.10	0.1001	0.190
8806	LEVEL FLT, 70 KIASB, CWS=.10	0.0999	0.204
8817	LEVEL FLT, 74 KIASB, CWS=.10	0.1013	0.222
8818	LEVEL FLT, 84 KIASB, CWS=.10	0.1013	0.256
8819	LEVEL FLT, 97 KIASB, CWS=.10	0.1014	0.289
8820	LEVEL FLT, 105 KIASB, CWS=.10	0.1015	0.312
8821	LEVEL FLT, 114 KIASB, CWS=.10	0.1006	0.335
8822	LEVEL FLT, 119 KIASB, CWS=.10	0.1004	0.349
8823	LEVEL FLT, 123 KIASB, CWS=.10	0.1008	0.355
8913	LEVEL FLT, 20 KIASB, CWS=.11	0.1131	0.076
8912	LEVEL FLT, 24 KIASB, CWS=.11	0.1102	0.089
8911	LEVEL FLT, 31 KIASB, CWS=.11	0.1100	0.106
8910	LEVEL FLT, 35 KIASB, CWS=.11	0.1095	0.111
8909	LEVEL FLT, 46 KIASB, CWS=.11	0.1093	0.145
8908	LEVEL FLT, 55 KIASB, CWS=.11	0.1092	0.173
8907	LEVEL FLT, 65 KIASB, CWS=.11	0.1095	0.204
8827	LEVEL FLT, 75 KIASB, CWS=.11	0.1123	0.221
8906	LEVEL FLT, 75 KIASB, CWS=.11	0.1094	0.230
8914	LEVEL FLT, 75 KIASB, CWS=.11	0.1099	0.231
8915	LEVEL FLT, 85 KIASB, CWS=.11	0.1098	0.264
8916	LEVEL FLT, 96 KIASB, CWS=.11	0.1103	0.298
8919	LEVEL FLT, 101 KIASB, CWS=.11	0.1092	0.311
8917	LEVEL FLT, 105 KIASB, CWS=.11	0.1101	0.324
8918	LEVEL FLT, 109 KIASB, CWS=.11	0.1107	0.337
9027	LEVEL FLT, 20 KIASB, CWS=.12	0.1206	0.080
9026	LEVEL FLT, 24 KIASB, CWS=.12	0.1202	0.088
9025	LEVEL FLT, 31 KIASB, CWS=.12	0.1207	0.108
9024	LEVEL FLT, 36 KIASB, CWS=.12	0.1200	0.123
9023	LEVEL FLT, 45 KIASB, CWS=.12	0.1205	0.149
9022	LEVEL FLT, 54 KIASB, CWS=.12	0.1199	0.178
9021	LEVEL FLT, 64 KIASB, CWS=.12	0.1205	0.212
9020	LEVEL FLT, 75 KIASB, CWS=.12	0.1208	0.244
9028	LEVEL FLT, 77 KIASB, CWS=.12	0.1209	0.252
9029	LEVEL FLT, 87 KIASB, CWS=.12	0.1204	0.286
9030	LEVEL FLT, 90 KIASB, CWS=.12	0.1203	0.296
9016	LEVEL FLT, 28 KIASB, CWS=.13	0.1326	0.066
9015	LEVEL FLT, 33 KIASB, CWS=.13	0.1310	0.115
9014	LEVEL FLT, 45 KIASB, CWS=.13	0.1310	0.150
9013	LEVEL FLT, 52 KIASB, CWS=.13	0.1303	0.179
9012	LEVEL FLT, 64 KIASB, CWS=.13	0.1311	0.219
9011	LEVEL FLT, 68 KIASB, CWS=.13	0.1314	0.230
9017	LEVEL FLT, 69 KIASB, CWS=.13	0.1335	0.236

Table 37.– Referred rotor speeds for six airspeed sweeps.

C_T/σ	$N_r/\bullet\theta$, RPM	ERROR (NOMINAL), %
0.079	255.6	–1.0
0.089	254.1	–1.6
0.101	259.3	0.5
0.110	263.4	2.1
0.120	266.5	3.3
0.132	267.0	3.4

Table 38.– Flat plate area corrections used for power coefficient comparisons.

COMPONENT	FIRST YEAR	SIXTH YEAR		12^{TH} YEAR
	REF. 24	REF. 27	REF. 16	REF. 28
ESSS fairing	2.50	—	—	—
IR & chaff brackets	—	–1.50	–1.50	—
misc. (ref. 27)	1.00	—	—	—
wire strike	1.00	1.00	1.00	—
HIRSS	—	—	—	–2.00
extended sponson	—	—	—	–0.76
misc. (ref. 28)	—	—	—	–0.50
BMH/LASSIE	2.00	2.00	—	2.00
test instrumentation	0.83	0.83	0.83	0.83
RDAS	2.81	2.81	2.81	2.81
TOTAL	10.14	5.14	3.14	2.38

Table 39.– Level flight cases from ground-acoustic testing; prefix-4 data base.

FLIGHT	COUNTER	DESCRIPTION	DURATION
91	49104	LEVEL, 104 KIASB, RUN 140	31.69 Seconds
91	49105	LEVEL, 102 KIASB, RUN 141	31.15 Seconds
91	49106	LEVEL, 143 KIASB, RUN 160	20.98 Seconds
91	49107	LEVEL, 143 KIASB, RUN 161	28.98 Seconds
91	49114	LEVEL, 60 KIASB, RUN 120	39.40 Seconds
91	49121	LEVEL, 80 KIASB, RUN 130	35.23 Seconds
92	49204	LEVEL, 41 KIASB, RUN 110	48.20 Seconds
92	49218	LEVEL, 101 KIASB, RUN 142	26.08 Seconds
92	49219	LEVEL, 99 KIASB, RUN 143	25.92 Seconds
93	49309	LEVEL, 99 KIASB, RUN 140	26.61 Seconds
93	49310	LEVEL, 145 KIASB, RUN 160	22.25 Seconds
93	49317	LEVEL, 60 KIASB, RUN 120	32.51 Seconds
93	49325	LEVEL, 80 KIASB, RUN 130	10.69 Seconds
94	49421	LEVEL, 102 KIASB, RUN 141	22.95 Seconds
95	49505	LEVEL, 100 KIASB, RUN 141	19.13 Seconds
95	49523	LEVEL, 100 KIASB, RUN 142	23.83 Seconds
96	49615	LEVEL, 100 KIASB, RUN 141	21.22 Seconds
97	49705	LEVEL, 100 KIASB, RUN 142	15.72 Seconds
98	49810	LEVEL, 100 KIASB, RUN 140	22.77 Seconds
98	49811	LEVEL, 100 KIASB, RUN 141	21.59 Seconds
98	49813	LEV, 100 KIASB, CON.FIX, RUN 142	21.98 Seconds
98	49814	LEV, 100 KIASB, CON.FIX, RUN 143	22.11 Seconds
99	49927	LEVEL, 250', 100 KIASB, RUN 144	22.98 Seconds

Table 40.– Time slices for level flight cases in prefix-4 and BH2 data bases.

PREFIX-4 DATA BASE			BH2 DATA BASE		
COUNTER	START TIME SEC	END TIME SEC	COUNTER	START TIME SEC	END TIME SEC
49104	0.00	31.69	9104	23.68	28.68
49105	0.00	31.15	9105	19.16	24.14
49106	0.00	20.98	9106	12.93	17.92
49107	0.00	28.98	9107	4.74	9.73
49130	0.00	28.98	9130	14.74	19.73
49114	0.00	39.40	9114	4.78	9.77
49121	0.00	35.23	9121	4.82	9.82
49204	0.00	48.20	9204	34.66	39.66
49218	0.00	26.08	9218	17.25	24.24
49219	0.00	25.92	9219	14.21	19.20
49309	0.00	26.61	9309	8.00	13.00
49310	0.00	22.25	9310	1.00	7.00
49317	0.00	32.51	9317	5.01	10.00
49325	0.00	10.69	9325	0.00	5.00
49421	0.00	22.95	9421	10.01	15.00
49505	0.00	19.13	9505	7.00	12.00
49523	0.00	23.83	9523	5.01	10.00
49615	0.00	21.22	9615	5.01	10.00
49705	0.00	15.72	9705	0.00	5.00
49810	0.00	22.77	9810	10.00	15.00
49811	0.00	21.59	9811	2.01	7.00
49813	0.00	21.98	9813	1.00	6.00
49814	0.00	22.11	9814	5.01	10.00
49927	0.00	22.98	9927	9.01	14.00

Table 41.– Level flight cases from ground-acoustic testing; BH2 data base.

FLIGHT	COUNTER	DESCRIPTION	DURATION
91	9104	LEVEL, 104 KIASB, RUN 140	5.00 Seconds
91	9105	LEVEL, 102 KIASB, RUN 141	4.99 Seconds
91	9106	LEVEL, 143 KIASB, RUN 160	4.99 Seconds
91	9107	LEVEL, 143 KIASB, RUN 161	4.99 Seconds
91	9114	LEVEL, 60 KIASB, RUN 120	4.99 Seconds
91	9121	LEVEL, 80 KIASB, RUN 130	4.99 Seconds
91	9130	LEVEL, 143 KIASB, RUN 161*	4.99 Seconds
92	9204	LEVEL, 41 KIASB, RUN 110	4.99 Seconds
92	9218	LEVEL, 101 KIASB, RUN 142	6.99 Seconds
92	9219	LEVEL, 99 KIASB, RUN 143	4.99 Seconds
93	9309	LEVEL, 99 KIASB, RUN 140	4.99 Seconds
93	9310	LEVEL, 145 KIASB, RUN 160	5.99 Seconds
93	9317	LEVEL, 60 KIASB, RUN 120	4.99 Seconds
93	9325	LEVEL, 80 KIASB, RUN 130	4.99 Seconds
94	9421	LEVEL, 102 KIASB, RUN 141	4.99 Seconds
95	9505	LEVEL, 100 KIASB, RUN 141	4.99 Seconds
95	9523	LEVEL, 100 KIASB, RUN 142	4.99 Seconds
96	9615	LEVEL, 100 KIASB, RUN 141	4.99 Seconds
97	9705	LEVEL, 100 KIASB, RUN 142	5.00 Seconds
98	9810	LEVEL, 100 KIASB, RUN 140	5.00 Seconds
98	9811	LEVEL, 100 KIASB, RUN 141	4.99 Seconds
98	9813	LEV, 100 KIASB, CON.FIX, RUN 142	4.99 Seconds
98[a]	9814	LEV, 100 KIASB, CON.FIX, RUN 143	4.99 Seconds
99	9927	LEVEL, 250', 100 KIASB, RUN 144	4.99 Seconds

[a]No tracking data.

Table 42.– Flightpath angles for ground-acoustic level flight cases in Ames data base.

COUNTER	DESCRIPTION	γ DEG	$S_e(\gamma)$ DEG	α_{TPP} DEG	$\sigma(\alpha_{TPP})$, DEG
9104	LEVEL, 104 KIASB, RUN 140	–0.04	0.17	–6.18	0.68
9105	LEVEL, 102 KIASB, RUN 141	–3.23	0.34	–3.03	0.90
9106	LEVEL, 143 KIASB, RUN 160	0.07	0.07	–11.49	0.54
9107	LEVEL, 143 KIASB, RUN 161	1.59	0.09	–11.92	0.31
9114	LEVEL, 60 KIASB, RUN 120	–0.98	0.19	–2.58	0.30
9121	LEVEL, 80 KIASB, RUN 130	–0.23	0.24	–3.98	0.53
9130	LEVEL, 143 KIASB, RUN 161*	–0.83	0.04	–11.69	0.19
9204	LEVEL, 41 KIASB, RUN 110	–4.46	0.13	2.89	0.44
9218	LEVEL, 101 KIASB, RUN 142	0.04	0.61	–5.32	0.41
9219	LEVEL, 99 KIASB, RUN 143	1.76	0.11	–6.41	0.38
9309	LEVEL, 99 KIASB, RUN 140	–0.04	0.06	–5.06	0.24
9310	LEVEL, 145 KIASB, RUN 160	0.00	0.09	–11.79	0.17
9317	LEVEL, 60 KIASB, RUN 120	–1.48	0.09	–2.10	0.24
9325	LEVEL, 80 KIASB, RUN 130	–0.64	0.18	–3.34	0.61
9421	LEVEL, 102 KIASB, RUN 141	0.06	0.07	–5.68	0.24
9505	LEVEL, 100 KIASB, RUN 141	1.52	0.69	–7.82	5.75
9523	LEVEL, 100 KIASB, RUN 142	–0.18	0.16	–6.09	0.71
9615	LEVEL, 100 KIASB, RUN 141	0.55	0.35	–6.55	0.56
9705	LEVEL, 100 KIASB, RUN 142	0.15	0.06	–5.52	0.57
9810	LEVEL, 100 KIASB, RUN 140	1.79	0.14	–4.47	0.66
9811	LEVEL, 100 KIASB, RUN 141	–0.79	0.11	–5.23	0.14
9813	LEV, 100 KIASB, CON.FIX, RUN 142	–0.61	0.14	–4.52	1.02
9927	LEVEL, 250', 100 KIASB, RUN 144	–1.16	0.18	–4.79	0.58

Table 43.– IRAP level flight cases.

FLIGHT	COUNTER	DESCRIPTION	DURATION
100	10006	LEVEL, 65 KIASB, PT C	13.99 Seconds
100	10007	LEVEL, 65 KIASB, PT C	13.99 Seconds
102	10206	LEVEL FLT, 75 KIASB, PT D	13.99 Seconds
102	10207	LEVEL FLT, 75 KIASB, PT D	13.99 Seconds

Table 44.– Rotor speed sweep for four airspeeds in level flight.

FLIGHT	COUNTER	DESCRIPTION	DURATION
115	11505	HOVER OGE, 70 FT, 100% NR	4.99 Seconds
115	11506	HOVER OGE, 70 FT, 98% NR	4.99 Seconds
115	11507	HOVER OGE, 70 FT, 96% NR	4.99 Seconds
115	11508	HOVER OGE, 70 FT, 102% NR	4.99 Seconds
115	11509	HOVER OGE, 70 FT, 104% NR	4.99 Seconds
115	11529	LEVEL, 120 KIASB, 100% NR	4.99 Seconds
115	11530	LEVEL, 120 KIASB, 98% NR	4.99 Seconds
115	11531	LEVEL, 120 KIASB, 96% NR	4.99 Seconds
115	11532	LEVEL, 120 KIASB, 102% NR	4.99 Seconds
115	11533	LEVEL, 120 KIASB, 104% NR	4.99 Seconds
115	11534	LEVEL, 80 KIASB, 100% NR	4.99 Seconds
115	11535	LEVEL, 80 KIASB, 98% NR	4.99 Seconds
115	11536	LEVEL, 80 KIASB, 96% NR	11.99 Seconds
115	11537	LEVEL, 80 KIASB, 102% NR	4.99 Seconds
115	11538	LEVEL, 80 KIASB, 104% NR	4.99 Seconds
116	11652	LEVEL, 30 KIASB, 100% NR	4.99 Seconds
116	11653	LEVEL, 30 KIASB, 98% NR	4.99 Seconds
116	11654	LEVEL, 30 KIASB, 96% NR	4.99 Seconds
116	11655	LEVEL, 30 KIASB, 102% NR	4.99 Seconds
116	11656	LEVEL, 30 KIASB, 104% NR	4.99 Seconds

Table 45.– Stabilator angle sweep at $\mu = 0.27$, $C_w/\sigma = 0.08$.

FLIGHT	COUNTER	DESCRIPTION	DURATION
115	11518	LEV, 100KIASB, CWS=.08, STAB 0.0	4.99 Seconds
115	11519	LEV, 100KIASB, CWS=.08, STAB 2.5	4.99 Seconds
115	11520	LEV, 100KIASB, CWS=.08, STAB 5.0	4.99 Seconds
115	11521	LEV, 100KIASB, CWS=.08, STAB –2.5	4.99 Seconds
115	11522	LEV, 100KIASB, CWS=.08, STAB –5.0	4.99 Seconds

Table 46.– Roll angle/sideslip trim comparison.

FLIGHT	COUNTER	DESCRIPTION	DURATION
110	11010	LEVEL FLT, 109 KIASB, CWS=.08	4.99 Seconds
110	11011	LEVEL, 0 S/S, 109 KIASB, CWS=.08	4.99 Seconds
115	11514	LEVEL, 35 KIASB, CWS=.08	4.99 Seconds
115	11515	LEVEL, 35 KIASB, CWS=.08, 0 S/S	4.99 Seconds
115	11516	LEVEL, 85 KIASB, CWS=.08	4.99 Seconds
115	11517	LEVEL, 85 KIASB, CWS=.08, 0 S/S	4.99 Seconds

Table 47.– Roll and sideslip angles for roll angle/sideslip comparison cases.

COUNTER	DESCRIPTION	ϕ, DEG	β, DEG
11010	LEVEL FLT, 109 KIASB, CWS=.08	–0.55	–4.64
11011	LEVEL, 0 S/S, 109 KIASB, CWS=.08	0.99	–0.60
11514	LEVEL, 35 KIASB, CWS=.08	1.22	5.89
11515	LEVEL, 35 KIASB, CWS=.08, 0 S/S	1.32	–0.04
11516	LEVEL, 85 KIASB, CWS=.08	0.69	–4.09
11517	LEVEL, 85 KIASB, CWS=.08, 0 S/S	1.99	–0.57

Table 48.– Level flight in atmospheric turbulence.

FLIGHT	COUNTER	DESCRIPTION	DURATION
106	10605	ATM TURBULENCE, 120 KIASB	20.00 Seconds
106	10606	ATM TURBULENCE, 80 KIASB	9.99 Seconds
106	10607	ATM TURBULENCE, 120 KIASB	9.99 Seconds
106	10608	ATM TURBULENCE, 120 KIASB	5.99 Seconds
106	10609	ATM TURBULENCE, 80 KIASB	10.00 Seconds

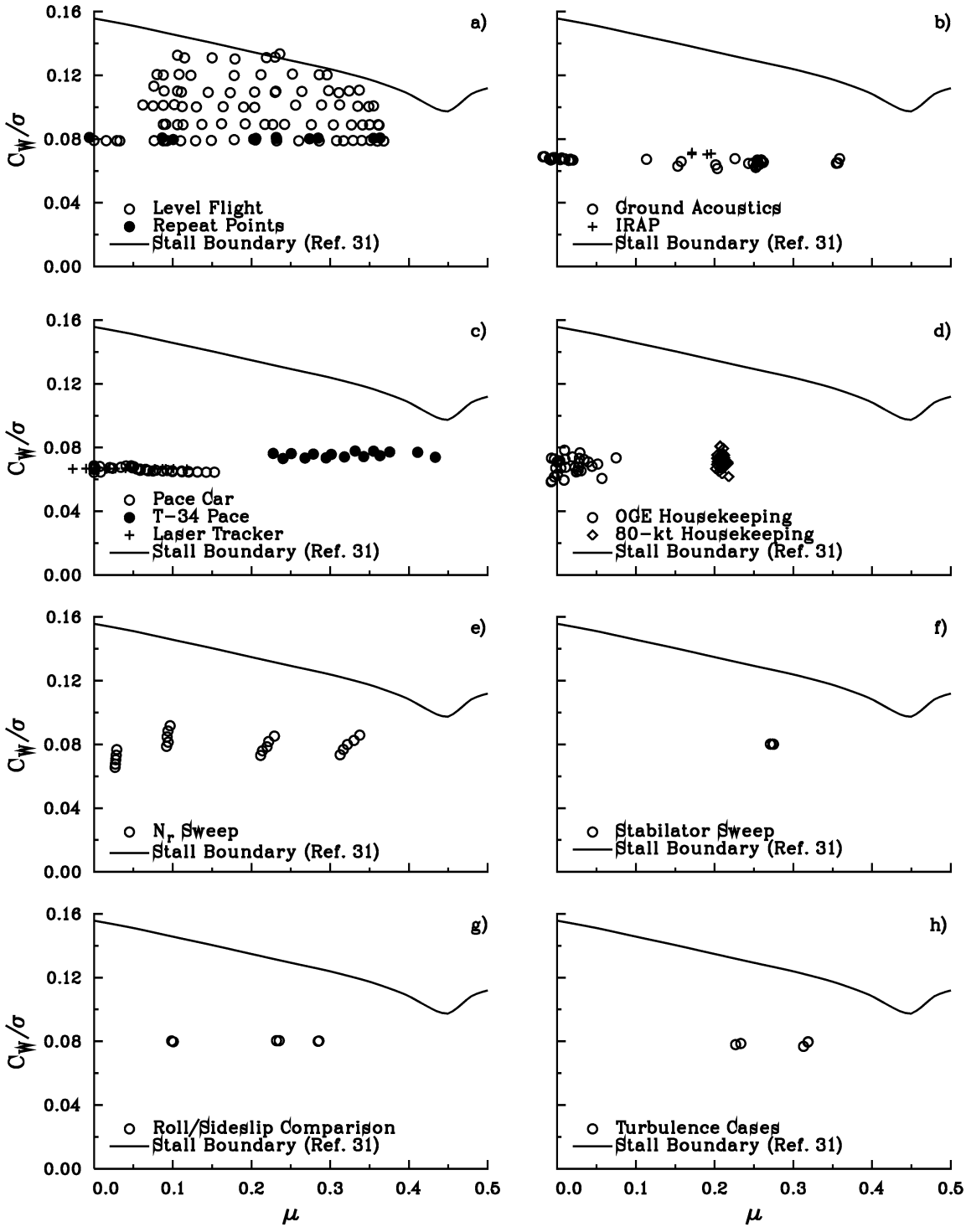

Figure 26.– Weight coefficient as a function of advance ratio for Airloads Program level flight data: a) airspeed sweeps, b) acoustic data, c) calibration data, d) housekeeping points, e) N_r sweeps, f) stabilator sweep, g) roll angle/sideslip angle comparison, and h) turbulence data.

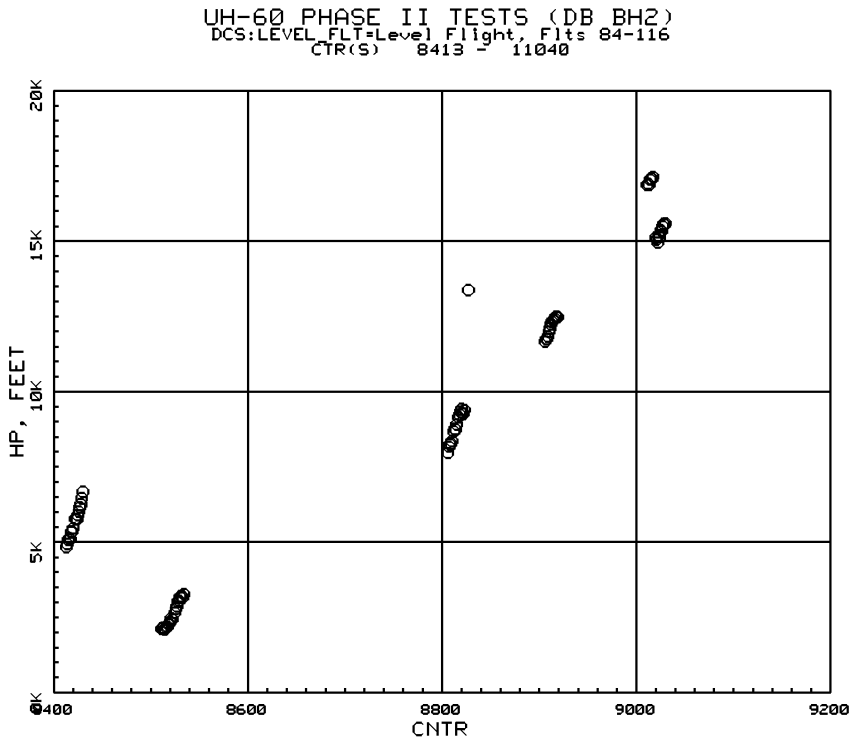

Figure 27.– Pressure altitudes for six airspeed sweeps.

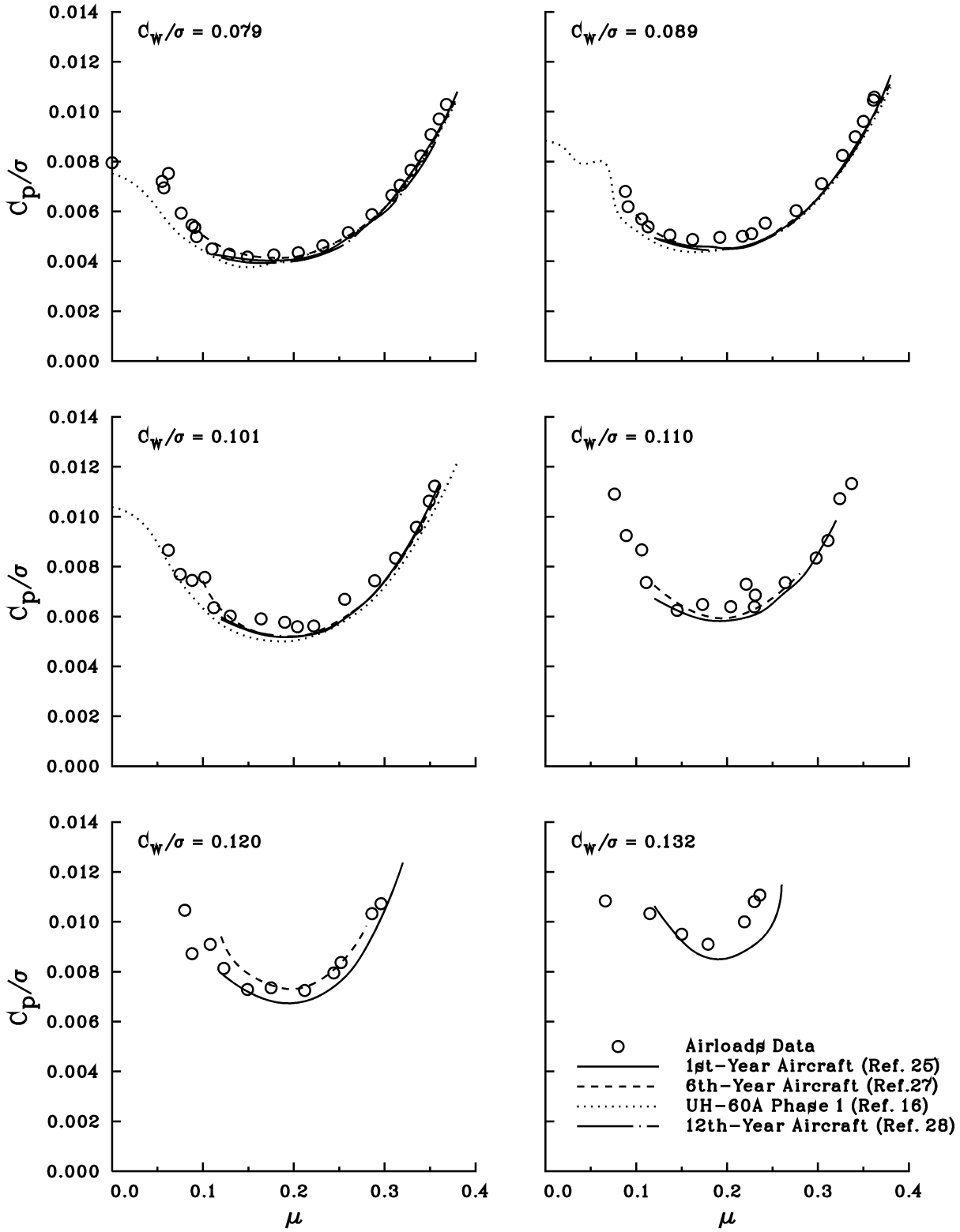

Figure 28.– Power coefficient as a function of advance ratio for Airloads Program compared to previous AEFA data (refs. 16, 25, 27, and 28).

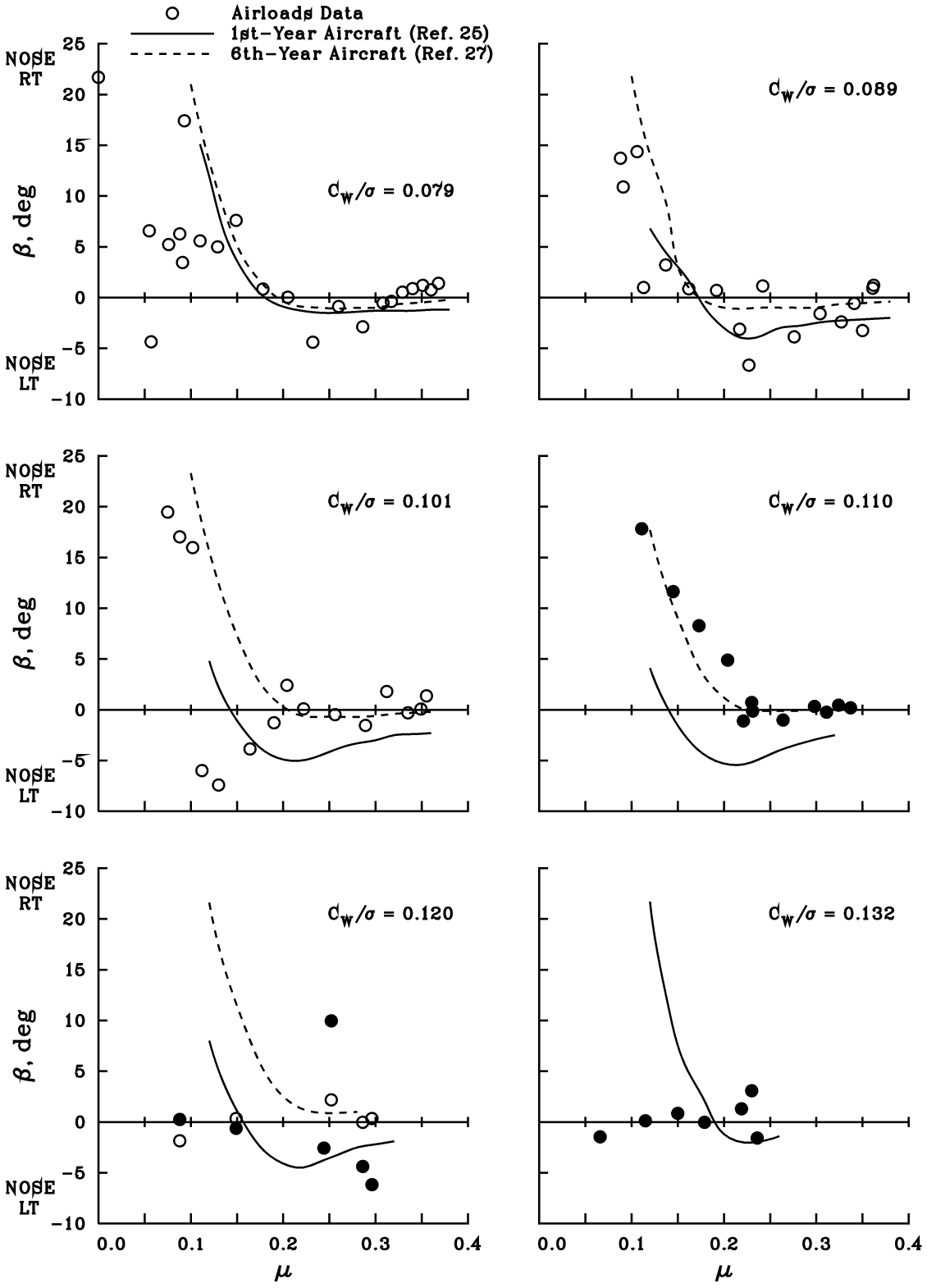

Figure 29.– Comparison of sideslip angles measured in Airloads Program with inherent sideslip angles of AEFA performance measurements (refs. 25, 27). Solid circles have been corrected for a bias error of –39.77 deg.

Figure 30.– Rotating Data Acquisition System (RDAS) installed on UH–60A.

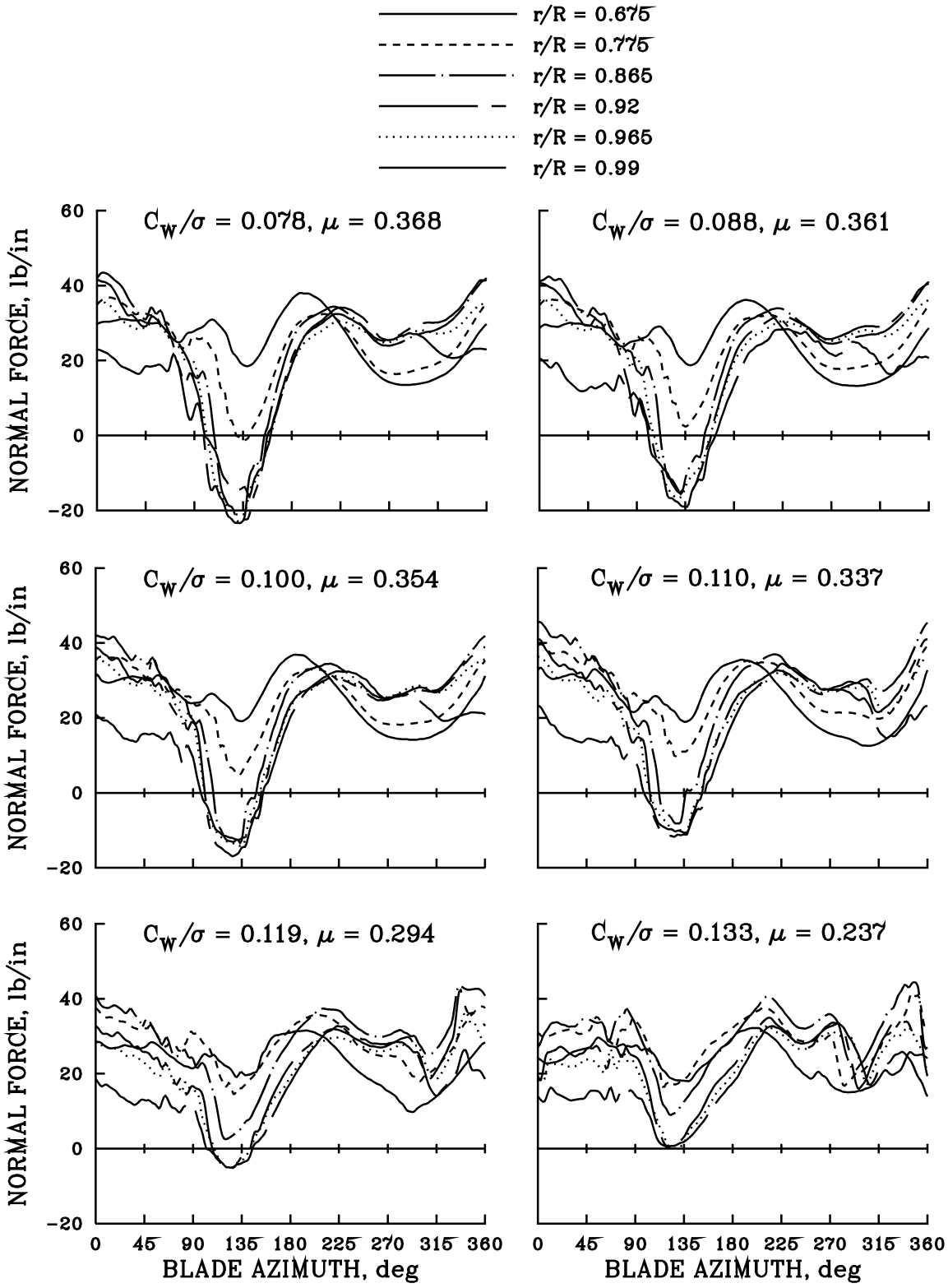

Figure 31.– Measured normal force for maximum velocity points for six airspeed sweeps.

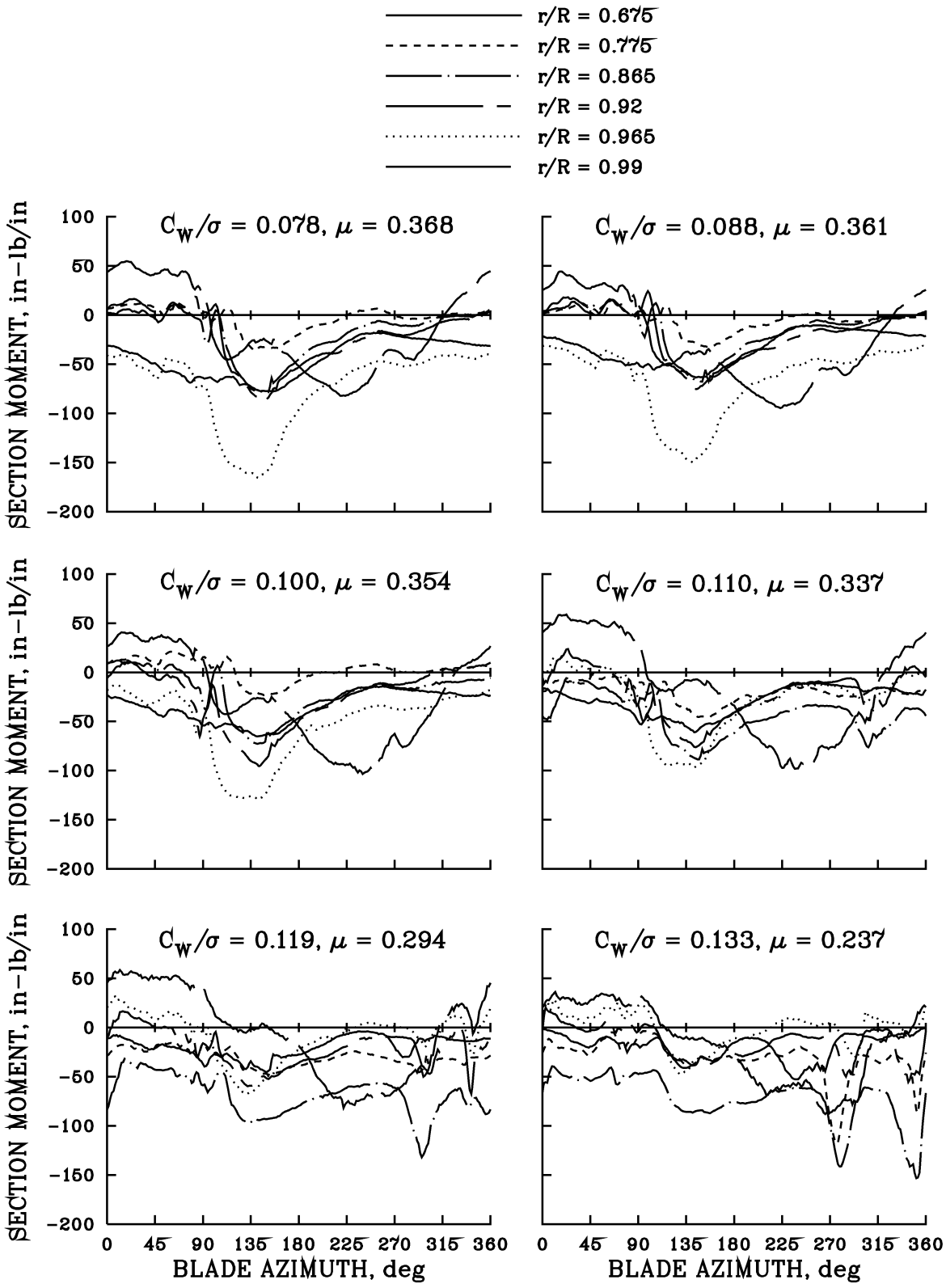

Figure 32.– Measured pitching moment for maximum velocity points for six airspeed sweeps.

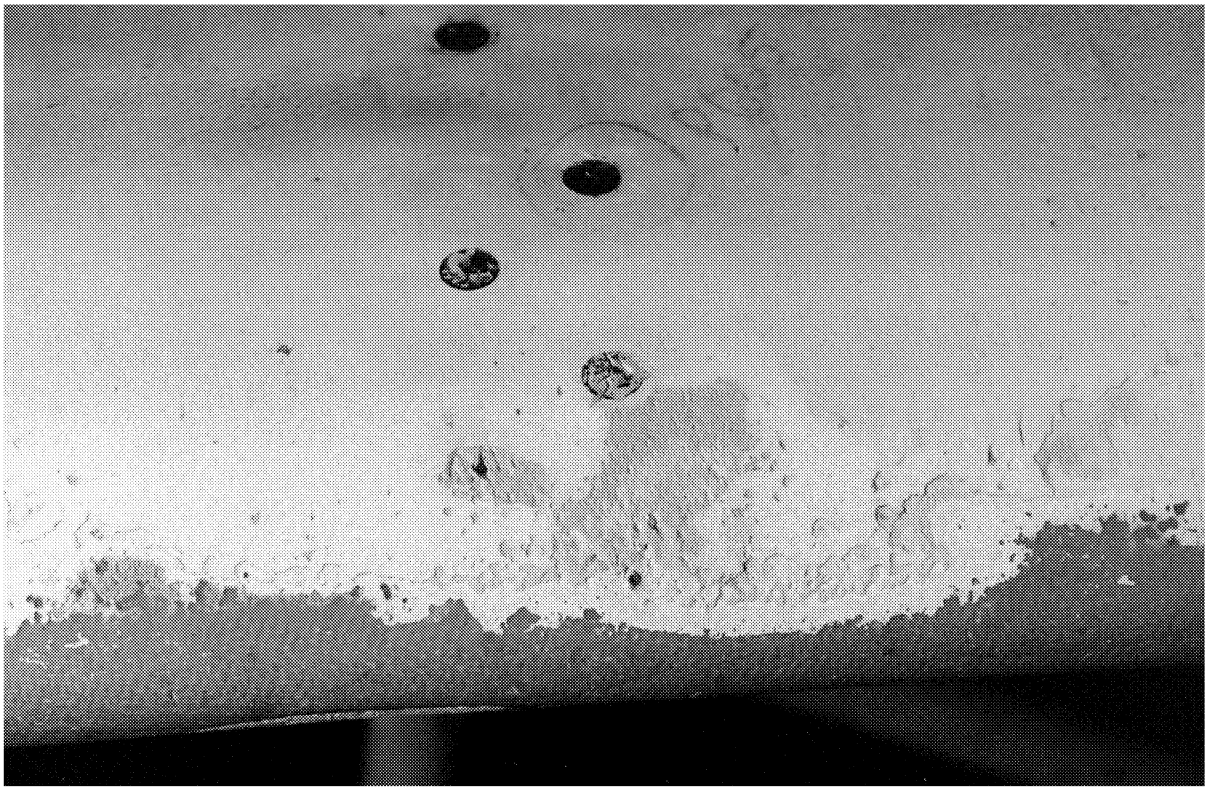

Figure 33.– Blade erosion at 0.865R, observed at the end of the flight test program.

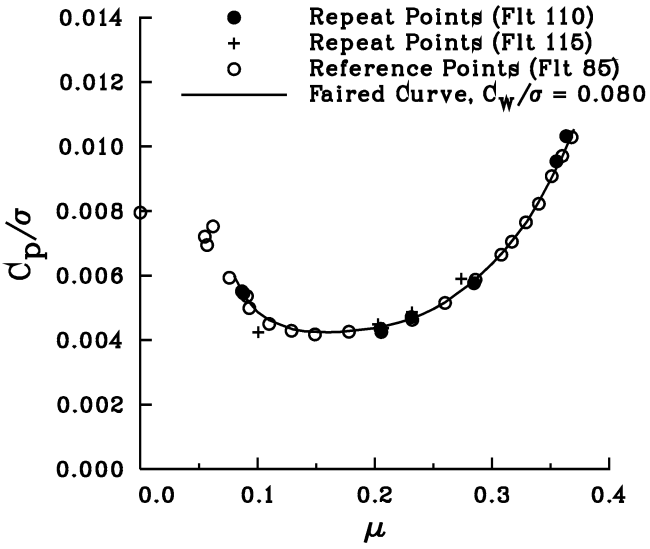

Figure 34.– Repeat points compared to Flight 85 data and best fit.

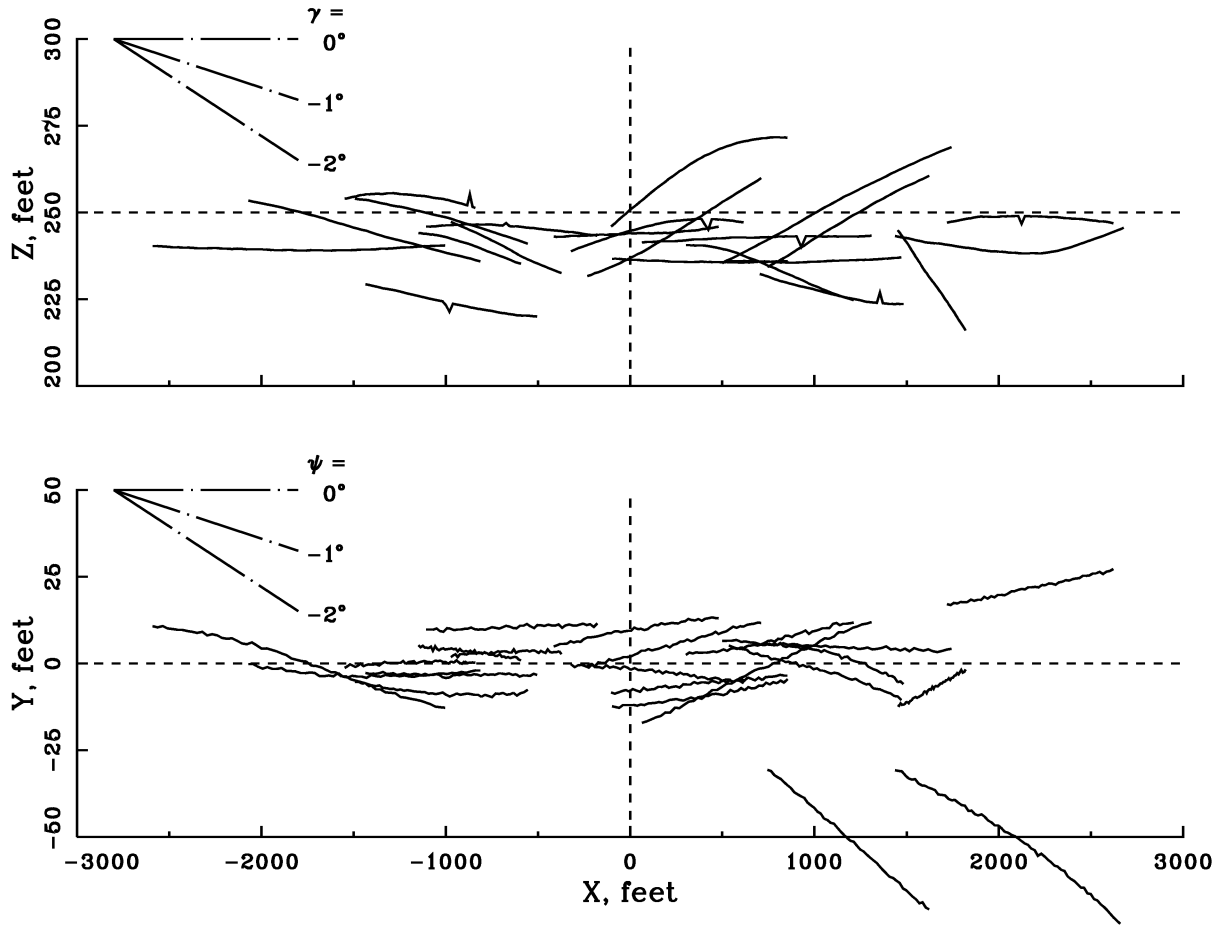

Figure 35.– Z- and y-position data as a function of x-position for Ames data base time slices (BH2) for level flight data obtained in Ground Acoustics tests. The zero reference represents the center of the acoustical array. Vertical and lateral scales have 20X exaggeration.

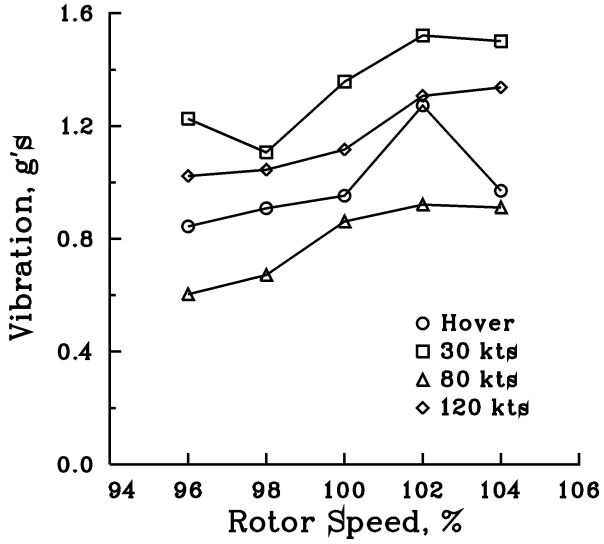

Figure 36.– Hub vertical vibration (AH0Z) as a function of rotor speed for four airspeeds.

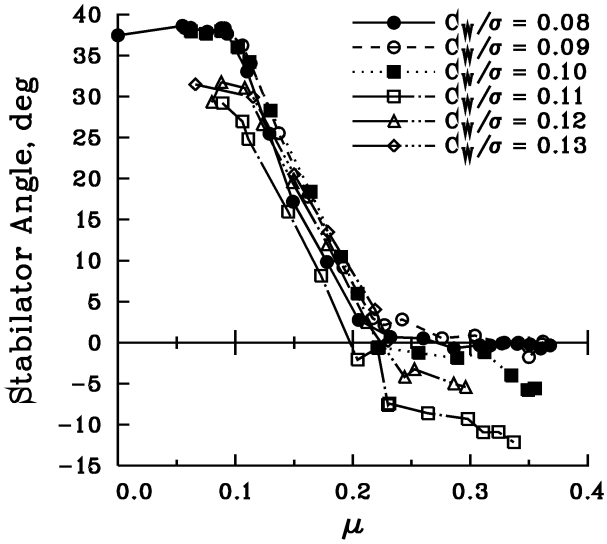

Figure 37.– Stabilator angle as a function of advance ratio for six level flight conditions.

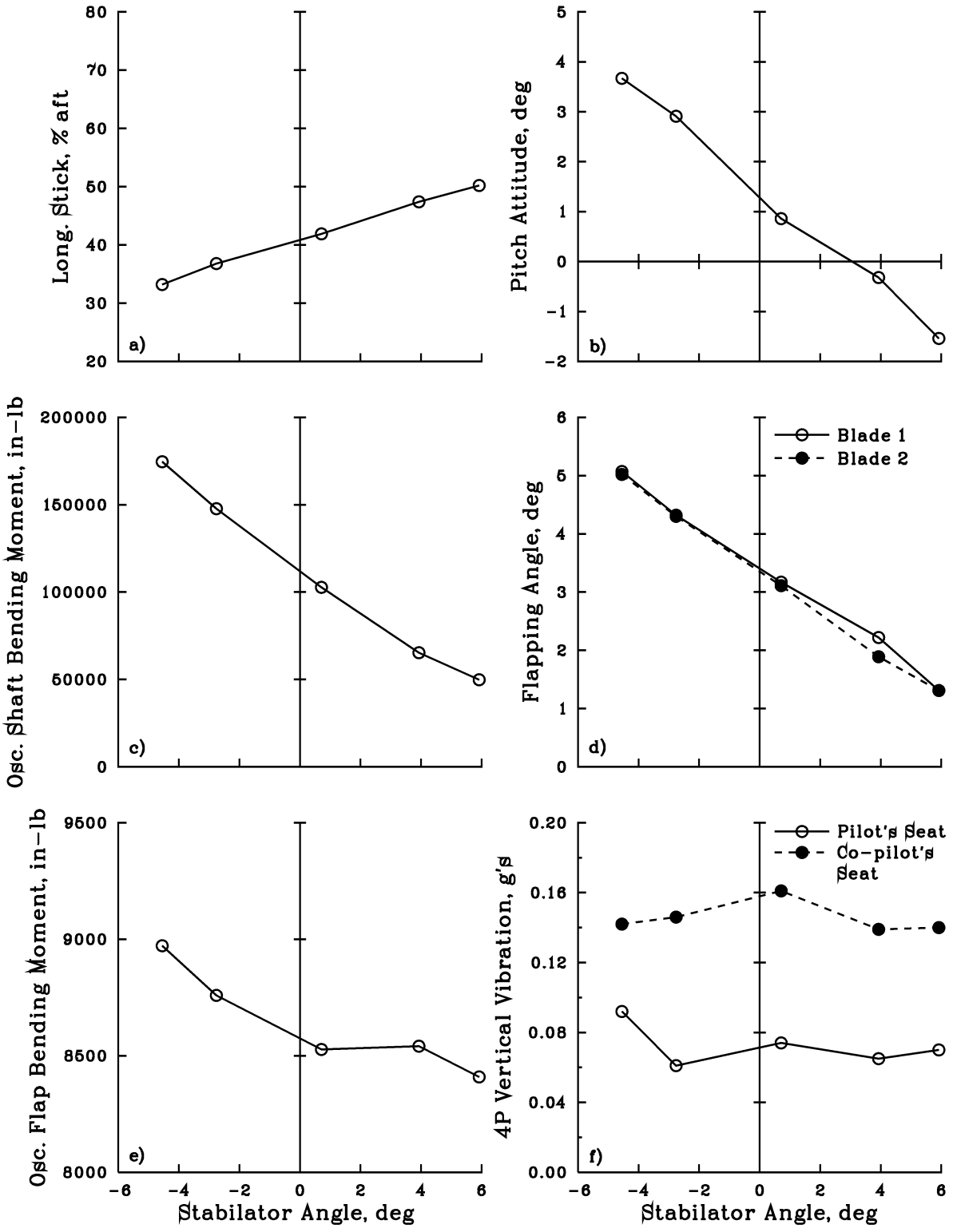

Figure 38.– Variation of six parameters as a function of stabilator angle at $\mu = 0.27$: a) longitudinal stick position, b) aircraft pitch attitude, c) oscillatory shaft bending moment, d) first harmonic blade flap angle, e) oscillatory flap bending moment at 0.50*R*, and f) cockpit 4/rev vertical vibration.

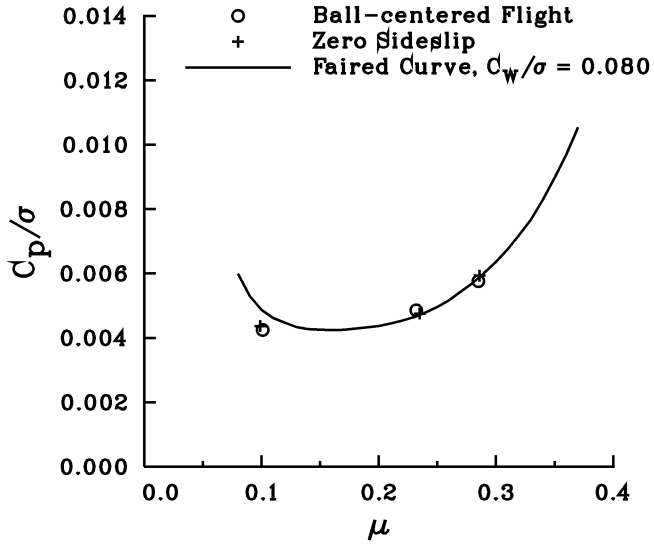

Figure 39.– Comparison of power coefficient for ball-centered flight and zero sideslip conditions at three airspeeds. Faired curve from Flight 85 for $C_w/\sigma = 0.08$ shown as reference.

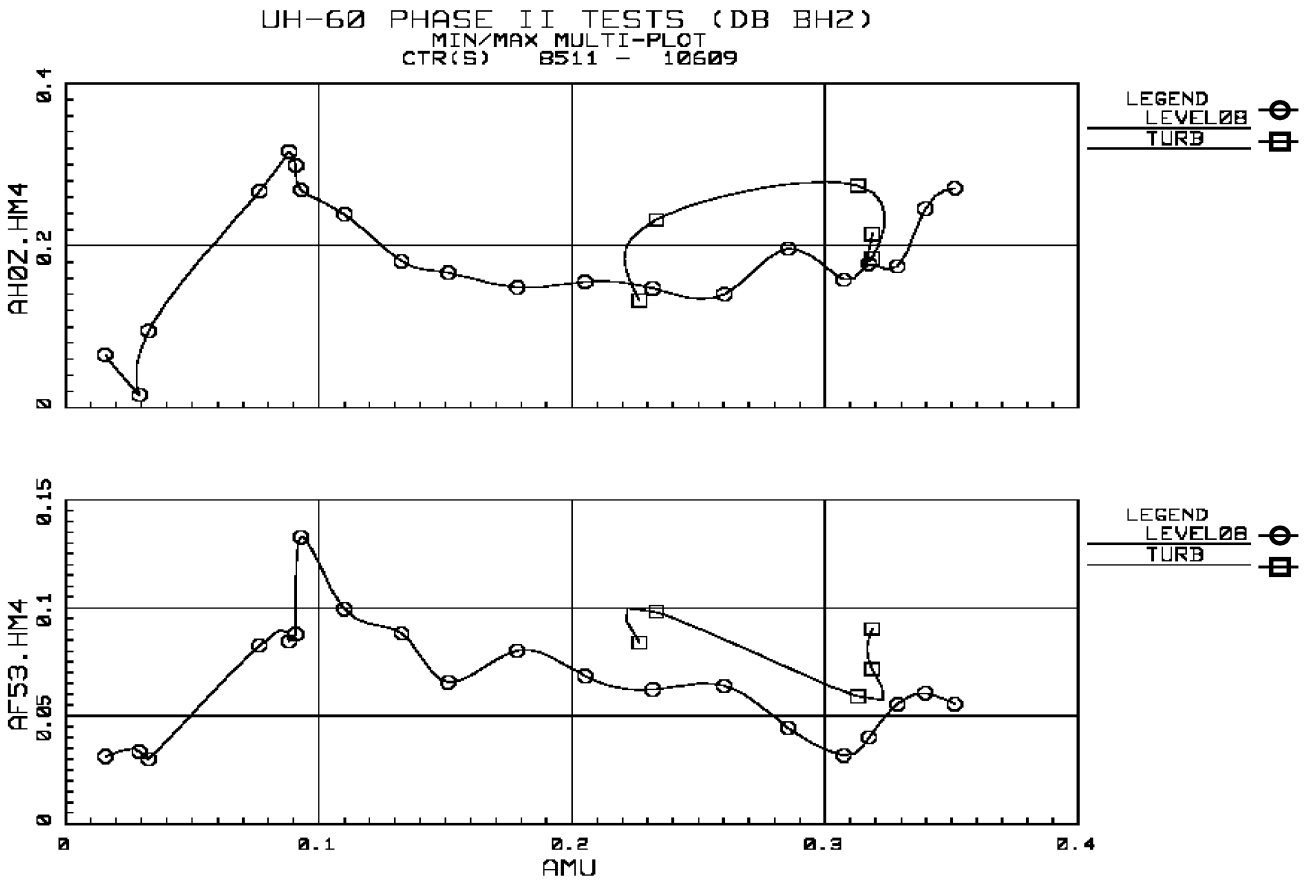

Figure 40.– Atmospheric turbulence compared to steady level flight for the 4/rev vertical vibration at the rotor hub (AH0Z.HM4) and the pilot's seat (AF53.HM4) as a function of advance ratio (AMU).

7. CLIMBS AND DESCENTS

Flight test data were obtained in climbs and descents during the Airloads Program including: 1) ascending and descending flight over a ground-acoustic array at the Crows Landing Naval Auxiliary Air Field (NAAF), 2) accelerated or dynamic ascending and descending flight over the array at Crows Landing NAAF, 3) a limited number of vertical climbs centered over the acoustic array at Crows Landing, 4) steady climbs at altitude including a combined climb and steady maneuver condition, 5) steady descending flight cases obtained during the in-flight acoustics portion of the program, 6) powered descents at airspeeds beyond the maximum level flight speed, and 7) data from autorotational descents.

Ascents and descents were flown over a ground-acoustic array to obtain acoustic data for a variety of flightpath angles and airspeeds. For the majority of these conditions the aircraft position and velocity were determined with a laser tracker and this provides accurate measurements of the aircraft's inertial velocity. These data are discussed below in the section titled "Steady Climbs and Descents (Ground-Acoustic Testing)." Associated with the climb and descents during the ground-acoustic testing were a number of flight counters where the aircraft was in accelerated flight. That is, it was either transitioning from level flight to a climb condition, referred to here as a "dynamic ascent" or it was transitioning from descending to level flight, which is called a "dynamic descent." These climb and descent related maneuvers are discussed below in the section "Dynamic Climbs and Descents (Ground-Acoustic Testing)." Flight data were obtained for a limited number of flight conditions with the aircraft in a vertical climb, starting from a hover condition. The data records include both the initial acceleration from hover to a vertical climb and the subsequent steady climb. These cases are discussed below in "Vertical Climbs (Ground-Acoustic Testing)."

Steady climb data were obtained at selected airspeeds and climb rates. The flight data include conventional test cases at different climb rates as well as a test sequence where data were obtained every three thousand feet in a continuous climb from sea level to 17,000 feet. These steady climbs are discussed below in "Steady Climbs." One case is also included of a combined climb and steady turn.

Under the Inflight Acoustics Rotor Program (IRAP), the UH–60A was flown in formation with a YO–3A to obtain in-flight acoustic data using microphones installed on the YO-3A. Most of the test conditions for the IRAP flights were for descending conditions and were selected to match descending flight cases from the model-scale wind tunnel tests of this rotor. These data are discussed below in "Steady Descents (In-flight Acoustics)."

Data were obtained at speeds above the aircraft's maximum level flight speed, V_H, in powered descents. These high-speed dive conditions are discussed below in "Powered Descents." Data were obtained during autorotational descents at two airspeeds and these cases are treated below in "Autorotational Descents."

Steady Climbs and Descents (Ground-Acoustic Testing)

The UH–60A was flown at the Crows Landing NAAF over a ground-acoustic array set up and maintained by NASA Langley Research Center personnel. A general discussion of the test procedures for these nine flights is provided in section 2. Ascending, level, and descending flight cases were flown for a matrix of airspeeds and flightpath angles as shown in table 49. The data from these flights were reduced in two steps. In the first step, the flight tape record, excluding the rotor data, was reduced and placed in the BH2 database with the prefix-4 added to the counter number. Thus, for Counter 9517, the data from this first step are stored in the BH2 database as Counter 49517. Typically these prefix-4 records extend from 20 to 40 seconds, with a few reaching approximately 60 seconds in length. The second step in the data reduction differed depending upon the research objectives of the Langley or Ames test personnel. The objective of the Langley researchers was to obtain steady data for flight conditions centered on the microphone array. For those counters that met their criteria, a time slice was selected and all of the data, including the rotor data, were reduced and placed in the Langley BHL database in TRENDS. Roughly half of the data counters obtained were reduced and placed in the BHL database. The ground-acoustic testing and the BHL database cases are discussed in more detail in section 9.

The objective of Ames researchers was to find appropriate steady conditions regardless of the aircraft's position relative to the acoustic array and time slices were selected for these conditions. The flight data, including the rotor data, were then reduced and placed in the BH2 database in TRENDS. These later cases are discussed in this section.

Thirty-one counters of steady climb data were obtained and placed in the prefix-4 database and are listed in table 50. The time slices for the counters placed in the BH2 database are shown in table 51. Two time slices were taken from Counter 49120: Counter 9120 and Counter 9131 (a pseudo-counter). Counter 49521 was an abbreviated flight record, so no time slice was made for the BH2 database. The resulting 31 counters of steady climb data are listed in table 52. In a similar fashion, 39 counters of steady descent data were obtained and the prefix-4 counters are listed in table 53. The time slices for these counters are shown in table 54. Two slices were taken from Counter 49108, providing the baseline case, Counter 9108, and a pseudo-counter, Counter 9132. A total of 40 counters with steady descent data are listed in table 55.

Three examples of x- and z-position tracking data obtained during climb and descent cases are shown in figure 41. For the climb cases, the aircraft flew towards the microphone array at the assigned airspeed at about 100 feet above the ground. Prior to reaching the array centerline, a climb was initiated so that the aircraft would pass over the array centerline at 250 feet elevation with the correct climb angle. In general, the pilots found it difficult to achieve the correct climb angle and also pass over the array at the target elevation. Figure 41a is representative of a climb case with substantial variance. Passing over the array centerline, the aircraft was still pulling up slightly. The climb rate was maintained for the next thousand feet, but then decreased. The climb example in figure 41(b) shows a case where the flight objectives were more closely met. The pilots were able to fly the descent cases more accurately, as illustrated in figure 41(c). In these cases, the aircraft could be set up in a steady descent well before the microphone array centerline, the descents were

reasonably steady, and the aircraft passed quite close to the target elevation. The pull-up at the end of the maneuver could be delayed until the aircraft was well past the microphone array.

The climb and descent examples in figure 41 also illustrate the differences in the time slices selected for the BH2 and BHL databases. The tracking data in each example are from the prefix-4 database. In figure 41(a), the primary climb record for the BH2 database, Counter 9120, was taken towards the end of the climb where the climb rate had decreased significantly. A pseudo-counter, Counter 9131, was also selected for the BH2 database, to record the higher climb rate condition. A portion of the entry to the climb, Counter 9142, was also selected and is referred to as a "dynamic ascent." It is discussed in the following section. The time slice selected for the BHL database was nearly the full length of the record and included a portion of the initial entry, the initial steeper climb, and the subsequent reduced climb angle portion.

Laser and radar tracking data were obtained for nearly all of the climb, level flight, and descent counters. The x- and z-position data for all of these counters are illustrated in figure 42. These data were extracted from the TRENDS database using the OUTDATA utility as a batch process under GATEWAY in the TRENDS menu. The tracking data were then post-processed to compute the average x- and z-position of the aircraft for each rotor revolution and these mean position data are plotted in figure 42. The center of the microphone array is located at $X = 0$ ft in figure 42 and this center point is indicated with a dashed vertical line. The ILS indicator in the aircraft cockpit was driven externally to provide guidance to the pilot so that the aircraft would pass over the microphone array centerline at an elevation of 250 ft. Good accuracy was achieved in matching the 250-ft target elevation for the level flight cases (see also figure 35). In descending and ascending flights, however, greater scatter in the vertical position at $X = 0$ ft is observed.

The aircraft flightpath angles for all climb, level flight, and descent conditions are shown in figure 43. The angles were determined from the laser tracking measurements by fitting a first-order regression curve to the x- and z-position data. The average standard error of the estimate for all of these cases was 0.32 deg. The variation in advance ratio averaged ±0.002.

Tables 56 and 57 show the flightpath and the tip-path-plane angles of attack for all of the climb and descent test conditions. The flightpath angles are based on a linear regression of the tracking data, as discussed above. The standard error of estimate based on the linear regression provides a measure of dispersion. The tip-path-plane angle of attack is

$$\alpha_{TPP} = \alpha_s - \beta_{1c} - \gamma \tag{1}$$

where α_s, β_{1c}, and γ were each calculated over one rotor revolution. The shaft angle of attack, α_s, was calculated from measured pitch attitude (PITCHATT) after subtracting 3 deg to account for the forward tilt of the rotor shaft relative to the aircraft datum. The cosine flapping angle, β_{1c}, was calculated from a Fourier analysis of the corrected flapping angle measurement for blade 1. The flightpath angle was calculated from the x- and z-position data. The mean and standard deviation were computed over the entire length of the record, generally, 19 to 20 revolutions, and these are the values shown in tables 56 and 57.

Dynamic Climbs and Descents (Ground-Acoustic Testing)

To obtain the steady climb data discussed in the previous section, it was necessary to fly the UH–60A at an elevation of about 100 feet above the ground towards the acoustic array. Then, depending upon the desired climb angle, the pilot would initiate a climb so that the correct airspeed and climb angle would be achieved as the aircraft passed through the 250-foot target elevation above the acoustic array center. The transition from level flight to climb is referred to here as a "dynamic climb." These records were obtained by examining the original prefix-4 counter from the first data reduction step and the record was time-sliced to capture the transition period. As these records are considered secondary to the steady climb data, it was necessary to provide a pseudo-counter number for the dynamic climb data in the TRENDS database. The time slices for 16 dynamic climb conditions are shown in table 58 and the dynamic climb counters are listed in table 59. The distinction between steady and dynamic climb is not always clear and, in a few cases, individual counters have been included in both categories.

"Dynamic descent" data were obtained at the end of steady descent cases. Just as for the dynamic climb data, the prefix-4 steady descent record was examined to identify when the aircraft transitioned from a steady descent to level flight and a time slice was obtained and a pseudo-counter assigned to the data. Time slices were defined for 17 dynamic descent cases as shown in table 60. The dynamic descent counters are listed in table 61.

The aircraft x- and z-positions, based on the laser tracker, are shown in figure 44 for all of the dynamic climb and descent data. The same 3.75X exaggeration is used for the vertical position as in figure 42 and a comparison of these two figures illustrates the overlap between the steady climb and descent cases and the dynamic climb and descent cases. The position data were obtained from the TRENDS database and processed in the same manner as described previously for the data in figure 42.

Vertical Climbs (Ground-Acoustic Testing)

Vertical climb data, starting from a stabilized hover, were obtained for three counters during testing over the ground-acoustic array at Crows Landing. The counters for the prefix-4 database are listed in table 62. The time slices used for the BH2 database are shown in table 63, while the BH2 database counters are listed in table 64. Figure 45 shows the vertical position of the aircraft, measured with the radar tracker, and the helicopter normalized power coefficient, both as functions of time for the three records. The laser tracker was inactivated for these tests, as test personnel were stationed on the airfield to assist the pilots with hover station keeping. The radar z-position data (ZRADAR) and power coefficient data (CP) were extracted from TRENDS using the PRINT command in TIMEHIST. For each counter, an initial segment of data was selected to represent stabilized hover. A mean value was computed for this segment and was used to normalize the calculated power coefficient plotted in the figure.

Figure 45 shows that there is an initial transient stage in all of the vertical climb cases where the engine power overshoots and then oscillates. An estimate was made of the time period when the

engine power was stabilized for each of the cases. For the time period of stabilized power the average climb rate and average power ratio were computed. These average values and the time period used are tabulated in table 65.

During the initial transition to a vertical climb, there was very little variation in the x- and y-position of the aircraft. However, once a stabilized climb was achieved, there was a tendency for the aircraft to drift from its starting point. This drift ranged from about 56 feet for Counter 9417 to about 135 feet for the other counters. The drift does not appear related to the approximately 8 knot wind conditions that were measured at this altitude just prior to the tests (see fig. 20). Although the engine power remained constant during the stabilized climb period, the aircraft showed a slight increase in climb rate throughout the record. This increase ranged from about 7% of the mean value shown in table 65 for Counter 9417 to about 11% for Counter 9419.

The climb rates tabulated in table 65 are greater than the 500 ft/min vertical rate of climb required in recent U.S. Army helicopter procurements. Harris (ref. 32) has shown that the climb rate is a nonlinear function of power ratio for values below approximately 1.1. Unfortunately, no data were obtained that cover the nonlinear region nor is there a significant overlap between published OH–58D vertical climb data, mostly for power ratios below 1.2, and the data included here.

In section 5, it was shown that even for the most stable hover conditions there is considerable unsteadiness—see figure 22 as an example. However, at a vertical rate of climb of approximately 1900 ft/min, the combination of induced flow and climb rate force the tip vortices well away from the blade, and the measured normal force on the blade is very steady as shown in figure 46. The normal forces shown in this figure were obtained by an integration of the measured blade pressures. The integration was performed after extracting the pressure data from TRENDS using the OUTDATA utility and post-processing the OUTDATA files to convert them from the TRENDS time base to an azimuth base.

Steady Climbs

Steady climb data were obtained using conventional flight test techniques and are listed in table 66. These test conditions also include a single combined climb/maneuver case: Counter 11525. Figure 47 shows the climb rates for the test conditions of table 66 as a function of the average pressure altitude. Climb rate was based on measurements of the boom pressure altitude (HPB). The boom pressure altitude data were extracted from the TRENDS database using the PRINT command in TIMEHIST. A linear regression of pressure altitude on time over the length of the record provided an estimate of the climb rate. In most cases, the standard error of estimate of the climb rate is smaller or the same size as the symbols used in figure 47. The pressure altitude shown in figure 47 is the mean value for the pressure measurement over the duration of the record.

Steady climb data were obtained on Flights 89 and 115 for climb rates between 600 and 2300 ft/min and advance ratios between 0.21 and 0.24 (aircraft best rate of climb speed). These test points also include one case, Counter 11523, which was flown at a lower advance ratio, $\mu = 0.18$.

Sequential climb data were obtained on Flight 90 as the aircraft climbed to 17,100 feet prior to performing a level flight airspeed sweep at $C_W/\sigma = 0.13$; see section 6. During this climb, data records were taken as the aircraft passed through 3,000, 6,000, 9,000, 12,000, and 15,000 feet. This sequence of counters is connected by a dotted line in figure 47 and, as expected, as the altitude increases the excess power available is reduced and the rate of climb decreases.

Climb data were obtained during a steady turn for one condition on Flight 115. The climb rate was held at 1887 ±27 ft/min over the 10 sec duration of this counter. However, the load factor in the turn was variable during the record. For the first five seconds of the record the load factor varied between 1.10 and 1.18 g's. Over the last five seconds the load factor increased from 1.18 to 1.46 g's.

Steady Descents (In-flight Acoustics)

Under NASA's In-flight Acoustic Research Program (IRAP), the UH–60A was flown in formation with a YO–3A airplane to obtain acoustic measurements (see fig. 5). The YO–3A was used as a microphone platform. Both acoustic and flight data were obtained on Flights 100–102, 113, and 114 and these flights are discussed in more detail in section 10. Level flight conditions for these tests were previously discussed in section 6 and were listed in table 43. Sixty-three test points were obtained for descending flight conditions and these are listed in table 67.

Figure 48 shows the aircraft's flightpath angle as a function of the advance ratio for all of the steady descent points flown during the IRAP tests. The rate of descent was determined in TRENDS by using the POLY (first order) fit in TIMEHIST. The mean value of advance ratio (AMU) was obtained from VIEW in TRENDS. The flightpath angle was calculated from the two velocities.

The descending flight data points were obtained at an advance ratio of either 0.17 or 0.20, as illustrated in figure 48. Most of these cases were flown for $C_W/\sigma = 0.071$. However, data were also obtained at a weight coefficient of 0.086 and an advance ratio of 0.17 on Flight 113. The boundary indicated by a dashed line on figure 48 shows the range of ascent and descent conditions obtained during ground-acoustic testing.

Powered Descents

Data were obtained in powered descents for advance ratios from 0.38 to 0.48. All of these counters were at airspeeds beyond the aircraft maximum level flight speed, V_H. Figure 49 shows the rate of climb for these conditions as a function of advance ratio and includes level flight data from Flight 85 for reference (see table 30). The nine powered descent conditions are listed in table 68.

The descent rates (negative rate of climb) and advance ratios shown in figure 49 were obtained by using the PRINT command in TIMEHIST in TRENDS to extract the boom pressure altitude (HPB) and the advance ratio (AMU). A linear regression of the pressure altitude with time was obtained to estimate the descent rate. The standard error of estimate of the regression slope varied from 14 to 31 ft/min for the nine cases.

The power coefficient, based on measured engine power, is shown as a function of advance ratio for the powered descent cases in figure 50. As before, level flight data from Flight 85 are included for reference. These data were obtained using the PRINT command as discussed previously for the pressure altitude and advance ratio. The power used in these descents was approximately the 30-minute power rating for the engines (MRP). The specific flight conditions for the nine cases are tabulated in table 69 to include the weight and power coefficients, the advance ratio, the rate of climb, the flightpath angle, and the mean pressure altitude. Test altitude was selected on Flights 110 and 116 to provide $C_W/\sigma = 0.08$. The weight coefficient is not available for Flight 83.

Rotor loads for these powered descent conditions have been examined in reference 9 and compared to other highly loaded conditions. Sample loads from the limit descent condition, Counter 11682, are compared with the maximum level flight case, Counter 8534, in figure 51. The data shown in this figure were extracted from TRENDS using OUTDATA and were converted from a time base to an azimuth base using the rotor azimuth encoder (AZIM). The measured normal force and pitching moment at $0.92R$ increase for the limit dive condition, as expected, and the structural loads increase as well. The pitching moment time history in the dive condition differs from level flight in showing rapid, large variations in the moment on the advancing side of the disk and only limited incipient stall in the fourth quadrant. As discussed in reference 9, the rapid changes in moment on the advancing side are a consequence of out-of-phase shock movements on the upper and lower surfaces of the blade. The high loads at this condition, then, is induced by unsteady transonic flow and not by dynamic stall.

Autorotational Descents

Data were obtained at two flight speeds for an autorotational entry, a steady autorotational descent, and a recovery from autorotation. The duration of the records was between 50 and 60 sec and, therefore, it was necessary to record the data as two segments. The counters for the two records are shown in table 70. The general features of these autorotational records are illustrated in figure 52 for Counters 11541 and 11542. The autorotational record based on Counters 11539 and 11540 is similar.

The five parameters in figure 52 were extracted from TRENDS using the PRINT command in TIMEHIST. The power coefficient is based on the power from both engines and is a derived parameter in TRENDS. The power coefficient for the main rotor was calculated from the main rotor shaft torque measurement (RQ10), using the boom density (SGMA) and the rotor speed (VR05) in the power coefficient calculation. The main rotor torque measurement show some “noise,” mostly caused by 4/rev torque loads. The CVF filter command was used in TRENDS to reduce the high-frequency torque oscillations with a cutoff frequency of 1 Hz and a half-cosine filter (see ref. 17). No attempt was made to filter the collective stick position measurement which shows some “jitter” for most flight conditions. The rotor speed (VR05) is shown normalized by the nominal rotor speed of 258 rpm.

Event markers have been added to figure 52 to show the different phases of the autorotational descent. Event 1 is the initiation of a simulated loss of power. This was accomplished by the copilot

reducing both throttles to idle. Event 2 marks the end of the autorotational entry and the start of the steady descent. Event 3 is the end of the first segment (during steady descent). Event 4 is the start of the second segment. Note that there is a time gap of about a second between the two segments (counters). Event 5 is the end of the steady descent where the throttles were brought back to their 100% or governing position. The times for the five events are shown in table 71 for both autorotational records as well as the start time for segment 1 and the end time of segment 2.

The power coefficient data in figure 52 show that the engine power was very close to zero, while the main rotor power was slightly negative. The nominal condition for autorotation is zero torque from the engines, that is, the loss of all power. The main rotor power is “negative” as it is generating power for the tail rotor and the accessories drive, as well as overcoming gearbox losses.

Table 49.– Test matrix for ascending, level, and descending flight conditions during ground-acoustic measurements at Crows Landing.

FLIGHTPATH		AIRSPEED, KNOTS					
ANGLE, DEG		40	60	80	100	120	140
12	BH2	9517, 9519	9513, 9514	9511	9120, 9323, 9324		
	BHL	9517	9513	9511	9120		
9	BH2	9518	9112, 9113, 9216, 9316, 9217	9123, 9327			
	BHL	9518	9113	9123			
8	BH2					9530	
	BHL					9530	
7	BH2			9507, 9508			
	BHL			9507			
6	BH2	9522	9429	9119, 9322	9509		
	BHL	9522	9429	9119	9509		
3	BH2		9512	9510	9515, 9516		
	BHL	9525	9512	9510	9515		
0	BH2	9204	9114, 9317	9121, 9325	9104, 9105, 9218, 9219, 9309, 9421, 9505, 9523, 9615, 9705, 9810, 9811, 9814, 9927		9106, 9107, 9130, 9310
	BHL	9204	9317	9121	9104, 9421, 9814		9310
–3	BH2	9426	9422	9423	9424		
	BHL		9422	9423			
–6	BH2	9427	9115, 9318, 9506, 9524, 9616, 9706, 9812, 9928	9109, 9221, 9312	9117, 9320		
	BHL	9427	9616	9109	9320		
–7	BH2			9116, 9319			
	BHL			9116			
–8	BH2					9122, 9326	
	BHL					9122	
–9	BH2	9220, 9428	9108, 9311	9118, 9321	9110, 9222, 9313, 9314		
	BHL	9428	9108	9118	9110		
–12	BH2	9111, 9223, 9315	9124, 9328	9125	9425		
	BHL	9111		9125	9425		

Table 50.– Steady climb cases from ground-acoustic testing; prefix-4 database.

FLIGHT	COUNTER	DESCRIPTION	DURATION
91	49112	CLIMB, 9DEG, 60KIASB, RUN 460	32.47 Seconds
91	49113	CLIMB, 9DEG, 60KIASB, RUN 461	35.83 Seconds
91	49119	CLIMB, 6DEG, 80KIASB, RUN 490	29.04 Seconds
91	49120	CLIMB, 9DEG, 100KIASB, RUN 550	27.92 Seconds
91	49123	CLIMB, 9DEG, 80KIASB, RUN 510	27.25 Seconds
91	49216	CLIMB, 9DEG, 60KIASB, RUN 462	30.72 Seconds
91	49217	CLIMB, 9DEG, 60KIASB, RUN 463	29.86 Seconds
91	49316	ASCENT, 9DEG, 60KIASB, RUN 460	31.68 Seconds
91	49322	ASCENT, 6DEG, 80KIASB, RUN 490	23.53 Seconds
91	49323	ASCENT, 9DEG, 100KIASB, RUN 550	26.00 Seconds
91	49324	ASCENT, 9DEG, 100KIASB, RUN 551	29.81 Seconds
91	49327	ASCENT, 9DEG, 80KIASB, RUN 510	26.58 Seconds
91	49429	ASCENT, 6DEG, 60KIASB, RUN 450	30.08 Seconds
91	49507	ASCENT, 7DEG, 80KIASB, RUN 500	27.28 Seconds
92	49508	ASCENT, 7DEG, 80KIASB, RUN 501	26.46 Seconds
92	49509	ASCENT, 6DEG, 100KIASB, RUN 540	24.06 Seconds
92	49510	ASCENT, 3DEG, 80KIASB, RUN 480	25.13 Seconds
93	49511	ASCENT, 12DEG, 80KIASB, RUN 520	24.41 Seconds
93	49512	ASCENT, 3DEG, 60KIASB, RUN 440	34.36 Seconds
93	49513	ASCENT, 12DEG, 60KIASB, RUN 470	30.83 Seconds
93	49514	ASCENT, 12DEG, 60KIASB, RUN 471	34.23 Seconds
94	49515	ASCENT, 3DEG, 100KIASB, RUN 530	21.26 Seconds
95	49516	ASCENT, 3DEG, 100KIASB, RUN 531	25.43 Seconds
95	49517	ASCENT, 12DEG, 40KIASB, RUN 430	42.81 Seconds
96	49518	ASCENT, 9DEG, 40KIASB, RUN 420	41.42 Seconds
97	49519	ASCENT, 12DEG, 40KIASB, RUN 431	41.08 Seconds
98	49520	ASCENT, 9DEG, 40KIASB, RUN 421	39.38 Seconds
98	49521	ASCENT, 6DEG, 40KIASB, RUN 410	6.43 Seconds
98	49522	ASCENT, 6DEG, 40KIASB, RUN 411	47.46 Seconds
98	49525	ASCENT, 3DEG, 40KIASB, RUN 400	59.23 Seconds
99	49530	ASCENT, 8DEG, 120KIASB, RUN 570	27.58 Seconds

Table 51.– Time slices for steady climbs in prefix-4 and BH2 databases.

PREFIX-4 DATABASE			BH2 DATABASE		
COUNTER	START TIME SEC	END TIME SEC	COUNTER	START TIME SEC	END TIME SEC
49112	0.00	32.47	9112	22.63	27.62
49113	0.00	35.83	9113	29.57	34.57
49119	0.00	29.04	9119	18.42	23.41
49120	0.00	27.92	9131	11.99	16.98
49120	0.00	27.92	9120	17.99	22.98
49123	0.00	27.24	9123	16.99	21.98
49216	0.00	30.72	9216	73.99	78.98
49217	0.00	29.86	9217	19.51	26.69
49316	0.00	31.68	9316	12.00	17.00
49322	0.00	23.53	9322	16.01	21.00
49323	0.00	26.00	9323	13.00	18.00
49324	0.00	29.81	9324	13.22	18.22
49327	0.00	26.57	9327	10.00	14.99
49429	0.00	30.08	9429	1.00	7.00
49507	0.00	27.28	9507	15.00	19.99
49508	0.00	26.46	9508	17.01	22.00
49509	0.00	24.05	9509	9.01	13.00
49510	0.00	25.13	9510	6.01	9.99
49511	0.00	24.41	9511	14.00	19.00
49512	0.00	34.36	9512	6.00	11.00
49513	0.00	30.82	9513	12.01	17.00
49514	0.00	34.22	9514	8.00	19.00
49515	0.00	21.26	9515	4.01	9.00
49516	0.00	25.43	9516	8.00	13.00
49517	0.00	42.80	9517	20.00	25.00
49518	0.00	41.42	9518	17.01	22.00
49519	0.00	41.08	9519	17.01	22.00
49520	0.00	39.37	9520	14.01	19.00
49521	0.00	6.43	—	—	—
49522	0.00	47.46	9522	26.00	31.00
49525	0.00	59.23	9527	44.01	48.99
49530	0.00	27.57	9530	16.01	20.99

Table 52.– Steady climb cases from ground-acoustic testing; BH2 database.

FLIGHT	COUNTER	DESCRIPTION	DURATION
91	9112	CLIMB, 9DEG, 60KIASB, RUN 460	4.99 Seconds
91	9113	CLIMB, 9DEG, 60KIASB, RUN 461	4.99 Seconds
91	9119	CLIMB, 6DEG, 80KIASB, RUN 490	4.99 Seconds
91	9120	CLIMB, 9DEG, 100KIASB, RUN 550	4.99 Seconds
91	9123	CLIMB, 9DEG, 80KIASB, RUN 510	4.99 Seconds
91	9131	CLIMB, 9DEG, 100KIASB, RUN 550*	4.99 Seconds
92	9216	CLIMB, 9DEG, 60KIASB, RUN 462	5.18 Seconds
92	9217	CLIMB, 9DEG, 60KIASB, RUN 463	7.18 Seconds
93	9316	ASCENT, 9DEG, 60KIASB, RUN 460	4.99 Seconds
93	9322	ASCENT, 6DEG, 80KIASB, RUN 490	4.99 Seconds
93	9323	ASCENT, 9DEG, 100KIASB, RUN 550	4.99 Seconds
93	9324	ASCENT, 9DEG, 100KIASB, RUN 551	4.99 Seconds
93	9327	ASCENT, 9DEG, 80KIASB, RUN 510	4.99 Seconds
94	9429	ASCENT, 6DEG, 60KIASB, RUN 450	5.99 Seconds
95	9507	ASCENT, 7DEG, 80KIASB, RUN 500	4.99 Seconds
95	9508	ASCENT, 7DEG, 80KIASB, RUN 501	4.99 Seconds
95	9509	ASCENT, 6DEG, 100KIASB, RUN 540	3.99 Seconds
95	9510	ASCENT, 3DEG, 80KIASB, RUN 480	3.99 Seconds
95	9511	ASCENT, 12DEG, 80KIASB, RUN 520	4.99 Seconds
95	9512	ASCENT, 3DEG, 60KIASB, RUN 440	4.99 Seconds
95	9513	ASCENT, 12DEG, 60KIASB, RUN 470	4.99 Seconds
95	9514	ASCENT, 12DEG, 60KIASB, RUN 471	10.99 Seconds
95	9515	ASCENT, 3DEG, 100KIASB, RUN 530	4.99 Seconds
95	9516	ASCENT, 3DEG, 100KIASB, RUN 531	4.99 Seconds
95	9517	ASCENT, 12DEG, 40KIASB, RUN 430	4.99 Seconds
95	9518	ASCENT, 9DEG, 40KIASB, RUN 420	4.99 Seconds
95	9519	ASCENT, 12DEG, 40KIASB, RUN 431	4.99 Seconds
95	9520	ASCENT, 9DEG, 40KIASB, RUN 421	4.99 Seconds
95	9522	ASCENT, 6DEG, 40KIASB, RUN 411	4.99 Seconds
95	9527	ASCENT, RUN 400 SEGMENT 3	4.99 Seconds
95	9530	ASCENT, 8DEG, 120KIASB, RUN 570	4.99 Seconds

Table 53.– Steady descents from ground-acoustic testing; prefix-4 database.

FLIGHT	COUNTER	DESCRIPTION	DURATION
491	49108	DESCENT, 9DEG, 60KIASB, RUN 260	54.38 Seconds
491	49109	DESCENT, 6DEG, 80KIASB, RUN 290	40.51 Seconds
491	49110	DESCENT, 9DEG, 100KIAB, RUN 350	34.87 Seconds
491	49111	DESCENT, 12DEG, 38KIAB, RUN 230	49.99 Seconds
491	49115	DESCENT, 6DEG, 60KIASB, RUN 250	39.78 Seconds
491	49116	DESCENT, 7DEG, 80KIASB, RUN 300	29.62 Seconds
491	49117	DESCENT, 6DEG, 100KIAB, RUN 340	30.05 Seconds
491	49118	DESCENT, 9DEG, 80KIASB, RUN 310	34.98 Seconds
491	49122	DESCENT, 8DEG, 120KIASB, RUN 370	32.27 Seconds
491	49124	DESCENT, 12DEG, 60KIASB, RUN 270	38.04 Seconds
491	49125	DESCENT, 12DEG, 80KIASB, RUN 320	36.77 Seconds
492	49220	DESCENT, 9DEG, 45KIASB, RUN 261	48.91 Seconds
492	49221	DESCENT, 6DEG, 75KIASB, RUN 291	32.76 Seconds
492	49222	DESCENT, 9DEG, 100KIASB, RUN 351	26.74 Seconds
492	49223	DESCENT, 12DEG, 40KIASB, RUN 231	49.78 Seconds
493	49311	DESCENT, 9DEG, 60KIASB, RUN 260	40.41 Seconds
493	49312	DESCENT, 6DEG, 80KIASB, RUN 290	28.67 Seconds
493	49313	DESCENT, 9DEG, 100KIASB, RUN 350	34.21 Seconds
493	49314	DESCENT, 9DEG, 100KIASB, RUN 351	31.94 Seconds
493	49315	DESCENT, 12DEG, 40KIASB, RUN 230	61.32 Seconds
493	49318	DESCENT, 6DEG, 60KIASB, RUN 250	36.84 Seconds
493	49319	DESCENT, 7DEG, 80KIASB, RUN 300	27.75 Seconds
493	49320	DESCENT, 6DEG, 100KIASB, RUN 340	27.98 Seconds
493	49321	DESCENT, 9DEG, 80KIASB, RUN 310	31.84 Seconds
493	49326	DESCENT, 8DEG, 120KIASB, RUN 370	27.00 Seconds
493	49328[a]	DESCENT, 12DEG, 60KIASB, RUN 270	43.33 Seconds
494	49422	DESCENT, 3DEG, 60KIASB, RUN 240	27.59 Seconds
494	49423	DESCENT, 3DEG, 80KIASB, RUN 280	32.43 Seconds
494	49424	DESCENT, 3DEG, 100KIASB, RUN 330	23.25 Seconds
494	49425	DESCENT, 12DEG, 100KIASB, RN 361	25.13 Seconds
494	49426	DESCENT, 3DEG, 40KIASB, RUN 200	45.13 Seconds
494	49427	DESCENT, 6DEG, 40KIASB, RUN 210	49.01 Seconds
494	49428	DESCENT, 9DEG, 40KIASB, RUN 220	46.48 Seconds
495	49506	DESCENT, 6DEG, 58KIASB, RUN 250	34.67 Seconds
495	49524	DESCENT, 6DEG, 60KIASB, RUN 251	38.19 Seconds
496	49616	DESCENT, 6DEG, 60KIASB, RUN 250	24.69 Seconds
497	49706	DESCENT, 6DEG, 60KIASB, RUN 257	31.91 Seconds
498	49812	DESCENT, 6DEG, 60KIASB, RUN 250	31.52 Seconds
499	49928	DESCENT, 6DEG, 60KIASB, RUN 253	18.08 Seconds

[a]Data corrupted.

Table 54.– Time slices for steady descents in prefix-4 and BH2 databases.

PREFIX-4 DATABASE			BH2 DATABASE		
COUNTER	START TIME SEC	END TIME SEC	COUNTER	START TIME SEC	END TIME SEC
49108	0.00	54.38	9108	5.37	10.36
49108	0.00	54.38	9132	18.37	23.36
49109	0.00	40.50	9109	19.37	24.36
49110	0.00	34.87	9110	15.22	20.21
49111	0.00	49.99	9111	21.81	26.80
49115	0.00	39.78	9115	5.03	10.03
49116	0.00	29.62	9116	15.73	20.73
49117	0.00	30.05	9117	12.45	17.45
49118	0.00	34.98	9118	8.88	13.87
49122	0.00	32.26	9122	7.31	12.30
49124	0.00	38.04	9124	4.30	9.29
49125	0.00	36.77	9125	8.42	13.41
49220	0.00	48.91	9220	16.14	21.13
49221	0.00	32.75	9221	16.90	21.89
49222	0.00	26.73	9222	9.29	14.28
49223	0.00	49.78	9223	21.42	26.41
49311	0.00	40.40	9311	0.28	6.27
49312	0.00	33.69	9312	8.00	12.99
49313	0.00	34.21	9313	7.00	12.00
49314	0.00	31.93	9314	6.00	11.00
49315	0.00	61.32	9315	32.01	37.00
49318	0.00	36.84	9318	4.00	8.99
49319	0.00	27.75	9319	4.01	9.00
49320	0.00	27.98	9320	0.00	5.00
49321	0.00	31.84	9321	16.01	20.99
49326	0.00	26.99	9326	4.00	8.99
49328	0.00	43.33	9328	12.01	17.00
49422	0.00	27.58	9422	15.00	19.99
49423	0.00	32.43	9423	14.00	18.99
49424	0.00	23.24	9424	11.01	16.00
49425	0.00	25.13	9425	10.00	14.99
49426	0.00	45.13	9426	4.01	9.00
49427	0.00	49.01	9427	22.00	26.99
49428	0.00	46.48	9428	20.01	25.00
49506	0.00	34.67	9506	15.01	20.00
49524	0.00	38.18	9524	19.00	24.00
49616	0.00	24.69	9616	13.00	18.00
49706	0.00	31.91	9706	5.01	10.00
49812	0.00	31.52	9812	5.01	10.00
49928	0.00	18.07	9928	12.00	17.00

Table 55.– Steady descents from ground-acoustic testing; BH2 database.

FLIGHT	COUNTER	DESCRIPTION	DURATION
91	9108	DESCENT, 9DEG, 60KIASB, RUN 260	4.99 Seconds
91	9109	DESCENT, 6DEG, 80KIASB, RUN 290	4.99 Seconds
91	9110	DESCENT, 9DEG, 100KIAB, RUN 350	4.99 Seconds
91	9111	DESCENT, 12DEG, 38KIAB, RUN 230	4.99 Seconds
91	9115	DESCENT, 6DEG, 60KIASB, RUN 250	4.99 Seconds
91	9116	DESCENT, 7DEG, 80KIASB, RUN 300	4.99 Seconds
91	9117	DESCENT, 6DEG, 100KIAB, RUN 340	4.99 Seconds
91	9118	DESCENT, 9DEG, 80KIASB, RUN 310	4.99 Seconds
91	9122	DESCENT, 8DEG, 120KIASB, RUN 370	4.99 Seconds
91	9124	DESCENT, 12DEG, 60KIASB, RUN 270	4.99 Seconds
91	9125	DESCENT, 12DEG, 80KIASB, RUN 320	4.99 Seconds
91	9132	DESCENT, 9DEG, 60KIASB, RUN 260*	4.99 Seconds
92	9220	DESCENT, 9DEG, 45KIASB, RUN 261	5.18 Seconds
92	9221	DESCENT, 6DEG, 75KIASB, RUN 291	5.19 Seconds
92	9222	DESCENT, 9DEG, 100KIASB, RUN 351	5.19 Seconds
92	9223	DESCENT, 12DEG, 40KIASB, RUN 231	5.19 Seconds
93	9311	DESCENT, 9DEG, 60KIASB, RUN 260	5.99 Seconds
93	9312	DESCENT, 6DEG, 80KIASB, RUN 290	4.99 Seconds
93	9313	DESCENT, 9DEG, 100KIASB, RUN 350	4.99 Seconds
93	9314	DESCENT, 9DEG, 100KIASB, RUN 351	4.99 Seconds
93	9315	DESCENT, 12DEG, 40KIASB, RUN 230	4.99 Seconds
93	9318	DESCENT, 6DEG, 60KIASB, RUN 250	4.99 Seconds
93	9319	DESCENT, 7DEG, 80KIASB, RUN 300	4.99 Seconds
93	9320	DESCENT, 6DEG, 100KIASB, RUN 340	4.99 Seconds
93	9321	DESCENT, 9DEG, 80KIASB, RUN 310	4.99 Seconds
93	9326	DESCENT, 8DEG, 120KIASB, RUN 370	4.99 Seconds
93	9328[a]	DESCENT, 12DEG, 60KIASB, RUN 270	4.99 Seconds
94	9422	DESCENT, 3DEG, 60KIASB, RUN 240	4.99 Seconds
94	9423	DESCENT, 3DEG, 80KIASB, RUN 280	4.99 Seconds
94	9424	DESCENT, 3DEG, 100KIASB, RUN 330	4.99 Seconds
94	9425	DESCENT, 12DEG, 100KIASB, RUN 361	4.99 Seconds
94	9426	DESCENT, 3DEG, 40KIASB, RUN 200	4.99 Seconds
94	9427	DESCENT, 6DEG, 40KIASB, RUN 210	4.99 Seconds
94	9428	DESCENT, 9DEG, 40KIASB, RUN 220	4.99 Seconds
95	9506	DESCENT, 6DEG, 58KIASB, RUN 250	4.99 Seconds
95	9524	DESCENT, 6DEG, 60KIASB, RUN 251	4.99 Seconds
96	9616	DESCENT, 6DEG, 60KIASB, RUN 250	4.99 Seconds
97	9706	DESCENT, 6DEG, 60KIASB, RUN 257	4.99 Seconds
98	9812	DESCENT, 6DEG, 60KIASB, RUN 250	4.99 Seconds
99	9928	DESCENT, 6DEG, 60KIASB, RUN 253	4.99 Seconds

[a]Data corrupted.

Table 56.– Flightpath and tip-path-plane angles for climbs at Crows Landing; ground-acoustic testing.

COUNTER	DESCRIPTION	γ	$S_e(\gamma)$	α_{TPP}	$\sigma(\alpha_{TPP})$
		DEG	DEG	DEG	DEG
9112	CLIMB, 9DEG, 60KIASB, RUN 460	3.56	0.08	–8.56	0.23
9113	CLIMB, 9DEG, 60KIASB, RUN 461	7.92	0.22	–10.62	0.17
9119	CLIMB, 6DEG, 80KIASB, RUN 490	2.56	0.16	–7.97	0.30
9120	CLIMB, 9DEG, 100KIASB, RUN 550	6.06	0.92	–14.23	1.15
9123	CLIMB, 9DEG, 80KIASB, RUN 510	6.23	0.30	–12.79	0.33
9131	CLIMB, 9DEG, 100KIASB, RUN 550*	14.02	0.42	–15.23	1.74
9216	CLIMB, 9DEG, 60KIASB, RUN 462	11.97	0.83	–10.82	2.07
9217	CLIMB, 9DEG, 60KIASB, RUN 463	10.04	1.48	–10.72	0.61
9316	ASCENT, 9DEG, 60KIASB, RUN 460	10.30	0.76	–12.48	0.77
9322	ASCENT, 6DEG, 80KIASB, RUN 490	7.06	0.70	–10.91	0.84
9323	ASCENT, 9DEG, 100KIASB, RUN 550	10.95	0.25	–14.20	0.69
9324	ASCENT, 9DEG, 100KIASB, RUN 551	12.15	0.43	–12.49	1.02
9327	ASCENT, 9DEG, 80KIASB, RUN 510	14.49	0.34	–14.10	0.74
9429	ASCENT, 6DEG, 60KIASB, RUN 450	2.97	4.15	–3.45	4.05
9507	ASCENT, 7DEG, 80KIASB, RUN 500	4.03	0.60	–11.95	0.94
9508	ASCENT, 7DEG, 80KIASB, RUN 501	7.25	0.39	–8.74	0.57
9509	ASCENT, 6DEG, 100KIASB, RUN 540	9.54	0.70	–13.64	0.93
9510	ASCENT, 3DEG, 80KIASB, RUN 480	6.69	0.15	–7.59	0.64
9511	ASCENT, 12DEG, 80KIASB, RUN 520	13.52	0.28	–17.59	0.37
9512	ASCENT, 3DEG, 60KIASB, RUN 440	7.23	1.28	–6.88	1.95
9513	ASCENT, 12DEG, 60KIASB, RUN 470	19.81	0.81	–17.21	1.39
9514	ASCENT, 12DEG, 60KIASB, RUN 471	12.89	10.15	–12.09	6.12
9515	ASCENT, 3DEG, 100KIASB, RUN 530	5.07	0.31	–9.56	0.88
9516	ASCENT, 3DEG, 100KIASB, RUN 531	1.44	0.13	–8.11	0.32
9517	ASCENT, 12DEG, 40KIASB, RUN 430	11.95	1.26	–13.43	1.81
9518	ASCENT, 9DEG, 40KIASB, RUN 420	5.92	0.24	–9.84	0.61
9519	ASCENT, 12DEG, 40KIASB, RUN 431	8.60	1.13	–9.55	1.39
9520	ASCENT, 9DEG, 40KIASB, RUN 421	13.55	1.40	–13.62	1.40
9522	ASCENT, 6DEG, 40KIASB, RUN 411	6.86	0.12	–12.24	0.49
9527	ASCENT, RUN 400 SEGMENT 3	4.66	0.07	–8.19	0.36
9530	ASCENT, 8DEG, 120KIASB, RUN 570	9.27	0.41	–14.19	0.68

Table 57.– Flightpath and tip-path-plane angles for descents at Crows Landing; ground-acoustic testing.

COUNTER	DESCRIPTION	γ DEG	$S_e(\gamma)$ DEG	α_{TPP} DEG	$\sigma(\alpha_{TPP})$, DEG
9108	DESCENT, 9DEG, 60KIASB, RUN 260	–9.28	0.18	6.78	0.16
9109	DESCENT, 6DEG, 80KIASB, RUN 290	–6.54	0.20	2.26	0.41
9110	DESCENT, 9DEG, 100KIAB, RUN 350	–9.25	0.09	4.38	0.12
9111	DESCENT, 12DEG, 38KIAB, RUN 230	–15.10	0.24	14.05	0.37
9115	DESCENT, 6DEG, 60KIASB, RUN 250	–5.40	0.21	3.14	0.34
9116	DESCENT, 7DEG, 80KIASB, RUN 300	–7.63	0.06	2.79	0.11
9117	DESCENT, 6DEG, 100KIAB, RUN 340	–4.72	0.34	–0.43	0.26
9118	DESCENT, 9DEG, 80KIASB, RUN 310	–8.76	0.08	5.73	0.17
9122	DESCENT, 8DEG, 120KIASB, RUN 370	–5.97	0.30	–0.52	0.47
9124	DESCENT, 12DEG, 60KIASB, RUN 270	–11.12	0.16	11.00	0.51
9125	DESCENT, 12DEG, 80KIASB, RUN 320	–12.13	0.40	9.16	0.25
9132	DESCENT, 9DEG, 60KIASB, RUN 260*	–6.90	0.04	5.54	0.24
9220	DESCENT, 9DEG, 45KIASB, RUN 261	–7.89	0.86	5.27	1.07
9221	DESCENT, 6DEG, 75KIASB, RUN 291	–6.06	0.59	2.09	0.90
9222	DESCENT, 9DEG, 100KIASB, RUN 351	–7.90	0.16	2.45	0.23
9223	DESCENT, 12DEG, 40KIASB, RUN 231	–13.53	0.41	12.59	0.51
9311	DESCENT, 9DEG, 60KIASB, RUN 260	–7.52	0.38	5.16	0.52
9312	DESCENT, 6DEG, 80KIASB, RUN 290	–5.85	0.08	3.98	0.21
9313	DESCENT, 9DEG, 100KIASB, RUN 350	–9.15	0.05	4.22	0.18
9314	DESCENT, 9DEG, 100KIASB, RUN 351	–8.95	0.34	5.42	0.47
9315	DESCENT, 12DEG, 40KIASB, RUN 230	–10.13	0.08	8.15	0.84
9318	DESCENT, 6DEG, 60KIASB, RUN 250	–6.10	0.20	0.93	0.51
9319	DESCENT, 7DEG, 80KIASB, RUN 300	–8.03	0.04	2.01	0.18
9320	DESCENT, 6DEG, 100KIASB, RUN 340	–5.70	0.22	1.37	0.26
9321	DESCENT, 9DEG, 80KIASB, RUN 310	–8.53	0.29	3.90	0.44
9326	DESCENT, 8DEG, 120KIASB, RUN 370	–6.22	0.09	–1.05	0.30
9328[a]	DESCENT, 12DEG, 60KIASB, RUN 270	–	–	–	–
9422	DESCENT, 3DEG, 60KIASB, RUN 240	–3.86	0.55	–1.16	1.41
9423	DESCENT, 3DEG, 80KIASB, RUN 280	–3.60	0.06	–0.72	0.33
9424	DESCENT, 3DEG, 100KIASB, RUN 330	–3.25	0.15	–2.55	0.24
9425	DESCENT, 12DEG, 100KIASB, RUN 361	–10.96	0.45	6.96	1.33
9426[a]	DESCENT, 3DEG, 40KIASB, RUN 200	–3.27	3.04	3.86	0.38
9427	DESCENT, 6DEG, 40KIASB, RUN 210	–5.08	0.41	1.34	0.77
9428	DESCENT, 9DEG, 40KIASB, RUN 220	–6.05	0.56	3.46	1.17
9506	DESCENT, 6DEG, 58KIASB, RUN 250	–5.24	0.17	1.78	0.20
9524	DESCENT, 6DEG, 60KIASB, RUN 251	–5.10	0.17	2.83	0.55
9616	DESCENT, 6DEG, 60KIASB, RUN 250	–6.04	0.05	3.90	0.22
9706	DESCENT, 6DEG, 60KIASB, RUN 257	–4.64	0.31	2.85	0.55
9812	DESCENT, 6DEG, 60KIASB, RUN 250	–6.50	0.14	4.34	0.20
9928	DESCENT, 6DEG, 60KIASB, RUN 253	–7.42	0.29	5.14	0.62

[a]Laser/radar tracking data erroneous.

Table 58.– Time slices for dynamic climbs in prefix-4 and BH2 databases.

PREFIX-4 DATABASE			BH2 DATABASE		
COUNTER	START TIME SEC	END TIME SEC	COUNTER	START TIME SEC	END TIME SEC
49112	0.00	32.47	9140	5.63	11.62
49113	0.00	35.83	9141	3.07	9.07
49119	0.00	29.04			
49120	0.00	27.92	9142	4.49	10.98
49123	0.00	27.24	9143	4.99	11.98
49216	0.00	30.72	9230	4.60	10.56
49217	0.00	29.86	9231	4.60	12.59
49316	0.00	31.68	9343	4.90	10.09
49322	0.00	23.53	9344	5.01	10.00
49323	0.00	26.00			
49324	0.00	29.81			
49327	0.00	26.57			
49429	0.00	30.08	9429	1.00	7.00
49429	0.00	30.08	9443	9.01	14.00
49507	0.00	27.28	9541	4.00	12.99
49508	0.00	26.46	9542	3.01	10.00
49509	0.00	24.05	9543	3.01	8.00
49510	0.00	25.13			
49511	0.00	24.41	9544	6.01	12.00
49512	0.00	34.36			
49513	0.00	30.82			
49514	0.00	34.22	9514	8.00	19.00
49515	0.00	21.26			
49516	0.00	25.43			
49517	0.00	42.80			
49518	0.00	41.42			
49519	0.00	41.08			
49520	0.00	39.37			
49521	0.00	6.43			
49522	0.00	47.46			
49525	0.00	59.23			
49530	0.00	27.57	9545	9.00	14.99

Table 59.– Dynamic climbs at Crows Landing; ground-acoustic testing.

FLIGHT	COUNTER	DESCRIPTION	DURATION
91	9140	CLIMB OUT, CNTR 9112, RUN 460*	5.99 Seconds
91	9141	CLIMB OUT, CNTR 9113, RUN 461*	5.99 Seconds
91	9142	CLIMB OUT, CNTR 9119, RUN 550*	6.49 Seconds
91	9143	CLIMB OUT, CNTR 9123, RUN 510*	6.99 Seconds
92	9230	CLIMB, 9DEG, 60KIASB, RUN 462*	5.96 Seconds
92	9231	CLIMB, 9DEG, 60KIASB, RUN 463*	8.18 Seconds
93	9343	ASCENT, 9DEG, 60KIASB, RUN 460*	4.99 Seconds
93	9344	ASCENT, 6DEG, 80KIASB, RUN 490*	4.99 Seconds
94	9429	ASCENT, 6DEG, 60KIASB, RUN 450	5.99 Seconds
94	9443	ASCENT, 6DEG, 60KIASB, RUN 450*	4.99 Seconds
95	9514	ASCENT, 12DEG, 60KIASB, RUN 471	10.99 Seconds
95	9541	ASCENT, 7DEG, 80KIASB, RUN 500*	8.99 Seconds
95	9542	ASCENT, 7DEG, 80KIASB, RUN 501*	6.99 Seconds
95	9543	ASCENT, 6DEG, 100KIASB, RUN 540*	4.99 Seconds
95	9544	ASCENT, 12DEG, 80KIASB, RUN 520*	5.99 Seconds
95	9545	ASCENT, 8DEG, 120KIASB, RUN 570*	5.99 Seconds

Table 60.– Time slices for dynamic descents in prefix-4 and BH2 databases.

PREFIX-4 DATABASE			BH2 DATABASE		
COUNTER	START TIME SEC	END TIME SEC	COUNTER	START TIME SEC	END TIME SEC
49108	0.00	54.38	9150	37.37	45.36
49109	0.00	40.50	9151	25.37	32.36
49110	0.00	34.87			
49111	0.00	49.99	9152	39.81	49.80
49115	0.00	39.78	9153	30.03	37.02
49116	0.00	29.62	9154	23.74	29.22
49117	0.00	30.05			
49118	0.00	34.98	9155	23.88	33.87
49122	0.00	32.26			
49124	0.00	38.04	9156	35.30	41.30
49125	0.00	36.77			
49220	0.00	48.91	9240	31.14	43.13
49221	0.00	32.75	9241	23.90	30.89
49222	0.00	26.73	9242	16.29	22.28
49223	0.00	49.78	9243	37.42	46.41
49311	0.00	40.40	9340	27.28	33.27
49312	0.00	33.69			
49313	0.00	34.21			
49314	0.00	31.93	9341	20.00	25.99
49315	0.00	61.32	9342	50.01	55.00
49318	0.00	36.84			
49319	0.00	27.75			
49320	0.00	27.98			
49321	0.00	31.84			
49326	0.00	26.99			
49328	0.00	43.33			
49422	0.00	27.58			
49423	0.00	32.43	9440	23.00	29.99
49424	0.00	23.24	9441	18.00	23.00
49425	0.00	25.13	9442	17.00	21.99
49426	0.00	45.13			
49427	0.00	49.01			
49428	0.00	46.48			
49506	0.00	34.67			
49524	0.00	38.18			
49616	0.00	24.69			
49706	0.00	31.91			
49812	0.00	31.52			
49928	0.00	18.07			

Table 61.– Dynamic descents at Crows Landing; ground-acoustic testing.

FLIGHT	COUNTER	DESCRIPTION	DURATION
91	9150	PULLUP, CNTR 9108, RUN 260*	7.99 Seconds
91	9151	PULLUP, CNTR 9109, RUN 290*	6.99 Seconds
91	9152	PULLUP, CNTR 9111, RUN 230*	9.99 Seconds
91	9153	PULLUP, CNTR 9115, RUN 250*	7.19 Seconds
91	9154	PULLUP, CNTR 9116, RUN 300*	5.68 Seconds
91	9155	PULLUP, CNTR 9118, RUN 310*	10.19 Seconds
91	9156	PULLUP, CNTR 9124, RUN 270*	6.00 Seconds
92	9240	DESCENT, 9DEG, 45KIASB, RUN 261*	12.18 Seconds
92	9241	DESCENT, 6DEG, 75KIASB, RUN 291*	7.19 Seconds
92	9242	DESCENT, 9DEG, 100KIASB, RUN 351*	6.19 Seconds
92	9243	DESCENT, 12DEG, 40KIASB, RUN 231*	9.19 Seconds
93	9340	DESCENT, 9DEG, 60KIASB, RUN 260*	5.99 Seconds
93	9341	DESCENT, 9DEG, 100KIASB, RUN 351*	5.99 Seconds
93	9342	DESCENT, 12DEG, 40KIASB, RUN 230*	4.99 Seconds
94	9440	DESCENT, 3DEG, 80KIASB, RUN 280*	6.99 Seconds
94	9441	DESCENT, 3DEG, 100KIASB, RUN 330*	4.99 Seconds
94	9442	DESCENT, 12DEG, 100KIASB, RUN 361*	4.99 Seconds

Table 62.– Vertical climbs at Crows Landing; prefix-4 database.

FLIGHT	COUNTER	DESCRIPTION	DURATION
94	49417	HOVER/ASCENT, 1600FPM, RUN 880	38.80 Seconds
94	49418	HOVER/ASCENT, 900FPM, RUN 881	42.11 Seconds
94	49419	HOVER/ASCENT, 2200FPM, RUN 890	28.55 Seconds

Table 63.– Time slices for vertical climbs in prefix-4 and BH2 databases.

PREFIX-4 DATABASE			BH2 DATABASE		
COUNTER	START TIME SEC	END TIME SEC	COUNTER	START TIME SEC	END TIME SEC
49417	0.00	38.79	9417	3.00	30.00
49418	0.00	42.10	9418	8.00	38.00
49419	0.00	28.55	9419	8.00	28.00

Table 64.– Vertical climbs at Crows Landing; BH2 database.

FLIGHT	COUNTER	DESCRIPTION	DURATION
94	9417	HOVER/ASCENT, 1600FPM, RUN 880	27.00 Seconds
94	9418	HOVER/ASCENT, 900FPM, RUN 881	30.00 Seconds
94	9419	HOVER/ASCENT, 2200FPM, RUN 890	20.00 Seconds

Table 65.– Measured rates of climb and power ratios for vertical climbs.

COUNTER	CLIMB RATE, FT/MIN	POWER RATIO	DURATION, SEC
9417	1287.	1.252	9.52 to 26.93
9418	600.	1.165	10.75 to 29.95
9419	1871.	1.519	4.17 to 19.93

Table 66.– Steady climbs.

FLIGHT	COUNTER	DESCRIPTION	DURATION
89	8929	CLIMB, 80KIASB, 500FPM	10.20 Seconds
89	8931	CLIMB, 80KIASB, 1000FPM	10.28 Seconds
89	8932	CLIMB, 80KIASB, 1500FPM	10.69 Seconds
90	9006	CLIMB, 80KIASB, 3000FT HPB	4.99 Seconds
90	9007	CLIMB, 80KIASB, 6000FT HPB	4.99 Seconds
90	9008	CLIMB, 80KIASB, 9000FT HPB	4.99 Seconds
90	9009	CLIMB, 80KIASB, 12000FT HPB	4.99 Seconds
90	9010	CLIMB, 67KIASB, 15000FT HPB	4.99 Seconds
115	11523	CLIMB, 1000FPM, 62KIASB	4.99 Seconds
115	11524	CLIMB, MAX RATE, 62KIASB	4.99 Seconds
115	11525	CLIMBING TURN, 1000FPM, 62KIASB	9.99 Seconds

Table 67.– Steady descents; in-flight acoustic testing.

FLIGHT	COUNTER	DESCRIPTION	DURATION
100	10008	DESCENT, 300FPM, 65KIASB, PT D	13.99 Seconds
100	10009	DESCENT, 300FPM, 65KIASB, PT D	14.00 Seconds
100	10010	DESCENT, 400FPM, 65KIASB, PT E	13.99 Seconds
100	10011	DESCENT, 400FPM, 65KIASB, PT E	13.99 Seconds
100	10013	DESCENT, 500FPM, 65KIASB, PT F	13.99 Seconds
100	10014	DESCENT, 500FPM, 65KIASB, PT F	12.00 Seconds
100	10015	DESCENT, 600FPM, 65KIASB, PT G	13.99 Seconds
101	10106	DESCENT, 600FPM, 65KIASB, PT G	13.99 Seconds
101	10110	DESCENT, 700FPM, 65KIASB, PT H	13.99 Seconds
101	10111	DESCENT, 700FPM, 65KIASB, PT H	13.99 Seconds
101	10112	DESCENT, 800FPM, 65KIASB, PT I	13.99 Seconds
101	10113	DESCENT, 800FPM, 65KIASB, PT I	14.00 Seconds
101	10114	DESCENT, 900FPM, 65KIASB, PT J	13.99 Seconds
101	10115	DESCENT, 900FPM, 65KIASB, PT J	13.99 Seconds
101	10117	DESCENT, 400FPM, 75KIASB, PT E	13.99 Seconds
102	10208	DESCENT, 400FPM, 75KIASB, PT E	13.99 Seconds
102	10209	DESCENT, 400FPM, 75KIASB, PT E	13.99 Seconds
102	10210	DESCENT, 500FPM, 75KIASB, PT F	13.99 Seconds
102	10211	DESCENT, 500FPM, 75KIASB, PT F	14.04 Seconds
102	10213	DESCENT, 600FPM, 75KIASB, PT G	14.00 Seconds
102	10214	DESCENT, 600FPM, 75KIASB, PT G	14.00 Seconds
102	10216	DESCENT, 700FPM, 75KIASB, PT H	13.99 Seconds
102	10217	DESCENT, 700FPM, 75KIASB, PT H	13.99 Seconds
102	10218	DESCENT, 800FPM, 75KIASB, PT I	13.99 Seconds
102	10219	DESCENT, 800FPM, 75KIASB, PT I	13.99 Seconds
102	10220	DESCENT, 900FPM, 75KIASB, PT J	13.99 Seconds
103	10306	DESCENT, 300FPM, 95KIASB, PT D	13.90 Seconds
103	10309	DESCENT, 400FPM, 95KIASB, PT E	14.00 Seconds
103	10311	DESCENT, 400FPM, 95KIASB, PT E	14.00 Seconds
113	11306	DESCENT, 200FPM, 65KIASB, PT C	13.99 Seconds
113	11307	DESCENT, 200FPM, 65KIASB, PT C	10.99 Seconds
113	11308	DESCENT, 300FPM, 65KIASB, PT D	13.99 Seconds
113	11309	DESCENT, 300FPM, 65KIASB, PT D	13.99 Seconds
113	11310	DESCENT, 400FPM, 65KIASB, PT E	13.99 Seconds
113	11311	DESCENT, 400FPM, 65KIASB, PT E	13.99 Seconds
113	11312	DESCENT, 500FPM, 65KIASB, PT F	13.99 Seconds
113	11313	DESCENT, 500FPM, 65KIASB, PT F	13.99 Seconds
113	11314	DESCENT, 600FPM, 65KIASB, PT G	13.99 Seconds
113	11315	DESCENT, 600FPM, 65KIASB, PT G	10.61 Seconds
113	11317	DESCENT, 700FPM, 65KIASB, PT H	13.99 Seconds
113	11318	DESCENT, 700FPM, 65KIASB, PT H	14.00 Seconds
113	11319	DESCENT, 800FPM, 65KIASB, PT I	14.00 Seconds
113	11320	DESCENT, 800FPM, 65KIASB, PT I	13.99 Seconds
113	11321	DESCENT, 900FPM, 65KIASB, PT J	13.99 Seconds
113	11322	DESCENT, 900FPM, 65KIASB, PT J	13.99 Seconds

Table 67.– Concluded.

FLIGHT	COUNTER	DESCRIPTION	DURATION
114	11409	DESCENT, 200FPM, 68KIASB, PT C	13.99 Seconds
114	11410	DESCENT, 200FPM, 68KIASB, PT C	13.99 Seconds
114	11411	DESCENT, 300FPM, 68KIASB, PT D	13.99 Seconds
114	11412	DESCENT, 300FPM, 68KIASB, PT D	13.99 Seconds
114	11413	DESCENT, 400FPM, 68KIASB, PT E	13.99 Seconds
114	11414	DESCENT, 400FPM, 68KIASB, PT E	13.99 Seconds
114	11415	DESCENT, 500FPM, 68KIASB, PT F	13.99 Seconds
114	11416	DESCENT, 500FPM, 68KIASB, PT F	13.99 Seconds
114	11417	DESCENT, 600FPM, 68KIASB, PT G	6.82 Seconds
114	11418	DESCENT, 600FPM, 68KIASB, PT G	13.99 Seconds
114	11419	DESCENT, 700FPM, 68KIASB, PT H	13.99 Seconds
114	11420	DESCENT, 700FPM, 68KIASB, PT H	13.99 Seconds
114	11421	DESCENT, 800FPM, 68KIASB, PT I	13.99 Seconds
114	11422	DESCENT, 800FPM, 68KIASB, PT I	13.99 Seconds
114	11423	DESCENT, 900FPM, 68KIASB, PT J	13.99 Seconds
114	11424	DESCENT, 900FPM, 68KIASB, PT J	13.99 Seconds
114	11425	DESCENT, 1000FPM, 68KIASB, PT K	13.99 Seconds

Table 68.– Powered descents.

FLIGHT	COUNTER	DESCRIPTION	DURATION
83	8329	DESCENT, 150KIASB, 5000'HP	4.99 Seconds
83	8330	DESCENT, 160KIASB, 5000'HP	4.99 Seconds
110	11014	POWER DES, 145KIASB, CWS=.08	4.99 Seconds
110	11015	POWER DES, 150KIASB, CWS=.08	4.40 Seconds
110	11016	POWER DES, 155KIASB, CWS=.08	4.99 Seconds
110	11017	POWER DES, 160KIASB, CWS=.08	9.99 Seconds
110	11018	POWER DES, 165KIASB, CWS=.08	6.99 Seconds
110	11019	POWER DES, 170KIASB, CWS=.08	6.99 Seconds
116	11682	DESCENT, 186KIAS (VNE)	10.99 Seconds

Table 69.– Parameters for powered-descent cases.

COUNTER	C_W/σ	C_P/σ	μ	RATE OF CLIMB, FT/MIN	γ, DEG	H_p, FT
8329	—	0.00937	0.411	–1615.	–5.16	5408.
8330	—	0.00992	0.434	–2049.	–6.20	4449.
11014	0.080	0.01019	0.381	–589.	–2.03	4369.
11015	0.080	0.00987	0.393	–861.	–2.89	4372.
11016	0.080	0.01025	0.407	–1419.	–4.58	4577.
11017	0.079	0.00955	0.418	–2008.	–6.31	4457.
11018	0.079	0.00976	0.432	–2756.	–8.34	4594.
11019	0.079	0.00995	0.444	–3574.	–10.48	4781.
11682	0.082	0.00971	0.478	–4410.	–11.98	5088.

Table 70.– Autorotational descents.

FLIGHT	COUNTER	DESCRIPTION	DURATION
115	11539	AUTOROTATION, 60KIASB, SEG 1	27.00 Seconds
115	11540	AUTOROTATION, 60KIASB, SEG 2	26.99 Seconds
115	11541	AUTOROTATION, 80KIASB, SEG 1	26.00 Seconds
115	11542	AUTOROTATION, 80KIASB, SEG 2	20.99 Seconds

Table 71.– Event times for autorotational descents. The combined time is based on the time defined by the first counter. Time based on the second segment is shown in a separate column.

EVENT	COUNTER 11539/11540[a]		COUNTER 11541/11542[b]	
	TIME (COMBINED) SEC	TIME (2ND) SEC	TIME (COMBINED) SEC	TIME (2ND) SEC
Record start (Seg. 1)	0.00	—	0.00	—
Power failure transient	9.18	—	6.92	—
Steady descent start	15.45	—	12.01	—
Record end (Seg. 1)	26.95	—	25.91	—
Record start (Seg. 2)	28.00	0.00	26.98	0.00
Steady descent end	39.15	11.17	34.69	7.69
Record end (Seg. 2)	54.92	26.91	47.91	20.93

[a] 1.055 sec gap between counters.

[b] 1.069 sec gap between counters.

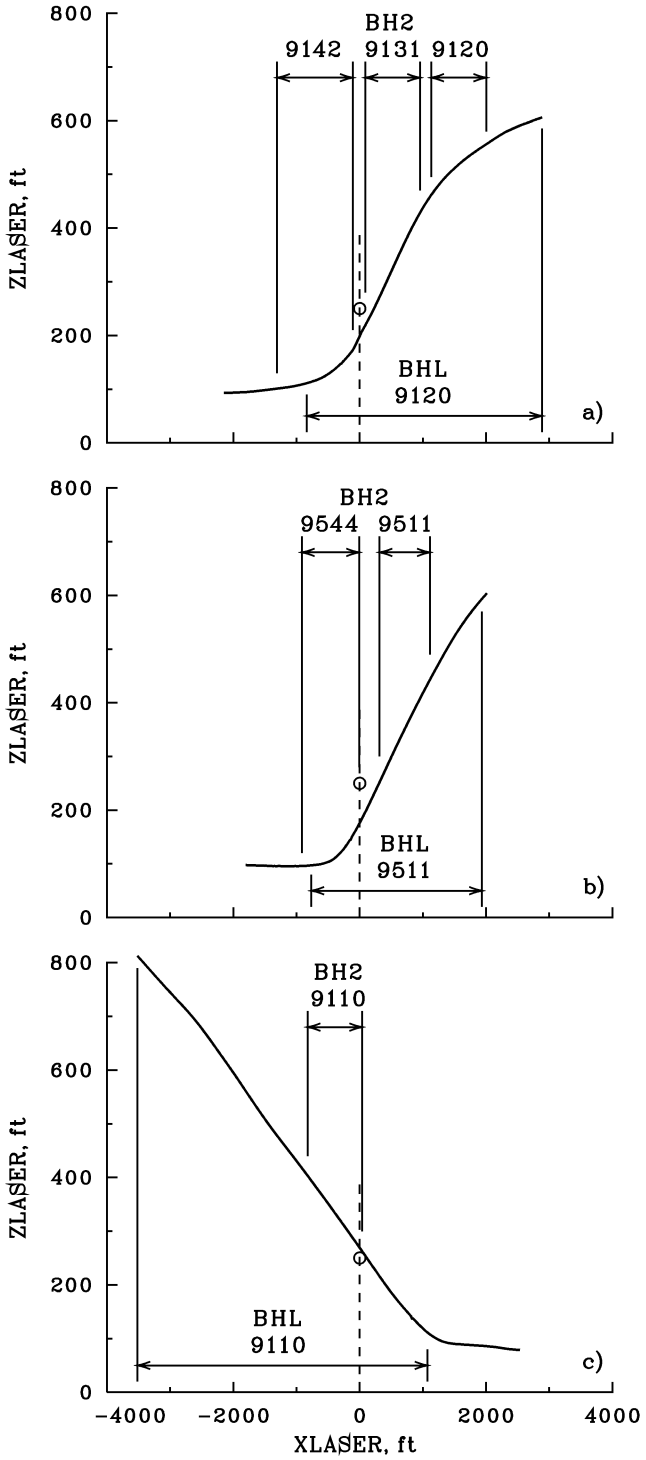

Figure 41.– Three sample climb and descent trajectories during ground-acoustic testing; 8.5X vertical scale exaggeration. Open circle shows target elevation for flight over microphone array centerpoint: a) Counter 49120, 100 KIASB, 9 deg climb; b) Counter 49511, 80 KIASB, 12 deg climb; c) Counter 49110, 100 KIASB, 9 deg descent.

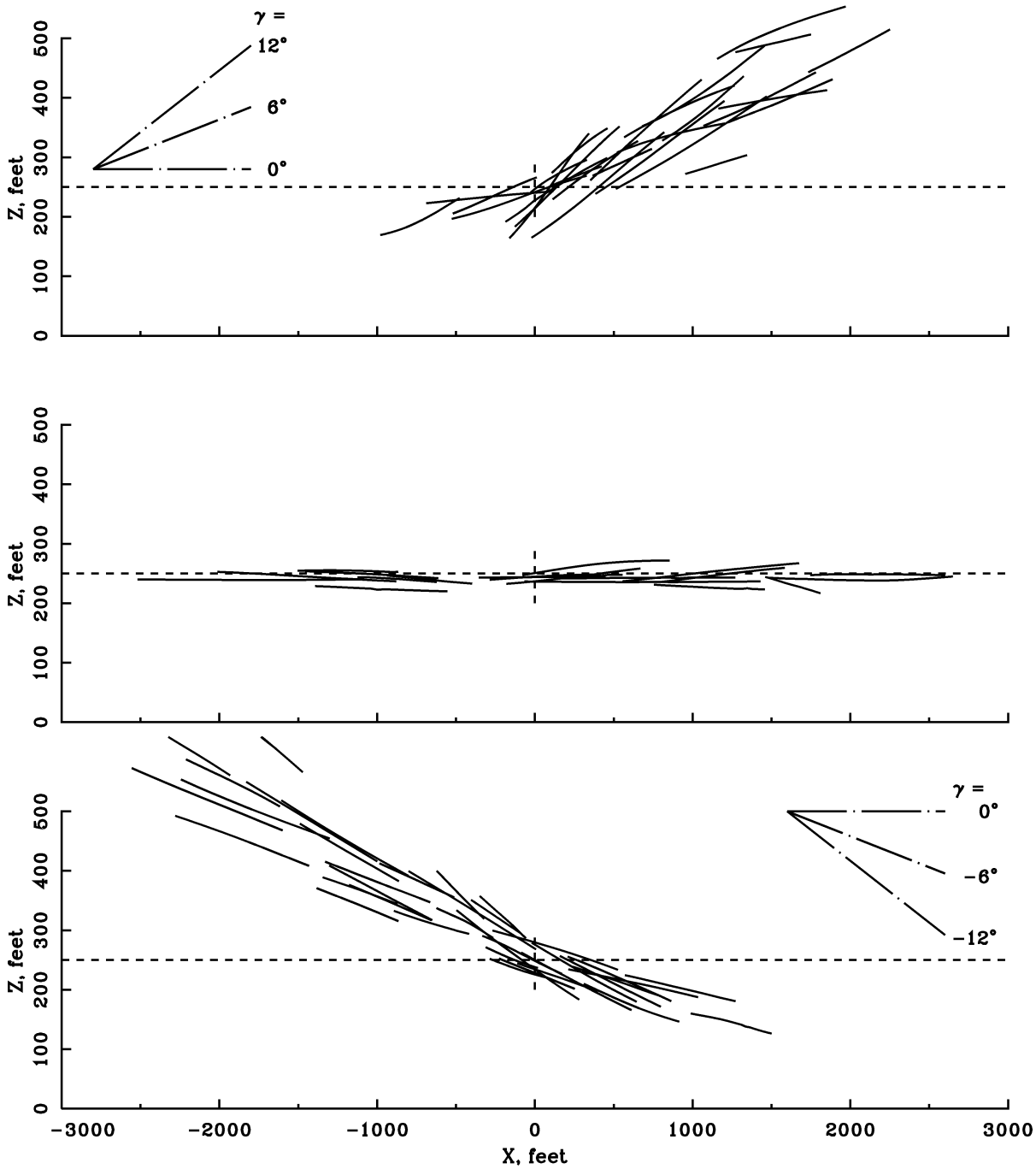

Figure 42.– Vertical position as a function of horizontal position during climb, level flight and descending flight conditions as obtained with a laser tracker. Vertical scale has a 3.75X exaggeration.

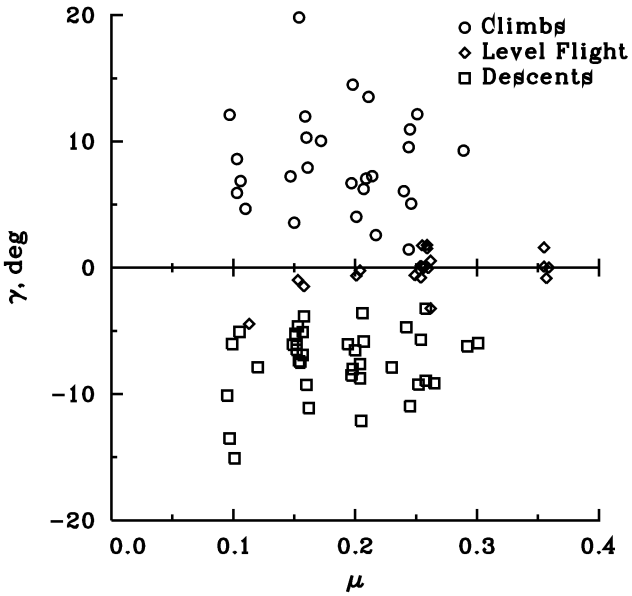

Figure 43.– Flightpath angles measured using a laser tracker for climbs, level flight, and descending flight conditions during ground-acoustic testing at Crows NAAF.

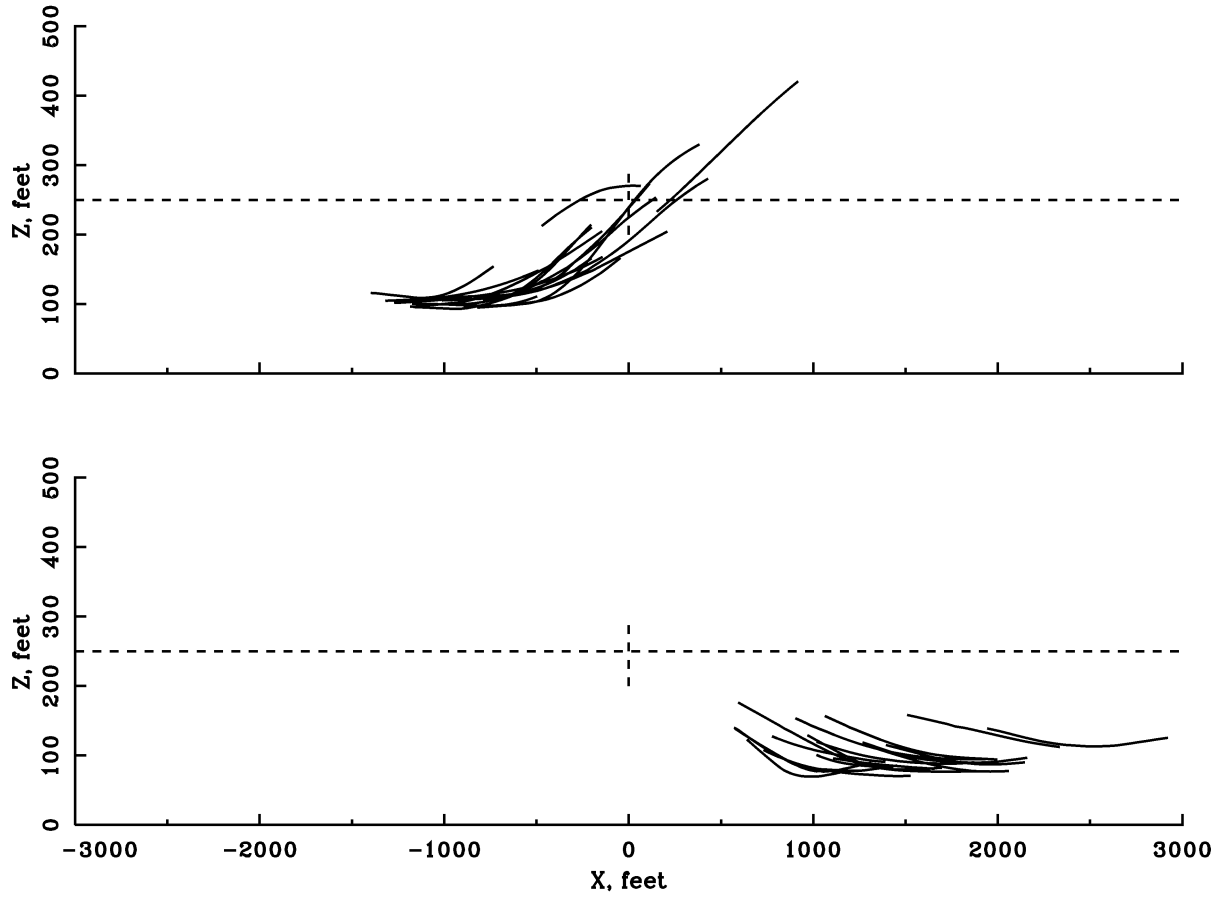

Figure 44.– Vertical position as a function of horizontal position during dynamic ascents and descents as obtained with a laser tracker. Vertical scale has a 3.75X exaggeration.

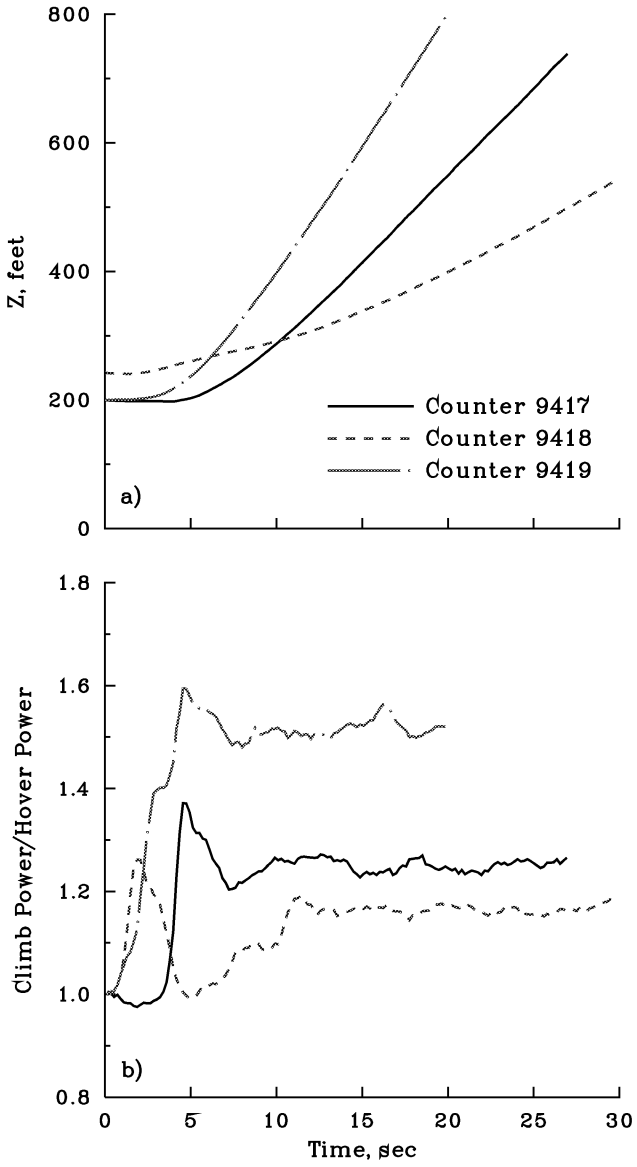

Figure 45.– Vertical climb cases at Crows Landing: a) vertical position as a function of time; b) power ratio as a function of time.

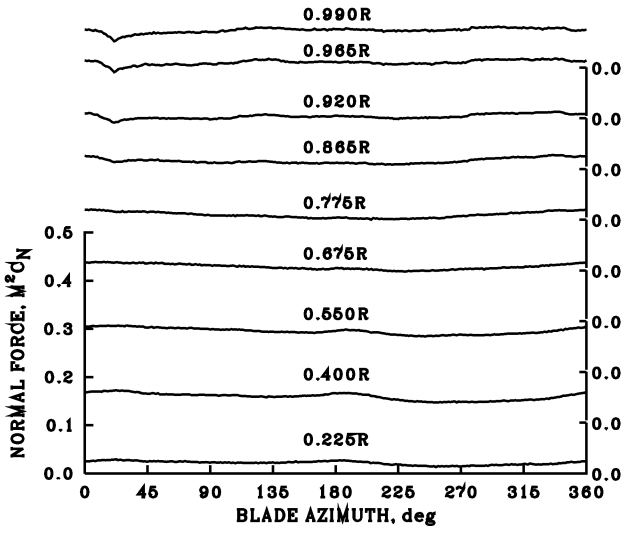

Figure 46.– Measured normal force for maximum vertical climb condition; counter 9419.

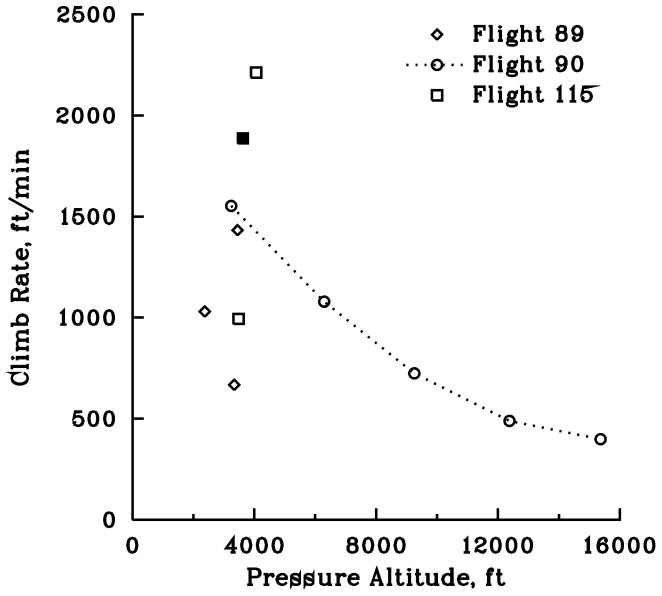

Figure 47.– Climb rates as a function of pressure altitude for steady climb data. Solid square symbol represents a climbing turn condition; counter 11525.

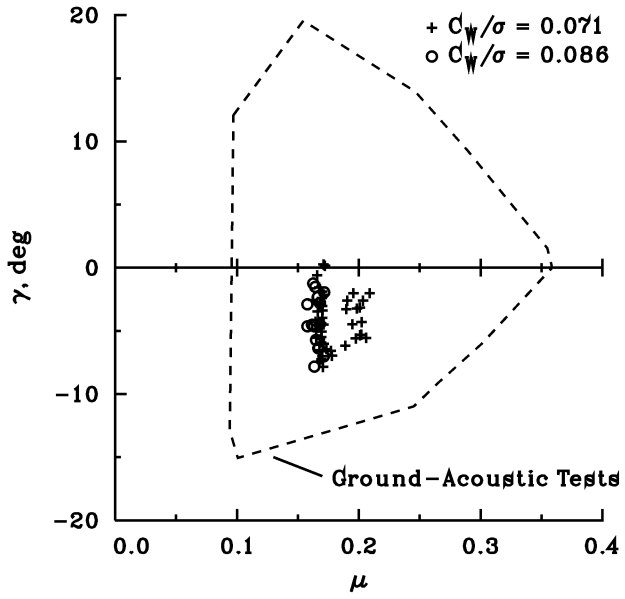

Figure 48.– Flightpath angles for in-flight acoustic descent conditions.

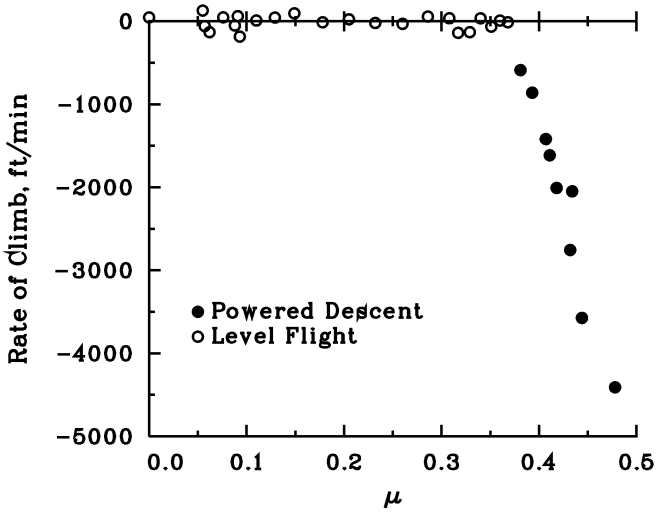

Figure 49.– Rate of climb during powered descents. Level flight data from Flight 85 shown for reference; $C_W/\sigma = 0.08$.

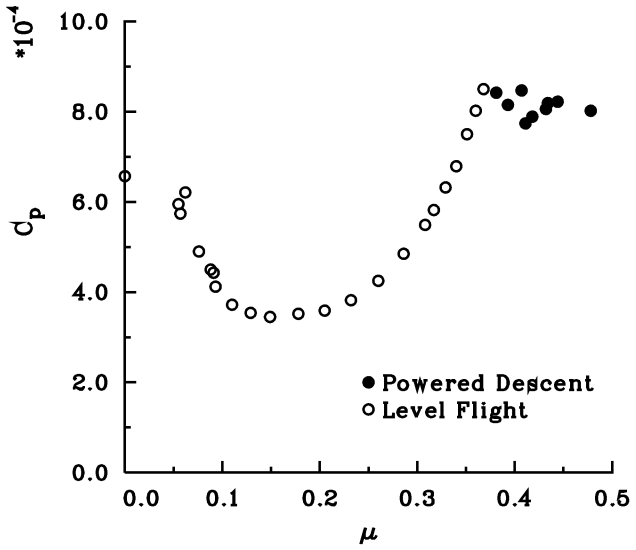

Figure 50.– Engine power coefficient during powered descents. Level flight data from Flight 85 shown for reference; $C_W/\sigma = 0.08$.

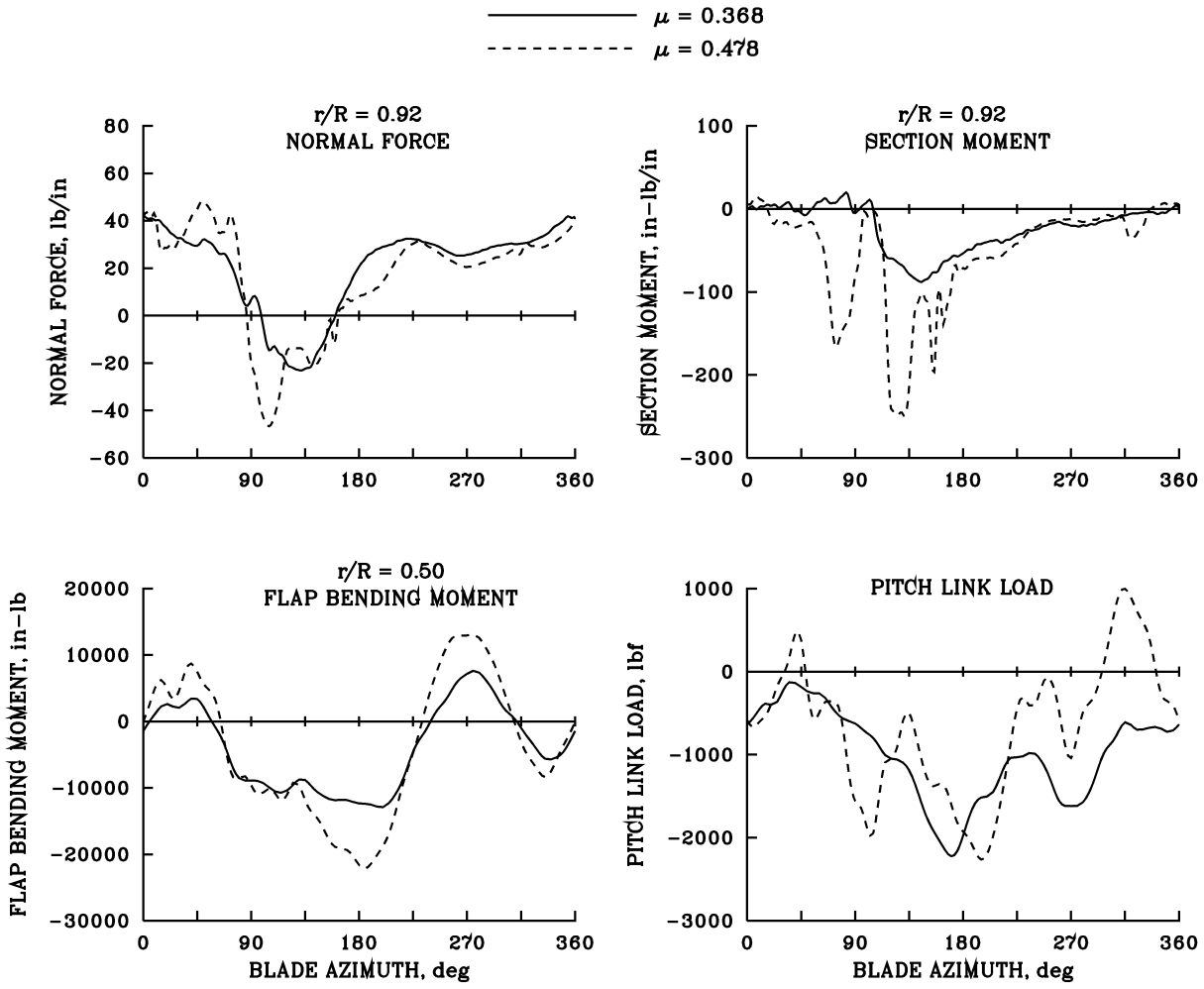

Figure 51.– Comparison of rotor airloads and structural loads for maximum level flight condition, $\mu = 0.368$, and for maximum dive speed, $\mu = 0.478$.

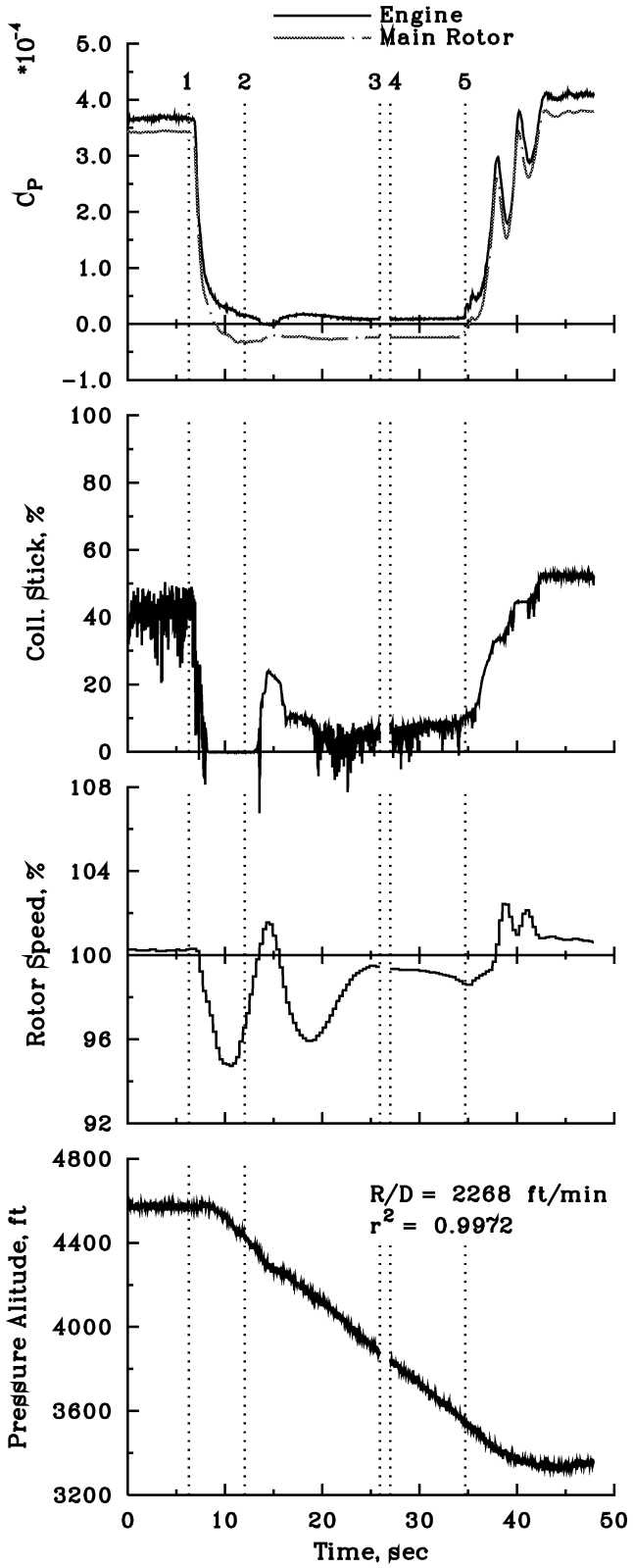

Figure 52.– Autorotational descent; $\mu = 0.222$. Combined record from Counters 11539 and 11540.

8. MANEUVERS

Maneuvers are generally defined as flight conditions where the aircraft is in some form of accelerated flight. Maneuvers can be steady, for instance in a bank-angle turn in level flight, where the pitch and yaw rates are non-zero, but all angular and linear accelerations are zero. Or maneuvers can be unsteady where one or more angular and linear accelerations are non-zero. However, the distinction between steady and unsteady maneuvers is sometimes difficult to make. The piloting of a steady maneuver state often results in significant periods of unsteady flight and the steady portion of such a maneuver may be quite short in duration. From a rotor loading standpoint, however, even short-duration maneuvers may provide multiple consecutive rotor revolutions which for comparison purposes may be considered steady or quasi-steady.

Maneuvering flight data were obtained in the Airloads Program for a variety of flight conditions including: 1) level bank-angle turns, 2) diving bank-angle turns, 3) symmetric pull-ups, 4) rolling pullouts, 5) pushovers, 6) UTTAS maneuvers, 7) roll reversals, 8) control pulses in bank-angle turns, 9) accelerating and decelerating flight, 10) settling with power, 11) moderate and aggressive heading turns for acoustic testing, and 12) constant radius turns for acoustic testing. The extrema in rotor loading are shown in figure 53 as a function of advance ratio for a number of these maneuvering flight cases. In this figure the weight coefficient has been multiplied by the aircraft load factor. For comparison purposes, the rotor thrust limit as determined by wind tunnel testing (ref. 31) is included in the figure.

To obtain the maximum and minimum load factor data in figure 53, the aircraft's vertical acceleration (AZCG) and advance ratio (AMU) were extracted from TRENDS using the PRINT command in TIMEHIST. As the vertical accelerometer measurement was noisy, the convolution filter (CVF) in TRENDS was used to reduce the noise. The cutoff frequency was set at 2 Hz and a half cosine window was used. The data were decremented within the PRINT command (/S=5), resulting in an effective sample rate of about 40 Hz. The weight coefficient (CT) in the rotor loading term was obtained using the average value obtained with the VIEW command. Unless otherwise noted, this procedure has been used for the figures in this section.

The maneuvers shown in figure 53 include several cases where the peak loading is well beyond the rotor thrust limit, and these types of maneuvers may size rotor components as well as the fixed-system controls. A number of the maneuvers are more moderate, for instance the conditions for level bank-angle turns in figure 53(a). The maneuvers performed during ground-acoustic testing (see figs. 53(e) and (f)) are benign. In reference 9, the present authors calculated the relative severity of all of the maneuvers in this section by examining representative loads. In addition, this maneuver data set was augmented with the powered descent cases discussed in section 7. For each selected measurement, the rank order of each maneuver was determined, that is, a rank of one was the most severe maneuver at this station, a rank of two was the next most severe maneuver, and so on. A composite ranking was then devised based on a subset of six measurements: the pitch-link load, the torsion moment at 0.30R, and the flap and chord bending measurements at 0.113R and 0.60R. The severity of the test maneuvers based on the composite ranking is shown in table 72 for the 12 most severe maneuvers. The most severe maneuver in the Airloads Program was a 60° diving bank-angle turn to the right at a nominal airspeed of 140 knots (Counter 11680). Note, however, that although

this maneuver was the most severe case encountered for three of the measurements, that is, the pitch-link load, the torsion moment at 0.30*R*, and the chord bending moment at 0.113*R*, other maneuvers were more severe at other measurement locations. For the flap bending moment at 0.113*R*, the most severe case was the UTTAS pull-up (Counter 11029); for the flap bending moment at 0.60*R*, the greatest severity occurred in a high-speed dive (Counter 11682); and for the chord bending moment at 0.60*R*, the most severe case was a 55° diving bank-angle turn to the left at a nominal airspeed of 120 knots (Counter 11659).

In the sections below, the maneuvers flown in the Airloads Program are placed in appropriate groups and discussed. The first section, "Level Bank-angle Turns," discusses bank-angle turns that were flown at moderate air speeds where there was sufficient power to maintain level flight. The next section, "Diving Bank-angle Turns," addresses flight counters obtained in diving turns where the kinetic energy available in the descent provided the necessary power for these high-speed and high-load factor turns. The next four sections treat unsteady maneuvers that result in either very high or low load factors: "Symmetric Pull-ups," "Rolling Pullouts," "Pushovers," and "UTTAS Maneuvers." The "Roll Reversals" section discusses flight counters where the aircraft was rolled rapidly to provide a high roll rate to either the left or right.

In a number of level bank-angle turns, a longitudinal control pulse was made, which rapidly increased the load factor. These counters, discussed in the section "Control Pulse in Bank-angle Turns," have aspects related both to maneuvering flight and flight dynamics. The counters described in the section "Accelerating and Decelerating Flight" include accelerating flight cases starting from a hover and their converse, decelerating cases approaching a hover.

The final sections contain maneuver data obtained during the ground-acoustic test portion of the program. The section dealing with "Moderate and Aggressive Heading Turns" examine flight cases where the aircraft approached the microphone array on one heading and then turned over the array and departed with a different heading. The rapidity of the heading change is used to distinguish between the moderate and aggressive turns. Finally, the section "Constant Radius Turns" includes data obtained in turns centered on the ground-acoustic array, and include three different radii.

Level Bank-Angle Turns

Fifteen level bank-angle turns were flown during the Airloads Program and the counters are listed in table 73. The load factor and advance ratio for these maneuvers are shown with open symbols in figure 53(a). The flight card called for the pilot to maintain a fixed bank-angle and airspeed for five seconds without gaining or losing altitude. Of the 15 level bank-angle turns in table 73, 13 are for right turns and two are for left turns. The level bank-angle turns were obtained at nominal C_W/σ values of 0.08, 0.10, 0.11, 0.12, and 0.13.

The distinction between the level bank-angle turns discussed here and the diving bank-angle turns discussed in the next section is illustrated in figure 54. This figure shows the average rate of climb during the bank-angle turns as a function of the advance ratio. The rate of climb data for the level bank-angle turns range from –267 ft/min to 470 ft/min, with a mean of 54 ft/min and a standard deviation of 252 ft/min. The rate of climb in the diving bank-angle turns vary from –252 ft/min to

–5704 ft/min. Bank-angle turns in level flight can only be accomplished if sufficient power is available. At higher speeds, it is necessary to descend to overcome the power deficit. The rates of climb shown in figure 54 were determined by fitting a linear regression curve to the boom pressure altitude measurements (HPB) as a function of time. These pressure altitude data were obtained from TRENDS using the PRINT command in TIMEHIST.

The level bank-angle counters in table 73 are from 8.10 to 33.00 seconds in length. The test objective was to obtain a specific bank angle and airspeed and then hold these values for five seconds. Many of these counters include the entry or exit from the maneuver as well as the time spent at the maneuver load factor. Two examples of level bank-angle turn maneuvers are shown in figure 55. In the first example, Counter 8539, the first 12 seconds of the record includes the maneuver entry to a “stabilized” load factor of about 1.5 g. In this case, however, the maneuver point is held only briefly and then the load factor decreases. In the second example, Counter 8826, the entry to the maneuver takes only about 5 seconds and then the maneuver point is held for about 13 seconds These two examples illustrate differences between maneuvers in the degree of steadiness, although quantification of the steadiness is difficult.

The approach used in this report to quantify the steadiness of the level bank-angle turn data is based on the following steps. First, a maximum load factor value is identified in the filtered acceleration time history. In the example shown in figure 55(a) this maximum is 1.52 g. A cutoff acceleration is then defined that is 98% of the maximum, as shown in the figure by the dashed line at 1.49 g. The maneuver point duration is then defined for the period where the load factor exceeds the 98% level. In this example, the duration, T_d, is about 1.1 seconds. This duration, then, is a measure of the steadiness of the maneuver. In the second example in figure 55(b), this approach results in a duration of 4.2 seconds. The definition used here is somewhat arbitrary. If the cutoff acceleration was defined as 95%, for instance, the duration of the maneuver in both examples would increase significantly.

Using the definition of the maneuver duration, the level bank-angle maneuvers are characterized in table 74. The tabulated values of pressure altitude, advance ratio, load factor, and rotor loading, $n_z C_W/\sigma$, are mean values over the maneuver duration. The climb rate is obtained from a regression fit of the boom pressure altitude data computed over the entire record.

Diving Bank-Angle Turns

Twenty-eight diving bank-angle turns were flown during the Airloads Program and the counters are listed in table 75. The load factor and advance ratio for these maneuvers are shown with solid symbols in figure 53(a). Of the 28 diving bank-angle turns in table 75, 12 were for right turns and 16 were for left turns.

The diving bank-angle counters in table 75 are from 5.99 to 28.00 seconds in length. Just as in the case of level bank-angle turns, the test objective was to obtain a specific bank angle and airspeed and then hold these values for five seconds. However, unlike the level bank-angle turns, it was not necessary to maintain altitude and the aircraft was allowed to descend. As with the level bank-angle turns, many of the counters include the entry or exit from the maneuver as well as the time spent at

the maneuver load factor. Two examples of diving bank-angle turn maneuvers are shown in figure 56. In the first example (Counter 11668), the steady portion of the maneuver occurs at the beginning of the counter, while the last 10 to 15 seconds of the record are part of the recovery. In the second example (Counter 11683), the entire record length is fairly steady, except that there is a brief increase in load factor at the very end. The maneuver duration was defined similarly to the level bank-angle turns. However, one difference is illustrated in figure 56(b). In this case, approximately the last second of data was not used to define the duration to avoid spurious effects caused by the rapid rise in load factor at the end of the record.

Using the definition of the maneuver duration from the previous section, the diving bank-angle maneuvers are characterized in table 76. Again, the tabulated values of pressure altitude, advance ratio, load factor, and rotor loading, $n_z C_W/\sigma$, are mean values over the maneuver duration. The climb rate is computed for the entire record. An interesting aspect of table 76 is that it illustrates how the sequence of diving bank-angle maneuvers were flown. The aircraft climbed to an initial altitude between 6700 and 7900 feet and the aircraft was put into a shallow dive. The aircraft was then turned to achieve a 30° bank-angle and a record was taken. The bank-angle was then increased and the dive was steepened to maintain airspeed and the next record was taken. This was repeated until the final record was obtained with a 60° bank-angle and a rate of descent from 3900 to 5700 ft/min. By this time the aircraft was at or below 4000 feet altitude. The process was then repeated for a new airspeed, or in the opposite turn direction.

Symmetric Pull-ups

Data were obtained for five symmetric pull-up maneuvers and these are listed in table 77. The peak load factor obtained during these maneuvers is illustrated in figure 53(b). Counter 11023 is considered the fifth most severe maneuver in the data base, as shown in table 72. Counters 8338 and 11022 include the entire maneuver sequence from entry to recovery. Counters 8926 and 8927 do not include the entry or initial portion of the maneuver. The initial portion of Counter 11023 has been processed as a pseudo-counter, Counter 11041, which is included in this table although it is not a separate maneuver.

A typical symmetric pull-up is illustrated in figure 57. The maneuver follows a roller-coaster type of trajectory. On entry to the maneuver, the pilot raises the nose of the aircraft and the aircraft develops increased load factor and altitude as it loses some airspeed. The nose is then lowered and there is an interval of reduced load factor (less than 1 g). As the airspeed increases, the pilot rapidly pulls back on the longitudinal stick to raise the aircraft's nose again and develop the target load factor. Subsequently, the pitch rate is reduced and the aircraft's nose is brought down to a normal angle as the pilot exits the maneuver. During these pull-ups, there was a general elevation gain in the initial pull-up phase that ranged from 400 to 800 feet, and then a drop of 100 to 300 feet in the pushover portion of the maneuver. Then in the final part of the maneuver the aircraft gained from 50 to 400 feet.

The symmetric pull-ups in the Airloads data base show similar characteristics. Figure 58 compares the load factor time histories for the five symmetric pull-ups, where the time axis has been shifted so that the zero times correspond to the maximum load factor. These maneuvers are

characterized in table 78 which shows the time, advance ratio, load factor, pitch attitude, and pitch rate at the time that the maximum load factor occurred. As can be seen in figure 57, supplementary load factor extrema occur prior to the symmetric pull-up. A positive load factor is observed in the initial pitch up and a reduced load factor is seen in the following pushover. These supplementary load factor extrema are listed in table 79.

Rolling Pullouts

Two rolling pullout maneuvers were flown; one in a left turn and the other in a right turn. The counters for these maneuvers are listed in table 80. The maximum load factor obtained in these maneuvers is shown in figure 53(b). The second of these rolling pullouts, Counter 11028, is fourth in the list of the most severe maneuvers in the Airload Program data base.

The pilot's objective for the rolling pullout maneuver was to obtain a target load factor and airspeed by pulling up the aircraft's nose while the aircraft was rolled to the left or right. A time history of the maneuver is shown in figure 59. An initial roll angle was established with little increase in load factor, and the aircraft was then pitched up which caused the load factor to build rapidly to the target value. Approximately 100 feet of elevation were gained during the maneuver, hence the "diving" in the counter description is a misnomer.

The two rolling pullouts are characterized in table 81, which shows the time, advance ratio, load factor, roll angle, and roll rate that were recorded at the maximum load factor. Counter 11027 is a left rolling pullout (negative roll angle) and 11028 is a right rolling pullout.

Pushovers

Flight test data were obtained for three pushover maneuvers and these are listed in table 82. The minimum load factors measured in these maneuvers are shown in figure 53(b). Counter 11024 is considered the 11th most severe maneuver in the Airload Program data base.

A typical pushover maneuver is shown in figure 60. A similar roller-coaster trajectory is observed for the pushover as for the symmetric pull-up. The maneuver is initiated by lowering the aircraft's nose, and the aircraft then descends and there is a reduction in load factor. The controls are then moved to bring the nose up, the aircraft develops an increased load factor, and the descent is arrested. Following the peak load factor the aircraft's nose is rapidly lowered and the target load factor and airspeed are obtained. The aircraft's nose is brought up once again to exit the maneuver, and this results in a second or trailing pull-up before the nose is once again brought down and the maneuver is complete.

The three pushovers are quite similar, as shown in figure 61. The time axes in this figure are aligned so that zero corresponds to the minimum load factor point. However, an exception was made for Counter 11024, in that the first of the two minima (0.33g) was used for alignment instead of the second minima (0.32g). The time, advance ratio, load factor, pitch angle, and pitch rate at the minimum load factor are shown in table 83. Parameters for the supplementary extrema, that is, the

initial and trailing pull-ups, are listed in table 84. Although these extrema are referred to as supplementary, the load factor during the initial pull-up for the Counter 11024 pushover is greater than two of the five symmetric pull-ups shown in table 78.

The symmetric pull-ups and pushovers show considerable similarity as illustrated in figure 62. However, the pull-up is initiated with a climb, while the pushover is started with a descent. Although both maneuvers follow a roller-coaster trajectory, the pull-up follows a slightly ascending flightpath, while the pushover takes a slightly descending flightpath.

UTTAS Maneuvers

A terrain avoidance maneuver was made part of the performance specification for the U.S. Army's procurement of the Utility Tactical Transport Aerial System (UTTAS) program in the early 1970s. This procurement, which funded prototype aircraft from two manufacturers, led to the development of the UH–60A. The UTTAS maneuver was defined in two parts: a pull-up and a pushover. The specification for the UTTAS pull-up was that the maneuver was to be entered at maximum level flight speed and the pilot was to pull the aircraft's nose up to quickly obtain a load factor of 1.75g, and the load factor was to be held for three seconds without loosing more than 30 knots of airspeed. Similarly, the UTTAS pushover was also initiated at maximum level flight speed and the pilot pitched the aircraft's nose down to quickly obtain 0.25g load factor and maintain this reduced load factor for three seconds. Two UTTAS pull-ups and two UTTAS pushovers were flown during the Airloads Program and the four counters are listed in table 85. The maximum load factors for the pull-ups and the minimum load factors for the pushover are shown in figure 53(c). Counter 11029, a 2.1g UTTAS pull-up, was the second most severe maneuver in the flight program, while Counter 11031, a 1.8g pull-up, was the tenth most severe maneuver (see table 72).

The two UTTAS pull-up time histories are shown in figure 63. The time scales of the two maneuvers have been shifted so that $T = 0$ sec corresponds to the time at which a load factor of 1.75g was obtained. This maneuver differs from the symmetric pull-up in that there is no initiating pull-up and pushover (no roller-coaster-like trajectory), instead the aircraft load factor builds quickly to its maximum value. Figure 63(a) also shows the three-second interval for which the aircraft was to maintain a 1.75g load factor. As can be seen, the specification requirement was not achieved for either counter. For Counter 11029, the load factor was maintained for about 2.56 sec, while for Counter 11031, it was maintained for 2.95 sec. However, as shown in figure 63(b), there was no excessive loss of airspeed in these maneuvers: –11.8 and –11.4 knots respectively for Counters 11029 and 11031.

The two UTTAS pushover time histories are shown in figure 64. For this figure the time scales have been shifted so that $T = 0$ sec corresponds to the time at which a load factor of 0.25g was obtained. Compared to the pushovers, there is no initiating pushover and pull-up; rather the aircraft enters the pushover from level flight. Relative to the UTTAS performance specification, the 0.25g condition was held for only 0.70 sec for Counter 11030 and 0.87 sec for Counter 11032.

The UTTAS pull-ups and pushovers are characterized in table 86, which shows values of time, advance ratio, load factor, pitch attitude, and pitch rate for the maximum or minimum load factor,

depending upon the maneuver. Note that the times indicated in this table are the record time, not the shifted time.

The UH–60A has been flown in free-engagement air-to-air combat tests in a program referred to as the Air-to-Air Combat Test or AACT (ref. 33). Reference 33 provided a number of examples of severe maneuvers that were encountered during free-engagement tests between a UH–60A and an AUH–76 aircraft. One of these maneuvers, Run 29, included high pitch-link loads in a pull-up and it is interesting to compare this combat maneuver with some of the Airloads Program flight test maneuvers. Figure 65 compares 25 seconds of the AACT Run 29 maneuver with Counters 8927 and 11029. In this figure the time scales have been shifted so that $T = 0$ sec corresponds with the maximum load factor observed in the maneuver. table 87 compares the calibrated airspeed, load factor, pitch attitude, and alternating pitch-link load at the peak load factor.

All three maneuvers are similar in that the peak load factor is of relatively short duration, although the AACT maneuver is notable in that a higher load factor is obtained and is held longer (about four seconds above 1.75g). The AACT combat maneuver is similar to the UTTAS pull-up in that it is entered from level flight. The entry airspeed is about 110 knots for the AACT maneuver as compared to 140 knots for the UTTAS pull-up. The symmetric pull-up, however, follows a roller-coaster like trajectory and as a consequence the aircraft is at a lower pitch attitude at the point of maximum load factor in this maneuver. It is interesting to note that for the two symmetric flight test maneuvers, Counters 8927 and 11029, the pilot recovers from the maneuver by dropping the nose of the aircraft and developing some reduced load factor. In the combat maneuver, the aircraft's pitch attitude continues to increase, eventually reaching nearly 60 deg. The pilot recovers by rolling out of the maneuver.

The comparison of the alternating pitch-link loads in figure 65(c) shows that these loads are greater for Counter 11029 as compared to AACT Run 29, even though the latter had a higher load factor which was sustained longer. However, the maneuver airspeed was higher for Counter 11029 and this shows the importance of both airspeed and load factor in the development of extreme maneuver loads.

Roll Reversals

Seven roll reversals were flown during the Airloads Program and these are listed in table 88. The peak rotor loading measured during these maneuvers is shown in figure 53(d). It is noted that the data base is now contaminated for Counter 8537 and some of the data for this case are no longer accessible. Of the other six reversals, four are reversals to the left, one is a reversal to the right, and one is a double reversal (Counter 11026).

The roll reversal is essentially a level-flight maneuver with no gain or loss of altitude. For a roll reversal to the left, the pilot banks the aircraft to the right and then makes a rapid input with the lateral stick so that the aircraft quickly rolls left. The pilot's objective is to reach the target roll rate with wings level and at the target airspeed. Then, as the aircraft continues to roll left, the pilot exits the maneuver by moving the lateral stick to stop the roll, and return to normal level flight.

The five roll reversals to the left and the two reversals to the right are shown in figure 66 where the aircraft roll attitude is shown as a function of time. The time scales for the maneuvers have been aligned by setting $T = 0$ sec corresponding to the maximum roll rate. For the higher speed roll reversals, the bank angle used in the entry to and exit from the maneuver is about the same. However, at lower speeds the peak roll rate occurs before the aircraft reaches a zero roll angle and the maneuver is completed with little overshoot in bank angle. The peak roll rates and load factors obtained in these maneuvers are tabulated in table 89.

The roll rates in the double roll reversal, Counter 11026, were the highest obtained in the flight test program. Rapid roll rates affect rotor torque which in turn affects the engine fuel control circuit. These aspects are examined in figure 67, which shows the measured rotor torque, the rotor speed, and the roll attitude for Counter 11026. It is observed that rotor torque generally follows the aircraft roll rate, but the torque is modified by rotor speed changes caused by the fuel control response.

Control Pulse in Bank-Angle Turns

Test data were obtained for a longitudinal control pulse during a bank-angle turn in level flight at two different airspeeds. The three cases of longitudinal control pulses are listed in table 90. The inclusion of these data in this section is somewhat arbitrary, as the response of the aircraft to a longitudinal pulse is also appropriate for the flight dynamics testing that is discussed in section 11.

An example of a longitudinal control pulse and the aircraft response in a steady turn is shown in figure 68 for Counter 11528. At the initiation time of the pulse, the aircraft advance ratio is 0.32, the bank angle is 29 deg, and the load factor is 1.14g. The pilot made a quick, aft pulse of about 1.3 in stick movement and the duration of the pulse was less than a half second. The load factor increased briefly from 1.14g to 1.43g and the pitch attitude increased about two degrees and then slowly returned to the initial value. The initial conditions and the aircraft input and response are shown in table 91 for each of the three cases. The data in figure 68 have been obtained with the PRINT command in TIMEHIST, as for the other time histories in this section. However, only the accelerometer data (AZCG) have been filtered.

Accelerating and Decelerating Flight

Flight data records were obtained for five accelerating and four decelerating flight conditions and the counters are listed in table 92. Note that Counter 10321, a pseudo-counter, is the second segment of the record in Counter 10305. Although these nine conditions are considered maneuvers, as the aircraft is in accelerated flight, the conditions are in general relatively benign. An exception is Counter 11681, which is an acceleration in diving flight to the limit dive speed condition. Half of these counters were flown near the ground and in this sense are representative of takeoff or approach conditions. The rest of the counters were flown at altitudes from 2500 to 6200 feet.

Two counters, 11510 and 11650, were accelerating takeoffs from IGE hover conditions. The time histories of airspeed and altitude for Counter 11650 are shown in figure 69. Two airspeed measurements are shown for this accelerating flight condition: the test boom pitot-static system and

a special-purpose, low-airspeed system called HADS, for Helicopter Airspeed Data Sensor. As discussed in section 3, the HADS system was considered accurate for airspeeds below 20 knots, while the boom system was used at higher airspeeds. However, as discussed in section 3, the accuracy of the HADS system was degraded for in-ground-effect conditions. Figure 69(a) shows spurious values for the test boom pitot-static system over the first ten to twenty seconds of the record, which is expected. Although 20 knots is considered the break point for this system, it appears that this measurement does not show the expected trend of accelerating flight until 25 or 30 knots. Obviously neither measurement can be used as a reference for the entire record, but in this case the two systems show reasonable agreement near the break-point conditions. The test boom pressure altitude in figure 69(b) shows large excursions over the first 15 seconds of the record, and the measurement then settles down and shows good agreement with the radar altimeter except for a negative offset of about 12 feet. Once past 30 or 40 knots, the test boom pressure measurement appears trustworthy in terms of rate of change, but there is an offset error.

Three counters: 8836, 11543, and 11688, are for decelerating flight in approaches to landing. Figure 70 shows the airspeed and altitude time histories for Counter 11688. In the approach, the HADS system airspeed is about 10 knots lower than the test boom system. This discrepancy is fairly typical of the difference observed in steady level flight (see fig. 10). The break point for the HADS measurement occurs about 16 sec into the record. However, the HADS airspeed shows a substantial oscillation as the airspeed is reduced and is not trustworthy. A similar oscillation was seen during the pace-car calibration discussed in section 3 (see fig. 9). Beyond about 18 sec the boom airspeed shows excessive variance and this is expected because of the low airspeed and perhaps the influence of rotor downwash. The boom pressure altitude measurement shown in figure 70(b) shows a bias of –120 feet, although the trend agrees well with the radar altimeter measurement until the boom measurement becomes unusable beyond 15 or 20 sec.

Counter 8432 is an accelerating flight condition similar to the takeoff conditions discussed above, but occurs at about 3000 feet pressure altitude. Counter 8431 is a decelerating case and is also well above ground level. Counters 10305 and 10321, as mentioned above, are two segments of a single record, and this represents a case of acceleration from 65 to 90 kts over a period of 50+ sec. Counter 11681 is an acceleration in diving flight to the aircraft’s limit dive speed.

The airspeed records for acceleration from or decelerations to hover are uncertain near the HADS/test boom pitot-static system breakpoint or crossover. Although it appears possible to create a combined airspeed signal in the case shown in figure 69, other counters are less satisfactory (for example as shown in fig. 70). Caution needs to be used in employing these airspeed references for these maneuvers. The test boom pressure altitude measurements show variable bias errors for these counters. At airspeeds above the HADS break point, these measurements generally agree with the radar altimeter, except for the bias error. At lower speeds pressure altitude measurements derived from the test boom pressure are unreliable. It is noted that on Flight 115, the boom pressure measurement failed and has been replaced with the less accurate ship’s system measurement. This affects the measurements for Counters 11510 and 11543.

Settling with Power

Twice during level flight airspeed sweeps, the pilots reported “settling with power” while setting up on a flight condition and at this point the flight engineer took a data record. In both cases, the pilots were in level flight and were recording data at five-knot intervals in a descending sequence. These settling with power cases occurred as the pilots reduced the airspeed to set up on the next test point. However, by the time the data were recorded, the aircraft was in steady descent condition rather than in level flight. The two settling with power counters are listed in table 93.

Settling with power, “power settling”, and flying within the vortex ring state (VRS) are all conditions characterized by descending flight at low airspeeds. However, there is little quantitative information that characterizes these conditions and it is not known whether these different terms are just imperfect descriptions of the same phenomenon or whether more than one phenomenon is involved. Moreover, little is known as to what helicopter design features affect the aircraft’s behavior when these conditions are encountered.

French investigators (ref. 34) have developed a semi-empirical model of induced flow in descending flight to define the VRS boundary, and they have successfully compared this model with extensive flight data obtained with a Dauphin 6075. Normalized forward and descent velocities for the two settling with power points are compared to the VRS (ref. 34) boundary in figure 71. The descent rates computed for the two test points are observed to be above the VRS boundary, although Counter 8421 is close to the upper edge. There is substantial uncertainty in the horizontal velocity, as the test boom and HADS systems are least accurate in the area between 20 and 30 knots. If the HADS system is correct, then the two counters are in the correct horizontal velocity range for an entry into the vortex state. If the test boom pitot-static speed is more accurate, then both of the settling with power cases are well outside the VRS boundary.

Some insight into these the two settling with power cases is obtained by comparing the flight time histories to the preceding level flight point. Comparative values are shown in table 94 for the settling with power points and the reference conditions. For Counter 8421, the means speed is between 8 and 12 knots lower than the preceding condition, while for Counter 8816, it is about 6 knots lower. The rates of climb for the reference cases are within the normal range of level flight conditions (see fig. 49, for example). Time histories of Counters 8420 and 8421 are compared in figure 72 for the boom airspeed, the main rotor shaft torque, and the pressure altitude. The airspeed for Counter 8421 is reduced from Counter 8420, as this was the next test point in the test card. The main rotor torque is slightly higher for 8421, which is not unexpected as more power is required at lower airspeeds on the back side of the power curve. Two increases in torque are observed for Counter 8421 and these are directly related to step increases of the collective of 1.7% and 1.9%. Although the rotor torque has increased, there is no apparent change in the rate of descent. This ineffectiveness of the collective control is considered a characteristic of power settling (ref. 34).

One of the more surprising aspects of the settling with power cases is an unexpected reduction in vibration. One of the characteristics noted in power settling or within the VRS boundary is an increase in vibration and torque oscillations. However, in both of these cases, the vertical vibration and the rotor oscillatory torque decreased by a factor of three. These levels are comparable to what

is observed in normal flight conditions between 70 and 100 knots and suggests the absence of the wake-excited vibration that is normally observed at low speeds.

Moderate and Aggressive Heading Turns

During the ground-acoustics portion of the Airloads Program, the aircraft's acoustics were recorded during standardized turning maneuvers (ref. 6). These maneuvers required the aircraft to approach the center of the microphone array on a specific heading in level flight and, over the center of the array, make a specified heading change. The pilot was asked to use two levels of quickness in performing these turns; referred to here as "moderate" and "aggressive." As was generally the case for ground-acoustic tests, the data were reduced in two steps. In the first step, the flight tape record excluding the rotor measurements was reduced and placed in the BH2 data base with a prefix-4 added to the counter number. In the second step, the different time slices were defined by Ames and Langley personnel for records to be installed in the BH2 (Ames) or BHL (Langley) data bases. The time slices in the second step include the rotor data.

Thirty-two counters for moderate heading turns were obtained and the counters in the prefix-4 data base are listed in table 95. Data for ten of these counters were accomplished on Flight 92, using the standard microphone array. Data for the remaining counters were obtained after the microphone array was changed to the non-standard layout (see section 9). The time slices used for the moderate heading turns are shown in table 96. The moderate heading turn counters in the BH2 data base are listed in table 97. This table also includes six counters that were flown on Flight 88 to develop and practice appropriate piloting techniques. These practice counters were flown at an elevation of about 1100 feet rather than the approximately 250 feet elevation used during the ground-acoustic testing.

Twenty-four aggressive heading turns were flown during the ground-acoustic testing and the prefix-4 data base counters are listed in table 98. The "CA" in the counter description refers to "collision avoidance." The time slices used for the counters to be placed in the BH2 data base are shown in table 99. Table 100 lists the BH2 data base aggressive heading turn counters. The peak rotor loading during the moderate and aggressive heading turns is shown in figure 53(e). These maneuvers are benign as concerns structural loads on the blades and controls.

The differences between the moderate and aggressive heading turns are somewhat subjective. Figure 73 shows the peak load factor recorded in a turn as a function of the absolute value of the peak roll rate, and this provides a means of comparing the various cases. Although most of the aggressive maneuvers show a higher load factor than the moderate turns, there is considerable overlap between the two sets of data. Time histories of two representative heading turns are shown in figure 74. Both of these maneuvers are right turns, with an approach speed of 60 knots and a nominal 60 deg heading change. The initial lateral stick motion is about 12% for the moderate case, Counter 9209, while the initial stick movement for the aggressive case, Counter 9721, is about 30%. In the moderate case the maximum bank angle is about 20 deg, while for the aggressive maneuver, a 40 deg bank angle is reached.

Two approach angles to the microphone array were used for these maneuvers. A nominal 0 deg approach, perpendicular to the array, was used for the majority of the heading turns (see fig. 4). In

addition, –40 deg approaches to the array along Runway 12 were also used. The approach speed was normally 60 KIAS and nominal turns to the left and right were made at angles from 15 to 90 deg. Figure 75 illustrates the aircraft track for these records for all of the moderate heading turns using a 0 deg approach, with the exception of one case that used a 35 deg turn. Figure 76 shows the equivalent tracking data for the –40 deg moderate turn approaches. The laser tracking data (XLASER, YLASER) were extracted from TRENDS using the PRINT option in TIMEHIST without filtering.

Tracking data, absolute peak roll rates, and peak load factors are shown in table 101 for all of the ground-acoustic moderate turns at a 0 deg approach angle. The equivalent data for the –40 deg approaches are shown in table 102 for the moderate turns. The 0 deg approach cases for the aggressive turns are shown in table 103 and the –40 deg approaches are in table 104.

Constant Radius Turns

Constant radius turns were performed at three radii as part of the ground-acoustic testing. Seven constant radius turns were flown on Flight 96 and six turns were flown on Flight 98. The thirteen prefix-4 counters for these turns are listed in table 105. The load factor measured in these turns is shown in figure 53(f).

Three concentric circles centered on the microphone array were laid out using standard surveyor instrumentation and techniques. The circle radii were 1000, 1400, and 1800 feet. A mixture of orange highway cones, painted four-foot boards, and strobe lights were placed on the surveyed circles to provide guidance for the pilots. The pilots approached each circle on a tangent and then followed the circular path. Generally, between one and one-and-a-half revolutions of flight data were recorded as the aircraft followed the circular paths. The approach speed in most cases was 60 KIASB and the elevation above the ground was 250 feet. Both clockwise and counterclockwise turns were flown. Turn performance, based on laser tracking data, is shown in table 106. The measured mean radius shows good agreement with the nominal value. The standard deviation varies from 9.5 to 43.9 feet and in most cases is less than 20 feet.

Figure 77 shows three examples of the x- and y-position data for the prefix-4 counters. Also shown in this figure is the non-standard microphone layout (ref. 6) as well as the time slices extracted from these runs for the BH2 data base. The example for the 1000-ft radius turn is Counter 49839. This is a counterclockwise turn with slightly more than one turn recorded. Three roughly five-second segments or slices were chosen for the BH2 data base: Counters 9839, 9840, and 9841. Similar examples are shown for radii of 1400 and 1800 feet. The tracking data shown in this figure were extracted from TRENDS using PRINT in TIMEHIST, but without filtering.

As shown in figure 77, each of the prefix-4 counters may have one or more segments or slices extracted and installed in the BH2 data base. The relationship between the prefix-4 counters and the time slices used for the BH2 data base segments are shown in table 107. Each of the thirteen prefix-4 counters is listed, along with the 34 BH2 data base time segments. The counters written to the BH2 data base are listed in table 108. Figure 78 shows the x- and y-position data for all of the BH2 data base counters relative to the prescribed turn radii.

Table 72.– Maneuver severity.

		RANK					
		L_{PL}	M_θ	M_β	M_ζ	M_β	M_ζ
MANEUVER	COUNTER	0.047R	0.30R	0.011R	0.60R	0.11R	0.60R
RT TURN, 140 KIAS, 60° AOB	11680	1	1	15	4	1	14
UTTAS PULL-UP, 130 KIAS 2.1G	11029	3	8	1	15	8	4
RT TURN, 140 KIAS, 55° AOB	11679	2	2	23	7	23	15
ROLLING PULLOUT, 120 KIASB	11028	6	5	8	23	3	22
PULL-UP, 120 KIAS, 2.25G	11023	10	7	2	26	4	25
LT TURN, 130 KIAS, 60° AOB	11686	9	3	7	17	12	5
DESCENT, 186 KIAS (VNE)	11682	24	24	28	1	21	2
LT TURN, 120 KIAS, 60° AOB	11660	8	4	13	14	7	6
RT TURN, 130 KIAS, 60° AOB	11672	13	6	10	18	5	8
UTTAS PULL-UP, 130 KIAS, 1.8G	11031	4	14	5	13	11	9
PUSHOVER, 120 KIASB, 0.3G	11024	7	19	3	16	29	13
LT TURN, 120 KIASB, 55° AOB	11659	22	21	17	25	24	1

Table 73.– Level bank-angle turns.

FLIGHT	COUNTER	DESCRIPTION	DURATION
81	8119	RT TURN, 30AOB, 80KIASB	8.10 Seconds
81	8122	RT TURN, 30AOB, 120KIASB	9.17 Seconds
81	8123	RT TURN, 45AOB, 120KIASB	8.26 Seconds
85	8538	RT TURN, 120KIASB, 30AOB	9.99 Seconds
85	8539	RT TURN, 120KIASB, 45AOB	22.99 Seconds
88	8824	RT TURN, 110KIASB, CWS=.10	20.60 Seconds
88	8826	RT TURN, 108KIASB, CWS=.10	21.00 Seconds
89	8920	RT TURN, 95KIASB, 15AOB, CWS.11	17.66 Seconds
89	8921	RT TURN, 95KIASB, 30AOB, CWS.11	27.49 Seconds
90	9018	RT TURN, 50KIASB, 15AOB, CWS.13	20.00 Seconds
90	9019	RT TURN, 50KIASB, 30AOB, CWS.13	33.00 Seconds
90	9031	RT TURN, 80KIASB, 15AOB, CWS.12	23.00 Seconds
90	9032	RT TURN, 83KIASB, 30AOB, CWS.12	30.00 Seconds
110	11020	LT TURN, 120KIASB, 30AOB	12.00 Seconds
110	11021	LT TURN, 120KIASB, 45AOB	9.61 Seconds

Table 74.– Maneuver characterization for level bank-angle turns.

COUNTER	PRESSURE ALTITUDE FT	RATE OF CLIMB FT/MIN	μ	n_z Gs	$n_z C_W/\sigma$	DURATION SEC
8119	1967	–123	0.224	1.14	0.0846	3.6
8122	2046	344	0.311	1.18	0.0896	1.7
8123	2023	418	0.317	1.41	0.1044	3.0
8538	3097	207	0.311	1.13	0.0878	3.2
8539	3078	145	0.331	1.50	0.1161	1.1
8824	9544	470	0.290	1.07	0.1078	6.4
8826	9370	–214	0.296	1.11	0.1107	4.2
8920	12480	88	0.293	1.04	0.1145	3.2
8921	12491	189	0.292	1.14	0.1260	1.8
9018	17024	–55	0.167	1.06	0.1374	4.6
9019	16946	–252	0.189	1.14	0.1478	4.3
9031	15761	221	0.264	1.04	0.1260	3.2
9032	15645	–267	0.279	1.15	0.1381	3.8
11020	5097	–201	0.307	1.16	0.0919	0.4
11021	5200	–158	0.325	1.29	0.1028	0.7

Table 75.– Diving bank-angle turns.

FLIGHT	COUNTER	DESCRIPTION	DURATION
116	11657	LT TURN, 120KIASB, 30DEG AOB	27.00 Seconds
116	11658	LT TURN, 120KIASB, 45DEG AOB	21.99 Seconds
116	11659	LT TURN, 120KIASB, 55DEG AOB	5.99 Seconds
116	11660	LT TURN, 120KIASB, 60DEG AOB	9.99 Seconds
116	11661	RT TURN, 120KIASB, 30DEG AOB	28.00 Seconds
116	11662	RT TURN, 120KIASB, 45DEG AOB	7.03 Seconds
116	11663	RT TURN, 120KIASB, 55DEG AOB	8.00 Seconds
116	11664	RT TURN, 120KIASB, 60DEG AOB	8.99 Seconds
116	11665	LT TURN, 130KIASB, 30DEG AOB	15.00 Seconds
116	11666	LT TURN, 130KIASB, 45DEG AOB	16.99 Seconds
116	11667	LT TURN, 130KIASB, 55DEG AOB	18.00 Seconds
116	11668	LT TURN, 130KIASB, 60DEG AOB	18.03 Seconds
116	11669	RT TURN, 130KIASB, 30DEG AOB	26.17 Seconds
116	11670	RT TURN, 130KIASB, 45DEG AOB	20.99 Seconds
116	11671	RT TURN, 130KIASB, 55DEG AOB	10.20 Seconds
116	11672	RT TURN, 130KIASB, 60DEG AOB	12.03 Seconds
116	11673	LT TURN, 140KIASB, 30DEG AOB	15.99 Seconds
116	11674	LT TURN, 140KIASB, 45DEG AOB	9.99 Seconds
116	11675	LT TURN, 140KIASB, 55DEG AOB	16.99 Seconds
116	11676	LT TURN, 140KIASB, 60DEG AOB	9.99 Seconds
116	11677	RT TURN, 140KIASB, 30DEG AOB	15.99 Seconds
116	11678	RT TURN, 140KIASB, 45DEG AOB	7.99 Seconds
116	11679	RT TURN, 140KIASB, 55DEG AOB	9.99 Seconds
116	11680	RT TURN, 140KIASB, 60DEG AOB	12.99 Seconds
116	11683	LT TURN, 130KIASB, 30DEG AOB	16.99 Seconds
116	11684	LT TURN, 130KIASB, 45DEG AOB	11.99 Seconds
116	11685	LT TURN, 130KIASB, 55DEG AOB	9.99 Seconds
116	11686	LT TURN, 130KIASB, 60DEG AOB	9.99 Seconds

Table 76.– Maneuver characterization of diving bank-angle turns.

COUNTER	PRESSURE ALTITUDE FT	RATE OF CLIMB FT/MIN	μ	n_z Gs	$n_z C_W/\sigma$	DURATION SEC
11657	6948	–252	0.334	1.17	0.1055	11.3
11658	6296	–2105	0.352	1.53	0.1362	5.9
11659	5917	–3157	0.347	1.59	0.1384	5.2
11660	5254	–4733	0.344	1.76	0.1505	1.7
11661	7059	–1083	0.334	1.32	0.1192	0.7
11662	6850	–2099	0.339	1.46	0.1310	2.3
11663	6485	–3215	0.330	1.57	0.1384	1.8
11664	5800	–4948	0.349	1.64	0.1418	4.1
11665	7318	–1202	0.367	1.19	0.1079	2.3
11666	6485	–3065	0.396	1.49	0.1321	5.5
11667	5223	–4706	0.396	1.74	0.1485	1.7
11668	3833	–5685	0.371	1.24	0.1010	5.1
11669	7273	–1560	0.363	1.23	0.1107	1.8
11670	6463	–2006	0.360	1.55	0.1370	1.7
11671	5943	–3142	0.355	1.65	0.1421	4.7
11672	5038	–4003	0.348	1.64	0.1373	3.1
11673	6910	–1478	0.386	1.15	0.1018	2.4
11674	6473	–2642	0.394	1.30	0.1135	1.1
11675	5354	–4671	0.389	1.78	0.1511	1.6
11676	4409	–5704	0.392	1.66	0.1355	2.2
11677	6703	–1349	0.388	1.28	0.1119	2.2
11678	6441	–2253	0.389	1.44	0.1249	2.2
11679	5880	–3878	0.393	1.69	0.1437	0.1
11680	4752	–5324	0.388	1.48	0.1219	0.7
11683	7894	–676	0.367	1.14	0.1012	2.6
11684	7549	–1860	0.372	1.32	0.1176	1.4
11685	7139	–2223	0.369	1.52	0.1332	3.3
11686	6664	–3898	0.376	1.68	0.1445	1.0

Table 77.– Symmetric pull-ups.

FLIGHT	COUNTER	DESCRIPTION	DURATION
83	8338	PULL-UP, 120 KIASB, 2.0G	34.00 Seconds
89	8926	PULL-UP, 80 KIASB, 1.5G	17.65 Seconds
89	8927	PULL-UP, 80 KIASB, 2.OG	24.10 Seconds
110	11022	PULL-UP, 120 KIASB, 1.85G	37.00 Seconds
110	11023	PULL-UP, 120 KIASB, 2.25G	14.79 Seconds
110	11041	PULL-UP, 120 KIASB, 2.25G*	19.00 Seconds

Table 78.– Characterization of symmetric pull-ups at maximum load factor.

COUNTER	TIME SEC	μ	n_z Gs	θ DEG	$\dot{\theta}$ DEG/SEC
8338	23.66	0.318	2.22	10.1	15.1
8926	9.56	0.226	1.91	8.5	13.0
8927	9.52	0.227	2.09	10.9	10.9
11022	25.74	0.274	1.91	7.6	11.4
11023	4.83	0.310	2.29	8.4	20.8

Table 79.– Supplementary load factor extrema in symmetric pull-ups.

COUNTER	INITIAL PULL-UP			PUSHOVER		
	TIME SEC	μ	n_z Gs	TIME SEC	μ	n_z Gs
8338	7.48	0.294	1.30	16.83	0.269	0.60
8926	—[a]	—[a]	—[a]	6.84	0.213	0.54
8927	—[a]	—[a]	—[a]	5.55	0.194	0.41
11022	3.28	0.296	1.35	19.99	0.232	0.58
11023[b]	—	—	—	0.69	0.273	0.54
11041[b]	1.72	0.315	1.39	—	—	—

[a] Initial pull-up not recorded.

[b] Record spread over two counters.

Table 80.– Rolling Pullouts.

FLIGHT	COUNTER	DESCRIPTION	DURATION
110	11027	DIVING ROLL PULLOUT, 120KIASB	17.00 Seconds
110	11028	DIVING ROLL PULLOUT, 120KIASB	22.00 Seconds

Table 81.– Characterization of rolling pullout at maximum load factor.

COUNTER	TIME SEC	μ	n_z Gs	ϕ DEG	$\dot{\theta}$ DEG/SEC
11027	10.81	0.291	2.19	–44.3	3.79
11028	13.13	0.296	2.27	62.8	5.24

Table 82.– Pushovers.

FLIGHT	COUNTER	DESCRIPTION	DURATION
89	8928	PUSHOVER, 80 KIASB, 0.5G	23.21 Seconds
89	8930	PUSHOVER, 80 KIASB, 0.25G	19.85 Seconds
110	11024	PUSHOVER, 120 KIASB, .3G	32.00 Seconds

Table 83.– Characterization of pushovers at minimum load factor.

COUNTER	TIME	μ	n_z	θ	$\dot{\theta}$
	SEC		Gs	DEG	DEG/SEC
8928	8.75	0.198	0.44	–5.6	–8.3
8930	9.83	0.213	0.27	–13.9	–9.1
11024	24.50	0.275	0.32	–24.5	–6.1

Table 84.– Supplementary load factor extrema in pushovers.

COUNTER	INITIAL PULL-UP			TRAILING PULL-UP		
	TIME	μ	n_z	TIME	μ	n_z
	SEC		Gs	SEC		Gs
8928	2.63	0.262	1.68	17.50	0.271	1.43
8930	1.94	0.289	1.74	16.42	0.296	1.65
11024	15.66	0.342	1.98	31.73	0.349	1.40

Table 85.– UTTAS maneuvers.

FLIGHT	COUNTER	DESCRIPTION	DURATION
110	11029	UTTAS PULL-UP, 130KIASB, 2.1G	20.00 Seconds
110	11030	UTTAS PUSHOVER, 130KIASB, .3G	15.00 Seconds
110	11031	UTTAS PULL-UP, 130KIASB, 1.8G	18.00 Seconds
110	11032	UTTAS PUSHOVER, 130KIASB, .3G	19.00 Seconds

Table 86.– Characterization of UTTAS pull-ups and pushovers at load factor extrema.

COUNTER	TIME	μ	n_z	θ	$\dot{\theta}$
	SEC		Gs	DEG	DEG/SEC
11029	4.04	0.304	2.15	27.5	10.8
11030	4.42	0.355	0.19	–19.1	–9.4
11031	6.86	0.307	1.98	26.6	9.6
11032	11.95	0.357	0.11	–22.8	–8.2

Table 87.– Comparison of AACT Run 29 with UTTAS and symmetric pull-up at peak load factor.

CASE	V_{cal}	n_z	θ	P-L LOAD
	KNOTS	Gs	DEG	LB
Run 29	122.8	2.45	17.	1717
8927	89.8	2.06	9.83	992
11029	137.1	2.12	25.85	2717

Table 88.– Roll reversals.

FLIGHT	COUNTER	DESCRIPTION	DURATION
85	8535	ROLL REV, 120 KIASB, 20 D/S	14.99 Seconds
85	8536	ROLL REV, 120 KIASB, 35 D/S	15.00 Seconds
85	8537[a]	ROLL REV, 120 KIASB, 45 D/S	9.99 Seconds
89	8924	ROLL REV, 80 KIASB, 27 D/S	20.64 Seconds
89	8925	ROLL REV, 80 KIASB, 32 D/S	19.84 Seconds
110	11025	ROLL REV, 120 KIASB, 38 D/S	14.99 Seconds
110	11026	ROLL REV, 120 KIASB, 35 D/S	22.00 Seconds

[a]Data base record contaminated.

Table 89.– Characterization of roll reversals.

COUNTER	MAXIMUM ROLL RATE			MAXIMUM LOAD FACTOR		
	TIME	μ	$\dot{\theta}$	TIME	μ	n_z
	SEC		DEG/SEC	SEC		Gs
8535	5.69	0.320	–18.4	5.36	0.320	1.10
8536	7.43	0.326	–28.7	7.84	0.325	1.23
8924	10.33	0.224	–24.6	10.35	0.224	1.12
8925	10.38	0.226	–28.1	10.38	0.226	1.13
11025	11.69	0.308	38.6	13.22	0.294	1.60
11026	8.86	0.278	51.7	5.76	0.286	1.29
11026	13.89	0.291	–35.5	12.96	0.281	1.40

Table 90.– Longitudinal control pulses in bank-angle turns.

FLIGHT	COUNTER	DESCRIPTION	DURATION
115	11526	TURN, AFT PULSE, 75KIASB, 30AOB	10.99 Seconds
115	11527	TURN, AFT PULSE, 75KIASB, 30AOB	13.99 Seconds
115	11528	TURN, AFT PULSE, 120KIASB, 30AOB	12.99 Seconds

Table 91.– Characterization of longitudinal control inputs.

COUNTER	INITIAL CONDITIONS (0.5 SEC)				PULSE	INPUT AND RESPONSE		
	μ	n_z	θ	ϕ	INITIATION	$\Delta\delta_{long}$	Δn_z	$\Delta\theta$
		Gs	DEG	DEG	SEC	%	Gs	DEG
11526	0.206	1.16	2.8	30.3	6.13	11.2	0.11	0.96
11527	0.209	1.14	2.6	30.5	5.37	14.7	0.17	1.41
11528	0.321	1.14	–1.3	28.8	5.70	13.4	0.30	1.95

Table 92.– Accelerating and decelerating flight.

FLIGHT	COUNTER	DESCRIPTION	DURATION
84	8431	LEVEL DECEL, 50-0 KTS, CWS=.09	40.00 Seconds
84	8432	LEVEL ACCEL, 0-50 KTS, CWS=.09	39.6 Seconds
88	8836	DECEL TO HOVER, 50 TO 0 KIASB	36.33 Seconds
103	10305	LEVEL ACCEL, 60-90 KIASB	32.90 Seconds
103	10321	LEVEL ACCEL, 60-90 KIASB*	19.24 Seconds
115	11510	ACCEL IGE, HOVER TO 50 KIASB	32.72 Seconds
115	11543	LANDING FLARE, 50 KIASB-HOVER	33.00 Seconds
116	11650	ACCEL, HOVER-50 KIASB, IGE	28.00 Seconds
116	11681	ACCEL TO VNE, 170-185 KIAS	5.99 Seconds
116	11688	LANDING FLARE, 50 KIASB-HOVER	30.00 Seconds

Table 93.– Settling with power.

FLIGHT	COUNTER	DESCRIPTION	DURATION
84	8421	SETTLING WITH POWER, 15 KIASH	9.99 Seconds
88	8816	SETTLING WITH POWER, 10 KIAS	5.99 Seconds

Table 94.– Comparison of settling with power and reference cases.

COUNTER	CASE	C_{w}/σ	TRUE AIRSPEED		RATE OF CLIMB	PRESSURE ALTITUDE
			BOOM KTS	HADS KTS	FT/MIN	FT
8420	ref.	0.0892	37.7	19.0	150	5458
8421	settling	0.0886	25.4	11.2	–779	5364
8815	ref.	0.1013	26.6	17.4	–212	8924
8816	settling	0.1011	20.9	10.2	–517	9060

Table 95.– Moderate heading turns in ground-acoustic testing; prefix-4 data base.

FLIGHT	COUNTER	DESCRIPTION	DURATION
92	49206	TURN, 25 DEG, 60 KIASB, RUN 701	26.56 Seconds
92	49207	TURN, 45 DEG, 60 KIASB, RUN 720	28.13 Seconds
92	49208	TURN, 35 DEG, 65 KIASB, RUN 710	26.35 Seconds
92	49209	TURN, 60 DEG, 63 KIASB, RUN 730	28.89 Seconds
92	49210	TURN, 90 DEG, 60 KIASB, RUN 740	33.88 Seconds
92	49211	TURN, 15 DEG, 80 KIASB, RUN 702	23.51 Seconds
92	49212	TURN, 30 DEG, 80 KIASB, RUN 711	22.90 Seconds
92	49213	TURN, 45 DEG, 80 KIASB, RUN 721	20.75 Seconds
92	49214	TURN, 60 DEG, 80 KIASB, RUN 731	27.87 Seconds
92	49215	TURN, 90 DEG, 80 KIASB, RUN 741	29.62 Seconds
97	49707	TURN, RT 30DEG, 60KIASB, RUN 745	19.08 Seconds
97	49708	TURN, RT 30DEG, 60KIASB, RUN 746	24.22 Seconds
97	49709	TURN, RT 45DEG, 60KIASB, RUN 750	26.86 Seconds
97	49710	TURN, RT 60DEG, 60KIASB, RUN 760	26.07 Seconds
97	49711	TURN, LT 30DEG, 60KIASB, RUN 700	27.08 Seconds
97	49712	TURN, LT 45DEG, 60KIASB, RUN 710	27.76 Seconds
97	49713	TURN, LT 60DEG, 60KIASB, RUN 720	30.66 Seconds
97	49722	TURN, LT 90DEG, 60KIASB, RUN 730	34.76 Seconds
97	49724	TURN LT 60DEG, 60KIASB, RUN 725	22.94 Seconds
97	49727	TURN RT 90DEG, 60KIASB, RUN 770	27.42 Seconds
97	49729	TURN RT 60DEG, 60KIASB, RUN 765	27.15 Seconds
99	49904	LT TURN 60DEG, 60KIASB, RUN 720	29.79 Seconds
99	49905	RT TURN 30DEG, 60KIASB, RUN 740	27.72 Seconds
99	49906	RT TURN 45DEG, 60KIASB, RUN 750	25.66 Seconds
99	49907	RT TURN 60DEG, 60KIASB, RUN 760	53.86 Seconds
99	49908	RT TURN 60DEG, 60KIASB, RUN 761	35.42 Seconds
99	49915	TURN LT 90DEG, 60KIASB, RUN 730	24.23 Seconds
99	49918	TURN LT 60DEG, 60KIASB, RUN 726	25.65 Seconds
99	49919	TURN LT 90DEG, 60KIASB, RUN 731	21.93 Seconds
99	49921	TURN RT 60DEG, 60KIASB, RUN 765	23.00 Seconds
99	49922	TURN RT 60DEG, 60KIASB, RUN 766	30.67 Seconds
99	49926	TURN RT 90DEG, 60KIASB, RUN 773	29.57 Seconds

Table 96.– Time slices for moderate heading turns in ground-acoustic testing; prefix-4 and BH2 data bases.

PREFIX-4 DATA BASE			BH2 DATA BASE		
COUNTER	START TIME SEC	END TIME SEC	COUNTER	START TIME SEC	END TIME SEC
49206	0.00	26.55	9206	6.64	17.63
49207	0.00	28.13	9207	7.30	20.30
49208	0.00	26.35	9208	0.00	18.96
49209	0.00	28.89	9209	5.60	21.59
49210	0.00	33.88	9210	6.21	33.88
49211	0.00	23.51	9211	4.13	13.12
49212	0.00	22.90	9212	4.90	14.89
49213	0.00	20.75	9213	4.75	12.74
49214	0.00	27.87	9214	4.31	24.31
49215	0.00	29.62	9215	4.65	23.64
49707	0.00	19.08	9707	0.00	10.00
49708	0.00	24.22	9708	4.01	13.99
49709	0.00	26.86	9709	7.00	18.00
49710	0.00	26.07	9710	3.01	16.00
49711	0.00	27.08	9711	7.01	16.00
49712	0.00	27.76	9712	5.00	16.00
49713	0.00	30.66	9713	3.01	18.00
49722	0.00	34.76	9722	10.00	28.00
49724	0.00	22.94	9724	1.01	16.00
49727	0.00	27.43	9727	7.01	22.00
49729	0.00	27.14	9729	7.00	19.99
49904	0.00	29.78	9904	8.00	29.78
49905	0.00	27.72	9905	9.00	17.00
49906	0.00	25.65	9906	8.00	18.99
49907	0.00	25.00	9907	7.21	19.00
49908	0.00	35.42	9908	9.01	20.00
49915	0.00	24.23	9915	2.00	20.00
49918	0.00	25.65	9918	7.01	20.00
49919	0.00	21.92	9919	1.00	18.00
49921	0.00	22.99	9921	7.00	19.00
49922	0.00	30.66	9922	8.00	22.00
49926	0.00	29.57	9926	8.00	22.00

Table 97.– Moderate heading turns; BH2 data base.

FLIGHT	COUNTER	DESCRIPTION	DURATION
88	8829	HEADING CHANGE, 60 KIASB	11.99 Seconds
88	8830	HEADING CHANGE, 60 KIASB	12.64 Seconds
88	8831	HEADING CHANGE, 45 KIASB	13.23 Seconds
88	8832	HEADING CHANGE, 45 KIASB	11.99 Seconds
88	8833	HEADING CHANGE, 30 KIASB	15.99 Seconds
88	8834	HEADING CHANGE, 30 KIASB	12.35 Seconds
92	9206	TURN, 25 DEG, 60 KIASB, RUN 701	11.19 Seconds
92	9207	TURN, 45 DEG, 60 KIASB, RUN 720	13.18 Seconds
92	9208	TURN, 35 DEG, 65 KIASB, RUN 710	19.15 Seconds
92	9209	TURN, 60 DEG, 63 KIASB, RUN 730	16.18 Seconds
92	9210	TURN, 90 DEG, 60 KIASB, RUN 740	27.86 Seconds
92	9211	TURN, 15 DEG, 80 KIASB, RUN 702	9.18 Seconds
92	9212	TURN, 30 DEG, 80 KIASB, RUN 711	10.19 Seconds
92	9213	TURN, 45 DEG, 80 KIASB, RUN 721	8.19 Seconds
92	9214	TURN, 60 DEG, 80 KIASB, RUN 731	20.00 Seconds
92	9215	TURN, 90 DEG, 80 KIASB, RUN 741	19.19 Seconds
97	9707	TURN, RT 30DEG, 60KIASB, RUN 745	9.99 Seconds
97	9708	TURN, RT 30DEG, 60KIASB, RUN 746	9.99 Seconds
97	9709	TURN, RT 45DEG, 60KIASB, RUN 750	10.99 Seconds
97	9710	TURN, RT 60DEG, 60KIASB, RUN 760	12.99 Seconds
97	9711	TURN, LT 30DEG, 60KIASB ,RUN 700	8.99 Seconds
97	9712	TURN, LT 45DEG, 60KIASB, RUN 710	10.99 Seconds
97	9713	TURN, LT 60DEG, 60KIASB, RUN 720	14.99 Seconds
97	9722	TURN, LT 90DEG, 60KIASB, RUN 730	18.00 Seconds
97	9724	TURN LT 60DEG, 60KIASB, RUN 725	15.00 Seconds
97	9727	TURN RT 90DEG, 60KIASB, RUN 770	14.99 Seconds
97	9729	TURN RT 60DEG, 60KIASB, RUN 765	12.99 Seconds
99	9904	LT TURN 60DEG, 60KIASB, RUN 720	21.78 Seconds
99	9905	RT TURN 30DEG, 60KIASB, RUN 740	7.99 Seconds
99	9906	RT TURN 45DEG, 60KIASB, RUN 750	10.99 Seconds
99	9907	RT TURN 60DEG, 60KIASB, RUN 760	12.00 Seconds
99	9908	RT TURN 60DEG, 60KIASB, RUN 761	10.99 Seconds
99	9915	TURN LT 90DEG, 60KIASB, RUN 730	18.00 Seconds
99	9918	TURN LT 60DEG, 60KIASB, RUN 726	13.00 Seconds
99	9919	TURN LT 90DEG, 60KIASB, RUN 731	17.00 Seconds
99	9921	TURN RT 60DEG, 60KIASB, RUN 765	12.00 Seconds
99	9922	TURN RT 60DEG, 60KIASB, RUN 766	13.99 Seconds
99	9926	TURN RT 90DEG, 60KIASB, RUN 773	13.99 Seconds

Table 98.– Aggressive heading turns in ground-acoustic testing; prefix-4 data base.

FLIGHT	COUNTER	DESCRIPTION	DURATION
97	49714	CA TURN L30DEG, 60KIASB, RUN780	23.19 Seconds
97	49715	CA TURN L45DEG, 60KIASB, RUN790	28.89 Seconds
97	49716	CA TURN L60DEG, 60KIASB, RUN800	27.55 Seconds
97	49717	CA TURN R30DEG, 60KIASB, RUN820	28.88 Seconds
97	49718	CA TURN R45DEG, 60KIASB, RUN830	24.57 Seconds
97	49719	CA TURN R45DEG, 60KIASB, RUN830	29.63 Seconds
97	49721	CA TURN R60DEG, 60KIASB, RUN841	25.36 Seconds
97	49723	CA TURN L90DEG, 60KIASB, RUN810	24.05 Seconds
97	49725	CA TURN L60DEG, 60KIASB, RUN805	30.42 Seconds
97	49728	CA TURN R90DEG, 60KIASB, RUN850	24.57 Seconds
97	49730	CA TURN R60DEG, 60KIASB, RUN845	26.59 Seconds
98	49842	CA LT TURN 30DEG RUN 700	26.85 Seconds
98	49843	CA LT TURN 45DEG RUN 710	26.26 Seconds
99	49909	CA TURN, L30DEG, 60KIASB, RUN780	22.17 Seconds
99	49910	CA TURN, L45DEG, 60KIASB, RUN790	21.32 Seconds
99	49911	CA TURN, L60DEG, 60KIASB, RUN800	22.87 Seconds
99	49912	CA TURN, R60DEG, 60KIASB, RUN820	22.88 Seconds
99	49913	CA TURN, R45DEG, 60KIASB, RUN830	23.69 Seconds
99	49914	CA TURN, R60DEG, 60KIASB, RUN840	25.51 Seconds
99	49916	CA TURN, L90DEG, 60KIASB, RUN805	27.86 Seconds
99	49917	CA TURN, L60DEG, 60KIASB, RUN806	33.03 Seconds
99	49920	CA TURN, L90DEG, 60KIASB, RUN810	25.20 Seconds
99	49923	CA TURN, R60DEG, 60KIASB, RUN845	22.74 Seconds
99	49924	CA TURN, R90DEG, 60KIASB, RUN771	27.39 Seconds

Table 99.– Time slices for aggressive heading turns in ground-acoustic testing; prefix-4 and BH2 data bases.

PREFIX-4 DATA BASE			BH2 DATA BASE		
COUNTER	START TIME SEC	END TIME SEC	COUNTER	START TIME SEC	END TIME SEC
49714	0.00	23.18	9714	3.00	12.99
49715	0.00	28.89	9715	7.00	17.00
49716	0.00	27.55	9716	8.01	18.00
49717	0.00	28.88	9717	8.01	17.00
49718	0.00	24.57	9718	5.01	14.99
49719	0.00	29.63	9719	8.01	17.99
49721	0.00	25.35	9721	5.01	19.00
49723	0.00	24.05	9723	0.01	10.00
49725	0.00	30.42	9725	10.01	21.00
49728	0.00	24.57	9728	7.00	18.00
49730	0.00	26.59	9730	7.00	14.75
49842	0.00	26.84	9842	9.00	19.00
49843	0.00	26.26	9843	3.01	16.00
49909	0.00	22.16	9909	9.00	17.00
49910	0.00	21.32	9910	5.00	14.00
49911	0.00	22.87	9911	6.01	16.00
49912	0.00	22.88	9912	7.00	17.00
49913	0.00	23.69	9913	9.01	19.00
49914	0.00	25.51	9914	9.00	17.99
49916	0.00	27.86	9916	11.01	21.00
49917	0.00	33.02	9917	16.01	27.00
49920	0.00	25.20	9920	8.01	18.00
49923	0.00	22.74	9923	6.00	15.99
49924	0.00	27.39	9924	9.00	19.99

Table 100.– Aggressive heading turns in ground-acoustic testing; BH2 data base.

FLIGHT	COUNTER	DESCRIPTION	DURATION
97	9714	CA TURN L30DEG, 60KIASB, RUN780	10.00 Seconds
97	9715	CA TURN L45DEG, 60KIASB, RUN790	9.99 Seconds
97	9716	CA TURN L60DEG, 60KIASB, RUN800	9.99 Seconds
97	9717[a]	CA TURN R30DEG, 60KIASB, RUN820	8.99 Seconds
97	9718	CA TURN R45DEG, 60KIASB, RUN830	9.99 Seconds
97	9719	CA TURN R45DEG, 60KIASB, RUN830	9.99 Seconds
97	9721	CA TURN R60DEG, 60KIASB, RUN841	13.99 Seconds
97	9723	CA TURN L90DEG, 60KIASB, RUN810	9.99 Seconds
97	9725	CA TURN L60DEG, 60KIASB, RUN805	10.99 Seconds
97	9728	CA TURN R90DEG, 60KIASB, RUN850	10.99 Seconds
97	9730	CA TURN R60DEG, 60KIASB, RUN845	7.94 Seconds
98	9842	CA LT TURN 30DEG RUN 700	9.99 Seconds
98	9843	CA LT TURN 45DEG RUN 710	13.00 Seconds
99	9909	CA TURN, L30DEG, 60KIASB, RUN780	7.99 Seconds
99	9910	CA TURN, L45DEG, 60KIASB, RUN790	8.99 Seconds
99	9911	CA TURN, L60DEG, 60KIASB, RUN800	9.99 Seconds
99	9912	CA TURN, R60DEG, 60KIASB, RUN820	10.00 Seconds
99	9913	CA TURN, R45DEG, 60KIASB, RUN830	9.99 Seconds
99	9914	CA TURN, R60DEG, 60KIASB, RUN840	8.98 Seconds
99	9916	CA TURN, L90DEG, 60KIASB, RUN805	10.00 Seconds
99	9917	CA TURN, L60DEG, 60KIASB, RUN806	10.99 Seconds
99	9920	CA TURN, L90DEG, 60KIASB, RUN810	10.00 Seconds
99	9923	CA TURN, R60DEG, 60KIASB, RUN845	9.99 Seconds
99	9924	CA TURN, R90DEG, 60KIASB, RUN771	10.99 Seconds

[a]Limited tracking data.

Table 101. – Tracking angles, roll rates, and load factors for moderate heading turns with a 0 deg approach angle. Counters sorted by nominal turn angle.

COUNTER	DIRECTION	APPROACH ANGLE		TURN ANGLE		PEAK	PEAK
		NOMINAL	MEASURED	NOMINAL	MEASURED	RATE	FACTOR
		DEG	DEG	DEG	DEG	DEG/SEC	Gs
9211	right	0.0	–0.3	–15.0	–13.8	16.9	1.19
9206	right	0.0	–1.0	–25.0	–22.9	23.4	1.15
9212	right	0.0	0.4	–30.0	–36.3	25.6	1.15
9707	right	0.0	–1.0	–30.0	–33.9	16.1	1.14
9708	right	0.0	0.3	–30.0	–34.1	19.6	1.14
9711	left	0.0	–0.2	30.0	37.7	14.8	1.13
9904	right	0.0	–0.5	–30.0	–27.0	8.3	1.10
9208	right	0.0	–0.5	–35.0	–32.9	26.4	1.14
9207	right	0.0	–2.1	–45.0	–44.8	18.6	1.17
9213	right	0.0	–12.0[a]	–45.0	–36.4	21.0	1.24
9709	right	0.0	–0.9	–45.0	–55.7	16.7	1.14
9712	left	0.0	0.4	45.0	57.0	14.6	1.14
9906	right	0.0	–1.4	–45.0	–46.6	13.5	1.21
9209	right	0.0	–0.7	–60.0	–56.3	11.3	1.19
9214	right	0.0	–3.4	–60.0	–63.5	13.2	1.20
9710	right	0.0	–0.9	–60.0	–70.7	15.8	1.24
9713	left	0.0	–0.5	60.0	78.0	15.8	1.17
9904	left	0.0	0.7	60.0	60.4	13.6	1.16
9907	right	0.0	0.5[b]	–60.0	–59.8[b]	13.6	1.19
9908	right	0.0	–1.4	–60.0	–52.6	13.6	1.16
9210	right	0.0	–0.4	–90.0	–94.0	10.2	1.13
9215	right	0.0	–2.3	–90.0	–94.4	23.4	1.23

[a]Tape record begins after the start of the turn.

[b]Based on HEADING measurement as tracker lost time synchronization.

Table 102.– Tracking angles, roll rates, and load factors for moderate heading turns with a –40 deg approach angle. Counters sorted by nominal turn angle.

COUNTER	DIRECTION	APPROACH ANGLE		TURN ANGLE		PEAK	PEAK
		NOMINAL	MEASURED	NOMINAL	MEASURED	RATE	FACTOR
		DEG	DEG	DEG	DEG	DEG/SEC	Gs
9724	left	–40.0	–41.8	60.0	71.2	12.2	1.16
9729	right	–40.0	–42.8	–60.0	–59.2	10.9	1.15
9918	left	–40.0	–41.8	60.0	48.4	14.7	1.15
9921	right	–40.0	–40.7	–60.0	–46.9	12.4	1.13
9922	right	–40.0	–40.7	–60.0	–52.4	9.4	1.14
9722	left	–40.0	–42.1	90.0	97.8	11.8	1.14
9727	right	–40.0	–42.4	–90.0	–83.6	9.6	1.15
9915	left	–40.0	–42.4	90.0	89.1	12.2	1.14
9919	left	–40.0	–42.8	90.0	98.3	12.7	1.25
9926	right	–40.0	–42.7	–90.0	–73.7	12.0	1.21

Table 103.– Tracking angles, roll rates, and load factors for aggressive heading turns with a 0 deg approach angle. Counters sorted by nominal turn angle.

COUNTER	DIRECTION	APPROACH ANGLE		TURN ANGLE		PEAK	PEAK
		NOMINAL	MEASURED	NOMINAL	MEASURED	RATE	FACTOR
		DEG	DEG	DEG	DEG	DEG/SEC	Gs
9714	left	0.0	0.7	30.0	34.9	31.6	1.13
9717	right	0.0	0.4	–30.0	–33.3[a]	24.1	1.19
9842	left	0.0	–1.1	30.0	32.7	14.0	1.08
9909	left	0.0	0.5	30.0	31.7	30.3	1.24
9715	left	0.0	–0.3	45.0	52.9	32.4	1.20
9718	right	0.0	–1.2	–45.0	–53.1	31.3	1.29
9719	right	0.0	–0.8	–45.0	–49.7	22.7	1.21
9843	left	0.0	–0.6	45.0	53.6	12.4	1.12
9910	left	0.0	–0.2	45.0	47.0	35.5	1.28
9913	right	0.0	–1.5	–45.0	–40.8	32.7	1.32
9716	left	0.0	0.4	60.0	76.0	22.3	1.29
9721	right	0.0	–0.6	–60.0	–69.2	30.2	1.38
9911	left	0.0	–0.6	60.0	64.5	36.0	1.36
9912	right	0.0	–1.5	–60.0	–26.3	23.4	1.12
9914	right	0.0	–1.7	–60.0	–61.2	36.5	1.43

[a]Based on HEADING measurement, as tracker failed after 1 sec.

Table 104.– Tracking angles, roll rates, and load factors for aggressive heading turns with a –40 deg approach angle. Counters sorted by nominal turn angle.

COUNTER	DIRECTION	APPROACH ANGLE		TURN ANGLE		PEAK	PEAK
		NOMINAL	MEASURED	NOMINAL	MEASURED	RATE	FACTOR
		DEG	DEG	DEG	DEG	DEG/SEC	Gs
9725	left	–40.0	–41.9	60.0	66.5	30.1	1.43
9730	right	–40.0	–41.8	–60.0	–59.1	26.4	1.30
9917	left	–40.0	–40.3	60.0	42.4	32.1	1.17
9923	right	–40.0	–40.4	–60.0	–49.6	32.2	1.27
9723	left	–40.0	–40.4	90.0	88.2	29.0	1.35
9728	right	–40.0	–42.0	–90.0	–79.8	26.5	1.29
9916	left	–40.0	–42.2	90.0	80.1	34.3	1.48
9920	left	–40.0	–40.5	90.0	84.4	36.7	1.55
9924	right	–40.0	–40.8	–90.0	–81.7	35.1	1.36

[a]Tape record begins after the start of the turn.

Table 105.– Constant radius turns from ground-acoustic testing; prefix-4 data base.

FLIGHT	COUNTER	DESCRIPTION	DURATION
96	49618	CW TURN, 1800', 58KIASB, RUN880	117.64 Seconds
96	49623	CCW TURN, 1800', 60KIASB, RUN910	103.25 Seconds
96	49628[a]	CW TURN, 1400', 60KIASB, RUN870	88.80 Seconds
96	49632	CCW TURN, 1400', 60KIASB, RUN900	77.87 Seconds
96	49636	CW TURN, 1000', 58KIASB, RUN860	58.31 Seconds
96	49639	CW TURN, 1000', 60KIASB, RUN861	65.64 Seconds
96	49642	CCW TURN, 1000', 60KIASB, RUN890	59.08 Seconds
98	49817	TURN CW 1800'RAD. R880 5 SEG	98.71 Seconds
98	49822	TURN CCW 1800'RAD. R910 6 SEG	126.19 Seconds
98	49828	TURN CW 1400'RAD. R870 4 SEG	30.37 Seconds
98	49832	TURN CCW 1400'RAD. R900 4 SEG	80.07 Seconds
98	49836	TURN CW 1000'RAD. R860 3 SEG	50.90 Seconds
98	49839	TURN CCW 1000'RAD. R890 3 SEG	56.38 Seconds

[a]No tracking data.

Table 106.– Constant radius turn performance; prefix-4 data base.

COUNTER	DIRECTION	TURNING ANGLE	TURN RADIUS		
			NOMINAL	MEAN	STD. DEVIATION
		DEG	FT	FT	FT
49618	CW	–405	1800	1813.1	13.7
49623	CCW	376	1800	1823.0	30.4
49628	CW	–[a]	1400	–[a]	–[a]
49632	CCW	369	1400	1402.3	23.6
49636	CW	–392	1000	1008.2	20.3
49639	CW	–457	1000	998.0	18.3
49642	CCW	367	1000	1029.6	43.9
49817	CW	–351	1800	1800.8	25.5
49822	CCW	462	1800	1804.2	11.7
49828	CW	–147	1400	1406.8	9.5
49832	CCW	364	1400	1406.0	10.8
49836	CW	–336	1000	990.1	11.0
49839	CCW	362	1000	1005.8	9.5

[a]No tracking data.

Table 107.– Time slices for constant radius turns in prefix-4 and BH2 data bases.

PREFIX-4 DATA BASE			BH2 DATA BASE		
COUNTER	START TIME SEC	END TIME SEC	COUNTER	START TIME SEC	END TIME SEC
49618	0.00	117.64	9620	53.00	58.00
49623	0.00	103.25	9625	46.00	51.00
	0.00	103.25	9627	96.00	100.99
49628	0.00	88.80	9629	30.01	35.00
	0.00	88.80	9631	70.00	75.00
49632	0.00	77.87	9633	30.02	35.01
	0.00	77.87	9634	47.02	52.01
49636	0.00	58.31	9637	19.51	24.50
	0.00	58.31	9638	53.01	58.00
49639	0.00	65.64	9639	15.01	20.00
	0.00	65.64	9640	36.00	40.99
49642	0.00	59.08	9642	7.00	12.00
	0.00	59.08	9643	28.00	32.99
49817	0.00	98.71	9817	11.01	16.00
	0.00	98.71	9818	25.00	30.00
	0.00	98.71	9819	44.96	49.99
	0.00	98.71	9820	69.01	74.00
49822	0.00	126.19	9822	20.00	24.99
	0.00	126.19	9823	44.01	48.99
	0.00	126.19	9824	60.00	64.99
	0.00	126.19	9825	77.00	82.00
	0.00	126.19	9826	97.01	102.00
49828	0.00	30.37	9828	7.00	12.00
	0.00	30.37	9829	23.01	28.00
49832	0.00	80.07	9832	6.00	11.00
	0.00	80.07	9833	28.01	33.00
	0.00	80.07	9834	50.01	55.00
	0.00	80.07	9835	68.01	73.00
49836	0.00	50.09	9836	15.01	20.00
	0.00	50.09	9837	35.01	40.00
	0.00	50.09	9838	43.00	48.00
49839	0.00	56.38	9839	12.00	17.00
	0.00	56.38	9840	24.00	29.00
	0.00	56.38	9841	48.00	53.00

Table 108.– Constant radius turns from ground-acoustic testing; BH2 data base.

FLIGHT	COUNTER	DESCRIPTION	DURATION
96	9620	CW TURN, 1800', 58KIASB, RUN880	4.99 Seconds
96	9625	CCW TURN, 1800', 60KIASB, RUN910	4.99 Seconds
96	9627	CCW TURN, 1800', 60KIASB, RUN910	4.99 Seconds
96	9629[a]	CW TURN, 1400', 60KIASB, RUN870	4.99 Seconds
96	9631[a]	CW TURN, 1400', 60KIASB, RUN870	4.99 Seconds
96	9633	CCW TURN, 1400', 60KIASB, RUN900	4.99 Seconds
96	9634	CCW TURN, 1400', 60KIASB, RUN900	4.99 Seconds
96	9637	CW TURN, 1000', 58KIASB, RUN860	4.99 Seconds
96	9638	CW TURN, 1000', 58KIASB, RUN860	4.99 Seconds
96	9639	CW TURN, 1000', 60KIASB, RUN861	4.99 Seconds
96	9640	CW TURN, 1000', 60KIASB, RUN861	4.99 Seconds
96	9642	CCW TURN, 1000', 60KIASB, RUN890	4.99 Seconds
96	9643	CCW TURN, 1000', 60KIASB, RUN890	4.99 Seconds
98	9817	TURN CW 1800' RAD. R880 SEG 1	4.99 Seconds
98	9818	TURN CW 1800' RAD. R880 SEG 2	4.99 Seconds
98	9819	TURN CW 1800' RAD. R880 SEG 3	5.03 Seconds
98	9820	TURN CW 1800' RAD. R880 SEG 4	4.99 Seconds
98	9822	TURN CCW 1800' RAD. R910 SEG 1	4.99 Seconds
98	9823	TURN CCW 1800' RAD. R910 SEG 2	4.99 Seconds
98	9824	TURN CCW 1800' RAD. R910 SEG 3	4.99 Seconds
98	9825	TURN CCW 1800' RAD. R910 SEG 4	4.99 Seconds
98	9826	TURN CCW 1800' RAD. R910 SEG 5	4.99 Seconds
98	9828	TURN CW 1400' RAD. R870 SEG 1	4.99 Seconds
98	9829	TURN CW 1400' RAD. R870 SEG 2	4.99 Seconds
98	9832	TURN CCW 1400' RAD. R900 SEG 1	4.99 Seconds
98	9833	TURN CCW 1400' RAD. R900 SEG 2	4.99 Seconds
98	9834	TURN CCW 1400' RAD. R900 SEG 3	4.99 Seconds
98	9835	TURN CCW 1400' RAD. R900 SEG 4	4.99 Seconds
98	9836	TURN CW 1000' RAD. R860 SEG 1	4.99 Seconds
98	9837	TURN CW 1000' RAD. R860 SEG 2	4.99 Seconds
98	9838	TURN CW 1000' RAD. R860 SEG 3	4.99 Seconds
98	9839	TURN CCW 1000' RAD. R890 SEG 1	4.99 Seconds
98	9840	TURN CCW 1000' RAD. R890 SEG 2	4.99 Seconds
98	9841	TURN CCW 1000' RAD. R890 SEG 3	4.99 Seconds

[a]No tracking data.

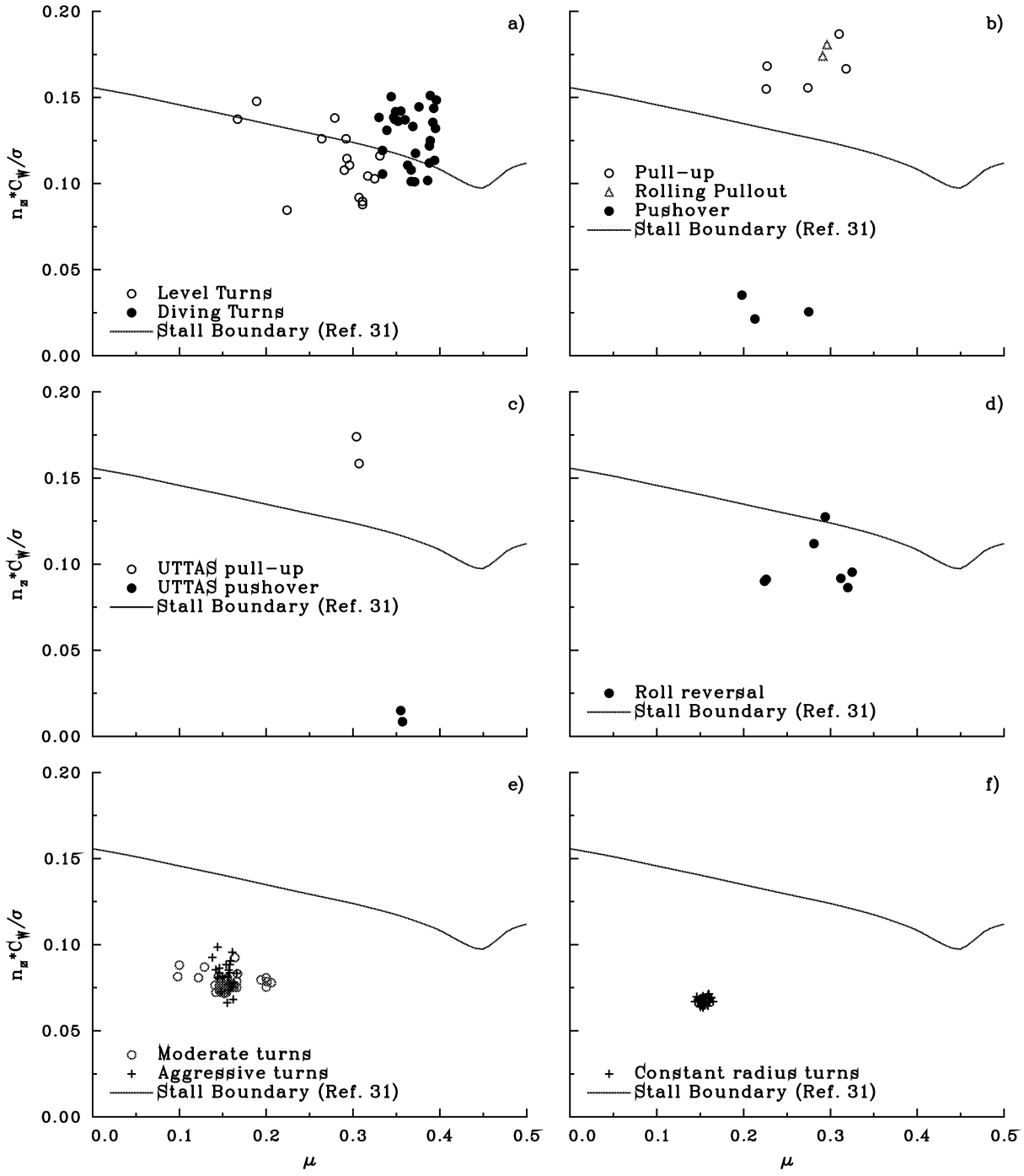

Figure 53.– Summary of maneuver conditions: a) bank-angle turns; b) pull-ups, rolling pullouts, and pushovers; c) UTTAS maneuvers; d) roll reversals; e) heading turns (acoustics); and f) constant radius turns (acoustics).

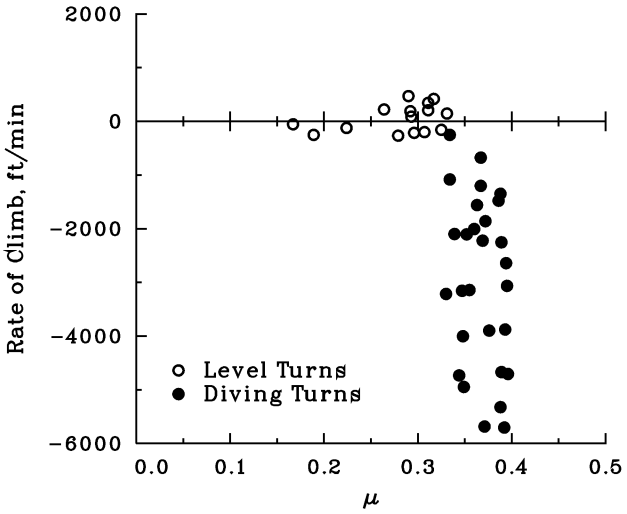

Figure 54.– Rate of climb for level and diving bank-angle turns.

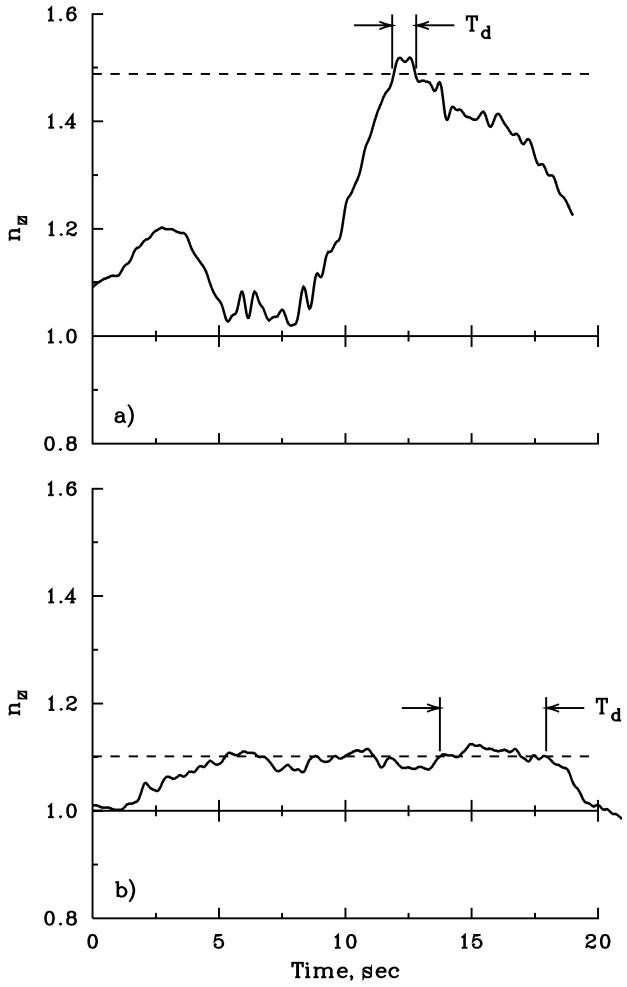

Figure 55.– Load factor time histories in two level bank-angle turns, illustrating maneuver steadiness. Duration time, T_d, indicates portion of time history where load factor is within 2% of maximum value: a) Counter 8539; b) Counter 8826.

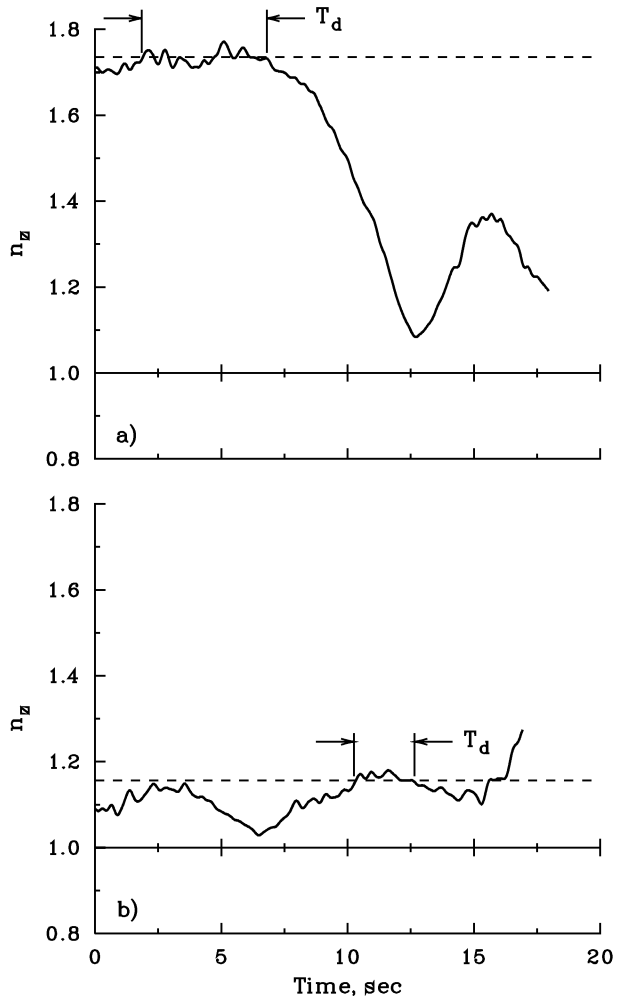

Figure 56.– Load factor time histories in two diving bank-angle turns, illustrating maneuver steadiness. Duration time, T_d, indicates portion of time history where load factor is within 2% of maximum value: a) Counter 11668; b) Counter 11683.

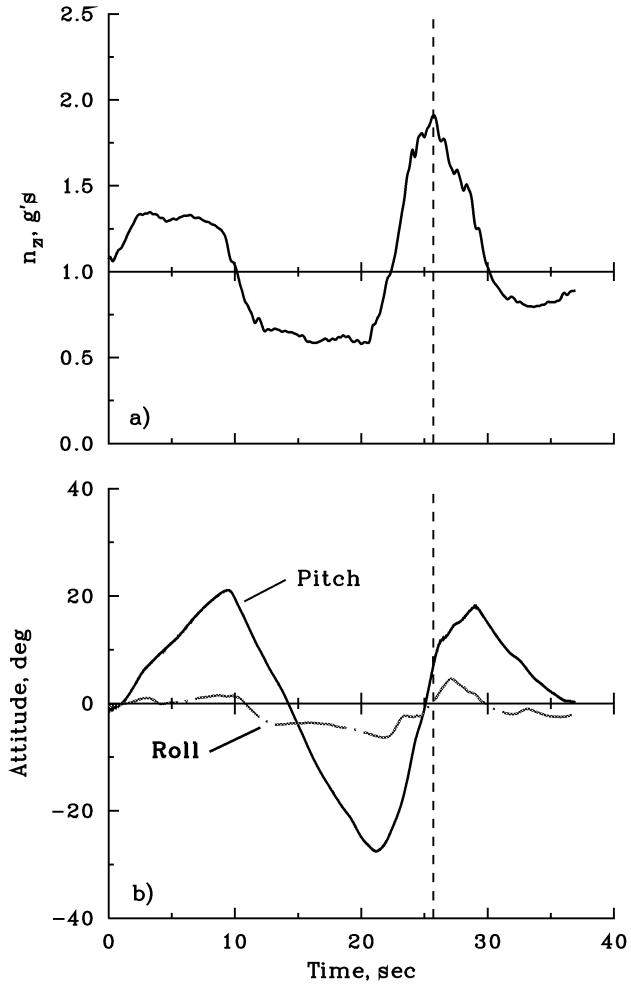

Figure 57.– Time history of symmetric pull-up (Counter 11022). Dashed line indicates time at maximum load factor: a) load factor; b) pitch and roll attitudes.

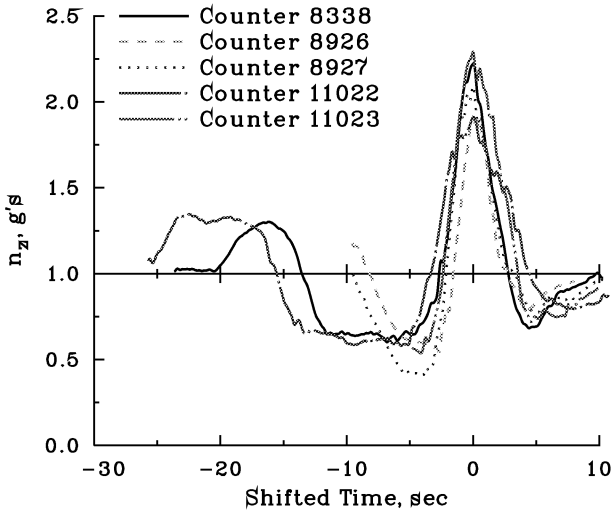

Figure 58.– Comparison of load factor time histories for five symmetric pull-ups. The time axis is shifted so that $T = 0$ sec corresponds to the maximum load factor.

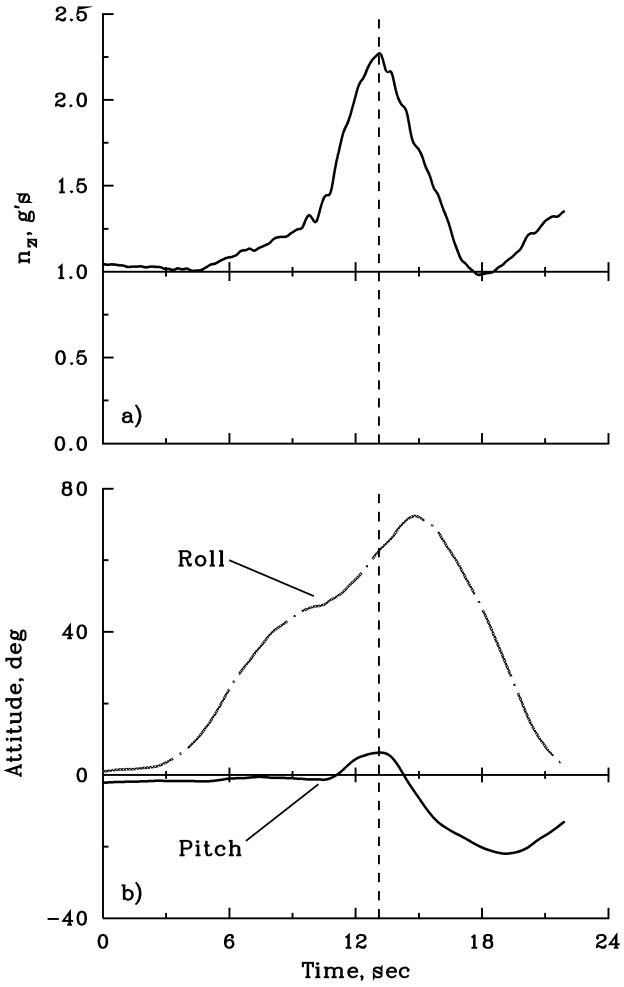

Figure 59.– Time history of rolling pullout (Counter 11028). Dashed line indicates time at maximum load factor: a) load factor; b) pitch and roll attitudes.

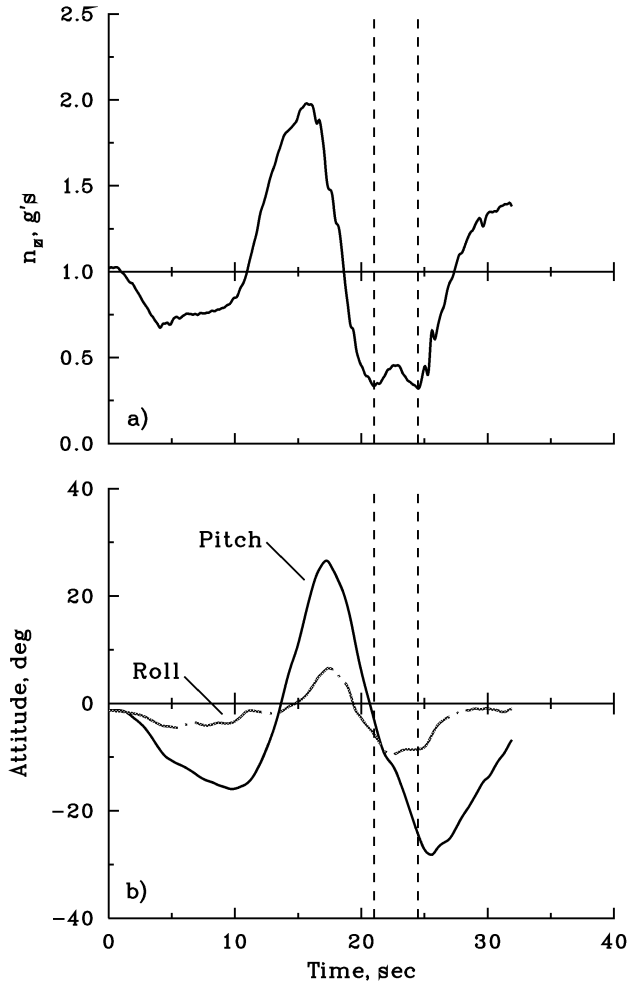

Figure 60.– Time history of pushover (Counter 11024). Dashed lines indicates time at two minimum load factors: a) load factor; b) pitch and roll attitudes.

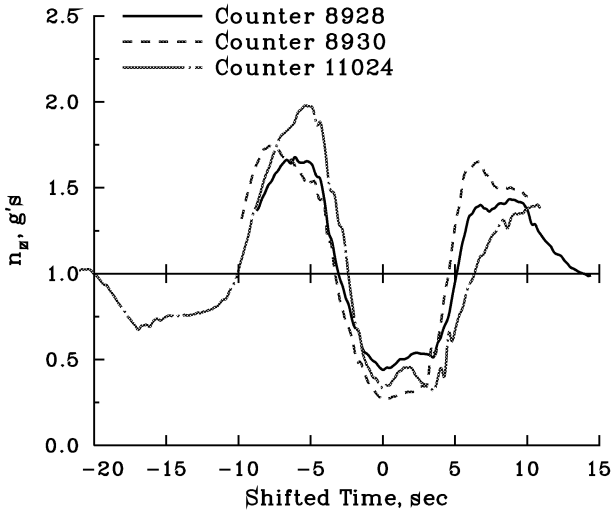

Figure 61.– Comparison of load factor time histories for three pushovers.

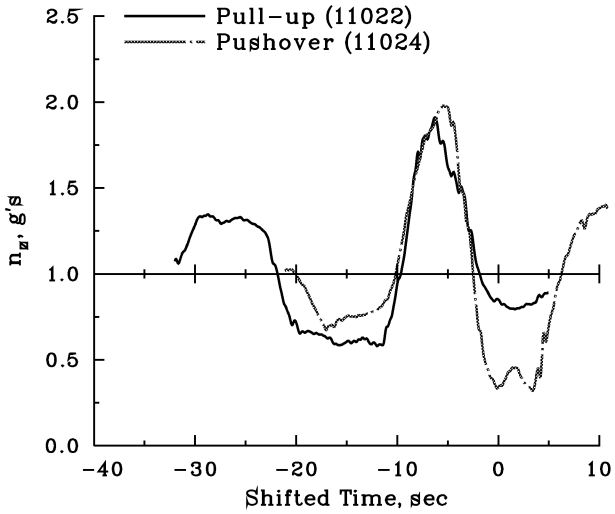

Figure 62.– Comparison of pull-up and pushover maneuvers.

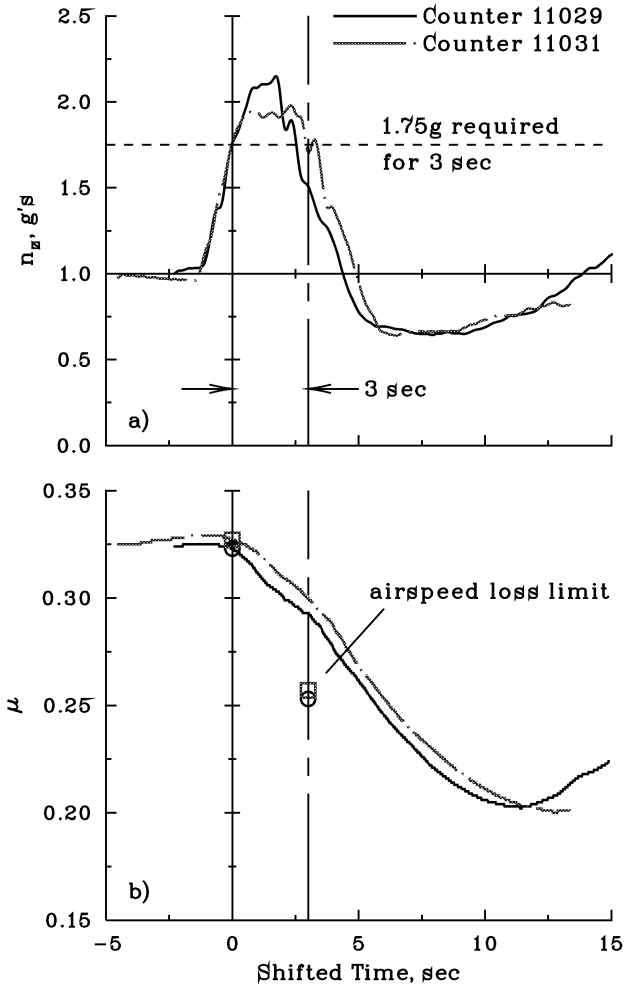

Figure 63.– Time histories of UTTAS pull-ups. $T = 0$ sec corresponds to initial attainment of 1.75g. Chain-dash line is used to mark three second period following $T = 0$: a) load factor; b) airspeed (symbols show allowable airspeed loss in maneuver).

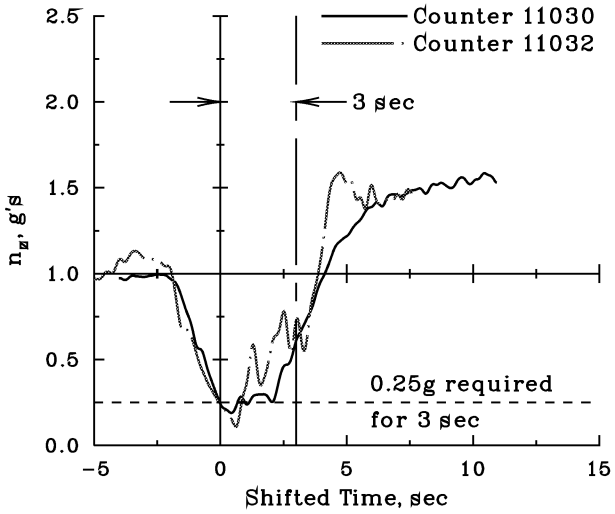

Figure 64.– Load factor time histories of UTTAS pushovers. $T = 0$ sec corresponds to initial attainment of 0.25g. Chain-dash line is used to mark three second period following $T = 0$.

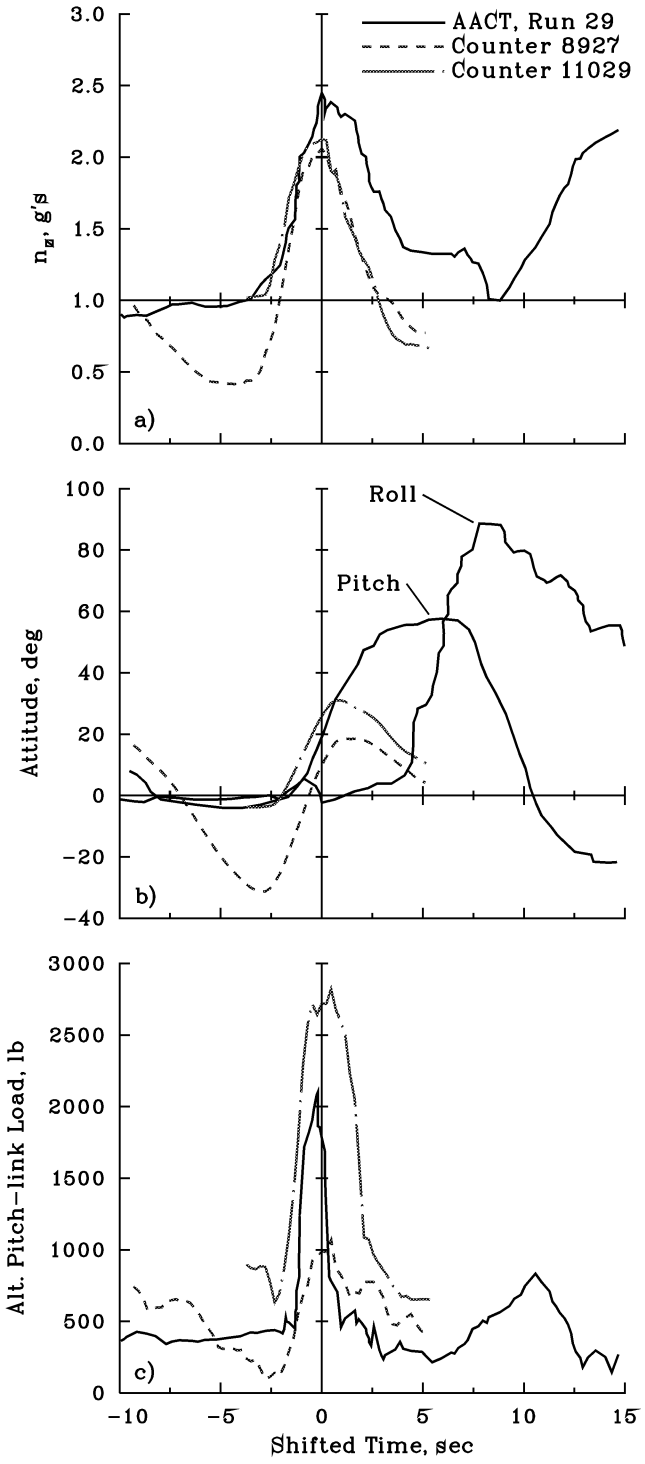

Figure 65.– Comparison of two maneuvers from Airloads Program with Air-to-Air Combat Maneuver (ref. 33): a) load factor; b) aircraft attitude (roll attitude included for AACT maneuver; c) alternating pitch-link load.

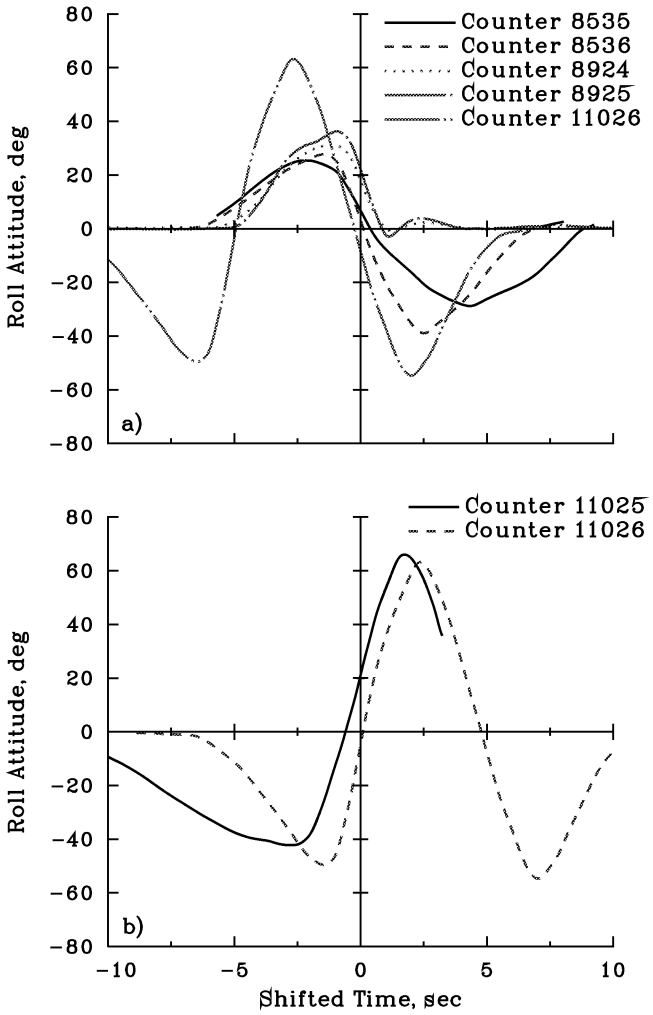

Figure 66.– Roll attitude time histories during roll reversals. $T = 0$ sec corresponds to time at maximum roll rate during roll reversal: a) Roll reversals to left; b) roll reversals to right.

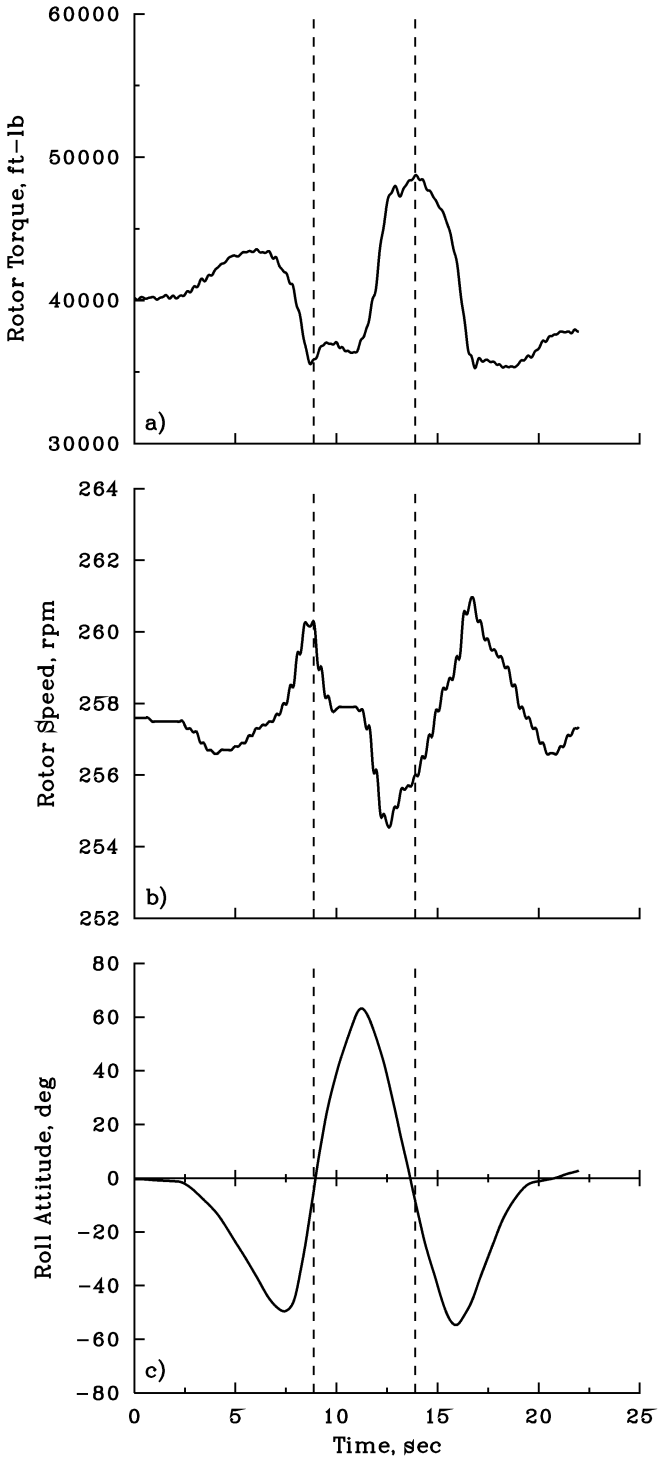

Figure 67.– Comparison of rotor torque, rotor speed, and roll attitude during a double roll reversal (Counter 11026). Dashed lines show time of maximum roll rate during right and left roll reversals: a) Main rotor torque; b) main rotor speed; c) aircraft roll attitude.

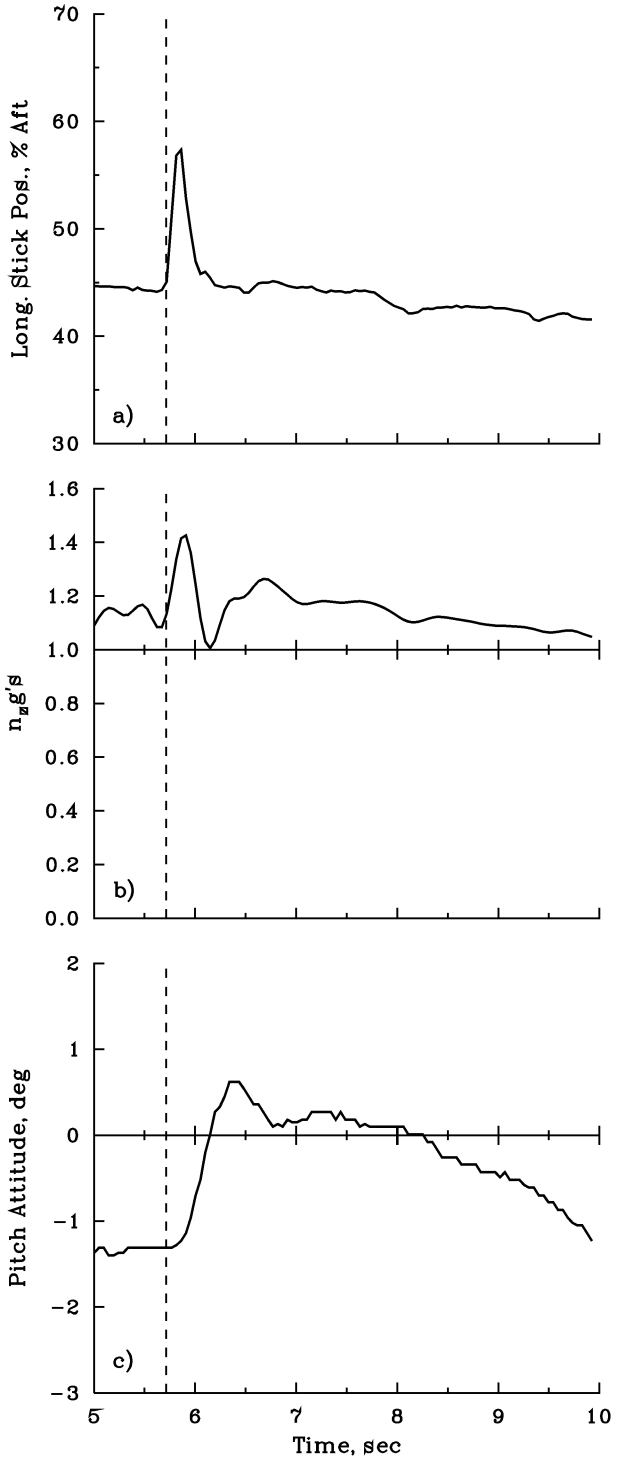

Figure 68.– Aft longitudinal control pulse in a bank-angle turn; $\mu = 0.32$ (Counter 11528). Dashed line shows time of initiation of the control pulse: a) Longitudinal stick position; b) aircraft load factor; c) aircraft pitch attitude.

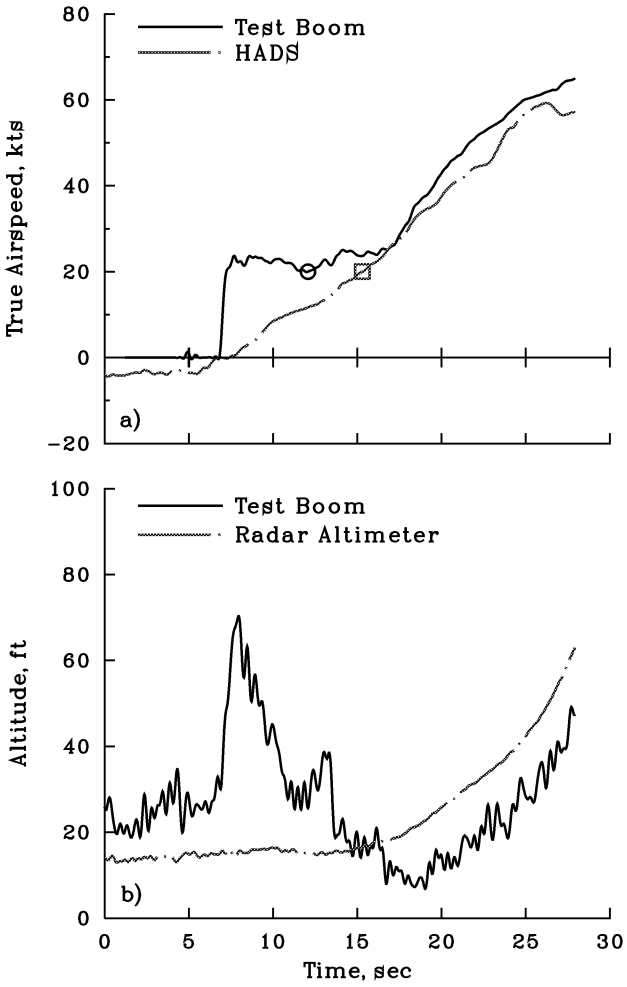

Figure 69.– Accelerating flight time history (Counter 11650). Open symbols indicate 20-knot break point for airspeed measurement systems: a) True airspeed; b) altitude above ground level.

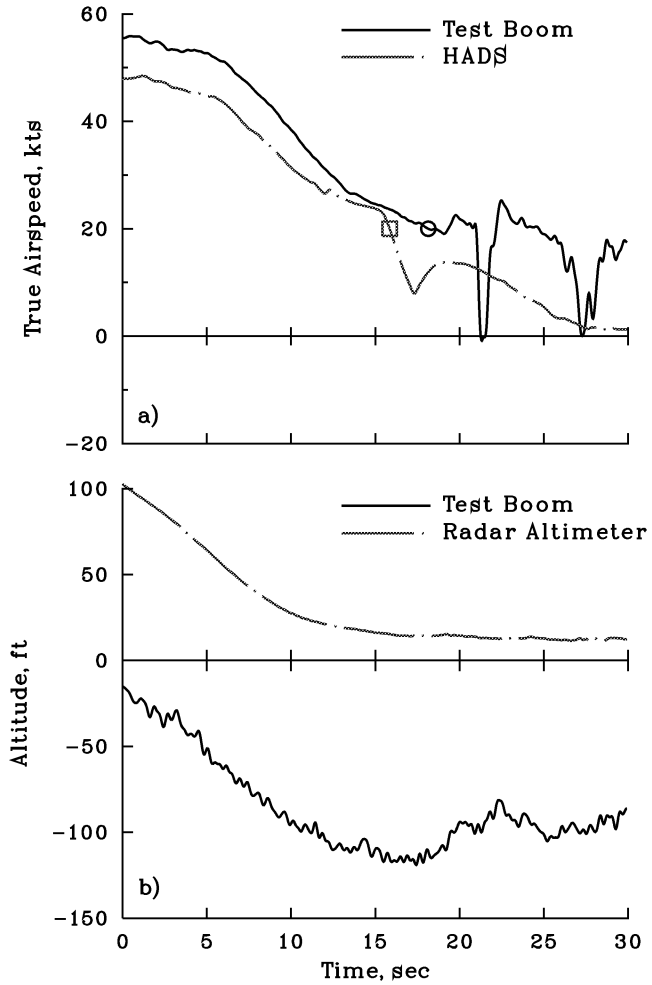

Figure 70.– Decelerating flight time history (Counter 11688). Open symbols indicate 20-knot break point for airspeed measurement systems: a) true airspeed; b) altitude above ground level.

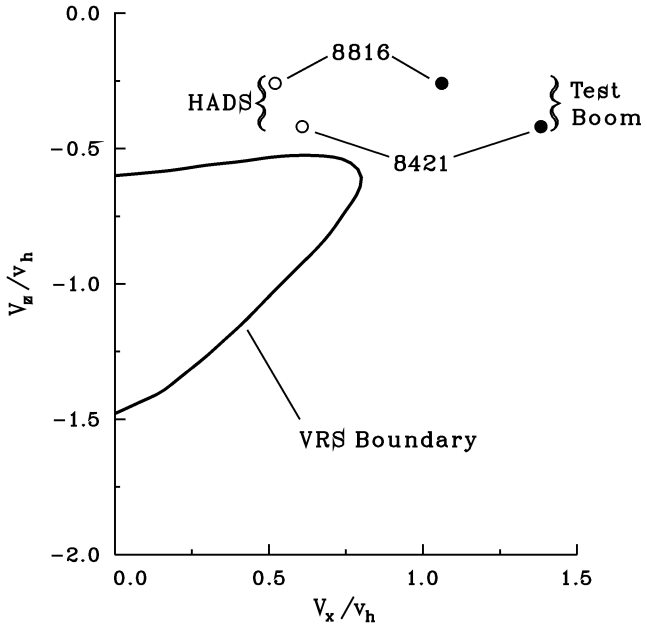

Figure 71.– Settling with power counters compared with vortex ring state (VRS) boundary from reference 34. Uncertainty in horizontal velocity indicated by differences in HADS and test boom measurements.

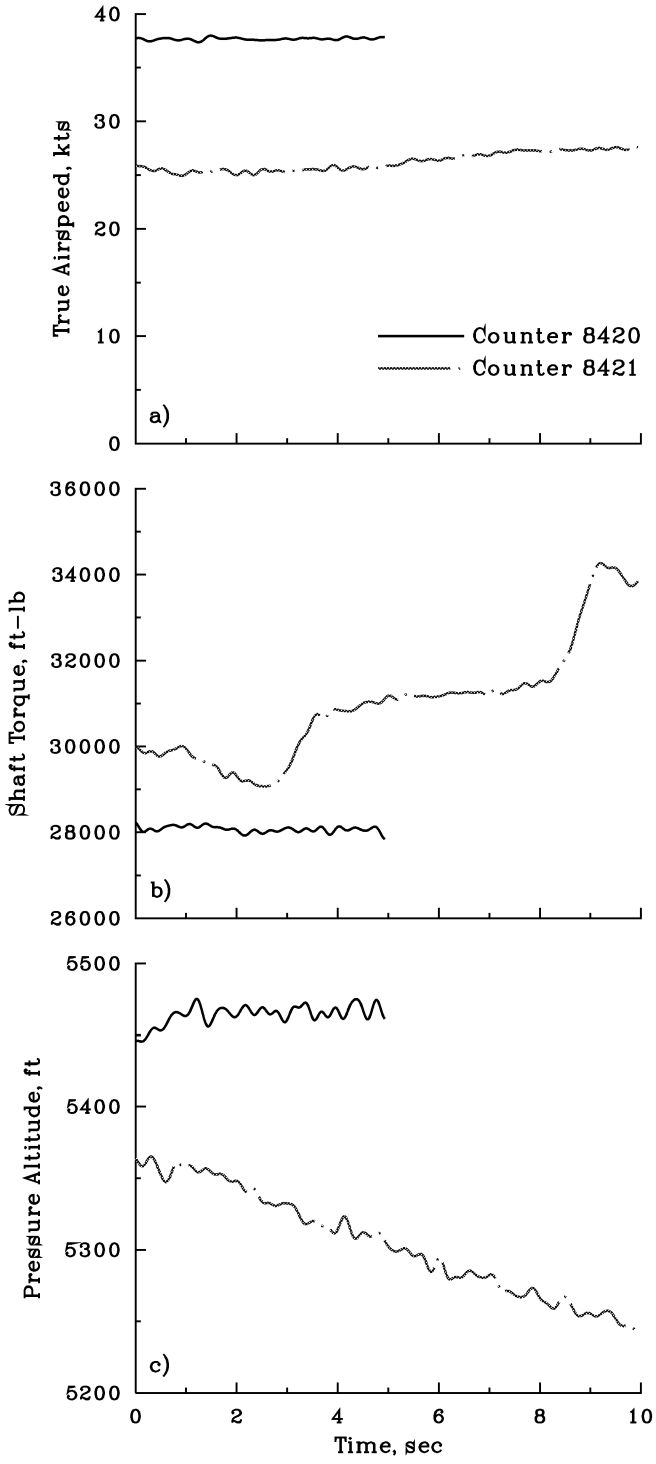

Figure 72.– Time histories of settling with power (Counter 8421) and reference condition (Counter 8420): a) True airspeed; b) main rotor shaft torque; c) pressure altitude.

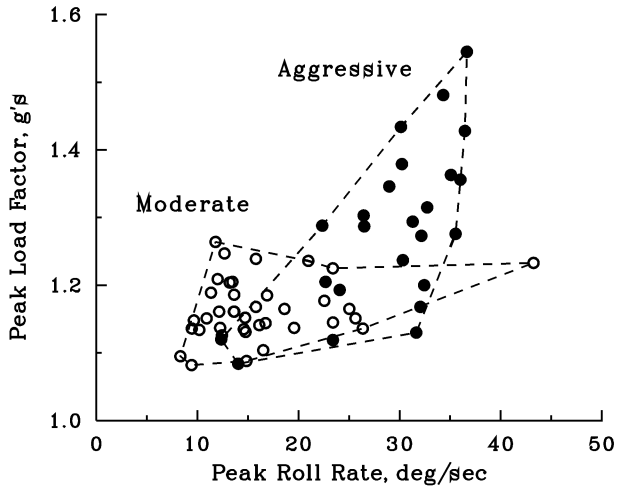

Figure 73.– Peak load factors and roll rates for moderate and aggressive heading turns.

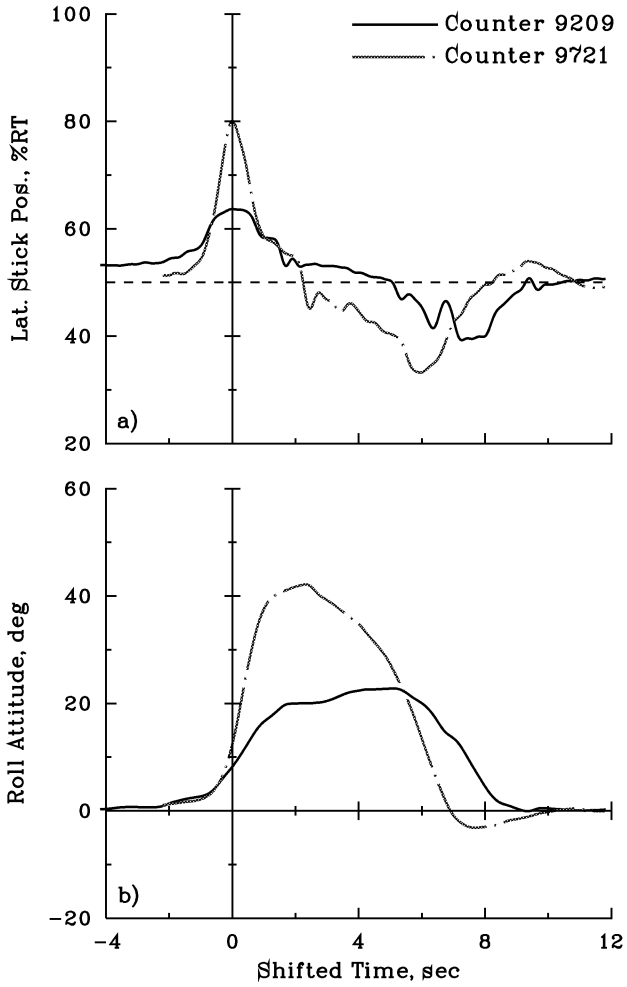

Figure 74.– Comparison of lateral control input and roll attitude time histories during moderate (Counter 9209) and aggressive (Counter 9721) heading turns; right turn, 60 KIAS approach speed, and 60 deg nominal turn angle. Time histories shifted so initial lateral control inputs are aligned: a) lateral stick position in percent of full travel; b) roll attitude, positive right wing down.

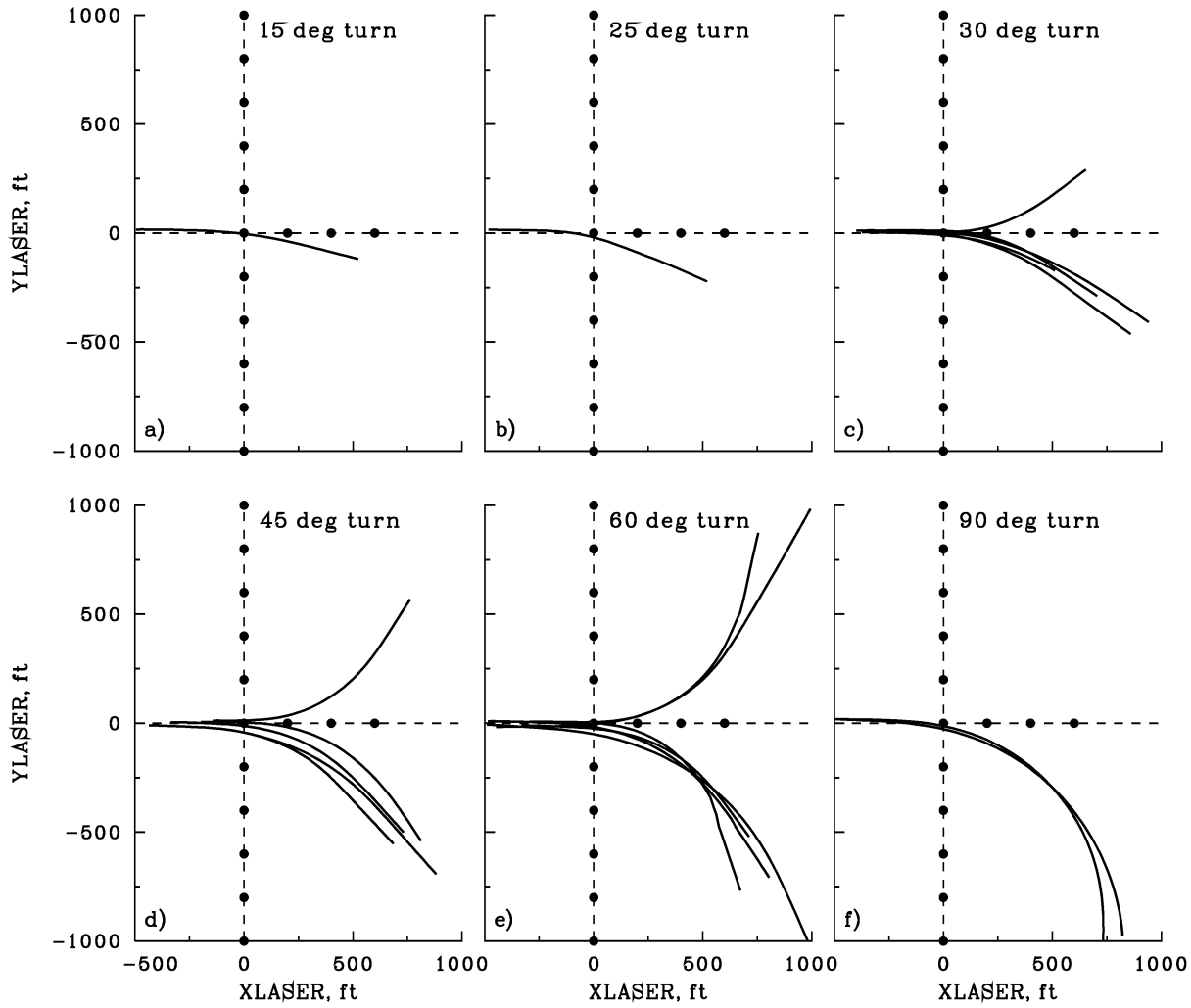

Figure 75.– X- and y-position of aircraft during moderate heading turns with 0 deg approach angle. Solid circles show microphone array locations for Flights 96 to 99.

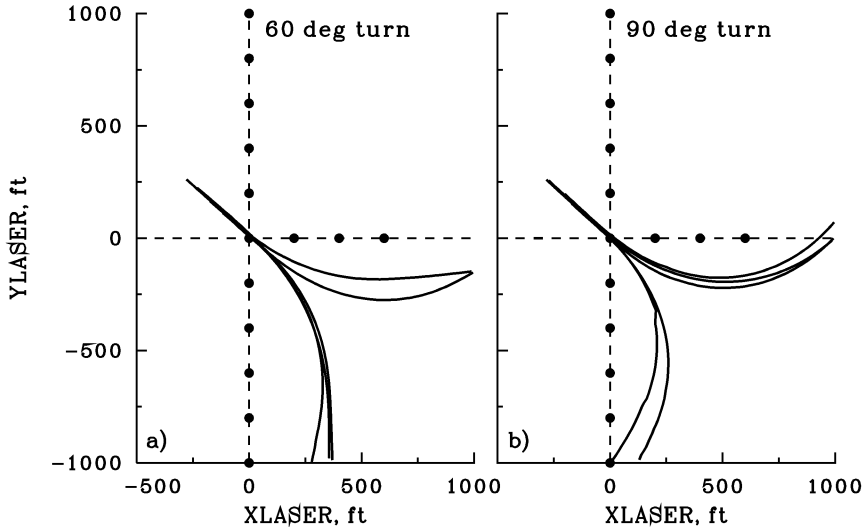

Figure 76.– X- and y-position measurements during moderate heading turns with –40 deg approach angle. Solid circles show microphone array locations for Flights 96 to 99.

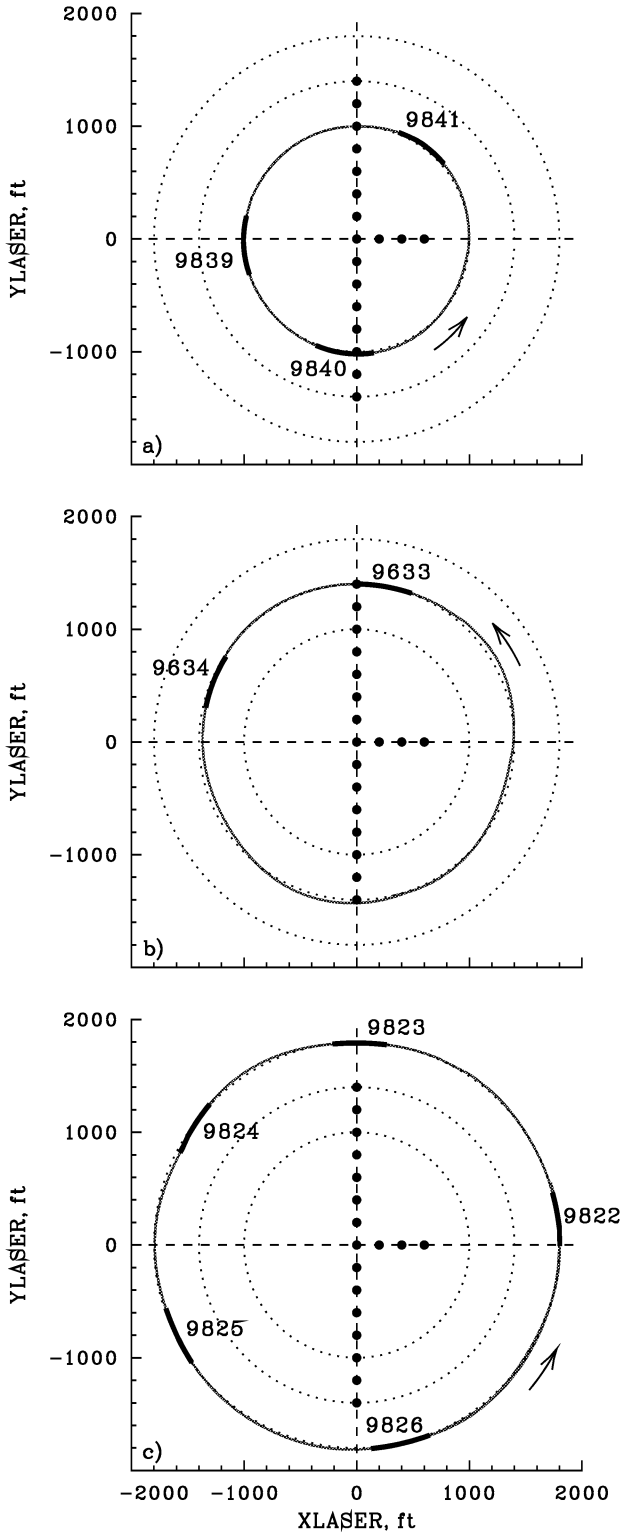

Figure 77.– X- and y-position track for constant radius turns on three radii, including selected BH2 data base segments. Solid circles show microphone array locations for Flights 96 to 99: a) 1000-ft radius (Counter 49839); b) 1400-ft radius (Counter 49632); c) 1800-ft radius (Counter 49822).

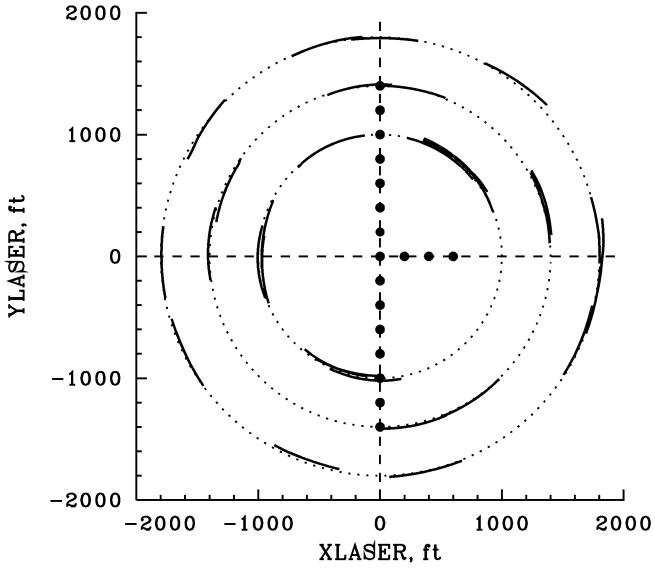

Figure 78.– X- and y-position measurements for BH2 data base constant radius turn segments centered on microphone array. Solid circles show microphone array locations for Flights 96 to 99.

REFERENCES

1. Kufeld, Robert M.; Balough, Dwight L.; Cross, Jeffrey L.; Studebaker, Karen F.; Jennison, Christopher D.; and Bousman, William G.: Flight Testing the UH–60A Airloads Aircraft. American Helicopter Society 50th Annual Forum, May 1994, pp. 557–578.

2. Balough, Dwight L.: Estimation of Rotor Flapping Response Using Blade-Mounted Accelerometers. American Helicopter Society Aeromechanics Specialists' Meeting, January 1994.

3. Coleman, Colin P.; and Bousman, William G.: Aerodynamic Limitations of the UH–60A Rotor. American Helicopter Society Aeromechanics Specialists' Meeting, January 1994.

4. Kufeld, Robert M.; Cross, Jeffrey L.; and Bousman, William G.: A Survey of Rotor Loads Distribution In Maneuvering Flight. American Helicopter Society Aeromechanics Specialists' Meeting, January 1994.

5. Studebaker, Karen: A Survey of Hub Vibration for the UH–60A Airloads Research Aircraft. American Helicopter Society Aeromechanics Specialists' Meeting, January 1994.

6. Mueller, Arnold W.; Conner, David A.; Rutledge, Charles K.; and Wilson, Mark R.: Full Scale Flight Acoustic Results for the UH–60A Airloads Aircraft. American Helicopter Society, Vertical Lift Aircraft Design Conference Proceedings, January 1995, pp. 5.1-1 to 5.1-25.

7. Rutledge, Charles K.; Mueller, Arnold W.; and Wilson, Mark: A Study of the Variability Difference Between Model Scale Wind Tunnel and Full Scale Flight Test Airloads Data. American Helicopter Society Vertical Lift Aircraft Design Conference Proceedings, January 1995, pp. 5.2-1 to 5.2-26.

8. Wilson, Mark R.; Mueller, Arnold W.; and Rutledge, Charles K.: A New Technique For Estimating Ground Footprint Acoustics For Rotorcraft Using Measured Sound Fields. American Helicopter Society Vertical Lift Aircraft Design Conference Proceedings, January 1995, pp. 5.3-1 to 5.3-9.

9. Kufeld, Robert M.; and Bousman, William G.: High Load Conditions on a UH–60A In Maneuvering Flight. American Helicopter Society 51st Annual Forum Proceedings, May 1995, pp. 421–433.

10. Tung, Chee; Bousman, William G.; and Low, Scott: A Comparison of Airload Data Between Model-Scale Rotor and Full-Scale Flight Test. American Helicopter Society 2nd International Aeromechanics Technology and Product Design Meeting Proceedings, October 1995, pp. 1-1 to 1-19.

11. Kufeld, Robert M.; and Bousman, William G.: UH–60A Helicopter Rotor Airloads Measured in Flight. The Aeronautical Journal, vol. 101, no. 1005, May 1997, pp. 217-227.

12. Bousman, William G.: A Qualitative Examination of Dynamic Stall from Flight Test Data. American Helicopter Society 53rd Annual Forum Proceedings, April–May 1997.

13. Bousman, William G.: A Note on Torsional Dynamic Scaling. J. of American Helicopter Society, vol. 43, no. 2, April 1998, pp. 172–175.

14. Kufeld, Robert M.; and Johnson, Wayne: The Effect of Control System Stiffness Models on the Dynamic Stall Behavior of a Helicopter. American Helicopter Society 54th Annual Forum Proceedings, May 1998, pp. 589–601.

15. Nguyen, Khanh; and Johnson, Wayne: Evaluation of Dynamic Stall Models with Flight Test Data. American Helicopter Society 54th Annual Forum Proceedings, May 1998, pp. 576–588.

16. Buckanin, Robert M.; Gould, Warren; Losier, Paul W.; Downey, David A.; Lockwood, Roy; Webre, James L.; Hagen, John F.; Cason, Randall W.; and Young, Christopher J.: UH–60A Rotor System Evaluation Phase I. AEFA Project No. 85–15, March 1988.

17. Bondi, M.; and Bjorkman, W.: TRENDS: A Flight Test Relational Database Users Reference Manual. NASA TM-108806, June 1994.

18. McCluer, M.; and Dearing, M.: Measuring Blade-Vortex Interaction Noise Using the YO-3A Acoustics Research Aircraft. 22nd European Rotorcraft Forum, Brighton, UK, September 1996.

19. Lorber, P. F.: Aerodynamic Results of a Pressure-Instrumented Model Rotor Test at the DNW. American Helicopter Society 46th Annual Forum, Washington D.C., May 1990.

20. Tischler, M. B.; and Cauffman, M. G.: Frequency-Response Method for Rotorcraft System Identification: Flight Application to BO–105 Coupled Rotor/Fuselage Dynamics. J. American Helicopter Society, vol. 37, no. 3, July 1992, pp. 3–17.

21. Davis, S. Jon: Predesign Study for a Modern 4-Bladed Rotor for the RSRA. NASA CR 166155, March 1981.

22. Shanley, John P.: Application of the Comprehensive Analytical Model of Rotorcraft Aerodynamics and Dynamics to the UH–60A Aircraft. SER-72126, 1986.

23. Gagnon, R.: Blade Motion Sensor System. SER-70486, October 1981.

24. Yamakawa, George M.; Bender, Gary L.; Buckanin, Robert M.; Robbins, Robert D.; Bailes, Edward E.; and Tulloch, Johns S.: Production Validation Test Government (PVT-G), Performance Guarantees UH–60A Black Hawk Helicopter. USAAEFA Project No. 77-23, October 1979.

25. Nagata, John I.; Skinner, Gary L.; Buckanin, Robert M.; Robbins, Robert D.; and Williams, Robert A.: Airworthiness and Flight Characteristics Evaluation UH–60A (Black Hawk) Helicopter. USAAEFA PROJECT NO. 77-17, September 1981.

26. Williams, Robert A.; Buckanin, Robert M.; MacMullin, Robert; Abbott, William; Miess, Joseph O.; and Skinner, Gary L.: UH–60A External Stores Support System Fixed Provision Fairings Drag Determinations. USAAEFA Project No. 82-15-1, May 1984.

27. Marshall, Arthur R. Jr.; Buckanin, Robert M.; MacMullin, Robert; Skinner, Gary L.; Lockwood, Roy A.; Herbst, Michael K.; Reynolds, Thomas L.; Cassil, Charles E.; Tavares, Edward J.; Sullivan, Patrick J.; and Williams, Robert A.: Airworthiness and Flight Characteristics Test of a Sixth Year Production UH–60A. USAAEFA Project No. 83-24, June 1985.

28. Nagata, John I.; Piotroski, Joseph L.; Young, Christopher J.; Lewis, William D.; Losier, Paul W.; and Lyle, Joseph A.: Baseline Performance Verification of the 12th Year Production UH–60A Black Hawk Helicopter. USAAEFA Project No. 87-32, January 1989.

29. Bousman, William G.; and Maier, Thomas H.: An Investigation of Helicopter Rotor Blade Flap Vibratory Loads. American Helicopter Society 48th Annual Forum Proceedings, June 1992, pp. 977–999.

30. Lim, Joon W.; and Anastassiades, Tassos: Correlation of 2GCHAS Analysis with Experimental Data. J. American Helicopter Society, vol. 40, no. 4, October 1995, pp. 18–33.

31. McHugh, F. J.: What Are the Lift and Propulsive Force Limits at High Speed for the Conventional Rotor? American Helicopter Society 34th Annual National Forum, Washington, D.C., May 15–17, 1978.

32. Harris, F. D.: AHIP: The OH-58D from Conception to Production. American Helicopter Society 42nd Annual Forum, Washington, D.C., June 2-5, 1986.

33. Washuta, Kevin W.; and Stocker, Barry P.: Air-to-Air Combat Test (AACT II) Maneuvering Flight Loads for UH–60A and AUH-76 Helicopters. USAAVSCOM TR 86-D-1, April 1986.

34. Taghizad, Armin; Jimenez, Jérémy; Binet, Laurent; and Heuzé, Daniel: Experimental and Theoretical Investigations to Develop a Model of Rotor Aerodynamics Adapted to Steep Descents. American Helicopter Society 58th Annual Forum Proceedings, Montréal, Canada, June 11-13, 2002.